APPLICATION OF EVOLUTIONARY COMPUTATION – GENETIC ALGORITHM IN THE UNIFIED MODEL DESIGN CONSIDERATIONS FOR ACSR

APPLICATION OF EVOLUTIONARY COMPUTATION – GENETIC ALGORITHM IN THE UNIFIED MODEL DESIGN CONSIDERATIONS FOR ACSR

By

HONGYAN LIU, B. Eng.

A Thesis

Submitted to the School of Graduate Studies

In Partial Fulfillment of the Requirements

For the Degree

Master of Engineering

McMaster University

MASTER OF ENGINEERING (2006) McMaster University

(Electrical and Computer Engineering) Hamilton, Ontario

TITLE:	APPLICATION OF EVOLUTIONARY COMPUTATION – GENETIC ALGORITHM IN THE UNIFIED MODEL DESIGN CONSIDERATIONS FOR ACSR
AUTHOR:	Hongyan Liu
	B. Eng. (North China Electrical Power University)
SUPERVISOR:	Dr. Raymond D. Findlay
NUMBER OF PAGES:	xxi, 258

ABSTRACT

Aluminum Conductor Steel Reinforced (ACSR) conductors have been applied in electric power transmission and distribution for over 80 years. Research about ACSR includes its possible properties in electrical, mechanical, and thermal areas. We postulate that these properties predict certain behaviours in power transmission and distribution lines.

Four models have been established by various authors for determining conductor behaviour. They are the electromagnetic, mechanical, radial conduction, and steady-state thermal models. These models were developed independently. Although they can be used in their fields individually, there are no experimental studies verifying a combined model. Also, using them separately does not yield the required information for determining conductor performance. The unified model connects these models probabilistically by considering power system loads and meteorological factors. Based on the unified model and its modules, it is possible to use mathematical tools to optimize ACSR design and analyze conductor characteristics when conductor parameters are changed.

Evolutionary Computation is an optimization process simulating natural evolution on the computer. Instances based on evolutionary principles are Evolutionary Algorithms that historically include Genetic Algorithms, Evolution Strategies, and Evolutionary Programming. Genetic Algorithms are used in the optimization of multi-dimensional problems in this work. Evolutionary Algorithms are empirically robust in finding near-

optimal solutions to complex problems through parallel searches of solution space. Evolution Computations imitates natural evolution and genetic variation, and lays the mathematical foundation for problems in which many inputs are variable. Especially, Genetic Algorithms are extensively applied in engineering to solve problems without satisfying gradient descent, deterministic hill climbing, or purely random search.

This project introduces the Evolutionary Algorithms and applies the Genetic Algorithms to the unified models. The problem solved by applying Genetic Algorithms to optimize the unified model is to select optimum multi-dimensional input parameters for the model. This provides an effective way to find conductor size for optimizing conductor design. The results give the variation of electrical, thermal, and mechanical characteristics according to conductor loss changes and predict the variation ranges of electric and magnetic fields of three-layer conductors within ASTM standards.

The procedure to apply Genetic Algorithms to optimize ACSR design is unique to the problem. Objective functions are found according to the characteristics of each model. The results are put into the unified model to analyze conductor performance and verify the robustness of the unified model. Comparing results gives rules to change geometrical parameters of ACSR to reach minimal Joule loss.

ACKNOWLEDGMENTS

I would like to thank my supervisor Dr. Raymond D. Findlay for his accurate prediction of thesis direction, guidance, encouragement, and patience in the accomplishment of this work.

I would like to thank the colleagues in power lab and appreciate their help. Thanks to my parents and my brother for their most unselfish support.

TABLE OF CONTENTS

LIST OF SYMBOLS

a^*	fitness individuals produced during the iteration
P^*	fitness population found during the iteration
$F(t)$	fitness value
$\Phi(a_\mu(t))$	fitness function
μ	size of parents population ($P(t)$) in generation t
λ	size of offspring population ($P(t)$) in generation t
l	termination criterion
$s : I^\lambda \rightarrow I^\mu$	selection operator
$m : I^k \rightarrow I^\lambda$	mutation operator
$r : I^\mu \rightarrow I^k$	recombination operator
Θ_s	parameter of selection operator
Θ_m	parameter of mutation operator
Θ_r	parameter of recombination operator
$P(t), P'(t), P''(t)$	populations consisting of μ, k, λ individuals.
t	generation number
$\Phi(a_k(t))$	fitness function
p_s	relative frequency of successful mutations measured over the

	interval of $10 * n$ trials
n_σ	number of standard deviation
$\delta_i(0)$	initial standard deviations
n_α	number of rotation angles
R_n	dc resistance of the nth layer (Ω / m)
k_{in}	coefficient takes into account the increase in length of the wires due to stranding
ρ	resistivity of the aluminum layer or the steel core $(\Omega \cdot m)$
α	temperature coefficient $(1/°C)$
D_n	center diameter of the nth layer (m)
s_n	layer length of the nth layer (m)
T	conductor temperature $(°C)$
d	diameter of aluminum wire or steel wire (m)
m	number of the wires of aluminum layer or steel wire
I	total current in the conductor (A)
N	number of turns
I_n	current in the layer n (A)
s_n	lay length (m)
A_s	cross section of the steel core (m^2)

A_n	area common to layer p and layer q (m^2)
k_0	factor of I_n contributing to the circular flux out of the ring
k_i	factor of I_n contributing to the circular flux in the inner of the ring
X_s	steel strain (N/m)
X_a	aluminum strain (N/m)
DT_s	thermal elongation of steel and aluminum (m/m)
DT_a	thermal elongation of aluminum (m/m)
σ_s	steel and aluminum axial stress (MPa)
σ_a	aluminum axial stress (MPa)
E_s	steel modulus of elasticity (Mpa)
E_a	aluminum modulus of elasticity (Mpa)
ST_s	settling strains of steel (m/m)
ST_a	settling strains of aluminum (m/m)
CRP_s	creep strain of steel (m/m)
CRP_a	creep strain of aluminum (m/m)
W	conductor weight per unit length (N/m)
B	half of the span (m)
H	horizontal tension (N)
P_J	Joule heating (W/m)

P_S	solar heating (W/m)
P_{con}	convective cooling (W/m)
P_R	radiative cooling (W/m)
α_S	absorptivity of the conductor surface in the short-wave radiation
D	overall diameter (m)
ξ	horizontal inclination
I_B	intensity of the direct solar beam on the area (W/m^2)
H_S	solar altitude (angle degree)
η	angle between the solar beam and the conductor axis (degree)
F	albedo
I_d	intensity of diffuse sky adiation (W/m^2)
N_u	Nusselt number
T_{sur}	temperatures of the surface $(°C)$
T_{amb}	temperatures of the ambient $(°C)$
λ_f	thermal conductivity of the air at the surface of the conductor
Gr	Grashof number
g	acceleration due to gravity (m/s^2)
υ_H	kinematic viscosity at the altitude H (m/s^2)
Pr	Prandtl number.
c_p	heat capacity at constant pressure,

Re	Reynolds number
u	fluid velocity normal to the axis of the conductor
υ	kinematic viscosity of the fluid at the surface of the conductor
σ_β	Stefan-Boltzman constant
ε_s	emissivity of the conductor
h	conduction $(Wm^{-2}K^{-1})$
A	contact area between layers n and n+1 per unit length (m^2)
m_n	number of the wires in layer n
$T^{'}$	total axial tension in the layer n (N)
β_n	angle of the wires in the layer n (degree)
F_{rn}	total radial force (N)
f_y	compressive yield stress (Mpa)
k_g	air thermal conductivity $(Wm^{-1}K^{-1})$
σ_v	effective void length (m)
$p_{N_{par}}$	population number
$_{N_{par}}$	gene number in one chromosome
h_i	highest bound in the parameter range
l_o	lowest bound in the parameter range
v_i	one chromosome

p_i	probability
q_i	cumulative probability
p_c	probability of crossover
p_m	mutation probability

LIST OF FIGURES

LIST OF TABLES

CHAPTER 1

INTRODUCTION

1.1 Background

Aluminum Conductor, Steel Reinforced (ACSR) is used in overhead transmission to transfer electric power from generation sites to major users. The conductor may have three, two or one aluminum strand layer wrapped around a steel core. The bimetallic structure satisfies practical needs where aluminum wires take most of the power load, and the steel core supports most of the conductor's mechanical tension for long spans.

The analysis of ACSR operation in a power system depends on the line length in two ways. Transmission capacity within power grids is calculated by system stability, voltage drop, and energy loss. However, the load capacity is also limited by conductor temperature, sag, and long time loss of the tensile strength in the nonferrous part of the conductor due to annealing. Analyzing the performance of the conductor from a power system consideration is to deal with the power flow and to reasonably arrange the power generation, transmission and distribution components, and load fluctuations. The analysis of the lines also relies on the conductor basic characteristics such as wire size, material properties and conductor geometry. The results can help to increase the current-carrying capacity of the conductor, reduce the Joule losses and improve conductor manufacture and design.

The short line operation includes efficiency, safety and reliability. The efficiency can be divided into two aspects. One is the power loss, which comes from the alternating current (ac) resistance of the conductor. Another is the capital and maintenance costs which are decided by the maximum sag and forces in the conductor. Safety and reliability depends on the sag and the loss of tensile strength in the nonferrous part of the conductor.

The power transfer capacity is first considered when conductors go into operation. It depends on the ampacity when the voltage stays constant. The temperature of the conductor and the mechanical characteristics such as maximum sag and tensile strength determine the maximum current carrying capacity. To improve the operational efficiency of ACSR conductors, it is necessary to calculate the electromagnetic, mechanic, and thermal properties.

The models used to calculate ACSR properties include the Electromagnetic Model, Mechanical Model, Radial Conduction Model, and the Steady-state Thermal Model. They are coupled in the unified model [1] to analyze the conductor performance considering load properties and meteorological factors. The variables affecting the performance of electrical conductors in these models can be classified as material properties of metals, meteorological data and geometrical size of conductors.

To deal with these input data and to optimize the conductor design, the optimization methods need parallel calculation capability. Evolutionary Algorithms, especially the Genetic Algorithm, is a possible choice among optimization methods. The problems they can handle are multi-dimensional. Also, these algorithms may be useful when other methods do not yield appropriate design information.

1.2 Problem Definition

1.2.1 Development of The Unified Model

The models used to express ACSR physical properties in mathematical formulas are developed independently.

In the research of electromagnetic properties, geometric mean distances were accounted for by Lewis and Matsch [2]. Lewis and Tuttle [3] calculated the resistance and reactance of the conductor. They treated the conductor as a hollow tube and added some coefficients to the dc resistance to account for skin effect, proximity effect, and core losses. Morgan and Price [4] and Barrett et al. [5] proposed models that considered the spiraling of strands. They calculated the longitudinal and circular inductances and layer resistances. Findlay, Morgan and Zhang [6] calculated the current density in ten slices of strands. The model developed was the Electromagnetic Model used in the unified model.

The Graphic Method [7][8] may be used to calculate sag, tension, and elongation. However, it does not account for creep. The Mechanical Model in the unified model was set up by Barrett and others [9–12]. It calculates the sag and tension with the accumulation of the creep within a certain load period, and also considers the settlement of the conductor.

The Radial Heat Conduction Model, which was established by Morgan and Findlay [13], calculates the radial temperature distribution within the stranded conductors.

The Steady-State Thermal Model came from Morgan's work [14][15]. The model balances heat transfer to calculate surface temperature when the conductor is loaded.

These four models were independently used and tested in their research fields without accounting for the inter-relationships amongst them. The models ignored load probability variations during conductor operation. When optimizing the conductor design, considering the single model by itself will result in design errors. Gledja, Morgan, and Findlay [1] sum up all these models in one procedure, which connects the Electromagnetic, Mechanic, Radial Conduction, and Steady-state Thermal Models together according to their physical connections, load history and environmental conditions. The results predict the performance of ACSR in electrical, magnetic, mechanic and thermal areas.

1.2.2 Optimization of Conductor Design

The development of mathematical models to represent the conductor's physical performance is an optimization procedure.

One suggestion to calculate conductor resistance and reactance is to view the conductor as a hollow tube adding factors from analytical and experimental data. This gives an approximate indication of conductor properties. However it does not reflect the actual performance of the conductor in the electromagnetic field model since it does not account for the spiral lay of the conductor. With improved experimental tools and knowledge of material properties and operation of the conductor, the recently developed EM model can reasonably interpret the configuration of the electrical and magnetic

structures in the stranded conductor. The model simulates the real physical structure and provides more accurate results regarding resistance and reactance.

The Graphic Method for calculating sag and tension of a conductor does not account for time increase but instead uses the beginning and end time during the whole load period. The mechanical model accumulates the mechanical deformation within the time intervals leading to steady-state temperature.

In prior thermal studies, the radial temperature distribution was assumed to be uniform, leading to errors in calculation of losses. The Radial Conduction Model accounts for radial temperature distribution. The Steady-State Model considers environment factors when the conductor is loaded, and establishes the surface temperature on the conductor.

With the occurrence of more precise experimental tools and new mathematical methods, the optimization scope becomes broader. There are many approaches by which the conductor can be improved [12][16]. From the macro viewpoint, the four independent models and the coupled unified model have covered ACSR studies. The analysis and modification of these models can be used to optimize the performance of the conductor. A comprehensive list of the involved parameters is obtained in Gledja's work [17]. Some inputs, for example environmental effects and material properties, cannot be changed, but the geometrical sizes and lay lengths of the conductor are variable. Calculating the fittest cable sizes and lay lengths, according to some purposes such as reducing Joule losses, is another optimization option. This procedure depends on existing models and conductor properties.

The types and values of conductor geometrical data used in this work come from ASTM standards or research papers [1][16][18]. In the usual calculations, conductor sizes are constant, but in ASTM standards, lay lengths can be changed and their ranges are proportional to the wire diameters of the corresponding layers. Thus, the idea that the conductor size can be changed is developed. In a three layer ACSR, wire diameters also have some variation in the same kind of conductor due to different specifications by countries or standards [5][16]. Different designs produce different results. Comparing the design and results to reduce losses or to meet some other special needs like reduced sags can be investigated.

Some typical conductor data for general applications are given in ASTM standards [18], and by some researches [16]. However, there are no published methods that can adequately compare various conductor designs, nor are there enough resources to find the general rule by which the designs vary. Some research [16] [19] calculated the effects of the different aluminum lay lengths in three-layer ACSR, but the lay lengths are chosen by rearrangement of the lay factor. Thus, the rules of the lay length changes according to ASTM standards do not necessarily produce a conductor with optimum design. If some factors are varied, such as wire diameters and steel lay lengths, new approaches will be needed.

1.2.3 Present Work and Contribution

The unified model predicts the conductor characteristics in electrical, mechanical and thermal fields. Compared to the former independently used models, the unified model takes account of the load history and meteorological changes to make ACSR

analysis dynamic and more practical. After the original unified model [1][17], there were many people who contributed to this work [16][19-21]. Xu [20] modified the program from MATLAB to C/C++ and improved program operation speed. Brocilo [19] developed the three-dimensional cubic spline function for the permeability calculation. This gives a more accurate simulation for the permeability of the steel core in the Electromagnetic Model. The work expanded the calculation from one span to multi-spans in the Mechanical Model and extended the range of short lines in the model. The work also improved the calculation of the hydraulic diameters in the Thermal Radial Conductor Model. Wang [21] put two-layer ACSR into the unified model and analyzed its electromagnetic properties by dividing the strand into slices to calculate the current distribution in layers.

The research broadened the application ranges of the unified model, improved the performance of the single module, and enhanced the functions in the unified model. These works aid to optimize the functions and modules of the unified model from the macro simulation structures. The next step is to find ways to apply this software package to analyze practical problems. In this work, the question lies in the effective use of conductors. Better performance of ACSR depends on reducing power loss with reasonable sag, good mechanical strength, and good heat conductivity. These micro points, which save materials and keep the operation highly efficient and safe, are the most important parts in the application of ACSR in power transfer. Predicting conductor parameters from experience with existing models is the best way to achieve this goal.

Optimization algorithms are divided into global and local types. Local algorithms use gradient descent, deterministic hill climbing, or purely random search to deal with individual functions. Global algorithms achieve results from the entire solution space and procedure. Evolutionary Computation is a typical global optimization procedure that gives inspiration to do multi-dimensional optimization. The algorithm comes from the idea of Darwin's Natural Evolutionary Theory. It is suitable to solve nonlinear and random distribution engineering problems.

The purpose of this work is to apply evolutionary computation optimization to the unified model and its modules. The algorithm used is established from the discussion of the algorithms in the Evolutionary Computation. There are several possible algorithms that could be used. In this case, Genetic Algorithms are applied after comparing and analyzing the basic Evolutionary Algorithms. The next procedure is to combine the algorithms with the unified model and its modules. The program inputs for the Unified Model are static and cannot be changed when the models run. Therefore, the whole program structure has been modified in order to apply the optimization algorithm. The results show the electrical field variation ranges within the ASTM standard.

1.3 Thesis Contents

Chapter one explains the previous and present work, basic problems and algorithms used in this project. Chapter two analyzes and compares the optimization algorithms in the Evolutionary Computation. Chapter three gives the modification of the unified model and its modules to meet the requests of applying the optimization algorithm. Chapter four introduces the procedure of utilizing the Genetic Algorithms to

the models. Chapter five provides the results of the calculation. Chapter six sums up conclusions and recommends some future work.

CHAPTER 2

INTRODUCTION OF EVOLUTIONARY COMPUTATION

2.1 Concept of Evolutionary Computation

Evolutionary Computation (EC) belongs to a class of global optimization algorithms. Essentially, it includes: Genetic Algorithms (GA), Evolution Strategies (ES) and Evolutionary Programming (EP). They simulate natural evolution [22]. These calculations use randomly varied populations to search over the fitness response surfaces [23]. There are common characteristics in approaches: reproduction, random variation, competition, and selection. The Genetic Programming (GP) and hybrid methods develop very quickly as further applications. The data structures in GP are executable computer programs. Hybrid methods mix the operators and processes of Evolutionary Algorithms to improve their capability to solve problems.

These algorithms are capable of handling the high dimensional and non-linear search spaces especially those with stochastic and temporal components. They provide a computation method for problems that are intractable in usual algorithms. EC has been used in many areas that include [24, 25]:

- Planning (routing, scheduling, packing)

  Typical applications: Traveling salesman problem; vehicle routing problem; robot route planning; job shop scheduling; computer task allocation

- Design.

Some applications in different fields are: Designing electronic or digital systems that implement a desired frequency response; designing artificial neural networks through searching the optimum weights.

- Simulation and identification

  Application fields: Time series prediction; models that produce a single-valued output in response to one or more input signals; some difficult problems in chemistry and biology.

- Control

- Classification

  Some Cases: Game playing; prediction of diseases; credit evaluation; risk assessment; classification of samples in biology; selection of particular features in image processing; and improvement of the efficiency of the storage and retrieval of information.

In these techniques, although EP and ES are similar, they are independent approaches and have less similarity to GA.

2.2 Structure of Evolutionary Computation

2.2.1 Evolutionary Computation Procedure

General steps of EC are:

1. Initializing the population of generation t with the population size μ.

2. Getting a fitness of the individuals in the initial population.

3. Beginning an iteration in which the termination criterion l may be the generation number or the errors of individuals between the last and present generation.

4. Using evolutionary operators to calculate a new population.

5. Iterating until a termination criterion is satisfied.

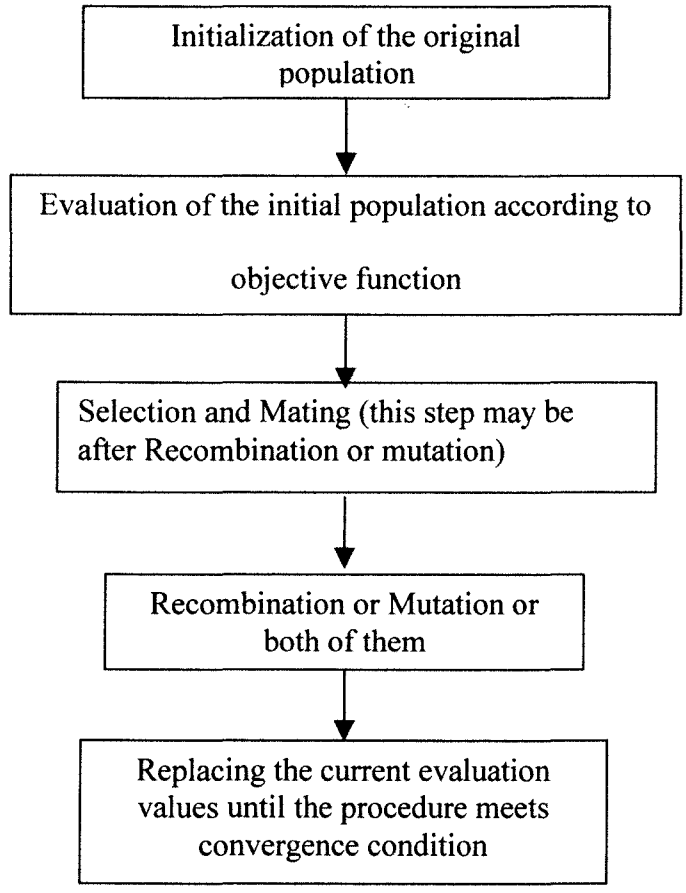

Figure 2.1 Structure of the Evolutionary Computation

2.2.2 General Scheme of EC Procedure

The following outline illustrates the basic components and procedure of Evolutionary Algorithms.

The algorithms work on the arbitrary space I and individuals $a \in I$, $F : I \to \Re$ is the fitness function of individuals.

Figure 2.2 Outline of an Evolutionary Algorithm

$input \quad \mu, \lambda, \Theta_l, \Theta_r, \Theta_m, \Theta_s$
$t \leftarrow 0;$
$P(t) \leftarrow initialize(\mu);$
$(P(t) = \{a_1(t), \cdots, a_\mu(t)\} \in I^\mu)$
$F(t) \leftarrow evaluate(P(t), \mu);$
$(F(t) = \{\Phi(a_1(t)), \cdots, \Phi(a_\mu(t))\})$
$while(_l(P(t), \Theta_l) \neq true)do$
$P'(t) \leftarrow recombine(P(t), \Theta_r);$
$P''(t) \leftarrow mutate(P'(t), \Theta_m);$
$F(t) \leftarrow evaluate(P''(t), \lambda);$
$(F(t) = \{\Phi(a_1''(t)), \cdots, \Phi(a_\lambda''(t))\})$
$P(t+1) \leftarrow select(P''(t), F(t), \mu, \Theta_s);$
$t \leftarrow t+1;$
end

Output:

a^* fitness individuals produced during the iteration

P^* fitness population found during the iteration

The parameters used in the structure:

$F(t)$ fitness value

$\Phi(a_\mu(t))$ fitness function

μ *and* λ sizes of parents and offspring population ($P(t)$) in generation t

l termination criterions which rely on the parameters summarized by the Θ_l

$s: I^\lambda \to I^\mu, m: I^k \to I^\lambda, r: I^\mu \to I^k$ selection, mutation, recombination operators

$\Theta_s, \Theta_m, \Theta_r$ parameters of these operators

$P(t), P'(t), P''(t)$ populations consisting of μ, k, λ individuals. In the main loop, $\mu = k$ with the absence of recombination and $k = \lambda$ without the mutation. In GAs $\mu = k = \lambda$. In EP $\mu = k$ without the recombination.

2.3 Frame of Genetic Algorithms

Genetic Algorithms (GAs) were first proposed by John Holland in 1975 [26]. The individuals in the population consist of the chromosomes composed by series of genes. Here these genes represent the parameters that need to be optimized. The whole procedure simulates biological genetics: Population → Mating pool → Mates selected → Mating →Offspring → New population. The algorithm structure is illustrated in figure 2.3.

Figure 2.3 Outline of the Genetic Algorithms

begin
$t = 0$;
initialize $P(0)$;
evaluate $P(0) : \{\Phi(a_1(0)), \cdots, \Phi(a_\mu(0))\}$;
while ter min *ation condition does not satisfied do*
$t = t + 1$;
select $P(t)$ *from* $P(t-1)$;
recombine and mutate $P(t)$;
form $P''(t)$;
evaluate $P''(t)$;
end

where

t generation number

$P(t), P''(t)$ populations in the procedure. Nearly all GAs maintain the fixed size population, which is made up by individuals. The bit string originally represented the individuals. Later the continuous parameter GA, using real value representation, came up in practical applications [27].

$\Phi(a_k(t))$ fitness function

The initial population $P(0)$ is randomly generated; each individual in it is evaluated by the fitness function. Some individuals are selected for mating. The crossover and mutation operators are then used to vary the population and produce offspring. There are several types of selection algorithms such as ranking, proportion and tournament selection [22]. The fitness is how individuals survive in the environment. The usual

fitness values should be kept positive, so in the algorithm some scale functions are adopted to make the results of the objective function positive. If there are some constraints in the objective function or procedure, GAs use local penalties or create representations that cause individuals to avoid violating the constraints. GA can solve multi objective problems.

GAs have many advantages in application:

1. Optimizing the continuous or discrete parameters according to a predetermined criterion.
2. Searching a large sampling cost (fitness) surface without derivative information.
3. Simultaneously optimizing parameters in a complex cost function to give the best parameters and to avoid local convergence.

2.4 Diagram of Evolution Strategies

The algorithm was established by I. Rechenberg and H-P. Schwefel in Germany during 1960s [28]. The main domain is the real value parameters. The parent population size is μ and the offspring population size is λ, $\lambda \geq \mu$. ES uses normally distributed mutations. The recombination has many forms since the process includes objective variables and strategy parameters such as standard deviations and rotation angles. The strategy parameters are self-adaptive to determine the mutation probability density function. The original form of ES is $(1+1)-ES$ with discrete, binomially distributed mutations in which there is one parent and one descendent per generation.

2.4.1 Structure of a Two-member Evolution Strategy $(1+1)-ES$

This is the first version of an evolutionary strategy. The rule is called the 1/5-successful rule. This ES requires that one result with the best convergence rates should be achieved with respect to the objective function values (see figure 2.4).

2.4.2 $(\mu+1)-ES$ and $(\mu+\lambda)-ES$

The first implementation of the population principle occurred in the multi-member ES ($(\mu+1)-ES$) in which μ parent individuals are recombined to form one offspring. This is infrequently used but is the basis of $(\mu+\lambda)-ES$ and $(\mu,\lambda)-ES$. The ES ($(\mu+\lambda)-ES$) is that μ best individuals come from the union of parents and offspring. While the latter form indicates μ individuals out of $\lambda(\lambda > \mu)$, pass to the next generation. This strategy incorporates the most important parameters: standard deviations and correlation coefficients of the normally distributed mutations in the search process. This makes optimization take place not only on the object variables, but also on the strategy parameters according to the actual local objective function.

When the situation is completely unknown, the following cases can be the first trials as default:

1. ES(1, 0, $r_{dl}, s_{(15,100)}$)
2. ES(n, 0, $r_{dl}, s_{(15,100)}$);
3. ES(2, 1, $r_{dl}, s_{(15,100)}$);
4. ES(n, n.(n-1)/2, $r_{dl}, s_{(15,100)}$)

The standard ES(1,0, r_{dI}, $s_{(15,100)}$) is given by

Parameter	Default
Number of standard deviation n_σ	$n_\sigma = n$
Initial standard deviations $\sigma_i(0)$	$\sigma_i(0) \approx 3.0$
Number of rotation angles n_α	$n_\alpha = 0$
Recombination operator r	$r = r_{dI}$
Selection operator s	$s = s_{(\mu,\lambda)}$
Parents population size μ	$\mu = 15$
Offspring population size λ	$\lambda = 100$

Figure 2.4 Outline of $(1+1)-ES$

begin

$t = 0;$

$P(0) \leftarrow initialize \ \{x_1(0), \cdots, x_n(0)\} \in I \ where \ I = \Re^n;$

$P(0) \leftarrow evaluate \{\Phi(x_1(0)), \cdots, \Phi(x_n(0))\};$

while $(_I(P(t) \neq true)$ *do*

$x'(t) \leftarrow mutate \ x(t);$

where $x_i' = x_i + \sigma(t) * N_i(0,1) \forall i \in \{1, \cdots, n\}$

$P'(t) \leftarrow evaluate \ \Phi(x'(t));$

$P(t+1) \leftarrow select \ (P(t) \bigcup P'(t));$

$t = t + 1;$

if $(t \mod n = 0)$ *then*

$$\sigma(t) = \begin{cases} \sigma(t-n)/c, & if \ p_s > 1/5 \\ \sigma(t-n) * c, & if \ p_s < 1/5 \\ \sigma(t-n), & if \ p_s = 1/5 \end{cases}$$

and $0.817 \le c \le 1;$

else $\sigma(t) = \sigma(t-1);$

endif

end

Where p_s is the relative frequency of successful mutations and is measured over the interval of $10 * n$ trials

Here, the algorithm does not use the population concept. From figure 2.4 we note that the parameter $\sigma(t)$ is carefully selected according to specific rules.

Figure 2.5 Outline of the general Evolution Strategies

begin

$t = 0;$

$P(0) \leftarrow initialize\ \{\vec{a}_1(0), \cdots, \vec{a}_\mu(0)\} \in I^\mu;$

where $\vec{a}_k = (x_i, \sigma_j)$

$i \in \{1,2,\cdots,n\}, j \in \{1,2,\cdots,n_\alpha\};$

$P(0) \leftarrow evaluate\{\Phi(\vec{a}_1(0)), \cdots, \Phi(\vec{a}_\mu(0))\};$

where $\Phi(\vec{a}_k(0)) = f(\vec{x}_k(0));$

while $(l(P(t) \neq true)$ *do*

$\vec{a}_k{}'(t) \leftarrow recombine\ r'(P(t)) \forall k \in \{1,\cdots,\lambda\};$

$\vec{a}_k{}''(t) \leftarrow mutate\ m'(\vec{a}'_k(t)) \forall k \in \{1,\cdots,\lambda\};$

$P''(t) \leftarrow evaluate\ \Phi(\vec{a}''_k(t)) \forall k \in \{1,\cdots,\lambda\};$

$P(t+1) \leftarrow select$

if (μ, λ)

then $s_{(\mu,\lambda)}(P''(t));$

else $s_{(\mu+\lambda)}(P(t) \cup P''(t));$

$t = t+1;$

end

2.5 Evolutionary Programming

Lawrence J. Fogel commenced work on this topic in the 1960s. The first EP was used in finite-state machines. In the 1980s David B. Fogel applied EP to parameter ptimization problems [23]. EP uses different operators depending on the problem. The self-adaptation of the strategy parameters for EP's characteristics is similar to that in ES.

The EP algorithm initializes the population randomly. The size of the population, μ, is larger than one. The original population is evaluated by the fitness function. In the strict EP, the recombination is not utilized and the parent variations come from the mutation with normalized distribution. In most cases the population size is fixed.

Figure 2.6 Outline of the standard EP

begin

$t = 0;$

$P(0) \leftarrow initialize \ \{\vec{a}_1(0), \cdots, \vec{a}_\mu(0)\} \in I^\mu;$

$where \ \vec{a}_k = (x_i, \upsilon_i) \qquad i \in \{1,2,\cdots,n\}$

$P(0) \leftarrow evaluate\{\Phi(\vec{a}_1(0)), \cdots, \Phi(\vec{a}_\mu(0))\};$

$where \ \Phi(\vec{a}_k(0)) = \delta(f(\vec{x}_k(0)), \kappa_k);$

$while\,(_l(P(t) \neq true) \quad do$

$\vec{a}_k'(t) \leftarrow mutate \ m'(\vec{a}'_k(t)) \forall k \in \{1,\cdots,\mu\};$

$P'(t) \leftarrow evaluate \ \Phi(\vec{a}''_k(t)) \forall k \in \{1,\cdots,\mu\};$

$P(t+1) \leftarrow select \ s(P(t) \cup P''(t));$

$t = t + 1;$

end

where δ *scaling function*

κ *a random noise term*

υ var*iance*

There are three main types in the basic paradigm:

1. Original EP, which has a continuous optimization function but performs without any self-adaptation.
2. Continuous EP, in which new individuals are inserted directly, and do not go through the generation iteration.

3. Self-adaptive EP, in which mutation parameters are governed by many factors and can be tuned to on-line adaptation according to the practical need.

2.6 Comparison of GA, EP and ES

Discussions [22-24][28-29] about the similarities and differences of these algorithms are extensive. They all simulate the natural evolution process and rely on randomly varied and selected population. They belong to the global optimization algorithm that is defined in [28]. They experience the same procedure as figure 2.1, in which they maintain the populations of potential solutions and make use of selection principles. In the procedure, the same concepts and operators are applied: recombination, crossover, mutation, selection, fitness, objective function and constraints. The differences among them appear in many aspects.

The classical GA usually uses binary strings to represent the individuals, whereas ES and EP operate on real value vectors, but this domain difference gets smaller: the real value comes up in GAs as a population representation, while ES and EP are used to solve discrete optimization problems.

EP and GA differ philosophically. The GA coding structure is very important because it contains the set of optimal building blocks set up through successive iterations. The building block hypothesis is the assumption that the fitness is a separable function in the whole process. Contrasting to this successively local optimization, EP is an entirely global approach. The solution of EP is judged only by fitness with respect to the environment. Crossover does not appear in EP.

When comparing ES and GA, the selection procedure produces differing processes. In a single generation, μ parents generate λ offspring by means of the recombination and mutation in the ES. The selection makes the parent's size of the next generation to μ by discarding the least fit individuals in the population. The selection in GA is a competition and the same individual can be selected several times. The selection in ES is deterministic, whereas it is random in GA, and the population size is not changeable in the selection.

In ES and EP, the selection process follows the recombination operation. In GA, the order is reversed.

Another difference is the reproduction parameters in GAs, in which the crossover and mutation usually remain constant. Whereas in EP and ES, the evolutionary parameters like the step size, σ are self-adaptive.

To handle constraints, ES and EP adjust control parameters when offspring cannot satisfy constraints, while GAs use penalty functions to get rid of the illegal offspring.

These algorithms have various applications in many fields [24,25]. This work utilizes GA in the design of ACSR. The input parameters for GAs are constant in length and volume, so it is suitable to configure the fixed length input series. There is no probability possibility for mutation. These conditions meet the requests of GAs. The inputs in ACSR calculation can comprise the fixed size population and the parameters of GAs are constant in every generation, so GA is adopted as the optimization algorithm in this work.

CHAPTER 3

IMPLEMENTATION OF GENETIC ALGORITHMS IN THE UNIFIED MODEL

To combine the optimization algorithm with the unified model, we have to consider two points. The first relies on the unified model and its four modules. It is necessary to find which parts in the models should be modified to fit the optimization algorithms. The second key problem is how to phrase the models as algorithms, which includes: stating the purpose in optimizing these models, and expressing the goals as optimizing procedures. The process depends on the model structures and input parameters. This chapter solves these two problems in the application of GAs in the unified model and its modules.

3.1 Optimization of The ASCR Calculation in The Unified Model and Its Modules

There are many factors affecting the calculation of ACSR characteristics. R. D. Findlay [30] noted that lay length is a major factor to optimize conductor design, and emphasized that lay length had a very important effect on the electromagnetic field associated with ACSR. In his paper, he indicated the importance to select proper conductor geometric parameters such as wire diameter, lay length, and in particular, the lay length variations within the ASTM specification. These values can reduce conductor power loss and improve the conductor ampacity.

Later, different lay factor combinations were analyzed in Zhang's [16] and Brocilo's [19] works. Zhang compared several three-layer ACSRs and changed the lay length to yield the minimum Joule loss conductor using the same wire size with different

lay factors. Brocilo arranged the lay factors to calculate the results of the different lay combinations. In the meantime, other people used different methods to find better conductor parameters to reduce the loss or for mechanical and thermal consideration. Barrett [12] used ideal space between the wires in each layer to approximately determine the number of layers and corresponding wires. The program evaluated the conductor sag, tension, and losses based on the changes of the aluminum and steel areas in the cross section. Although these works provide information in optimizing ACSR design, calculations in these papers about the optimization of conductor size or structure are limited by local events. Only some groups of selected results can be used to compare and analyze. Since the conductor sizes are multi-dimensional parameters, traditional tools cannot be used to optimize them. Genetic algorithms are one approach to achieve global optimization.

GA can select parallel parameters in the calculation. Lay length and wire size in layers can be simultaneously chosen. Hence it is a powerful tool to produce data used to analyze the relationship between the conductor parameters and the conductor properties in the loss, mechanical and thermal areas.

The unified model and its modules sum up every research area referring to ACSR performance. After the first model [1], some further works [19-21] enhance the function and structure of the unified model. Without changing the total configuration of the models, using these models to modify ACSR performance is the purpose of this paper. When applying GA to the unified model, problems exist in two parts: the parameters of the optimization algorithm and the object functions for getting the fittest conductor size.

To obtain the proper algorithm parameters and object functions, it is necessary to analyze the unified model and its modules and to modify them to accept the optimization algorithm.

3.2 Unified Model Analysis

The unified model is a toolbox that is used to calculate the characteristics of ACSR in the electromagnetic, mechanical, and thermal performances. There are four modules in the unified model: Electromagnetic, Mechanical, Static-state Thermal, and Radial Thermal Conduction Modules. The relationships among the modules are shown below (Gledja's work [17]):

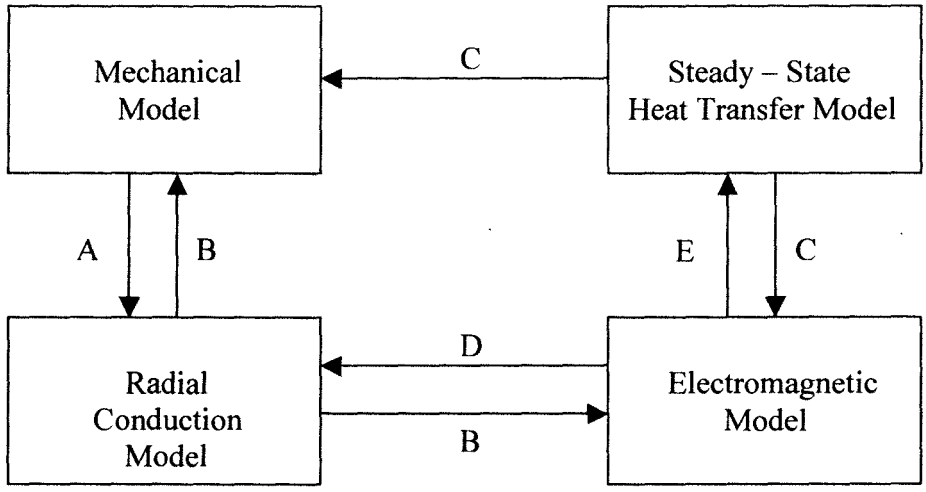

Figure 3.1 Structure of the unified model

Coupling variables are: A Aluminum and steel stress

B Radial temperature differences

C Surface conductor temperature

D Layer power losses

E Total power losses

The four models have been developed separately without any connection between them. The unified model combines them with the coupling variables and also considers ambient factors, annealing procedure, and system loads that belong to the long line or system stability analysis scope. Thus the model predicts the conductor behaviours in four areas versus the life time of the conductor.

The purpose of the work is to use the model to solve problems and not to optimize the model itself. To reach this goal, one way is to modify the model structure to adapt to the need of the optimization algorithm. For the conductor design, the wire size and lay pitch are the basic units. For the model application, these inputs are the only changeable input variables that affect the model objective functions. These parameters, with generic results, such as the outside diameter, mean diameters, weight, the areas of the aluminum wire and steel wire, constitute the geometrical characteristics of the conductor.

The geometrical parameters of the conductor can be altered according to practical need. Other inputs including the material and environment conditions are constant in the whole procedure and cannot be changed to meet the needs of optimization. Therefore, the inputs for GA are the lay length and wire diameters.

In the existing unified model, all inputs are global inputs and cannot be optimized. Thus, to combine GAs with the unified model and its modules, the structure of every module is modified and the geometrical parameters become local variables.

In determining optimal objective functions, there are two possible options. One is to use the unified model itself in the optimal process, while another is to select the single model to optimize. The single model has been proven to work well in its research field.

Compared to the separated models, the unified model is a four-module integration process and entirely embodies the properties of ASCR, but it does not particularly reflect the attributes of each area as the single model. Thus, the single module and its outputs are the objectives of the optimization. It is necessary to analyze the modules independently and describe their structures respectively so as to theoretically explain optimal results.

3.3 Electromagnetic Model

In ACSR, aluminum layers carry most of the total current. Although the steel core carries 1-2% of the current, it affects the conductor magnetic field since it is of ferrous material. It is assumed that there are no current leakages between the strands and all current is along the wires. Therefore, the layer impedances of the steel core and nonferrous wires determine the distribution of the alternating current in ACSR.

The recently used model is based on Morgan and Price's model [4]. The model first calculated the resistance and inductive reactance of the conductor in term of the layer resistances, circular and longitudinal inductances. Barrett et al. [5] modified the model by considering the effects of the complex permeability and loss angle in the steel core. Findlay, Morgan and Zhang [6] calculated the current distributions in the conductor cross-section through dividing the conductor strand into slices.

In the EM model, the lay length and wire diameters are used to calculate the direct current resistance and longitudinal inductance. The diameters are also applied in calculating the circular inductances. Thus changing their values will yield different resistance and reactance and will finally result in the changes of the current distribution and Joule loss. The current affects the layer temperature and the stress distribution within

wires, eventually changing the sag. Reducing conductor Joule loss is the basic topic in the research of the conductor electrical properties, good conduction means low loss and low heat. Therefore there will be a saving of capital, enlarging of the conductor thermal ampacity, and improvement of the operation safety and reliability. An objective to optimize this model is to obtain the least Joule loss conductor. This process involves current redistribution in conductor layers.

3.3.1 Resistance

The direct resistances vary with conductor size and temperature.

The dc resistance is

$$R_n = \frac{4\rho}{\pi d^2}\left[\frac{k_{\text{In}}}{m_n}\right] \quad \frac{\Omega}{m}$$

where

$R_n\ (\Omega/m)$ dc resistance of the nth layer

k_{in} coefficient takes into account the increase in length of the wires due to spiraling:

$$k_{in} = \sqrt{1+\left[\frac{\pi(D_n - d)}{s_n}\right]^2}$$

$\rho\ (\Omega \cdot m)$ resistivity of the aluminum layer or the steel core

$$\rho = \rho_{20}[1+\alpha(T-20)]$$

$\alpha\ (1/°C)$ temperature coefficient

$D_n\ (m)$ center diameter of the nth layer

s_n (m) layer length of the nth layer

T $(°C)$ conductor temperature

d (m) diameter of aluminum wire or steel wire

m number of the wires of the aluminum layer or the steel wire

The ac resistance

$$R_{ac} = R_{dc} + \Delta R_{ac}$$

The ac resistance increment ΔR_{ac} is due to current redistribution made by skin effect, transformer effect and proximity effect, and steel core losses including eddy current and hysteretic losses.

The Joule loss is

$$P_J = I^2 R_{ac}$$

3.3.2 Longitudinal Inductance

ACSR is a bimetallic structure. In the steel core, in addition to resistive losses, there are hysteretic losses and eddy losses. The eddy loss is determined by the longitudinal fluxes that are induced in the core wires by the currents within the aluminum layers. The hysteretic loss arises from the magnetic field which influences the permeability of the ferrous material. The magnetic field of the steel core causes the current to redistribute within the aluminum layers. The current is highest in the middle layer of a three-layer conductor due to the combination of skin effect and transformer effect in the research examples [6][31].

The magnetic field strength H around a closed path is equal to the current enclosed by a closed path according to Ampere's circuit law:

$$\oint \vec{H} dl = NI$$

$$\vec{H} = \frac{NI}{l} \qquad A/m$$

where

I (A) total current in the conductor

N number of the turns

l (m) path length around the conductor

In ACSR, the magnetic field strength contributed by the layer n is, approximately,

$$H_n = \frac{I_n}{s_n} \qquad A/m$$

where

I_n (A) current in the layer n

s_n (m) lay length

The aluminum stranding pitch affects the magnitude of magnetic field strength.

The magnetic strength for three layer ACSR is then approximated as:

$$H_n = \frac{I_1}{s_1} - \frac{I_2}{s_2} + \frac{I_3}{s_3} \qquad A/m$$

The permeability in the steel core can be estimated by

$$\mu = f(H)$$

The resultant longitudinal flux

$$\Psi_n = \mu_0 \mu_s A_n H_n \quad Wb$$
$$area \qquad A_n = A_s + ((D_n - d)^2 \pi / 4 - A_s) \quad m^2$$

$$\Psi_n = \mu_0 \left[\mu_s A_s + ((D_n - d)^2 \pi / 4 - A_s)\right] H_n \quad Wb$$

The self-inductance of layer n

$$L_{nn} = \Psi_n / I_n S_n = \mu_0 \left[\mu_s A_s + ((D_n - d)^2 \pi / 4 - A_s)\right] / s_n^2 \quad H/m$$

The self-reactance of layer n

$$X_{nn} = wL_{nn} = 2\pi f \mu_0 \left[\mu_s A_s + ((D_n - d)^2 \pi / 4 - A_s)\right] / s_n^2 \quad \Omega/m$$

The mutual reactance from layer p to the inner layer q is:

$$X_{pq} = 2\pi f \mu_0 \left[\mu_s A_s + ((D_p - d)^2 \pi / 4 - A_s)\right] / s_p s_q \quad \Omega/m$$

where

A_s (m^2) cross section of the steel core

A_n (m^2) area common to layer p and layer q

3.3.3 Circular Inductance

Currents distribute non-uniformly in ACSR. There are two opposing concepts that contribute to the distribution: the skin effect and the transformer effect. The impedance of the interior of a conductor is greater than that on the conductor surface. Hence there is a field driving the current toward the outer surface of the conductor. This is the skin effect. For the transformer effect, consider at least two layers of aluminum strands wound alternately left and right hand around the steel core. The net effect is to draw the current

distribution towards the center of the conductor, while reducing the net magnetic flux in the core.

If the current is not in the center of the layer and the current density in each layer or the slice is uniform, the inner and outer magnetic flux in the layers or slices are

$$\Psi_{n,outer} = [I_s + I_1 + k_0 I_n] \frac{\mu_0}{2\pi} \ln \frac{D_n}{D_n - d} \quad Wb$$

$$\Psi_{n,inner} = [I_s + I_1 + k_i I_n] \frac{\mu_0}{2\pi} \ln \frac{D_n - d}{D_{n-1}} \quad Wb$$

where

k_0 factor of I_n contributing to the circular flux out of the ring

k_i factor of I_n contributing to the circular flux in the inner of the ring

The reactances of the circular flux are:

$$X_{n,outer} = f\mu_0 \Psi_{n,outer}$$

$$X_{n,inner} = f\mu_0 \Psi_{n,inner}$$

In these equations, the diameters and lay lengths in three-aluminum layer conductor are the main factors in determining conductor electromagnetic characteristics. Changing them can make the current to redistribute among the layers. Using GAs to change the lay length or the wire diameters for three-layer ACSR provides the means to find the rules of variation of the conductor internal magnetic field and the current distribution to reduce power loss.

3.4 Mechanical Model

Current and resultant heating in the conductor contribute to sag and reduced tension at high temperature. In the calculation of the conductor sag and tension, the

Graphical Method [7,8] has been applied in engineering design. In the unified model, the Mechanical Model [1] assesses the accumulated creep that does not appear in the graph method. In some research [9-12], a new computer model to calculate the strain and tension took account of the metallurgical creep and geometrical settlement. Aluminum and steel have different strains in ACSR:

$$X_s = DT_s + \frac{\sigma_s}{E_s} + ST_s + CRP_s \qquad m/m$$

$$X_a = DT_a + \frac{\sigma_a}{E_a} + ST_a + CRP_a \qquad m/m$$

where

X_s *and* X_a (m/m)	total strain of steel and aluminum
DT_s *and* DT_a (m/m)	thermal elongation of steel and aluminum
σ_s *and* σ_a (MPa)	steel and aluminum axial stress
E_s *and* E_a (MPa)	moduli of the elasticity
ST_s *and* ST_a (m/m)	settling strains of metals
CRP_s *and* CRP_a (m/m)	creep strain of metals

Thermal elongation

$$DT_s = [11.3(T_s - 20) + 0.008(T_s^2 - 400)] \times 10^{-6} \qquad m/m$$

$$DT_a = [22.8(T_a - 20) + 0.009(T_a^2 - 400)] \times 10^{-6} \qquad m/m$$

The initial one-hour stress strain

$$ST_s = 5.75 \times 10^{-6}\sigma_s + 9.7 \times 10^{-22}\sigma_s^6 \qquad m/m$$

$$ST_a = 3.1 \times 10^{-5}\sigma_a + 2.5 \times 10^{-16}\sigma_a^6 \qquad m/m$$

The creep strains

$$CRP_s = 7\times10^{-8} e^{0.02(T_s-20)} S_s^{4.7} t^{0.133} \qquad m/m$$
$$CRP_a = 9\times10^{-6} e^{0.03(T_a-20)} S_a^{1.3} t^{0.2} \qquad m/m$$

The steel strain is equal to that of the aluminum within a certain time interval. When the temperatures in the steel and aluminum layers are known, the iterative procedure is used to get the stresses in the steel and aluminum layers. At the same time, the model predicts birdcaging.

From the equations and the calculation procedure, it is apparent that the variables in the Mechanical Model [MM] are the temperatures and stresses of different metals that they vary with the time. The average conductor tension may be expressed as [10]:

$$P = A_s\sigma_s + A_a\sigma_a \qquad N$$

or

$$P = \frac{H}{2}\left[\cosh\frac{WB}{H} + \frac{\frac{WB}{H}}{\sinh\frac{WB}{H}}\right]$$

The sag $D = \frac{H}{W}\left[\cosh\left(\frac{BH}{W}\right)-1\right] \qquad m$

Where W (N/m) conductor weight per unit

B (m) half of the span

H (N) horizontal tension

The conductor size affects sag and tension. Another point that demands attention is how to treat the constraints when applying GAs to search optimal parameters in this model. Sag can be an objective when using GAs in the MM, which is a key factor in the

safe operation of conductors. The objective functions in GA applications are selected according to strict criteria. In this model, the equations to calculate sag and tension are too complicated to produce local stagnancy. In addition, constraints are necessary when birdcaging occurs.

3.5 Steady-State Thermal Model

The acceptable currents in short lines rely mainly on conductor thermal characteristics. The surface temperature is a complex function of several conductor parameters as well as some meteorological parameters. Morgan [14,15] gave the heat loss, gain, and equilibrium relationship to calculate the heat transfer from the conductor as:

$$P_J + P_S = P_{con} + P_R$$

where

P_J Joule loss from electromagnetic model

P_S solar heating

P_{con} convective cooling

P_R radiative cooling

Each of these power functions is considered below.

3.5.1 Solar Heating

Solar heat gain from the isotropic diffuse sky radiation is

$$P_S = \alpha_s D[I_B(\sin\eta + \frac{\pi}{2} F \sin H_s \cos^2\frac{\xi}{2}) + \frac{\pi}{2}\cos^2\frac{\xi}{2} I_d(1+F)]$$

where

α_S absorptivity of the conductor surface in the short-wave radiation

D (m) overall diameter

ξ horizontal inclination

I_B (W/m^2) intensity of the direct solar beam on the area

H_S $(\deg ree)$ solar altitude

η $(\deg ree)$ angle between the solar beam and the conductor axis

F albedo

I_d (W/m^2) intensity of the diffuse sky radiation

In this procedure, the conductor's outside diameter is constant once given the wire diameters and lay length. Thus, wire diameters are changed to be local inputs.

3.5.2 Convective Cooling

Convection is the heat transferred by fluid or gas flowing over a solid body while temperature of the fluid and the solid surface are different. If the fluid motion is artificially induced by external means, the heat transfer is forced convection. If the fluid motion is set up by buoyancy effects resulting from density difference caused by temperature difference in the fluid, the heat transfer is natural convection. In this process, the Grashof number and Reynolds vary with conductor sizes. (The following equation is from Morgan [14, 15])

$$P_{con} = \pi Nu\lambda_f (T_{sur} - T_{amb})$$

where

N_u Nusselt number

T_{sur} *and* T_{amb} $(°C)$ temperatures of the surface and ambient

λ_f thermal conductivity of the air at the surface of the conductor

a. Natural convection

If there is no wind, the convective fluid flows upwards and the heat is lost by natural convection. In this procedure, the Grashof number, Gr, the Prandtl number, Pr, and their product, the Rayleigh number, Gr.Pr, are used to get the Nusselt number.

$$Nu = A(Gr.\Pr)^m$$

Where

A and m are coefficients, and

$$Gr = D^3 g(T_{sur} - T_{amb})/(T_f + 273)\upsilon_H{}^2$$

g (m/s^2) acceleration due to gravity

υ_H (m/s^2) kinematic viscosity at the altitude H(m)

$\Pr = c_p \mu / \lambda$ Prandtl number. c_p is specific heat capacity at constant pressure, μ is the dynamic viscosity of the fluid at the surface of the conductor, and λ is the thermal conductivity of the fluid at the surface of the conductor.

b. Forced convection

The Nusselt number for the wind velocity v which blows at right angles to the axis of the conductor is

$$Nu = 1.1C\,\mathrm{Re}^n$$

where

$\mathrm{Re} = uD/\upsilon$ Reynolds number, u is the fluid velocity normal to the axis of the

conductor and υ is the kinematic viscosity of the fluid at the surface of the conductor

C *and* n are coefficients depending on Re

The critical Reynolds number, decided by the roughness ratio of the Conductor, is

$$\mathrm{Re}_{cr} = 1500e^{\frac{0.035}{H_r/D}}$$

where

$$H_r / D = d / 2(D-d)$$

D and d (m) conductor and wire diameter

3.5.3 Radiative Cooling [15]

$$P_R = \pi D \sigma_\beta \varepsilon_s [(T_{sur} + 273)^4 - (T_{amb} + 273)^4]$$

where

σ_β Stefan-Boltzman constant

ε_s emissivity of the conductor

3.6 Radial Conduction Model

The Steady-state Thermal Model calculates the conductor surface temperature. Within the strand wires and layers, there is also heat from Joule loss. This heat is highest at he center of the conductor and lowest at the surface. Thus, the temperatures within the conductor are different among the strands and layers.

The module in the unified model set up by Morgan and Findlay [13] outputs the temperature differences between layers. The paths in which heat is transferred are mostly air gaps between metal-to-metal contacts and air voids between layers. Very little heat is

transferred through the metal-to-metal contacts. The total contact area includes the number of contacts per unit length and the area of each contact. The number of contacts depends on the construction of the conductor and the area of contact is decided by the total radial force on the wires of the inner layer and the compressive yield stress of the wire material.

The layer temperature differences from the king wire of steel core (i=0) are

$$T_n - T_{n+1} = \sum_{i=0}^{n} P_i / \sum (hA)_{n(n+1)} \qquad °C$$

Where $\sum_{i=0}^{n} P_i$ (W/m) the total power gain up to the layer n

$\sum (hA)_{n(n+1)}$ $(W/°C)$ the sum of the products of the heat coefficients due to the conduction h $(Wm^{-2}K^{-1})$ and the contact area is A (m^2) between layers n and n+1 per unit length.

The sum of the areas of the true metallic contacts A_m and the area of the air gaps between the metallic contacts A_g is equal to the product of the number of contacts q between wires in layers n and n+1 times the gross area of the contacts

$$A_{mn(n+1)} + A_{gn(n+1)} = q_{n(n+1)} A_{qn(n+1)} \qquad m^2$$

The area of voids A_v between layers n and n+1 is

$$A_{vn(n+1)} = \pi d(2n+1) - q_{n(n+1)} A_{qn(n+1)} \qquad m^2$$

The number of contacts between wires in layers n and n+1 with lay lengths s_n *and* s_{n+1} is

$$q_{n(n+1)} = m_n^2 \left[\frac{1}{s_n} + \frac{1}{s_{n+1}} \right]$$

where m_n is the number of the wires in the layer n and $1/s_0 = 0$ for the king wire

The total axial tension T' in the layer n with the total layer N is

$$T_n' = 6nT' \cos^2 \beta_n [1 - \sum_{n=1}^{N} 6n \cos^3 \beta_n]^{-1} \qquad N$$

where

β_n is the angle of the wires in the layer n

$$\cos \beta_n = s_n [s_n^2 + (\pi nd)^2]^{-1/2}$$

The total radial force

$$F_{rn} = T_n' \sin^2 \beta_n / nd \qquad N$$

The total radial force on the wires in the layer n is

$$F_{rn}' = \sum_{i=n+1}^{N} F_{rn} \qquad N$$

The radial force per contact is

$$F_{rqn} = F_{rn}' / q_{n(n+1)} \qquad N$$

The apparent area of each contact is

$$A_{qn(n+1)} = F_{rqn} / f_y \qquad m^2$$

where f_y is the compressive yield stress which is one of the material characters

All the above equations need the lay length and wire diameters that are module inputs modified to be local variables. Another change is the calculation of the hydraulic diameters of the voids between layers

The heat transfer in voids is

$$h_v = k_g / \sigma_v \qquad Wm^{-2}K^{-1}$$

where

k_g $(Wm^{-1}K^{-1})$ air thermal conductivity and

σ_v (m) effective void length

For triangular voids

$$\sigma_v = \left[\frac{2\sqrt{3}}{\pi} - 1\right] d = 0.1027d \qquad m$$

For rectangular voids

$$\sigma_v = \left[\frac{4}{\pi} - 1\right] d \qquad m$$

Brocilo [19] modified the formula to the more complicated but general equations considering void shapes that are neither triangular nor rectangular, and vary in terms of rotation angles.

From these equations, it appears that conductor lay length determines contact number, and affects contact area and radial force that result in the change of conductor area when the conductor is in operation. Because of stranding, there are angles between layers. Unifying wire diameter and lay length changes total tension of the conductor.

3.7 Unified Model

The unified model is the main function that connects the four modules according to the internal temperatures amongst the conductor surface and layers, and the stresses within the steel and aluminum layers.

From the analysis of the models, we can see there are many factors that have influences on conductor operation: environment, material parameters, and conductor geometric information. From a probabilistic viewpoint, the first two are usually constant. The last one, including wire diameters and lay lengths in above equations, is variable. The conductor wire mean diameters, the outer diameter, the steel and aluminum areas also vary. We can predict that to get the optimum design to meet practical needs, for instance the minimum loss or least sag, we expect to change wire diameters and lay lengths until an optimum value is reached.

In this work, the objective function is a procedure to calculate conductor losses. The inputs in the GAs are conductor wire sizes and lay lengths. The results are used to predict the rules of three-layer ACSR conductor heat, electrical, and mechanical characteristics.

CHAPTER 4

GENETIC ALGORITHM AND THE APPLICATION TO THE UNIFIED MODEL

4.1 Introduction of Genetic Algorithms

Genetic Algorithms (GAs) were studied in the 1960s, and were mathematically used by J. H. Holland [26] in 1975. The basic structure of GAs is shown in chapter 2. Its power lies in its methods of exploiting and exploring a multidimensional search space [32]. The applications of GAs [24, 25] are extensive in the scientific, financial, and engineering fields. GA optimization is a procedure in which process parameters are randomly changed and inputted into an evaluation function to get optimal results. It is necessary to have large sample space and multiple inputs.

The first step in applying GAs is to determine the physical range of inputs and the object function that defines the problem. The second is using GA operators, such as crossover and mutation, to change input parameters and evaluate them by iteration. After reaching some criteria, the procedure can be finished. The commonly used GA procedure is shown in figure 2.3.

The classical GA uses binary strings to represent inputs discretely. The real value expressions are applied in practical problems [29, 33] as well.

The initialization process generates a population similar to that of natural fitness. The individuals of the population randomly distribute throughout the search space. Population size is determined by the dimension of the solution space [32]. An excessively

small population cannot represent the whole search space and excessively large populations need a long time to reach convergence especially when input parameter lists are too long. There are no definitions about the size, which is normally based on the problem at hand.

As shown in figure 2.1, the iteration begins after population initialization. The selection is the first step in exploiting the population and relies on fitness results of evaluation functions. The selection is similar to nature surviving to the fittest that is to keep individuals with good performances to next generation and discard the poor ones.

When the population is selected, the next step is reproduction, which includes mating, crossover and mutation operators. Crossover is exchanging the segments between pairs of crossover points in parent individuals to produce new strings. Mutation is a random alteration of string elements in individuals to keep them diverse to prevent the current population from locally converging too quickly by excessive crossover and mating. In many cases, the elitist operator is used to keep the fittest from generation to generation. This ensures that the optimal fitness can survive until the end of the iteration.

The purpose of the variation of individuals in the population is to find the fitness values according to the objective function. The above operators generate randomly changed strings. They are evaluated by the objective function by which optimum strings can be selected. The elements in chromosomal strings are called schemata, which are the foundation of mathematic theory of GA [28, 29]. Although there are just a few operators in GA, many different forms of each operator broaden GA applications. In this work, two GA patterns are adopted to search maximal and minimal values respectively.

4.2 Program to Find The Near Optimum Values

4.2.1 Representation of Parameters

The initialization of the problem is to represent conductor parameters to apply algorithms. Here real values are the representation in chromosomes [24]. One individual can be expressed by chromosomes:

$$\text{Chromosome}=[p_1, p_2, p_3, \cdots, p_{N_{par}}]$$

Where

$p_{N_{par}}$ parameters as genes composing a chromosome

N_{par} parameter number which indicates the dimension of the problem

The fundamental form of the chromosome is the binary string, but for many real value problems, the expression using the real vector is simple to code and can reach the same near-optimum points. Therefore, the real vectors are used to establish the chromosomes in this instance. The initial population of N_{ipop} chromosomes and the matrix of $N_{ipop} \times N_{par}$ made up by random values are:

$$IPOP = (h_i - l_o) \times random\{N_{ipop}, N_{par}\} + l_o$$

where

h_i, l_o the highest and lowest values in the parameter range

$random\{N_{ipop}, N_{par}\}$ function that generates the $N_{ipop} \times N_{par}$ matrix of uniform random numbers between zero and one

4.2.2 Selection of Parents

The selection is to rank the population from best to worst. There are many selection methods [22]: proportionate, tournament, ranking, and Boltzmann. The most used is the best fitness value selection. All selected parents are copied into the next reproduction procedure. The Weighted roulette selection is used for this kind of selection as follows:

a. Calculate the fitness value $eval(v_i)$ for each chromosome v_i and find the total fitness of the population $F = \sum_{i=1}^{pop\_size} eval(v_i)$

b. Calculate the probability p_i and a cumulative probability q_i for each chromosome v_i, $i = 1, \cdots, pop\_size$

$$p_i = eval(v_i) / F$$
$$q_i = \sum_{j=1}^{i} p_j$$

c. Generate a random number r in the range [0...1]. If $r < q_i$ then select the first chromosome; otherwise select the $i\,th$ chromosome for each chromosome v_i $(q_{i-1} < r \leq q_i)$

4.2.3 Recombination Operators

GA operators include crossover and mutation.

a. Crossover operator

Given the probability of crossover p_c, there are $p_c \cdot pop\_size$ of chromosomes that undergo the crossover. The procedure is:

a.1 generate a random number r in the range [0...1]

a.2 if $r < p_c$ select the given chromosome to do the crossover. This random mating changes two chromosomes in randomly produced points. In the m –bit chromosome, the crossover in the pos –position is as follows

$$(p_{i1}p_{i2}\cdots p_{ipos}p_{ipos+1}\cdots p_{im})$$
$$(p_{j1}p_{j2}\cdots p_{jpos}p_{jpos+1}\cdots p_{jm})$$

After the crossover

$$(p_{i1}p_{i2}\cdots p_{ipos}p_{jpos+1}\cdots p_{jm})$$
$$(p_{j1}p_{j2}\cdots p_{jpos}p_{ipos+1}\cdots p_{im})$$

b. Mutation operator

Mutation is based on bit changes. Given the mutation probability p_m, the number of the mutated bits is $p_m.m.pop\_size$. The bits in all chromosomes of the whole population experience equal mutation.

In each chromosome:

b.1 Generate the random number r in the range [0...1]

b.2 If $r < p_m$, mutate the bit

4.2.4 Elitist Strategy

In every generation, the elitist procedure is to compare optimal values in the last generation with that of the present generation, then to keep the best one. Calculation methods are flexible. Keeping one or more than one relies on problems and calculation time. The strategies ensure good solutions in the population longer than one generation.

4.3 Program for Getting The Near Minimum Values

4.3.1 Initialization

The initialization procedure is the same as in 4.2.1. The only difference is that the population size is doubled in the beginning. After getting evaluation values, all individuals are sorted and ranked according to fitness values. Finally, discard half the population and keep the best half.

4.3.2 Crossover

Any two chromosomes can be paired for mating. The rate of crossover is P_{xover} that decides the number of the crossover $N_{crossover} = N_{pop} * P_{xover}$. From the best to the $N_{crossover}$ chromosome, adjacent two pairs are exchanged in the random crossover point. Thus, the parameter compositions are changed in these chromosomes. Keep the $N_{pop} - N_{crossover}$ best ones into the next generation and place $N_{crossover}$ chromosomes under them. The new generation is composed.

4.3.3 Mutation

The number of mutations is decided by the rate of mutation. $N_{mutation} = P_{mutation} * N_{pop} * N_{var}$. Here, let mutation points evenly distribute among every population, while the points can be among individuals.

4.3.4 Elitist

This is an operator to find the best chromosome within the sampling space from the initial population to the present generation. After all individuals are ranked according to the evaluation results, the best performance individual is kept generation to generation. An example in table 4.1 explains the procedure of searching minimum values.

Table 4.1 Chromosomes and generations

Generation 1				
Individual	Chromosome			
Number	1	2	3	
1	0.298	0.2695	0.3924	Population
2	0.3133	0.3109	0.4138	
3	0.2545	0.288	0.3726	
4	0.2843	0.324	0.4061	
5	0.2501	0.3588	0.4209	
6	0.1935	0.3254	0.41	
7	0.298	0.3485	0.4155	
8	0.2818	0.3342	0.3942	
9	0.2105	0.3098	0.407	
10	0.3203	0.3687	0.412	
Crossover				
1	0.298	0.2695	0.3924	
2	0.3133	0.3109	0.4138	
3	0.2545	0.288	0.3726	
4	0.2843	0.324	0.4061	
5	**0.3133**	0.2695	0.3924	
6	**0.298**	0.3109	0.4138	
7	**0.2843**	**0.324**	0.3726	
8	**0.2545**	**0.288**	0.4061	
9	**0.1935**	0.3588	0.4209	
10	**0.2501**	0.3254	0.41	

This is the initial population which has ten individuals. Every individual includes three parameters which are the inputs of fitness function.

The crossover is to change some points between individuals to make the population versatile. The bold ones show the results of this operation. Individuals 5 and 6 come from individuals 1 and 2, changing the parameters at the first position. Individuals 7 and 8 are produced by altering the 3 and 4 at the second point.

Mutation				
Number	1	2	3	
1	0.298	0.2695	0.3924	
2	0.3133	0.3109	0.4138	
3	**0.2263**	0.288	**0.3657**	
4	0.2843	0.324	0.4061	
5	0.3133	0.2695	0.3924	
6	0.298	**0.4037**	0.4138	
7	0.2843	**0.2703**	0.3726	
8	0.2545	0.288	0.4061	
9	**0.2473**	0.3588	0.4209	
10	0.2501	0.3254	**0.3764**	
Elitist				
Number	1	2	3	Evaluation Value
5	0.3133	0.2695	0.3924	45.9969
1	0.298	0.2695	0.3924	46.1619
7	0.2843	0.2703	0.3726	46.7485
2	0.3133	0.3109	0.4138	46.7936
8	0.2545	0.288	0.4061	47.2302
4	0.2843	0.324	0.4061	47.8607
3	0.2263	0.288	0.3657	48.6615
10	0.2501	0.3254	0.3764	49.3802
9	0.2473	0.3588	0.4209	49.6588
6	0.298	0.4037	0.4138	50.3195
Average				47.881

The mutation is the variation inside one individual. As shown, two parameters in individual 3 have been randomly changed.

For keeping the best individual to go to the next generation, the elitist operation is necessary. However, in most situations the best value is produced in the new generation, so there are no values kept from the old generation to the new generation in this calculation.

Generation 2				
Crossover				
Number	1	2	3	
1	0.3133	0.2695	0.3924	
2	0.298	0.2695	0.3924	
3	0.2843	0.2703	0.3726	
4	0.3133	0.3109	0.4138	
5	**0.298**	0.2695	0.3924	
6	**0.3133**	0.2695	0.3924	
7	**0.3133**	0.2703	0.3726	
8	**0.2843**	0.3109	0.4138	
9	**0.2843**	**0.324**	0.4061	
10	**0.2545**	**0.288**	0.4061	
Mutation				
Number	1	2	3	
1	0.3133	0.2695	0.3924	
2	0.298	0.2695	**0.3701**	
3	0.2843	0.2703	0.3726	
4	**0.2609**	0.3109	0.4138	
5	0.298	0.2695	**0.4354**	
6	0.3133	0.2695	0.3924	
7	**0.2997**	**0.323**	0.3726	
8	0.2843	0.3109	0.4138	
9	0.2843	0.324	0.4061	
10	0.2545	**0.3618**	0.4061	

The procedure in generation 2 is the same as that of generation 1. It includes crossover, mutation, selection, and elitist to configure new offspring.

Elitist				
Number	1	2	3	Evaluation value
5	0.298	0.2695	0.4354	45.64
1	0.3133	0.2695	0.3924	46.0207
6	0.3133	0.2695	0.3924	46.0207
2	0.298	0.2695	0.3701	46.593
3	0.2843	0.2703	0.3726	46.7716
8	0.2843	0.3109	0.4138	47.3472
4	0.2609	0.3109	0.4138	47.7697
9	0.2843	0.324	0.4061	47.9522
7	0.2997	0.2703	0.3726	48.39
10	0.2545	0.3618	0.4061	50.0318
Average				47.255

4.4 Genetic Algorithm Parameters

GA parameters are population size, crossover rate, and mutation rate. They decide the performance of GAs.

The population size in real value representation is the same as the dimension of the search space. The higher dimension needs more populations to randomly sample the search space than the lower one. Consequently, it will use more calculation time and machine memory. The proper number improves convergence [27, 29].

The crossover rate limits the numbers of chromosomes participating in the crossover. Suitable pair forms in practical applications can make the crossover more powerful. The mutation rate decides the chromosome number taking part in the mutation

and can be specified according to the situation. The number of chromosomes in the mutation is $P_{mutation} * N_{pop}$ or $P_{mutation} * N_{pop} * N_{vars}$.

Though there are some basic variation rules for these parameters, the application [33] prefers the crossover rate at 0.6. The rate depends on the random property of the GA application.

Convergence criteria vary according to requests. Most cases use the maximum generation to stop iteration after observing evaluation values converge to constant values or known physical optimal values. Another method is to use the errors of the evaluation values to stop the generation iterations.

4.5 GA Application in This Project

The main function in ACSR calculation is the unified model. It combines four modules through the equilibration of variables. The relationship of these four modules is introduced in chapter 3. There are two processes in the unified model: deterministic and probabilistic. The first considers the physical couplings of modules without using time division in the procedure. The second is established according to probabilistic load distribution along the time line. Time intervals are separated into small pieces including temperature and load characteristics.

Since the unified model is a probability process and connects all the sub modules together, the whole procedure is not suitable to be optimized. This needs the addition of constraints if applying optimization methods to it. GA is very strict with objective functions. Every module in the unified model has been applied to solve one aspect problem in ACSR operation. Their purposes are more distinct when separately used.

Therefore, the modules are independently used with GA in this work. Then input the results of the GA calculation into the unified model to calculate other conductor properties, observe the effect of GA, and get optimal conductor sizes.

CHAPTER 5

RESULT AND ANALYSIS

5.1 Inputs in The Unified Model

In this calculation, a sample conductor is used: 54/19 Grackle ACSR conductor [1][6][16]. Other samples include Finch, Pheasant, Martin, Plover, and Cardinal in the appendices. Inputs include constant environment and operation conditions, and changeable conductor size. Inputs in the unified model are listed in Appendix A.

Geometrical parameters of ACSR like lay lengths are changeable in terms of the ASTM 232M [18]. Wire diameters are specified in ASTM, but for optimizing the design, they are assumed to be altered.

5.2 Genetic Algorithm Parameters

GA parameters include population size, crossover rate and mutation rate. GA parameters are estimated by trial by changing one of them and keeping others constant.

5.2.1 Selecting Population Size

Table 5.1 Selecting the best population size

Generation	2000	1000	670	500	400	370
Pop size	10	20	30	40	50	60
Times to reach the minimum	397	197	525	73	184	63
Average Losses [W/m]	46.736	48.014	49.249	49.982	50.057	50.48

In this table, the crossover rate is 0.6 and the mutation rate is 0.2.

Population size is very important in deciding the sampling space. Proper sampling space makes the search converge well. In table 5.1, keeping $N_{pop} * generation$ constant means giving the same lifetime to all samples. Changing the population size from 10 to 60, checks the fitness value in generations. When the population size is 60, it takes 63 iterations to reach the minimal fitness value. However, the average fitness value is bigger than that in other population sizes. This indicates the sample changes to a greater degree. In addition, the space is too large and needs a long time to converge.

In some cases, such as searching the maximal fitness value in this paper, the maximal value can be found early when the population size is small (10 here). However, for a smaller population size, the sampling number is too limited for a stochastic search and the solution cannot be found from it. Therefore, excessively large or small population sizes should be avoided. The next optimal value is at 50 where average fitness is relatively small. Thus, in this calculation procedure, the population size adopted is 50.

5.2.2 Deciding Crossover Rate and Mutation Rate

The crossover rate and mutation rate are the basic parameters in the GA application. There are many criteria to select them. The direct method is to change one without changing others and then to compare the mean minimum values with optimal fitness values.

The check begins with crossover rate P_c from 0.1 to 0.9 and mutation rate P_m from 0.1 to 0.7. Table 5.2 gives the iteration times reaching near optimal solutions, the average values in these points and the standard deviation.

Table 5.2 Changing crossover rate and mutation rate to check GA performance

Crossover / Mutation	0.1	0.2	0.3	0.4	0.5	0.6	0.7	0.8	0.9
0.1	169	924	146	180	129	125	419	116	359
Average loss [W/m]	45.5309	45.6688	45.5952	45.7389	45.6187	45.6518	45.5395	45.5375	45.566
Std deviation	0.5461	0.8704	0.783	1.0238	0.9221	0.7172	0.6635	0.5505	0.625
0.2	345	198	256	224	304	73	257	90	114
Average loss [W/m]	45.9038	46.0523	45.9816	46.0714	45.8815	45.7783	45.8524	46.3154	45.815
Std deviation	1.1183	1.1328	1.3498	1.3763	1.0473	1.1794	1.05	1.6738	1.0234
0.3	78	329	74	82	534	165	146	422	49
Average loss [W/m]	46.6419	46.4573	46.6419	46.2994	46.507	46.3422	46.3491	46.1736	46.523
Std deviation	1.8329	2.0979	1.8329	1.305	1.6151	1.4912	1.4403	0.9713	1.575
0.4	128	306	136	133	851	128	153	112	76
Average loss [W/m]	46.7774	46.7605	46.6268	46.7099	46.8125	46.4974	46.9884	46.7728	47.438
Std deviation	1.8962	1.8388	1.7824	1.6454	2.1913	1.7348	2.0407	1.897	1.8682
0.5	114	354	110	108	107	105	327	196	55
Average loss [W/m]	46.898	47.1647	46.858	46.9126	46.8673	46.8579	47.3462	46.8864	46.74
Std deviation	1.9052	1.9373	1.9763	1.9426	1.6955	1.9763	2.0578	1.7448	1.7363
0.6	427	283	434	455	171	108	184	48	86
Average loss [W/m]	47.1201	47.0172	46.9608	47.4792	47.0034	47.791	47.0119	48.003	47.034
Std deviation	1.7953	1.9728	1.8193	1.9978	1.7231	2.5887	1.9165	1.8742	1.9521
0.7	381	217	374	429	246	244	476	145	236
Average loss [W/m]	47.5439	47.1983	47.2779	47.6526	47.6256	47.9158	47.0916	47.1615	47.852
Std deviation	2.3829	2.082	1.8709	2.2389	2.062	2.3909	1.4888	1.8759	2.0913

From Table 5.2, average fitness values and standard deviations are all increased with the increased rate of crossover and mutation. With the small variation of the chromosomes in one population when the crossover and mutation rates are small, the times reaching the same minimal values are large. When the rates are large enough, the times are also large because populations are almost changed and the whole procedure loses stability. Comparing times that reach near optimum and average values, reasonable values of the crossover and mutation are 0.6 and 0.2 in the process of calculating minimal values. In the calculation of maximal values, population size is 50, crossover rate is 0.6 and mutation rate is 0.2.

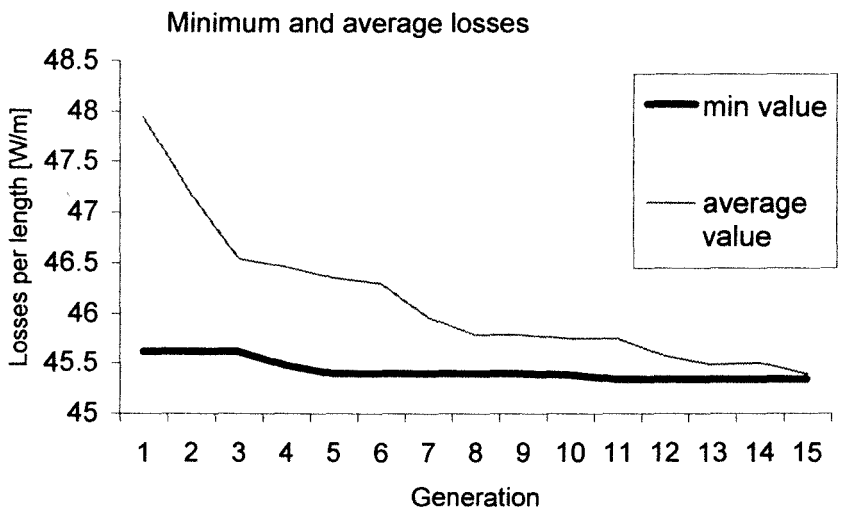

Figure 5.1 Average value and optimal value versus generation.

It can be seen from figure 5.1 how the algorithm converges. It shows that average values gradually decrease to the minimal values generation by generation in the calculation of minimal values when aluminum lay lengths are changed.

5.3 Results of The Genetic Algorithm Application

Applying GAs to the Electromagnetic Model calculates conductor characteristics in the electromagnetic field in terms of reducing Joule loss.

In all inputs, we postulate that wire diameters and lay lengths are the conductor manufacture parameters that decide ASCR operating characteristics. Within their physical limitations, changing their values can yield differing ACSR performances. The GA application can be divided into three situations: changing aluminum lay lengths and fixing other inputs; changing steel and aluminum lay lengths and fixing wire diameters; changing the aluminum lay lengths and wire diameters and fixing steel size.

Table 5.3 Standard in ASTM 232M

Ratio of lay length of a layer to nominal outside diameter of that lay									
Aluminum layer						Steel layer			
Outer		Middle		Inner		Outer		Inner	
Min	Max	Min	Max	Min	Max	Min	Max	Min	Max
10	13	10	16	10	17	16	24	18	30
Conversion of the lay length of Grackle conductor [mm]									
339	440	264	421	188	321	179	268.6	120.9	201.4

Table 5.3 gives the assumed bounds of wire diameters and lay lengths in this work, according to ASTM standards [18] for three layer ACSR. Also shown are the results from Grackle. The results from these values are shown from tables 5.6 to 5.9. We consider six conductors commonly cited in North American application. Physical characteristics are shown in Appendix A. These conductors will be used for comparison of results with changing parameters as shown for each case. The results will then be summarized.

Table 5.4 Results from different samples

Type of Conductor	Cardinal	Finch	Grackle	Pheasant	Martin	Plover
Weight [N/m]	17.93	20.81	22.25	23.78	25.25	26.75
Joule loss [W/m]	77.86	66.72	59.52	57.43	53.37	50.61
Sag [m]	12.89	13.94	14.46	15.13	15.75	16.41
Steel layer temperature [°C]	92.88	85.37	80.92	79.47	77.21	75.25
Alum layer temperature [°C]	91.53	84.24	79.90	78.50	76.30	74.39
Temperature dif of core to surface [°C]	2.49	2.16	1.96	1.86	1.75	1.65
Thermal conductivity [W/mK]	1.46	1.44	1.30	1.42	1.41	1.39
Core current [A]	22.00	21.44	20.02	21.19	21.10	21.04
Alum inner layer current [A]	203.23	197.51	216.68	199.51	199.93	200.27
Alum middle layer current [A]	368.78	386.28	328.63	382.95	382.11	381.62
Alum outer layer current [A]	411.46	406.55	444.07	411.07	413.01	414.84
Permeability	119.68	157.21	61.03	130.03	120.73	113.34
Magnetic field strength [A/m]	624.94	709.52	432.99	672.50	651.26	632.08
Reactance [Ω/m]	3.64E-06	1.97E-05	1.74E-05	1.95E-05	1.93E-05	1.92E-05
Resistance [Ω/m]	7.79E-05	6.67E-05	5.90E-05	5.74E-05	5.38E-05	5.06E-05
Steel stress [MPa]	0.70	303.09	288.52	272.40	259.37	247.24
Aluminum stress [Mpa]	14.00	14.58	15.26	14.36	14.09	13.71
Horizontal tension [N]	27850.62	29898.75	30830.18	31499.75	32125.05	32671.75

Note that all of the results citied below are for Grackle configuration. Similar results can be found for the remaining five conductor configurations in appendices B through F.

Table 5.5 Ranges of changed diameters and lay lengths

Steel diameter [mm]		Aluminum diameter [mm]	
Lower bound	Upper bound	Lower bound	Upper bound
		3.5	3.8
Steel lay length [mm]		Aluminum lay length [mm]	
Layer 1		Inner layer	
Lower bound	Upper bound	Lower bound	Upper bound
120.9	201.4	188	321
Layer 2		Middle layer	
Lower bound	Upper bound	Lower bound	Upper bound
179	268.6	264	421
		Outer layer	
		Lower bound	Upper bound
		339	440

Table 5.6 Min and max losses with changed aluminum lay lengths

Minimum Joule loss [W/m]		Weight [N/m]
59.0052		22.25
Aluminum lay length [mm]		
Inner	Middle	Outer
321	264	440
Maximum Joule loss [W/m]		Weight [N/m]
70.0135		22.31
Aluminum lay length [mm]		
Inner	Middle	Outer
188	421	339

Table 5.7 Min and max losses with changed steel and aluminum lay lengths

Minimum Joule loss [W/m]			Weight [N/m]	
59.0005			22.22	
Layer length [mm]				
Steel lay 1	Steel lay 2	Al inner	Al middle	Al outer
201.4	268.6	321	264	440
Maximum Joule loss [W/m]			Weight [N/m]	
70.0158			22.32	
Layer length [mm]				
Steel lay 1	Steel lay 2	Al inner	Al middle	Al outer
120.9	179	188	421	339

Table 5.8 Min and max losses with changed aluminum wire diameters

Minimum Joule loss [W/m]		Weight [N/m]
60.3614		22.44
Aluminum diameter [mm]		
Inner	Middle	Outer
3.8	3.8	3.8
Maximum Joule loss [W/m]		Weight [N/m]
71.7789		19.88
Aluminum diameter [mm]		
Steel lay 1	Steel lay 2	Inner
3.5	3.5	3.5

Table 5.9 Min and max losses with changed aluminum wire diameters and lay lengths

Minimum Joule loss [W/m]		Weight [N/m]
58.4914		22.39
Aluminum wire diameter [mm]		
Inner	Middle	Outer
3.8	3.8	3.8
Aluminum lay length [mm]		
Inner	Middle	Outer
321	264	440
Maximum Joule loss [W/m]		Weight [N/m]
82.6768		19.89
Aluminum wire diameter [mm]		
Inner	Middle	Outer
3.5	3.5	3.5
Aluminum lay length [mm]		
Inner	Middle	Outer
188	421	339

Table 5.10 Grackle used as a reference

Aluminum lay length [mm]			Steel lay length [mm]	
Inner	Middle	Outer	First layer	Second layer
251.41	294.30	375.50	150.0	187.4
Aluminum wire diameter [mm]			Steel wire diameter [mm]	
3.784			2.238	
Loss [W/m]		Weight [N/m]		Sag [m]
60.8891		22.29		14.5125

From the above combinations, the conductors whose losses are less than that of Grackle are listed in table 5.11. The Grackle in table 5.10 is used in Zhang's work. The line operation current is 1000 A.

Table 5.11 Low loss conductors

Results with changed aluminum lay lengths

Aluminum lay [mm]				Weight [N/m]	Loss [W/m]	Sag [m]
Number	Inner	Middle	Outer			
1	312.0	268.7	439.6	22.24	59.0477	14.456
2	320.3	268.7	419.6	22.26	59.1104	14.4617

Results with changed aluminum lay lengths and wire diameters

Aluminum lay [mm]				Aluminum wire diameter [mm]		
Number	Outer	Middle	Outer	Inner	Middle	Outer
1	316.1	268.9	439.5	3.7691	3.7855	3.7943
2	313.3	268.7	419.6	3.7364	3.777	3.793
Number	Weight [N/m]	Loss [W/m]	Sag [m]			
1	22.26	58.9559	14.4611			
2	22.18	59.398	14.4305			

Results with changed steel and aluminum lay lengths

Steel lay [mm]			Aluminum lay [mm]		
Number	Steel 1	Steel 2	Inner	Middle	Outer
1	200.0	230.0	321.0	264.0	440.0
2	172.4	229.3	320.7	283.3	439.9
Number	Weight [N/m]	Loss [W/m]	Sag [m]		
1	22.23	59.002	14.4487		
2	22.21	59.0256	14.4397		

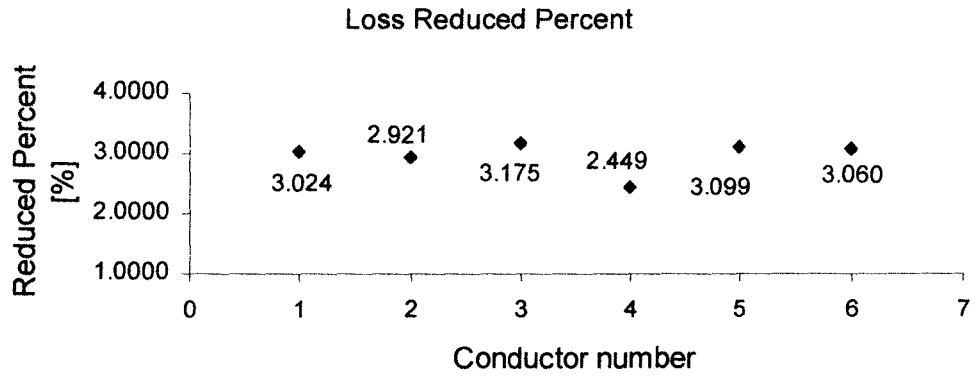

Figure 5.2 Percentage of reduced loss compared to the reference

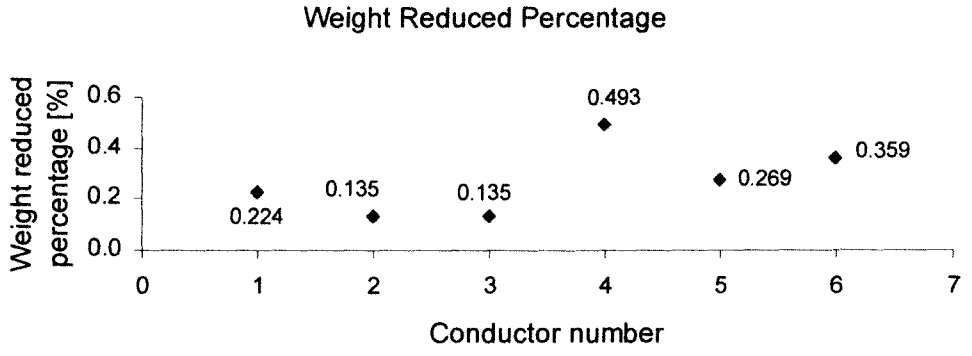

Figure 5.3 Percentage of reduced weight compared to the reference

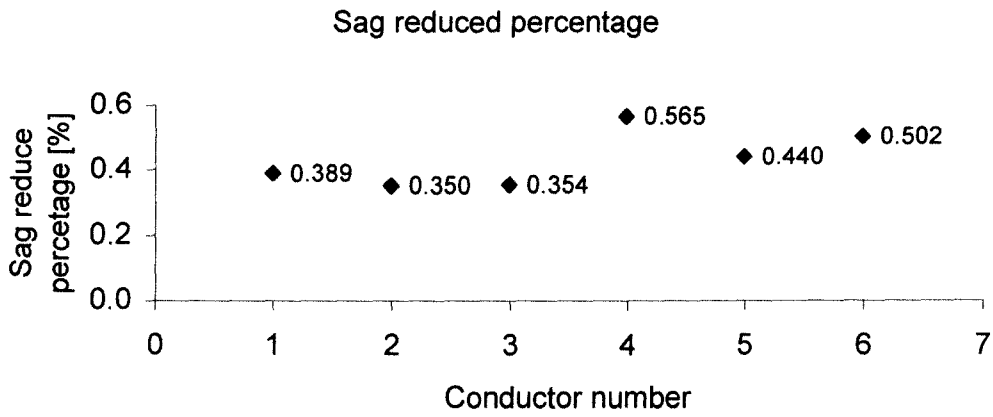

Figure 5.4 Percentage of reduced sag compared to the reference

Figure 5.2 shows that the least loss conductor can reduce loss by 3.175% compared to standard Grackle. Figure 5.3 indicates the weight can be reduced at most 0.494% compared to it. Figure 5.4 gives the shortest sag as 0.565% less than that of Grackle.

5.3.1 Fixing Wire Diameters and Steel Lay Lengths, Changing Aluminum Lay Lengths

Lay length is the key factor in affecting the magnetic field strength distribution. The magnetic field in the strand conductor is separated to circular and longitudinal directions. The longitudinal field is mainly connected to the lay factor. A suitable lay length can reduce magnetic field strength in the conductor. Various analyses about functions of lay length have been done by arranging lay factors, but few can find better conductors than the presently used types. The random selection and combination functions in the GA application make comparison possible.

Table 5.12 gives conductor input size in this GA application. Unchanged parameters include steel lay lengths and aluminum wire diameters.

Table 5.12 Unchanged wire and steel lay parameters

Steel wire diameter [mm]			Aluminum wire diameter [mm]		
Steel king	Steel lay 1	Steel lay 2	Inner	Middle	Outer
2.238	2.238	2.238	3.784	3.784	3.784
Steel layer outer diameter [mm]			Aluminum layer outer diameter [mm]		
Steel king	Steel lay 1	Steel lay 2	Inner	Middle	Outer
2.238	6.714	11.190	18.758	26.326	33.894
Steel lay length [mm]			Aluminum lay length [mm]		
Steel king	Steel lay 1	Steel lay 2	Inner	Middle	Outer
1000.0	150.0	187.4	Changed	Changed	Changed

Six sets of results from randomly changing aluminum lay lengths are listed in table 5.13. Conductor 2 is the type noted in Zhang's thesis.

In figure 5.5, there are two groups of aluminum lay lengths. The common point is that the length of the outer layer is always longer than that of the inner layer in the same conductor. The difference is that the lay length of the middle layer is under or above the connection line from the inner layer length to the outer layer length. In conductors 1 and 2, lay lengths of the middle layers are under the linear line from layer 1 to layer 3 and those of conductors 3 to 6 are in reverse. Conductors 1 to 6 are sorted according to the loss from low to high. Comparing lay lengths, the longer the middle aluminum layer ratios, the more Joule loss in that conductor.

Table 5.13 Changed aluminum lay lengths

Conductor number	Inner [mm]	Middle [mm]	Outer [mm]	Weight [N/m]
Conductor 1	321.00	264.00	440.00	22.25
Conductor 2	251.41	294.30	375.50	22.29
Conductor 3	277.80	395.10	439.90	22.16
Conductor 4	213.30	382.20	370.70	22.26
Conductor 5	202.10	406.70	359.20	22.28
Conductor 6	188.00	421.00	339.00	22.31

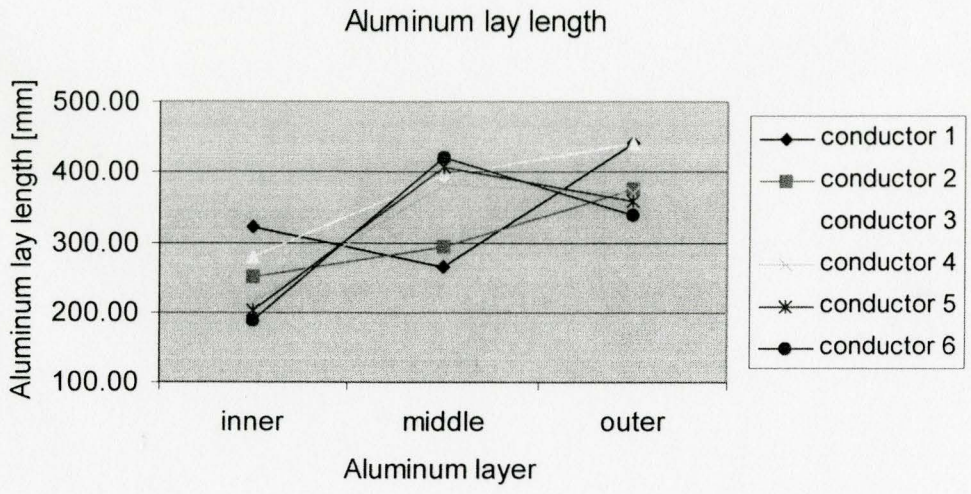

Figure 5.5 Changed lay lengths with fixed wire diameters

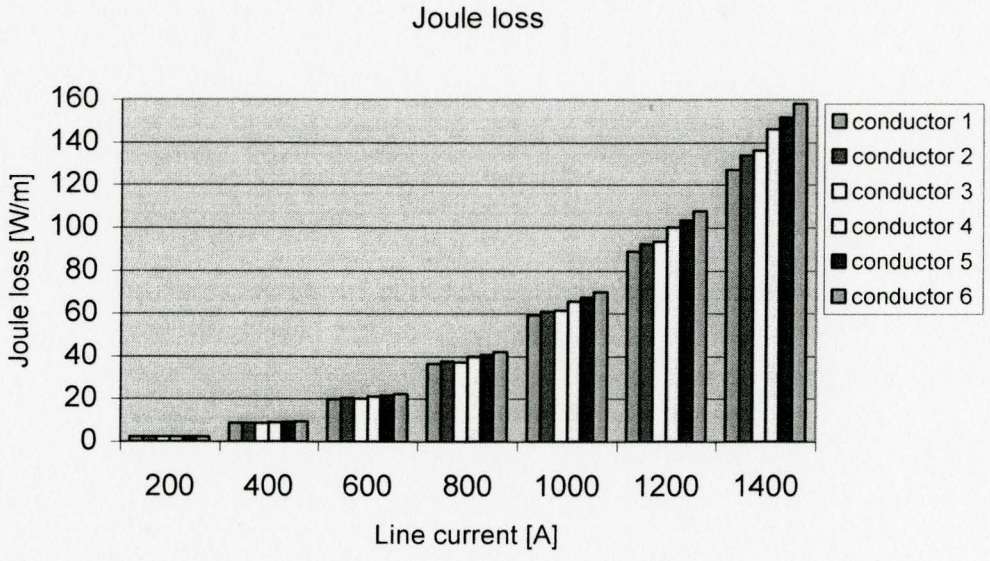

Figure 5.6 Variation of Joule losses in six conductors at various line currents

Note in each case that conductor one has losses either equal to or less than the other conductors for all values of currents. As the current increases, the variation between conductor one and the other conductors also increases.

Table 5.14 Joule losses at 1000A

Line current [A]	Conductor 1 [W/m]	Conductor 2 [W/m]	Conductor 3 [W/m]	Conductor 4 [W/m]	Conductor 5 [W/m]	Conductor 6 [W/m]
1000 A	59.01	60.89	61.17	65.42	67.48	70.01

Loss between conductor 1 and conductor 6 is 11W/m in 1000 A.

There are six samples. Five conductors are obtained from random selection; the second one comes from Zhang's thesis [16]. From the point of view of reducing Joule loss, the following properties of these six conductors are compared. The Joule losses are shown in table 5.14 when the total current is 1000A. The least loss conductor has 1.88 W/m loss less than that for Grackle. The loss variation range of changing aluminum lay length is 59.01 to 70.01 W/m.

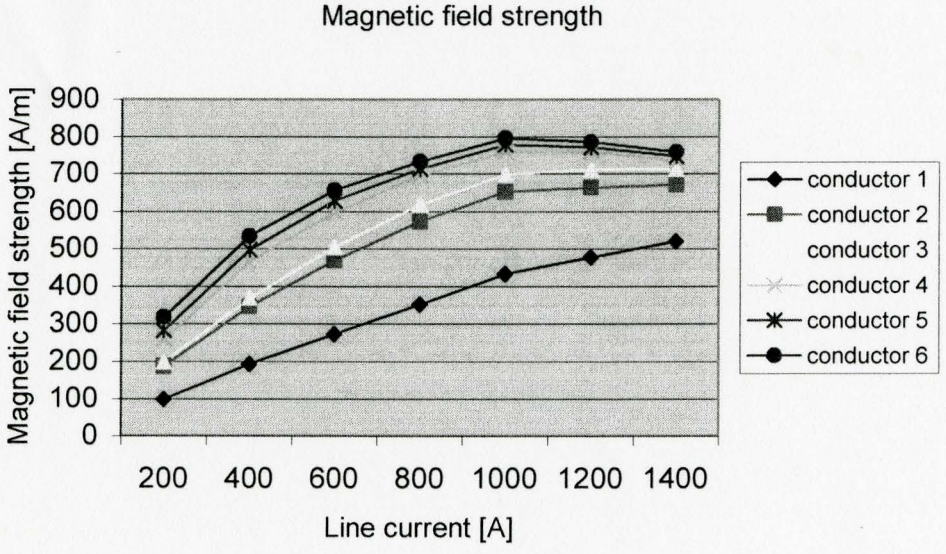

Figure 5.7 Variation of six-conductor magnetic field strength at various line currents

The critical point is 1000 A due to field saturation. In conductor 1 with the least loss, magnetic strength is almost linear. In conductors 4, 5 and 6, it reaches saturation at about 1000 A. Conductors 2 and 3 have not quite reached saturation by 1400A.

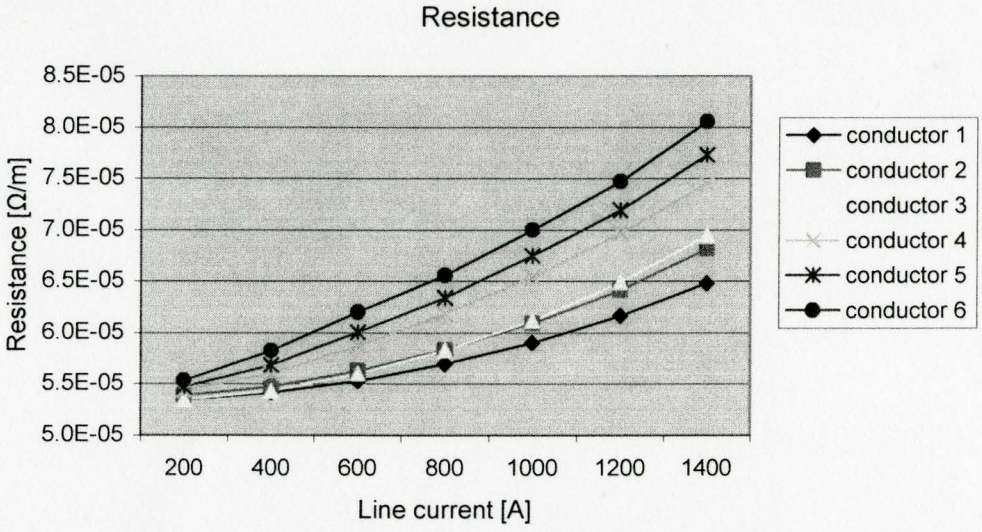

Figure 5.8 Variation of resistance in six conductors at various line currents

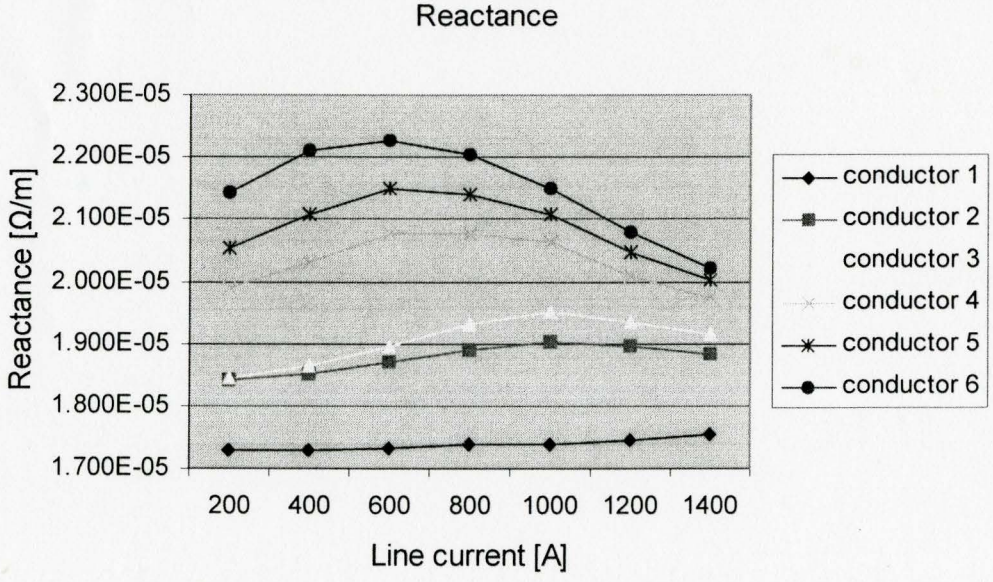

Figure 5.9 Variation of reactance in six conductors at various line currents

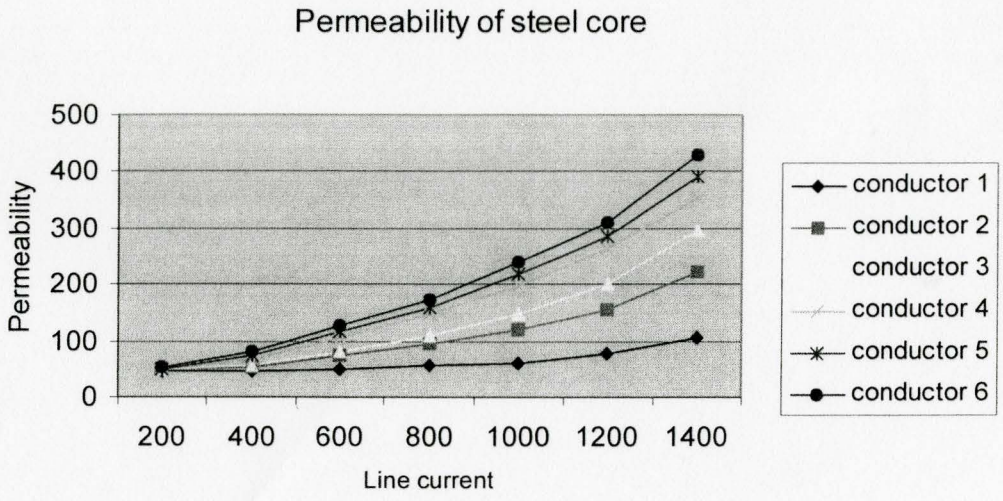

Figure 5.10 Variation of the permeability at various line currents

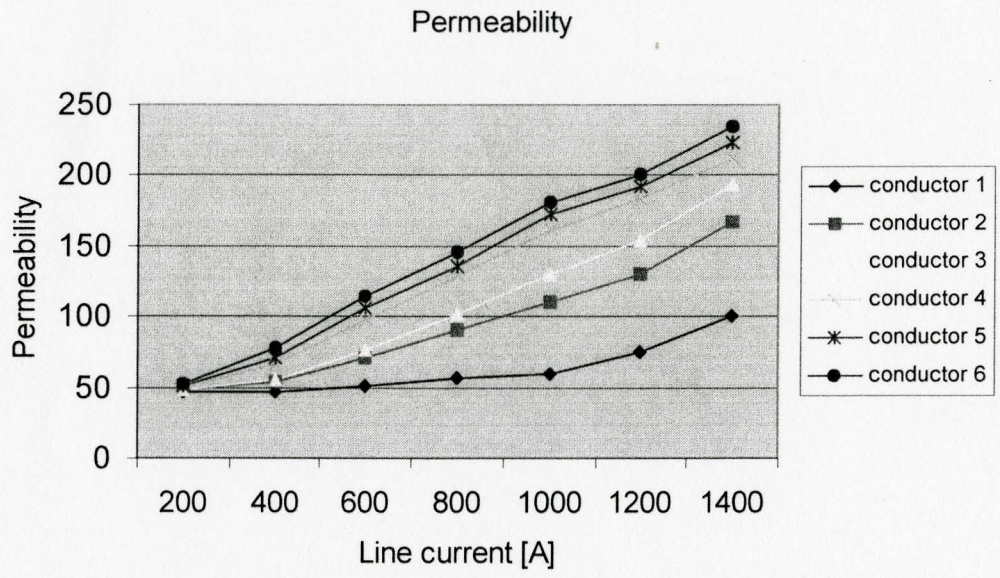

Figure 5.11 Variation of real part of the permeability at various line currents

Resistances increase with Joule loss and operating current. Reactance varies nonlinearly. In conductor 1, which does not reach saturation, the reactance continues to increase over the operating range. In conductors 2 and 3 the reactance decreases after 1000 A, and begins to decrease after 600 A in conductors 4 to 6.

Losses increase as permeability increases. In addition, differences among the conductors increase when the current increases.

The following figures show that currents in the steel core and aluminum middle layer increase when conductor losses rise. At the same time, current changes in the aluminum inner and outer layers are opposite to the middle layer current change. The outer layer of conductor 1 brings proportionally more current than that of any other conductors. The currents of each aluminum layer in conductor 1 change more than that in other conductors. When the current is above 800A, the differences among the conductors are more apparent.

The steel core currents increase when the loss increases. Aluminum current distributions among the layers in these six conductors vary with transformer effect produced by the steel core. In conductors 1 to 3, currents increase from inner layer to outer layer. From conductor 4, the current in the middle layer gradually overtakes the outer layer current for some operating currents. From conductor 4 to conductor 6, the middle layer current carries proportionately more of total current.

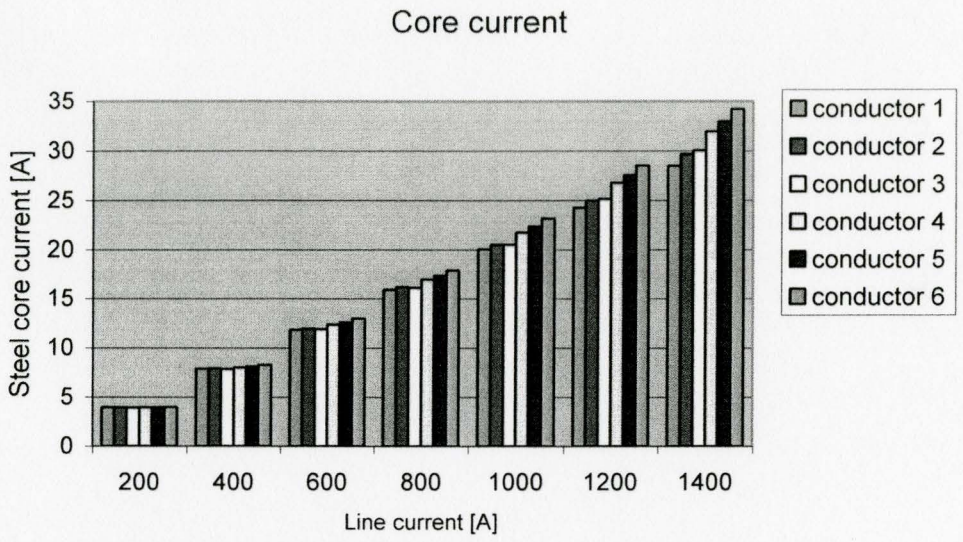

Figure5.12 Variation of steel core current at various line currents

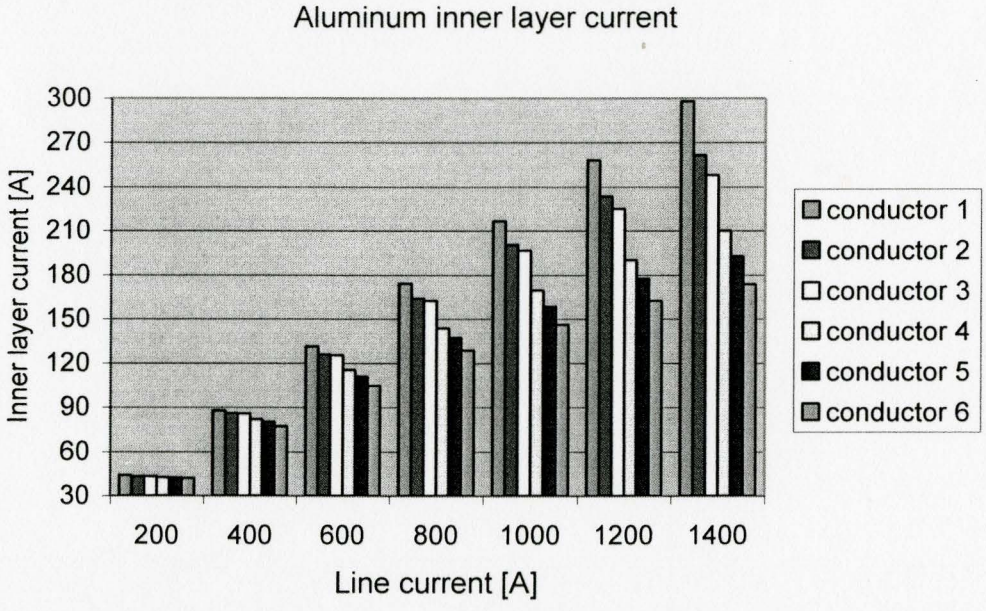

Figure 5.13 Variation of aluminum inner layer current at various line currents

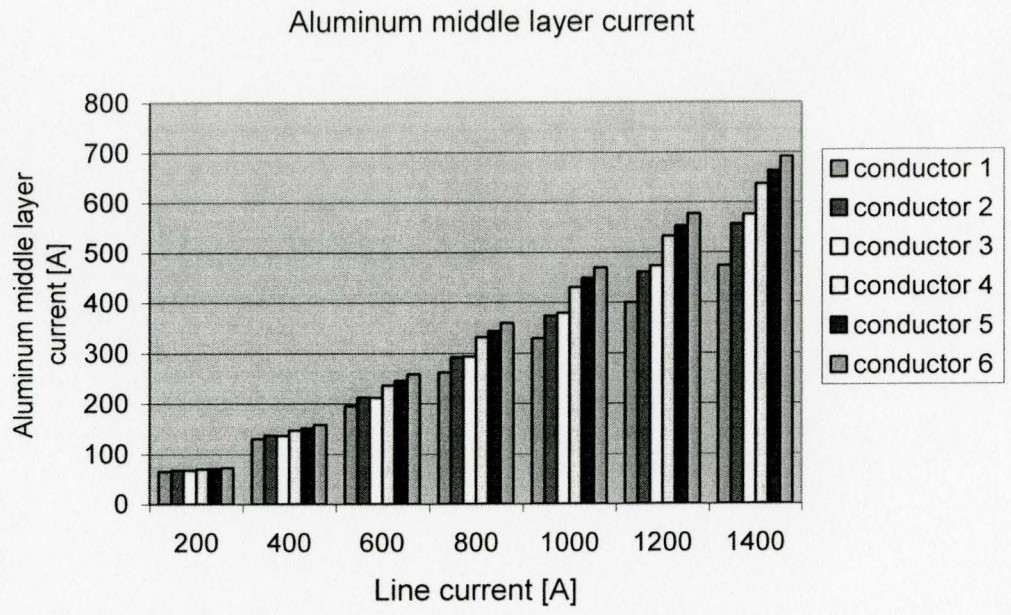

Figure 5.14 Variation of aluminum middle layer current at various line currents

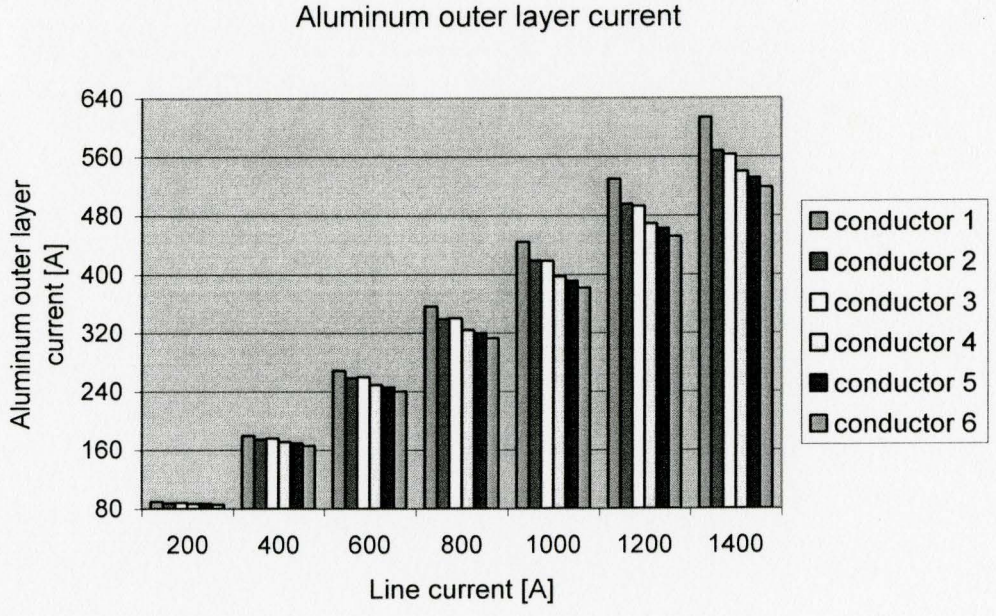

Figure 5.15 Variation of aluminum outer layer current at various line currents

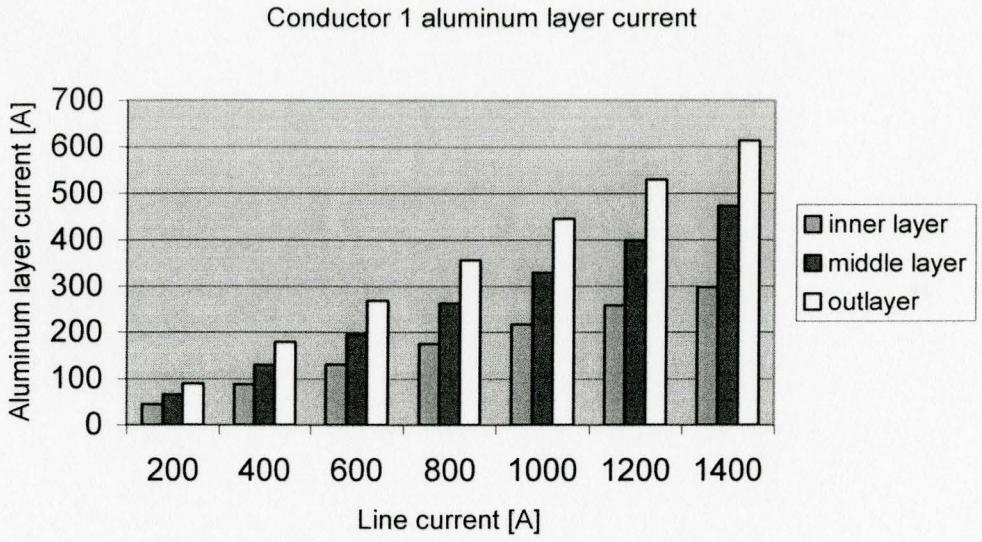

Figure 5.16 Variation of three aluminum layer currents in conductor 1 at various line currents

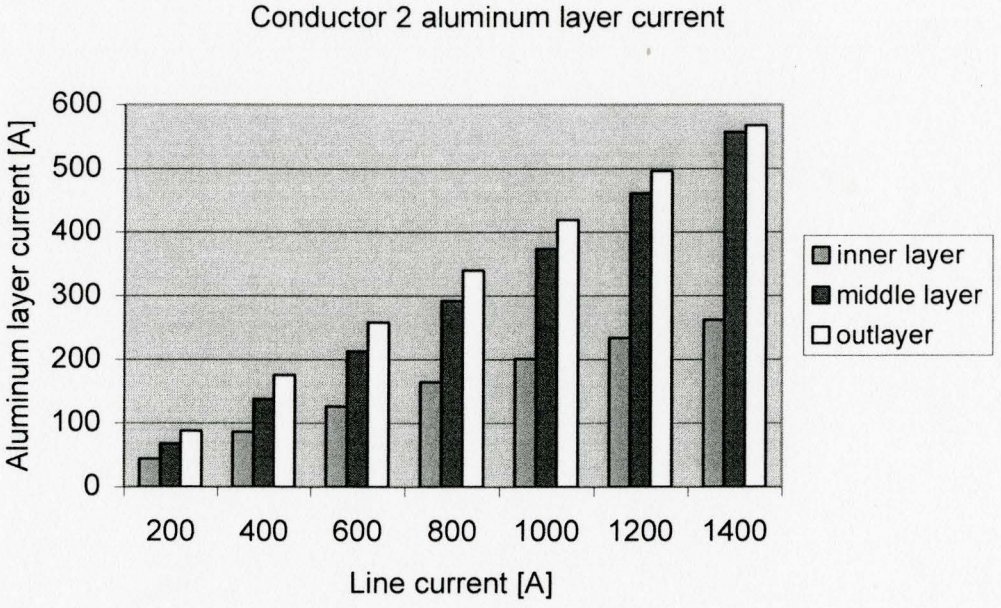

Figure 5.17 Variation of aluminum layer currents in conductor 2 at various line currents

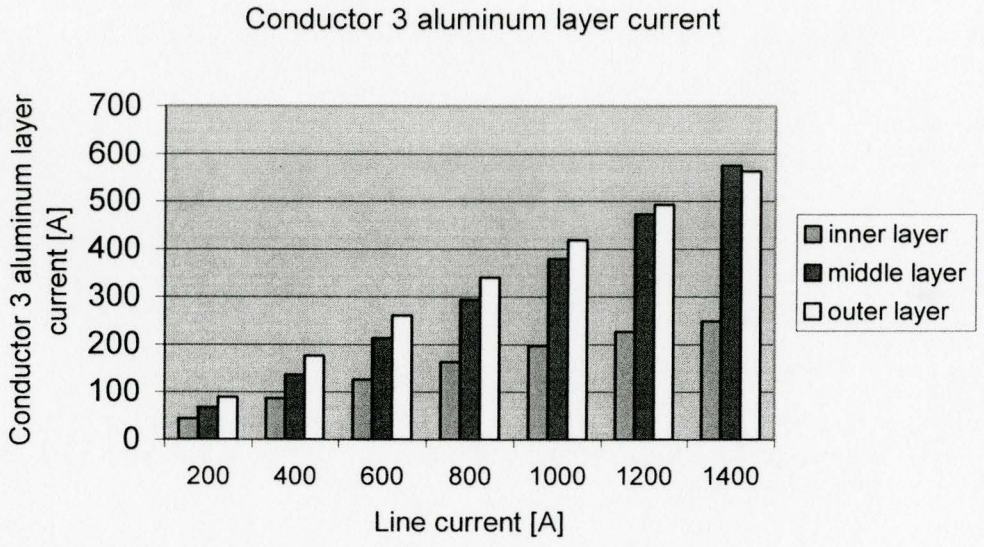

Figure 5.18 Variation of aluminum layer currents in conductor 3 at various line currents

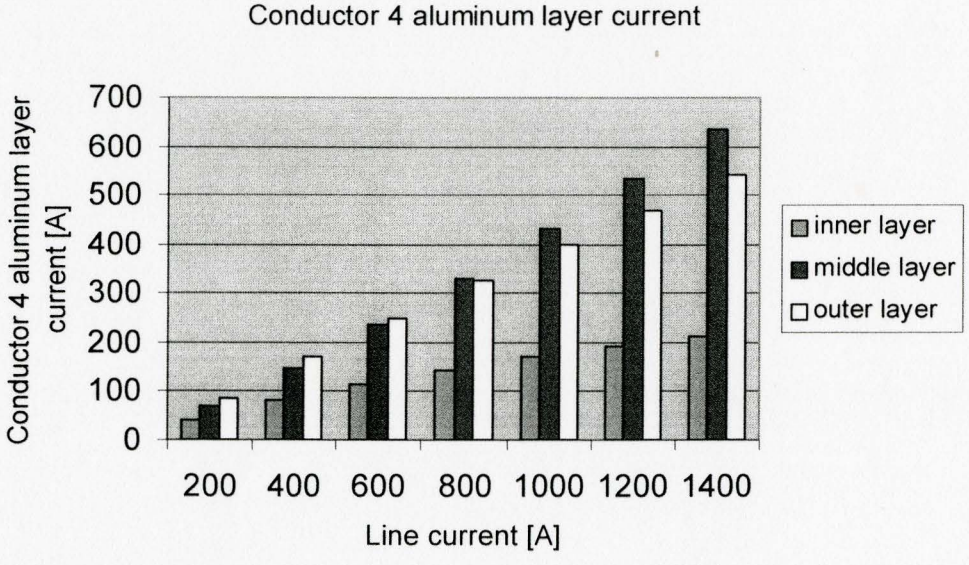

Figure 5.19 Variation of aluminum layer currents in conductor 4 at various line currents

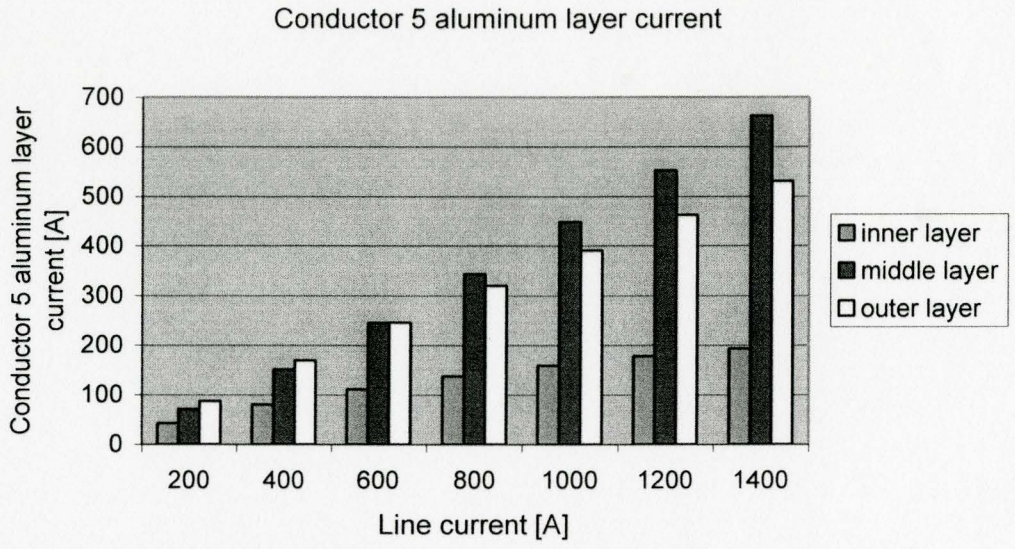

Figure 5.20 Variation of aluminum layer currents in conductor 5 at various line currents

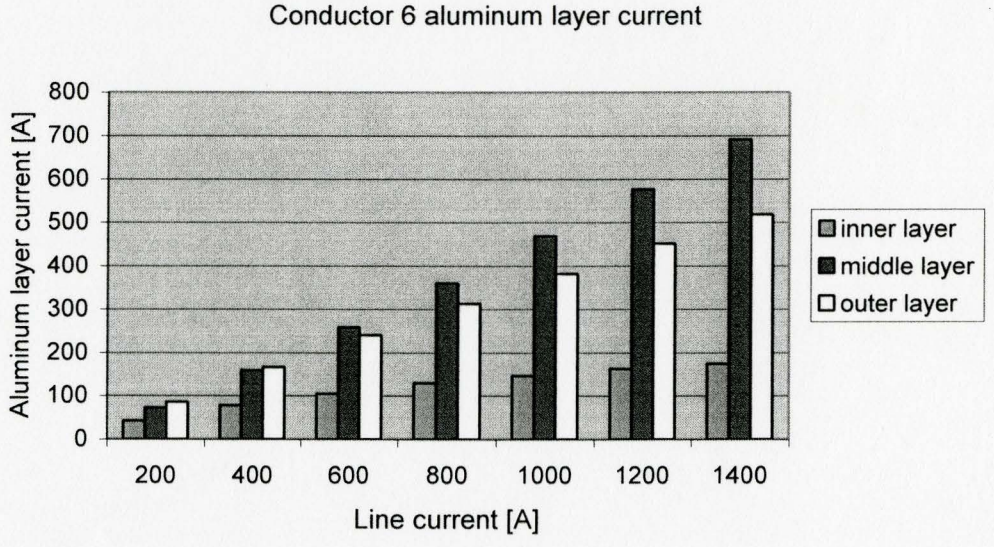

Figure 5.21 Variation of aluminum layer currents in conductor 6 at various line currents

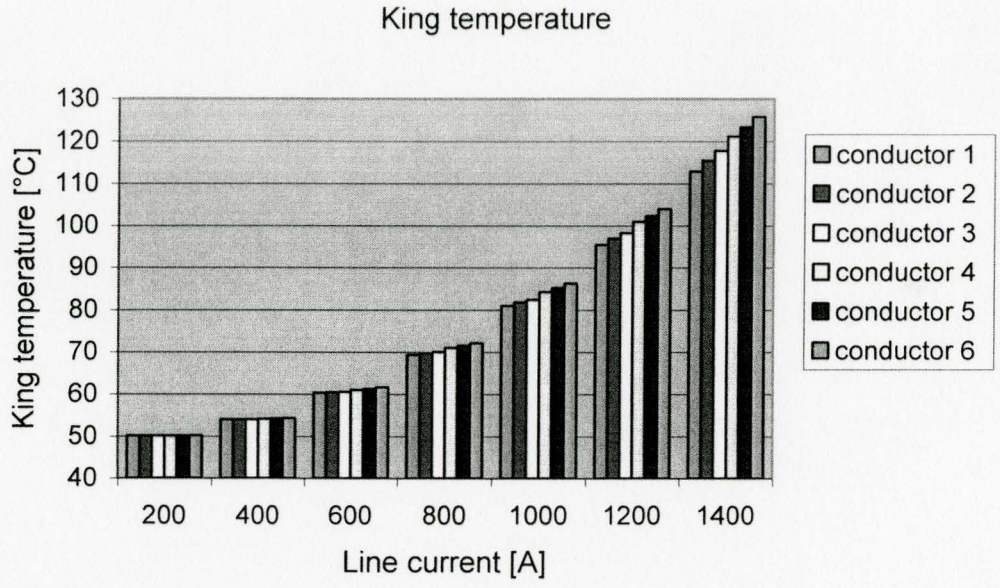

Figure 5.22 Variation of steel king layer temperature at various line currents

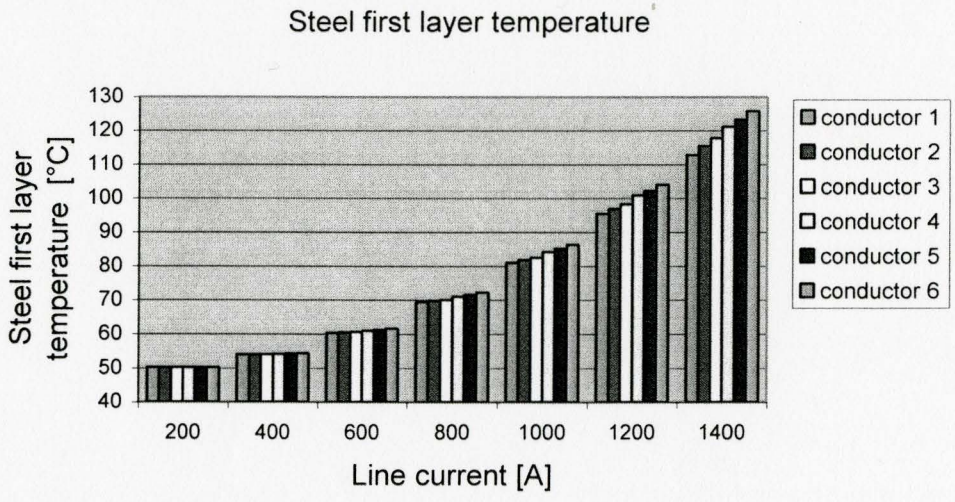

Figure 5.23 Variation of steel first layer temperature at various line currents

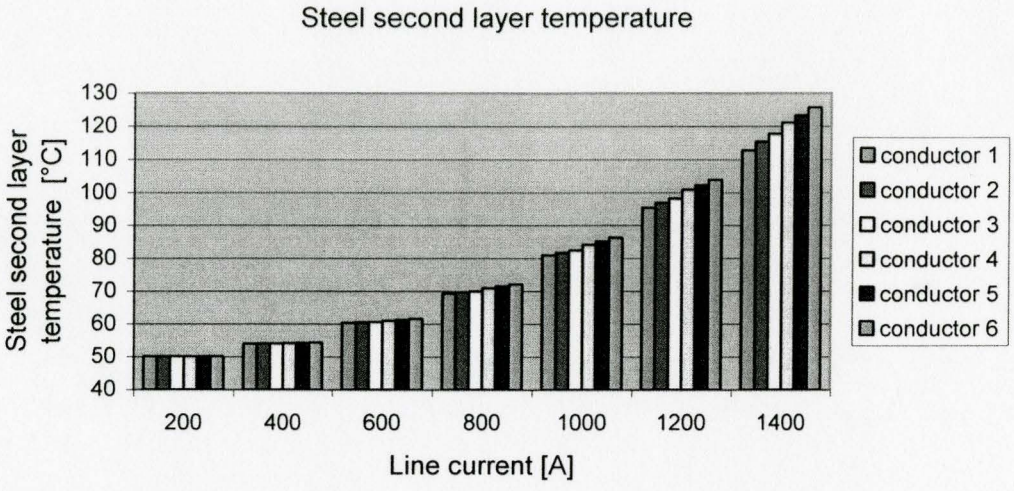

Figure 5.24 Variation of steel second layer temperature at various line currents

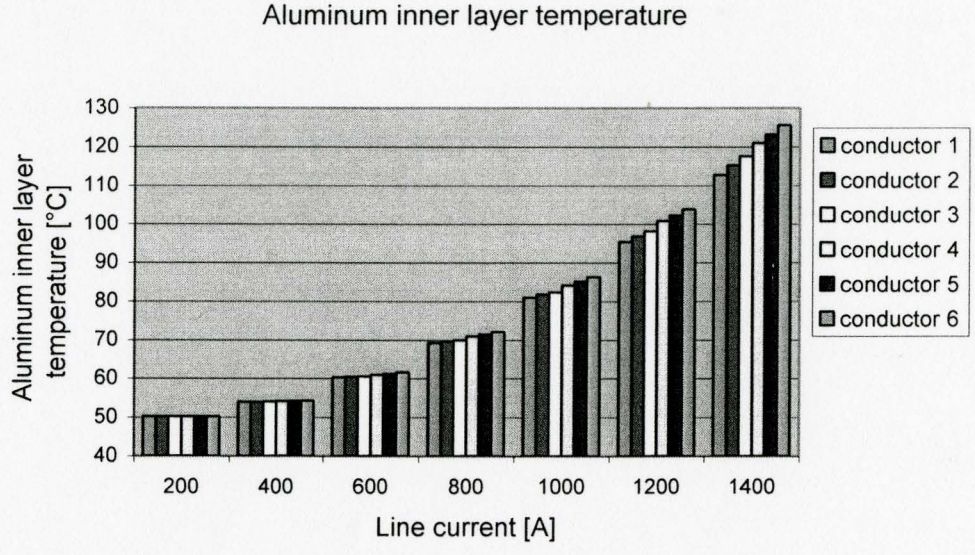

Figure 5.25 Variation of aluminum inner layer temperature at various line currents

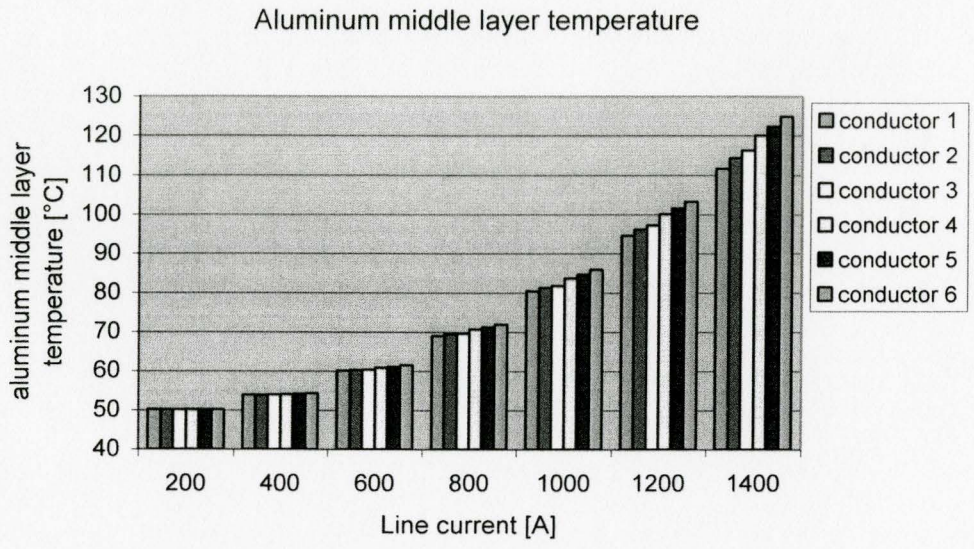

Figure 5.26 Variation of aluminum middle layer temperature at various line currents

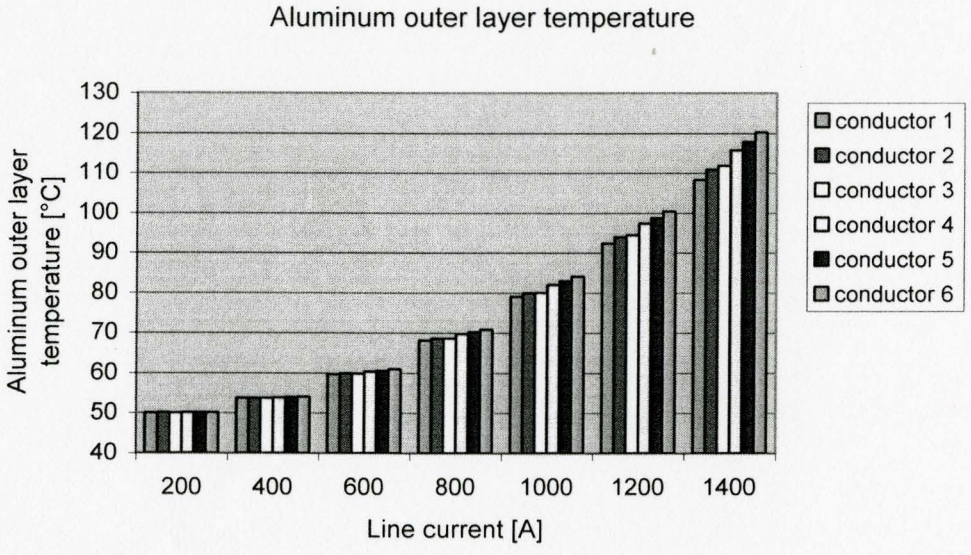

Figure 5.27 Variation of aluminum outer layer temperature at various line currents

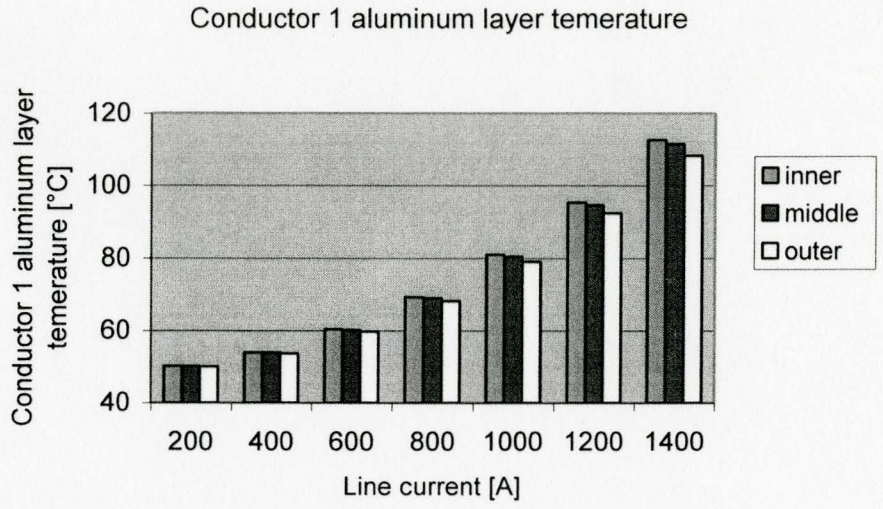

Figure 5.28 Variation of aluminum layer temperature in conductor 1 at various line currents

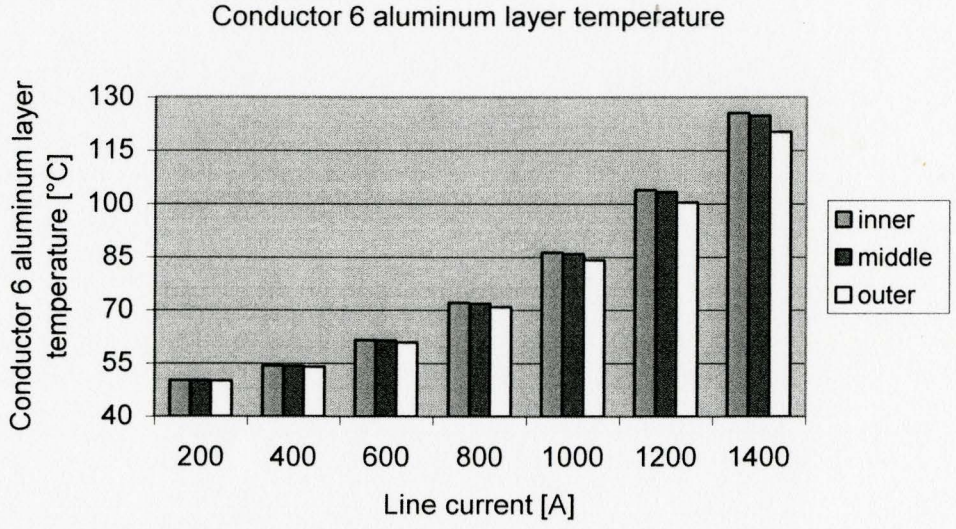

Figure 5.29 Variation of aluminum layer temperature in conductor 6 at various line currents

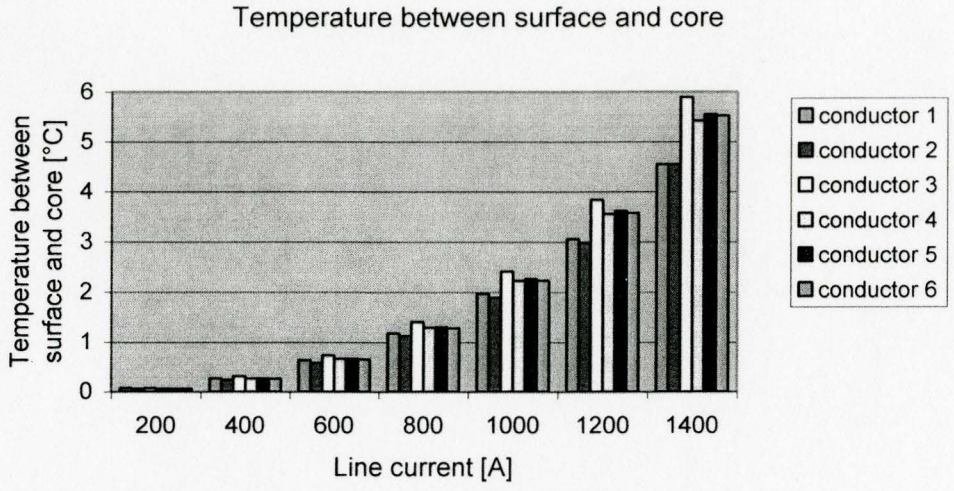

Figure5.30 Temperature differences between steel core and conductor surface

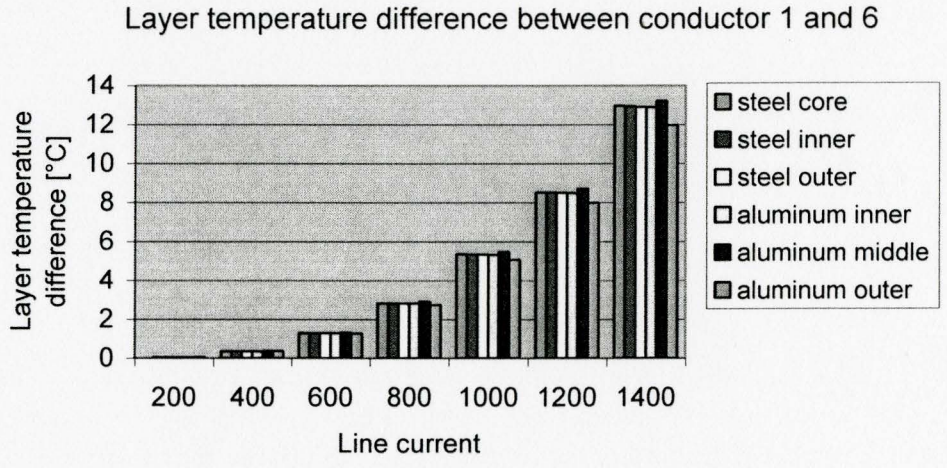

Figure 5.31 Layer temperature differences in layers between conductor 1 and 6

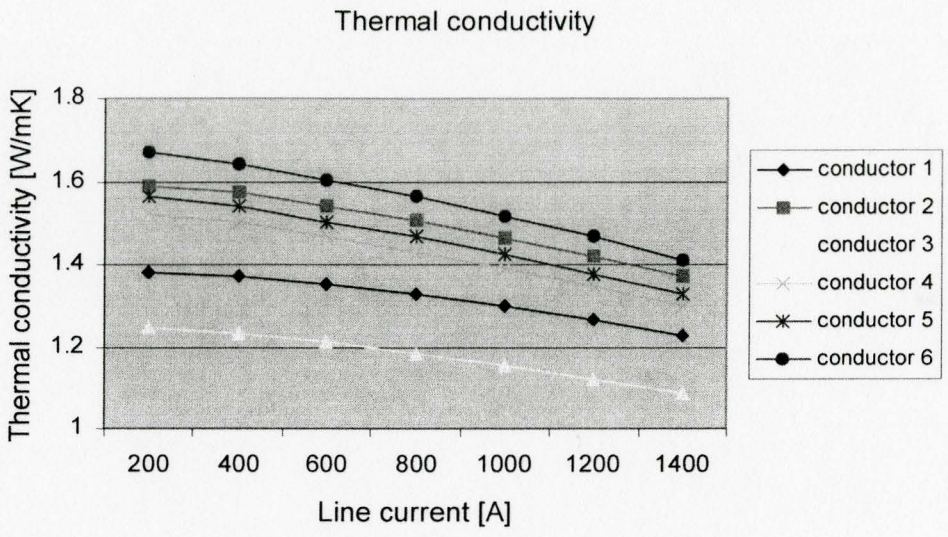

Figure 5.32 Variation of thermal conductivity at various line currents

Temperatures in all layers reduce from the inside to the outside of conductors. They increase from one conductor to the next one with the increase of Joule loss. The differences between conductor 1 and conductor 6 are shown in figure 5.31. The aluminum middle lay temperature changes are more significant than that of other layers. Conductor 2 has the smallest temperature changes between conductor core and surface. The temperature differences from core to surface in conductor 3 are biggest and reach 5.89 °C at 1400 A.

The thermal conductivity of conductor 3 is lowest. In conductors 1, 4, 5, and 6, it increases with an increase of the Joule loss. The value in conductor 2 is between the values for conductors 5 and 6. The thermal conductivity decreases as the operating current increases.

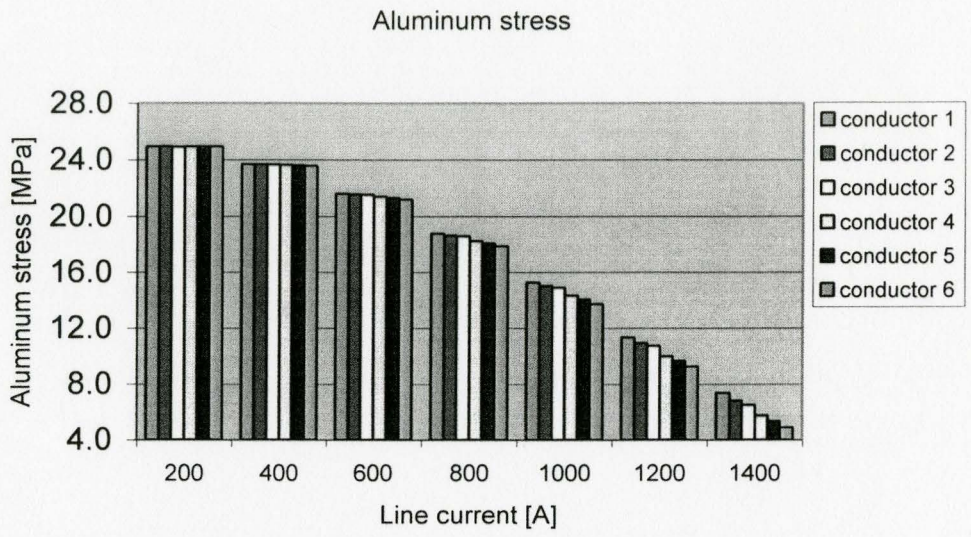

Figure 5.33 Variation of aluminum stresses at various line currents

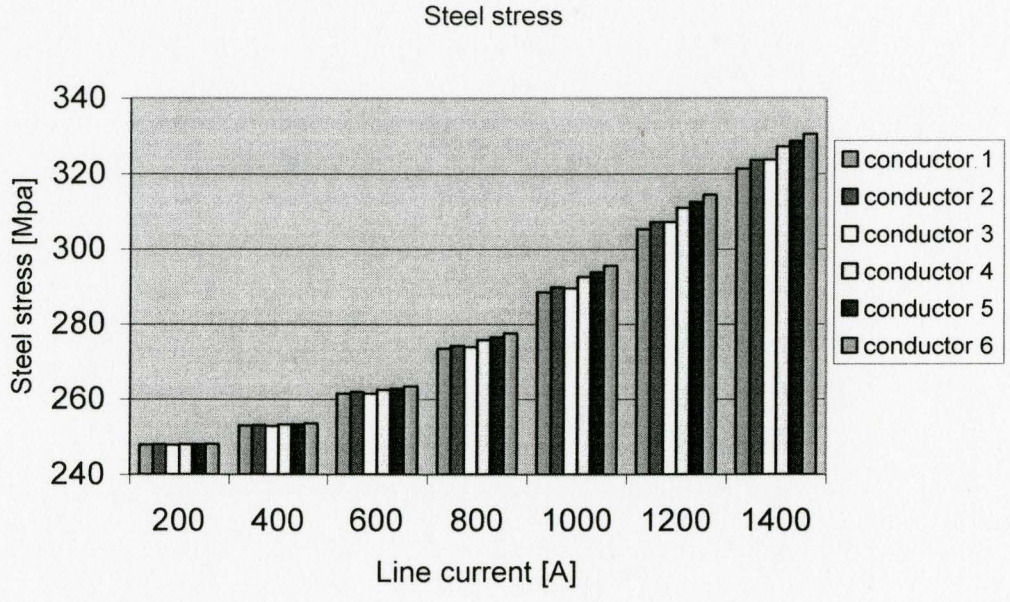

Figure 5.34 Variation of steel stresses at various line currents

The steel stress in conductor 3 is smaller than that of conductor 2 below 1400A. Steel stresses increase with the increase of the loss, while aluminum stresses change in the opposite direction except of that of conductor 3 compared to conductor 2.

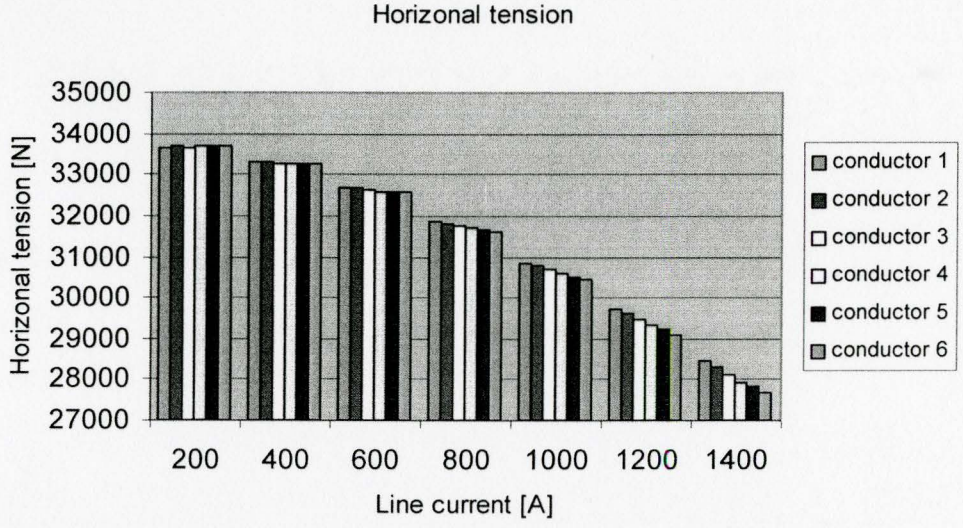

Figure 5.35 variation of horizontal tension at various line currents

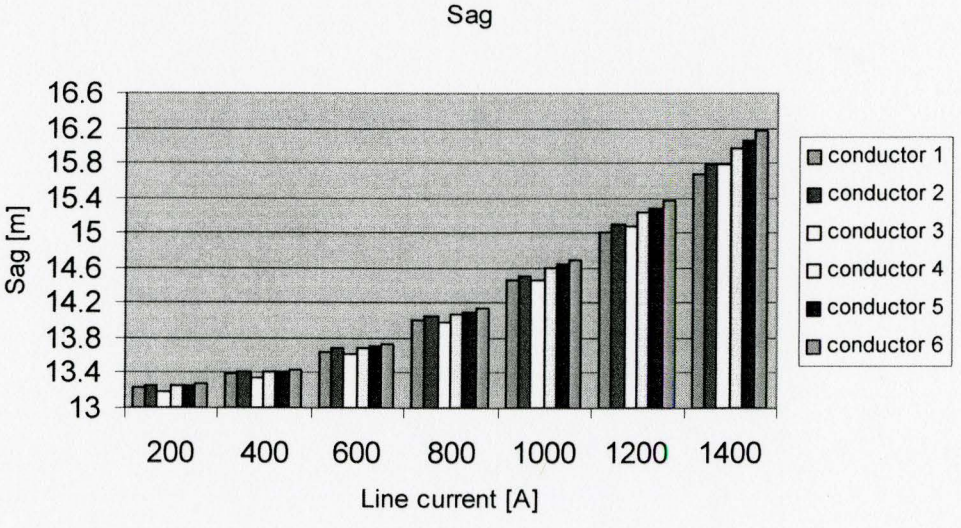

Figure 5.36 Variation of sags at various line currents with line length 400 meters

The horizontal tensions at the low current vary very little among all conductors. With the current increase, tensions fall down from conductor 1 to conductor 6 apparently.

The sag of conductor 3 is smaller than that of conductor 2, whereas the whole trend is that sags get bigger as Joule losses increase. At high operating current, the phenomenon is more apparent.

5.3.2 Fixing Wire Diameters, Changing Steel and Aluminum Lay Lengths

This experiment is to change all layer lengths including steel and aluminum layers. It is assumed that steel lay length can be altered. The transformer effect that the steel core produces can change the magnetic field of the conductor. Hence, to change steel lay lengths within a small variation can reduce the losses as well without substantially affecting the tension of a line.

Table 5.15 gives wire sizes of the conductor. The lay lengths of steel layers 1 and 2 are supposed to vary within [179,268.6] mm and [120.9,201.4] mm shown in table 5.5. The lay length ranges of aluminum layers are the same as case 1. The results can be used to compare with those of 5.3.1. The lay lengths are sorted by the losses in table 5.16. Within the steel and aluminum lay length variation ranges, six cables are selected.

Table 5.15 Unchanged steel wire and aluminum wire diameters

Steel wire diameter [mm]			Aluminum wire diameter [mm]		
King	Steel lay 1	Steel lay 2	Inner	Middle	Outer
2.238	2.238	2.238	3.784	3.784	3.784
Steel layer's outer diameters [mm]			Aluminum layer's outer diameters [mm]		
Steel lay 1	Steel lay 2	Steel lay 3	Inner	Middle	Outer
2.238	6.714	11.190	18.758	26.326	33.894

Table 5.16 Changed steel and aluminum lay lengths

Steel lay length [mm]			Aluminum lay length [mm]		
	Steel lay 1	Steel lay 2	Inner	Middle	Outer
Conductor 1	201.4	268.6	321	264	440
Conductor 2	141.3	181.8	294.1	292.6	364.6
Conductor 3	196.7	246.9	270.2	350.2	380.8
Conductor 4	194.3	253.3	244	375.8	353.5
Conductor 5	185.7	190.2	243.6	403.4	354.6
Conductor 6	120.9	179	188	421	339
Weight [N/m]					
Conductor 1	Conductor 2	Conductor 3	Conductor 4	Conductor 5	Conductor 6
22.22	22.3	22.22	22.25	22.25	22.32

The results are deduced from the physical limitations of the conductor performance and the variations of lay lengths. The aluminum middle layer lengths increase with an increase of line losses. Although other lay lengths sometimes do not change linearly in one direction, they decrease with an increase of power losses, especially that of inner layers. This can be seen from figure 5.37.

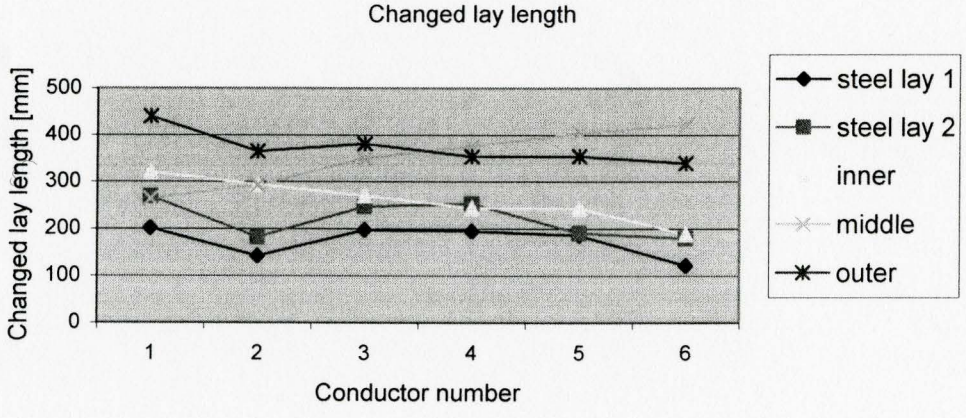

Figure 5.37 Variation of lay length for different conductors at 1000 A

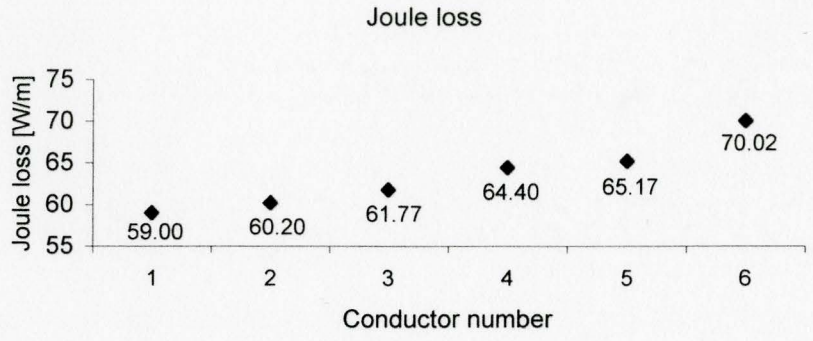

Figure 5.38 Variation of Joule losses for different conductors at 1000A

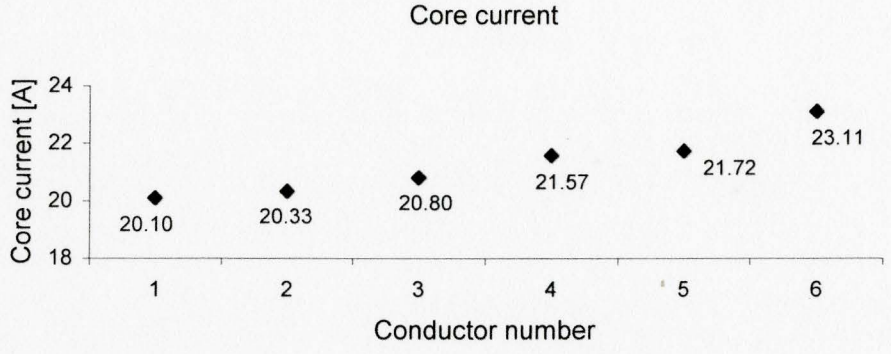

Figure 5.39 Variation of core current for different conductors at 1000A

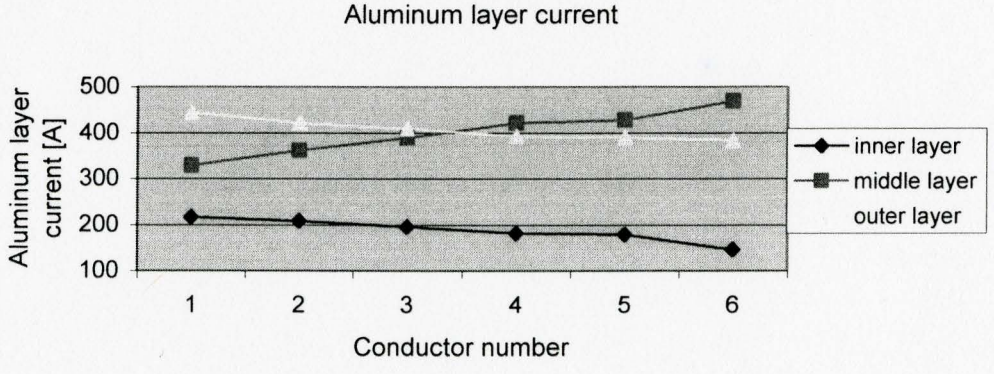

Figure 5.40 Variation of aluminum current for different conductors at 1000A

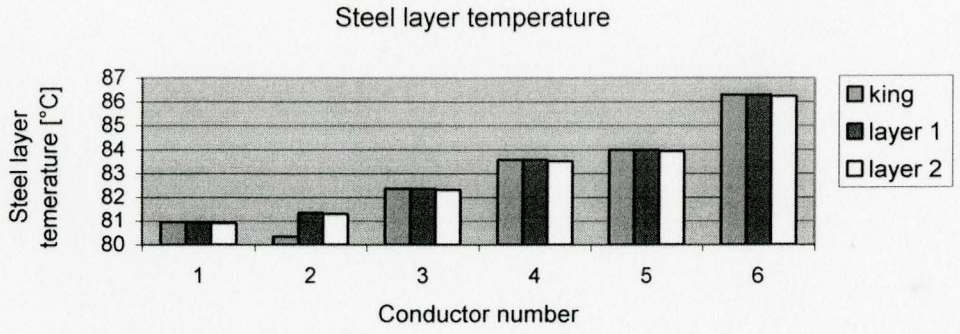

Figure 5.41 Variation of steel layer temperature for different conductors at 1000A

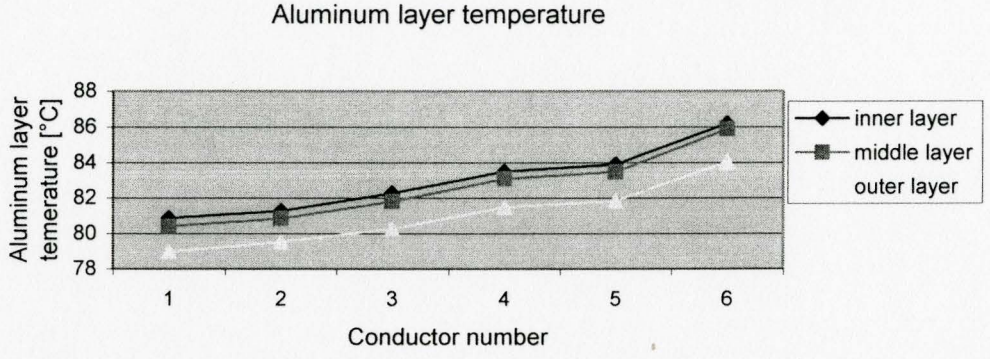

Figure 5.42 Variation of aluminum layer temperature for different conductors at 1000A

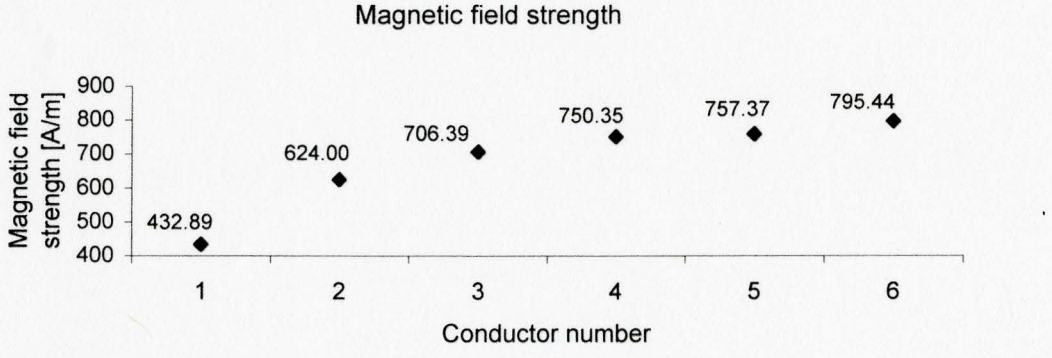

Figure 5.43 Variation of magnetic field strength for different conductors at 1000A

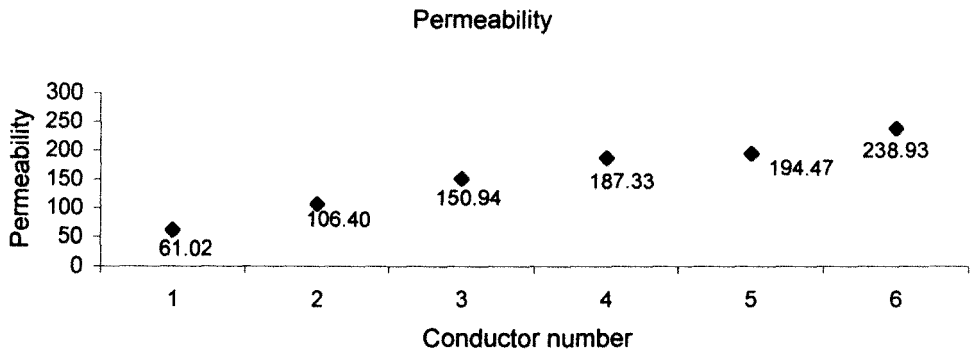

Figure 5.44 Variation of permeability for different conductors in 1000A

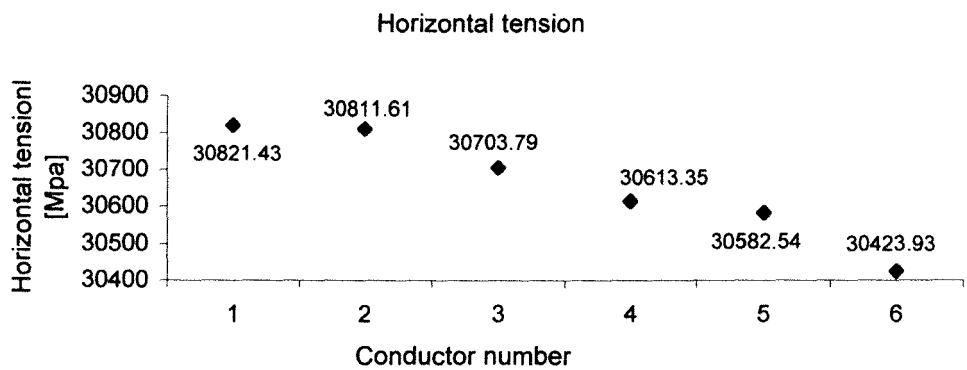

Figure 5.45 Variation of horizontal tension for different conductors at 1000A

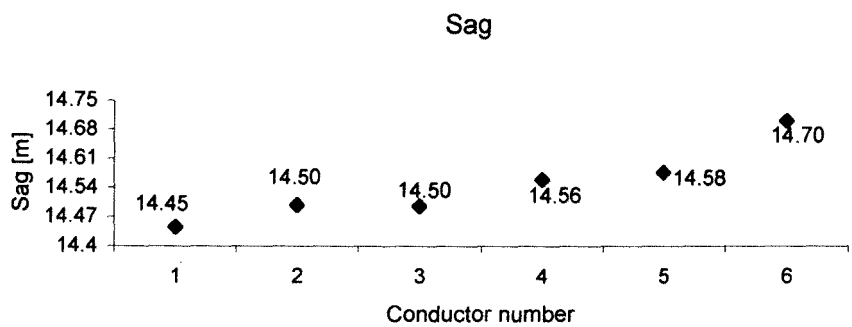

Figure 5.46 Variation of sags for different conductors at 1000A

The minimal and maximal losses are almost the same as achieved by only altering the aluminum lay length, since the steel lay lengths are varied over a very small range. Although lay lengths are randomly combined, steel inner layer lengths are always lower than those of the external layers. Variation trends of aluminum lay lengths are equal to the trends resulting from only changing aluminum lay length. Hence, changing steel lay lengths does not apparently affect conductor performance, but can be used as an option in the design of the low loss conductors.

5.3.3 Fixing Steel Core Size, Changing Aluminum Lay Lengths and Wire Diameters

Table 5.17 Changed aluminum wire and layer parameters

	Wire diameter [mm]			Aluminum lay length [mm]		
	Inner	Middle	Outer	Inner	Middle	Outer
Conductor 1	3.800	3.800	3.800	321.00	264.00	440.00
Conductor 2	3.784	3.784	3.784	251.41	294.30	375.50
Conductor 3	3.569	3.685	3.653	244.00	264.90	381.70
Conductor 4	3.681	3.528	3.506	219.30	305.40	348.80
Conductor 5	3.538	3.661	3.555	192.70	410.20	339.70
Conductor 6	3.500	3.500	3.500	188.00	421.00	339.00
	Outer diameter [mm]					
	Inner	Middle	Outer	Weight [N/m]		
Conductor 1	18.790	26.390	33.990	22.39		
Conductor 2	18.758	26.326	33.894	22.29		
Conductor 3	18.327	25.698	33.004	21.12		
Conductor 4	18.551	25.607	32.620	20.35		
Conductor 5	18.266	25.589	32.700	20.61		
Conductor 6	18.190	25.190	32.190	19.89		

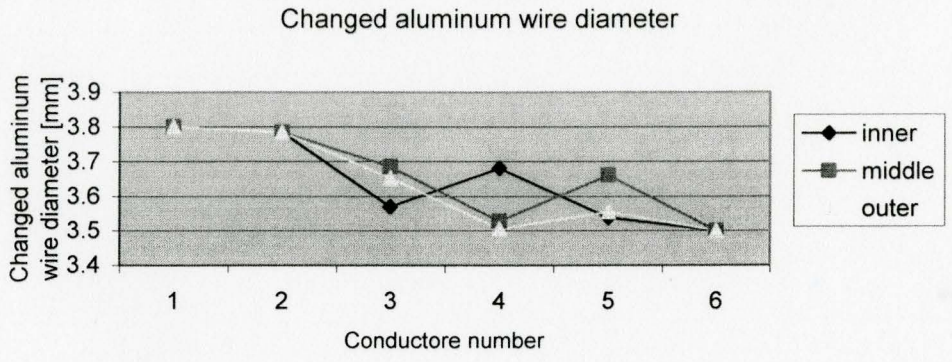

Figure 5.47 Changed aluminum diameters at 1000A

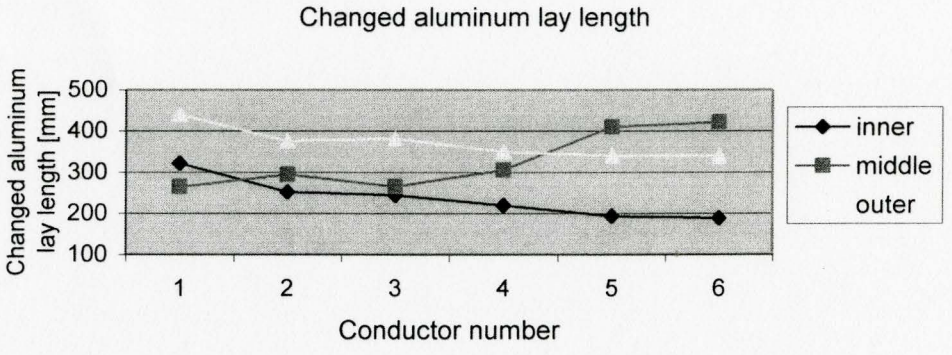

Figure 5.48 Changed aluminum lay lengths at 1000A

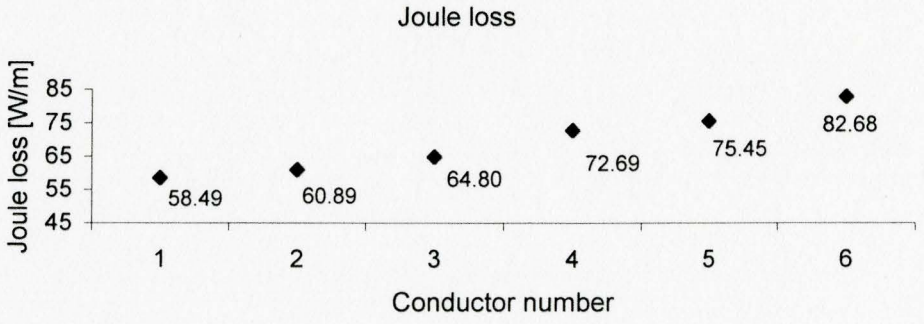

Figure 5.49 Variation of Joule losses among conductors at 1000A

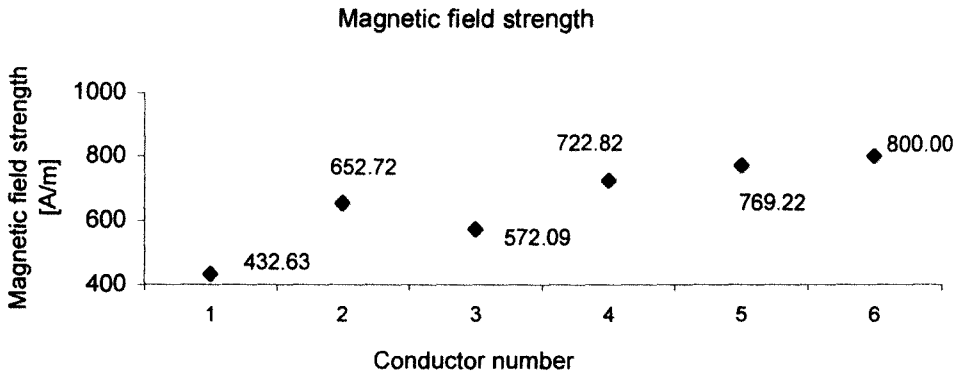

Figure 5.50 Variation of magnetic field strength among conductors at 1000A

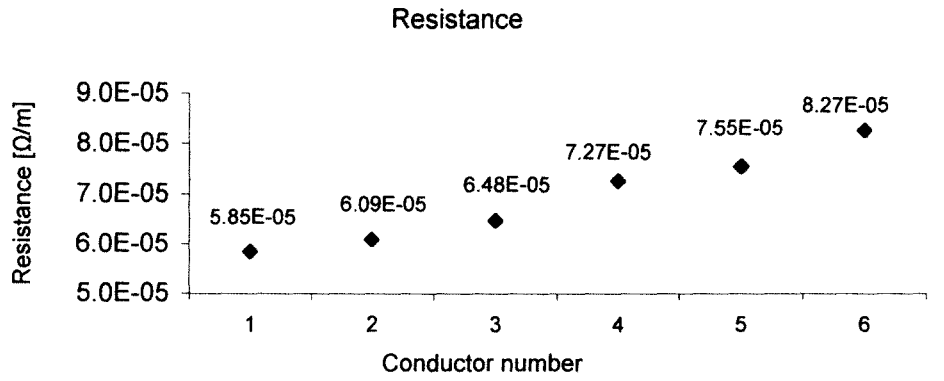

Figure 5.51 Variation of resistance among conductors at 1000A

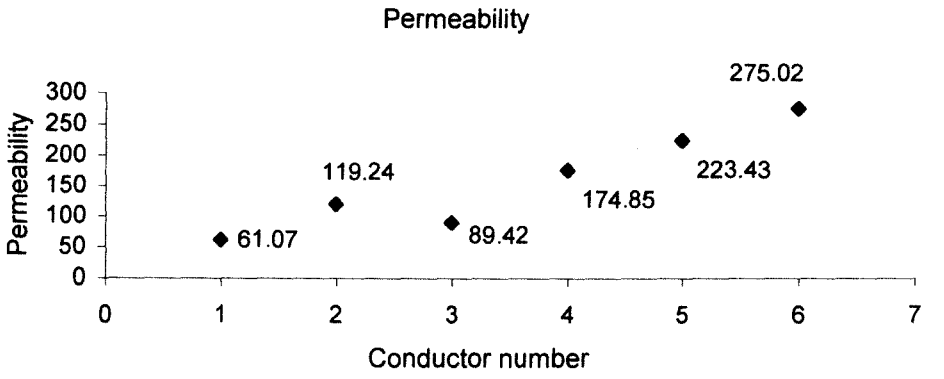

Figure 5.52 Variation of permeability among conductors at 1000A

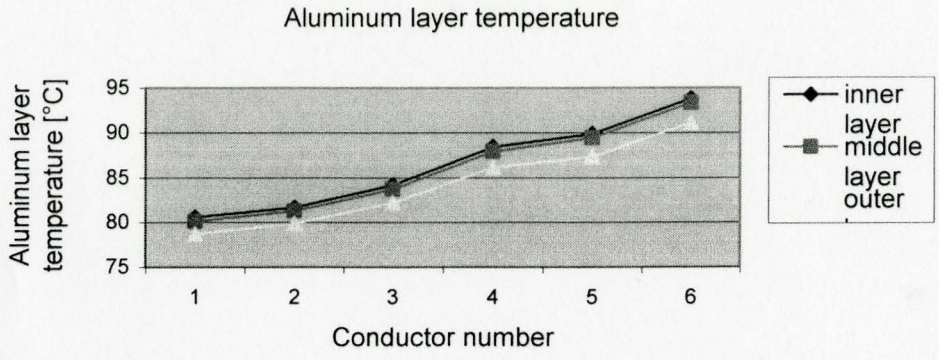

Figure 5.53 Variation of aluminum layer temperature among conductors at 1000A

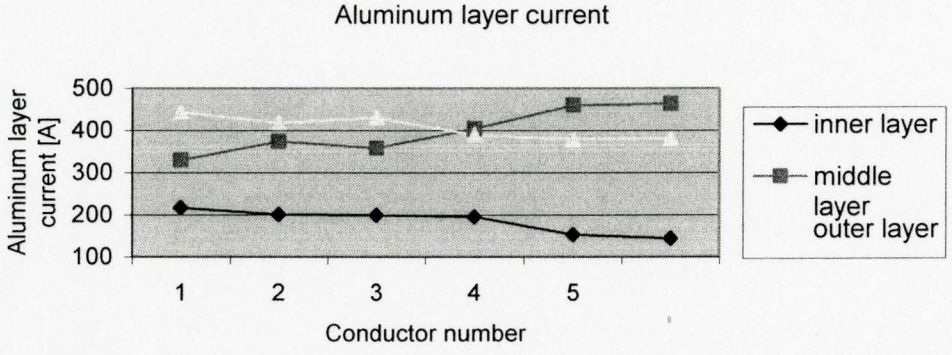

Figure 5.54 Variation of aluminum layer current among conductors at 1000A

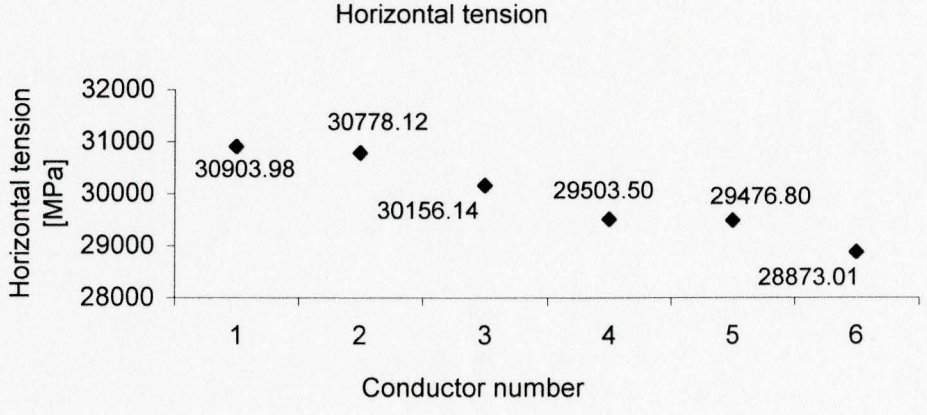

Figure 5.55 Variation of horizontal tension among conductors at 1000A

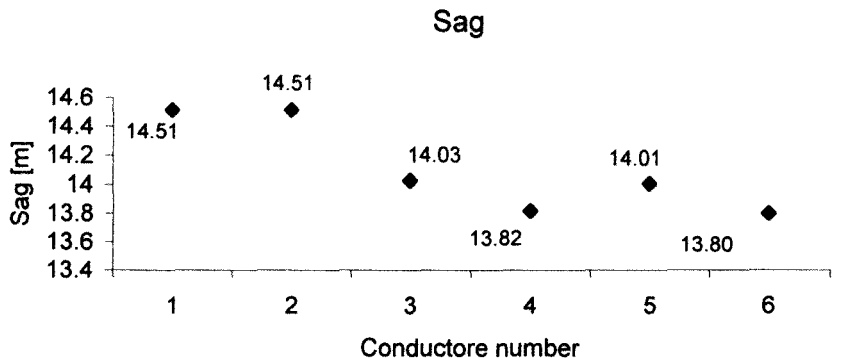

Figure 5.56 Variation of sags among conductors at 1000A

Changing aluminum wire diameters and lay lengths changes the loss from a minimum of 58.4914 W/m to a maximum of 82.6768 W/m. When the aluminum wire diameter is 3.8 mm, the middle layer lay length is lower than that of inner and outer layer and the conductor has minimum loss, but it is heavier. The magnetic field and aluminum layer temperatures increase with increasing loss. Currents of aluminum layers increase from the inside to the outer layer in low loss. From conductor 4 with loss 72.6873 W/m, the middle layer current begins higher than the current of the outer layer. The sag change is opposite to the previous situations in 5.3.1 and 5.3.2 since small wires reduce conductor weight.

CHAPTER 6

CONCLUSIONS

6.1 Conclusions for The Genetic Algorithm Application

This work was implemented to study the feasibility of applying Evolutionary Computation and in particular Genetic Algorithms to optimize the design of three layer ACSR using the unified model. This model combines the electromagnetic, mechanical, radial conduction, and thermal models. Through the analysis of Evolutionary Algorithms and from comparing their properties (in Chapter 2), Genetic Algorithms are implemented for the calculation of conductor geometrical parameters (in Chapter 4). The algorithm is global and includes the process of multi-parameter functions.

The results show that evolutionary algorithms can be used in the modules of the unified model. The evaluation is not a fitness function but a process applied to the modules. Therefore, the application is nonlinear. Inputs for the Genetic Algorithms are represented by vectors. The power loss is an objective fitness value. Search space is separated into two parts. One searches the near maximal losses and the other calculates the minimal values. The major contributions are:

1. The development of the process of applying Evolutionary Computation to the design of three layer ACSR.
2. Combining Genetic Algorithms with the unified model.
3. Analysis of ACSR using Genetic Algorithms and the Unified Model within the range of specifications indicated by ASTM Standards.

4. Finding the near optimum ACSR parameters in the unified model. The algorithm converges. The genetic operation parameters are selected by analyzing the problems at hand and they match the basic rules of the Genetic Algorithms.

For the different types of three-layer conductors:

1. The weights of three-layer ACSR increase gradually from Cardinal, Finch, Grackle, Pheasant, Martin to Plover. The Joule losses decrease with the increase of their weights. This indicates that the more materials used in the conductors, the more the losses are reduced.
2. The results show that the variation ranges of minimum and maximum losses when changing steel and aluminum lay lengths or just changing aluminum lay lengths according to ASTM standard are very similar. These losses are the electrical field limitation for three layer ACSR conductors.
3. Layer temperatures decrease with loss reduction amongst different types of conductors. The temperature differences from the core to the surface get smaller with loss decreases.
4. The sags increase with a decrease of Joule losses because of the increases of conductor weights for the different conductors. The horizontal tensions increase with the increases of conductor weights. The steel layer stresses, for example in Cardinal, are very low (under 1 Mpa in 1000A, 25 °C).
5. Core current is about 2% of the whole current. The aluminum outer layers carry the most current. The current distribution in the three aluminum layers in several

conductors, such as Finch, pheasant, Martin, and Plover are almost in the same proportion.

6. The maximum and minimum values of the losses, when changing wire diameters, are less than for changing both wire diameters and lay lengths.
7. The least loss conductor occurs when the length of the aluminum middle layer is shortest and other layer lengths are longest, except when calculating the maximum loss of changing all layer lengths of Finch conductor.
8. Thermal conductivity of the lowest loss conductor (conductor 1) is mostly below 1.4. There is no apparent saturation in the magnetic fields during 200A to 1400A in these conductors for the low-loss configurations.
9. Thermal conductivities slightly decrease with current increases.
10. The current distribution from low loss to high loss conductors shows that the currents in the aluminum middle layer increases and eventually gets larger than the current in the aluminum out layer, moving from the low-loss configuration to the high loss configuration.
11. When the unified model is used on the selected conductors, according to their losses, the variation trends are more linear in three steel layer conductors than that in two steel layer conductor for which the loss distribution becomes nonlinear as the core moves towards saturation.

For single three-layer conductor:

1. When the lay length of the middle layer is reduced in comparison with the outer layer, the transformer effects are low, so magnetic forces are low. Outer layer

currents are higher than the currents in the middle layers, where losses are lower. Layer temperatures rise at an increasing rate with an increase of power loss. Sag increases with the growth of power loss and current. Therefore, reducing power losses with changing lay lengths can increase thermal conductivity and decrease layer temperature and sag, thus improving the conductor performance.

2. The range of loss differences is larger than that of changing layer lengths when changing both aluminum lay lengths and wire diameters. The latter situation results in a larger variation of dc resistance compared to ac resistance. The conductor weight increases when the diameter increases. However, with good combination of the aluminum lay length and wire diameter, the weight variation can be kept small. Results show that some low loss conductors can be selected in this situation.
3. Through the application of Genetic Algorithms, the above random calculations generate some alterations for design options compared to the specified conductor size.

6.2 Future Work

This project gives the opportunity to use GAs in the unified model for calculation of conductor properties, and to check the robustness of the model. Positive results in this investigation ask for more application. Suggested further works are:

1. Expanding GA application in the unified model. Finding some other objective like tension or sag or alloy composition to optimize.

2. GAs can realize multi-objective optimization. Electrical, magnetic, thermal, mechanical properties can be calculated at once.
3. Results obtained in this project need to be verified by experiments.
4. GAs are not the only choice for applying evolutionary computation as any forms in Evolutionary Algorithms can be used. After using different evolutionary algorithms, it is possible to compare the efficiency of algorithms like calculation time, operator parameters, and calculation results.

Appendix A Input Parameters in The Unified Model

Type of conductor	Three-layer ACSR			
Number of layers	Steel layer		Aluminum layer	
	2 (excluding king)		3	
Number of wires in Layers	King	1	Inner	12
	Steel 1	6	Middle	18
	Steel 2	12	Outer	24

Conductor parameters

Specific density [kg/cm^3]	Steel	7.78E-03
	Aluminum	2.70E-03
Elasticity modulus [MPa]	Steel	190000.0
	Aluminum	55000.0
Linear expansion coefficient [°C^{-1}]	Steel	11.3E-6
	Aluminum	22.8E-6
Specific resistance at 20°C [Ω mm^2/m]	Steel	0.1775
	Aluminum	0.02818
Temperature coefficient of Resistance at 20°C [°C^{-1}]	Steel	0.0032
	Aluminum	0.00404
Air gap thickness [m]	Regular	0.000001
	Maximum	0.00001

Operation conditions

Frequency [Hz]		60
Tower parameters [m]	Span length	400
	Right tower height	30.0

	Left tower height	30.0
Running out conditions	Time	0.000114155
	Tension [N]	37288.0
	Temperature [°C]	20.0
Pretensioning conditions	Time [year]	0.000114155
	Tension [N]	0.0
	Temperature [°C]	0.0
String conditions	Time [year]	0.000114155
	Tension [N]	37288.0
	Temperature [°C]	20.0
Percentage loss of strength of aluminum in the fully annealed state [%]		56
Annealing constant	Aanncoeff	8.62
	Banncoeff	110
	Canncoeff	-5000
	Danncoeff	7.5
Percentage reduction in cross-section area during wire drawing [%]		90

Meteorological parameters

Ambient temperature [°C]	20
Standard deviation of ambient temperature [°C]	6.3
Wind speed [m/s]	0.6
Wind angle [degree]	0.0
Standard deviation of wind angle	15.0
Time duration of actual period	0.000057077
Stefan Boltzman constant [$Wm^{-2}K^{-4}$]	5.66997E-8

Gravity [ms^{-2}]	9.81
Actual clearance ratio	1
Day in a year	182
Azimuth [Degree]	0.0
Latitude [Degree]	44.0
Altitude [m]	0.0
Albedo	0.26
Absorptivity	0.9
Emissivity	0.95

Appendix B Results Using Genetic Algorithms in Three-layer Conductor Finch

B.1 Results of the application of the Genetic Algorithm

Table B.1 Standard in ASTM 232M

Ratio of lay length of a layer to nominal outside diameter of that lay									
Aluminum layer						Steel layer			
Outer		Middle		Inner		Outer		Inner	
Min	Max	Min	Max	Min	Max	Min	Max	Min	Max
10	13	10	16	10	17	16	24	18	30
Conversion of the lay length of Finch conductor [mm]									
328.3	426.8	255.3	408.5	182.4	310.1	175.1	262.7	118.2	197.0

Table B.2 Ranges of changed wire diameters and lay lengths

Steel diameter [mm]		Aluminum diameter [mm]	
Lower bound	Upper bound	Lower bound	Upper bound
2.189	2.189	3.5	3.8
Steel lay length [mm]		Aluminum lay length [mm]	
Layer 1		Inner layer	
Lower bound	Upper bound	Lower bound	Upper bound
118.2	197.0	182.4	310.1
Layer 2		Middle layer	
Lower bound	Upper bound	Lower bound	Upper bound
175.1	262.7	255.3	408.5
		Outer layer	
		Lower bound	Upper bound
		328.3	426.8

Table B.3 Min and max losses with changed aluminum lay lengths

Minimum Joule loss [W/m]		Weight [N/m]
63.9256		20.81
Aluminum lay length [mm]		
Inner	Middle	Outer
310.1	255.3	426.8
Maximum Joule loss [W/m]		Weight [N/m]
76.0349		20.88
Aluminum lay length [mm]		
Inner	Middle	Outer
182.4	408.5	328.3

Table B.4 Min and max losses with changed steel and aluminum lay lengths

Minimum Joule loss [W/m]				Weight [N/m]
63.9233				20.80
Layer length [mm]				
Steel lay 1	Steel lay 2	Al inner	Al middle	Al outer
197.0	262.7	310.1	255.3	426.8
Maximum Joule loss [W/m]				Weight [N/m]
76.0670				20.90
Layer length [mm]				
Steel lay 1	Steel lay 2	Al inner	Al middle	Al outer
119.0	177.0	182.0	408.0	328.0

Table B.5 Min and max losses with changed aluminum wire diameters and lay lengths

Minimum Joule loss [W/m]		Weight [N/m]
58.6575		22.14
Aluminum wire diameter [mm]		
Inner	Middle	Outer
3.8	3.8	3.8
Aluminum lay length [mm]		
Inner	Middle	Outer
310.1	255.3	426.8
Maximum Joule loss [W/m]		Weight [N/m]
83.0229		19.65
Aluminum wire diameter [mm]		
Inner	Middle	Outer
3.5	3.5	3.5
Aluminum lay length [mm]		
Inner	Middle	Outer
182.4	408.5	328.3

Table B.6 Min and max losses with changed aluminum wire diameters

Minimum Joule loss [W/m]		Weight [N/m]
61.2272		22.14
Aluminum diameter [mm]		
Inner	Middle	Outer
3.8	3.8	3.8
Maximum Joule loss [W/m]		Weight [N/m]
72.8515		19.59
Aluminum diameter [mm]		
Steel lay 1	Steel lay 2	Inner
3.5	3.5	3.5

Table B.7 Finch used as a reference

Aluminum lay length [mm]			Steel lay length [mm]	
Inner	Middle	Outer	Inner	Outer
273.634	331.983	361.152	164.211	218.948
Aluminum wire diameter [mm]			Steel wire diameter [mm]	
3.647			2.189	
Loss [W/m]		Weight [N/m]	Sag [m]	
66.7231		20.81	13.9437	

Table B.8 Low loss conductors

Results with changed aluminum lay lengths

Aluminum lay [mm]				Weight [N/m]	Loss [W/m]	Sag [m]
Number	Inner	Middle	Outer			
1	297.3	304.6	410.3	20.78	64.4444	13.8854
2	310.0	255.3	426.7	20.81	63.9275	13.8901

Results with changed aluminum lay lengths and wire diameters

Aluminum lay [mm]				Aluminum wire diameter [mm]		
Number	Outer	Middle	Outer	Inner	Middle	Outer
1	293.4	296.7	407.8	3.5225	3.6443	3.6239
2	259.5	272.9	400.6	3.5426	3.6065	3.6296
Number	Weight [N/m]	Loss [W/m]	Sag [m]			
1	20.46	65.6987	13.7620			
2	20.45	66.2837	13.7661			

Results with changed steel and aluminum lay lengths

Steel lay [mm]			Aluminum lay [mm]		
Number	Steel 1	Steel 2	Inner	Middle	Outer
1	157.6	258.7	251.0	356.0	421.8
2	196.7	262.1	310.0	255.3	426.7
Number	Weight [N/m]	Loss [W/m]	Sag [m]		
1	20.74	66.4223	13.9160		
2	20.80	63.9242	13.8854		

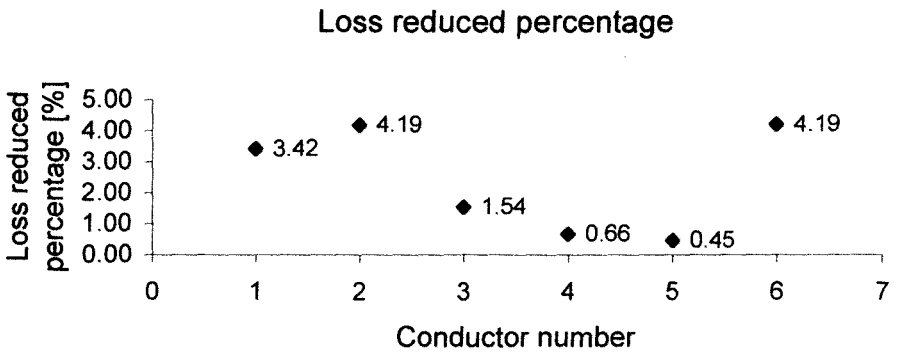

Figure B.1 Percentage of reduced loss compared to the reference

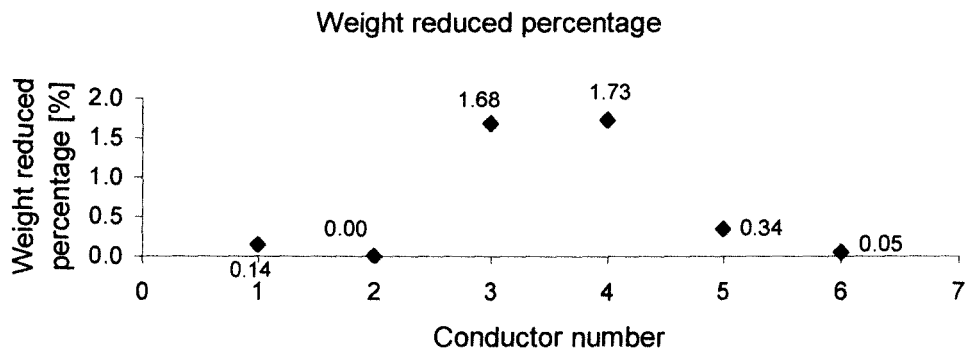

Figure B.2 Percentage of reduced weight compared to the reference

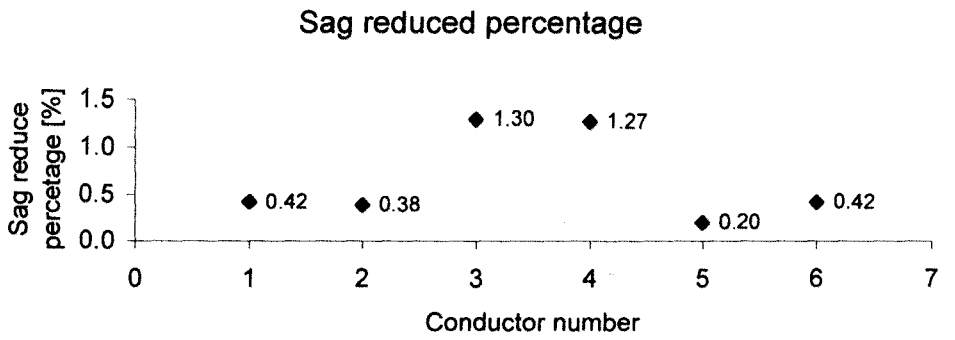

Figure B.3 Percentage of reduced sag compared to the reference

B.2 Fixing wire diameters and steel lay lengths, changing aluminum lay lengths

Table B.9 Unchanged wire and steel lay parameters

Steel wire diameter [mm]			Aluminum wire diameter [mm]		
Steel king	Steel lay 1	Steel lay 2	Inner	Middle	Outer
2.189	2.189	2.189	3.647	3.647	3.647
Steel layer outer diameter [mm]			Aluminum layer outer diameter [mm]		
Steel king	Steel lay 1	Steel lay 2	Inner	Middle	Outer
2.189	6.567	10.945	18.239	25.533	32.827
Steel lay length [mm]			Aluminum lay length [mm]		
Steel king	Steel lay 1	Steel lay 2	Inner	Middle	Outer
1000.0	164.211	218.948	Changed	Changed	Changed

Table B.10 Changed aluminum lay lengths

Conductor number	Inner [mm]	Middle [mm]	Outer [mm]	Weight [N/m]
Conductor 1	310.10	255.30	426.80	20.81
Conductor 2	284.30	283.20	353.20	20.86
Conductor 3	261.30	339.40	369.10	20.80
Conductor 4	207.80	391.00	394.40	20.78
Conductor 5	189.20	384.60	346.50	20.85
Conductor 6	182.4	408.50	328.30	20.88

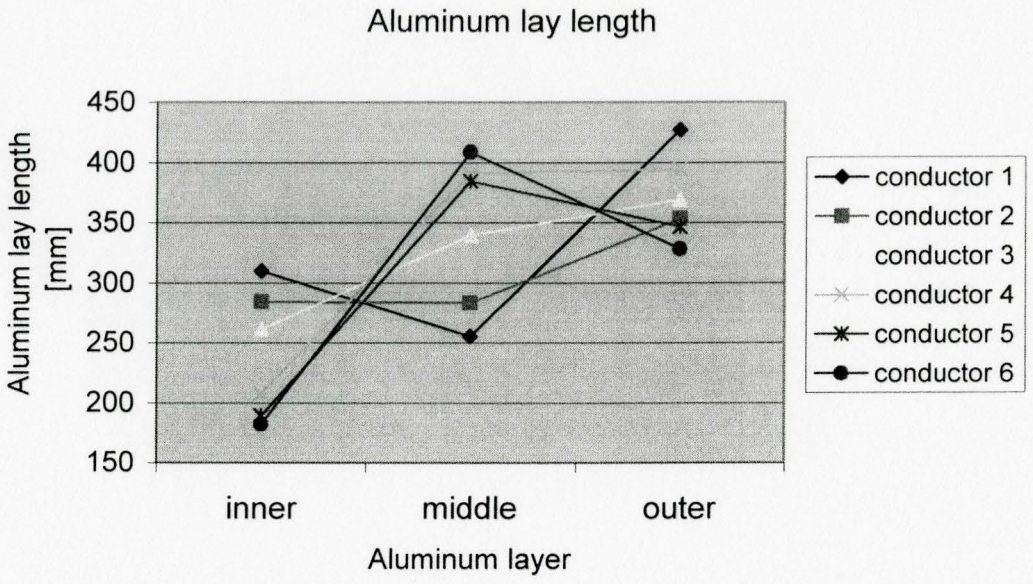

Figure B.4 Changed lay lengths with fixed wire diameters

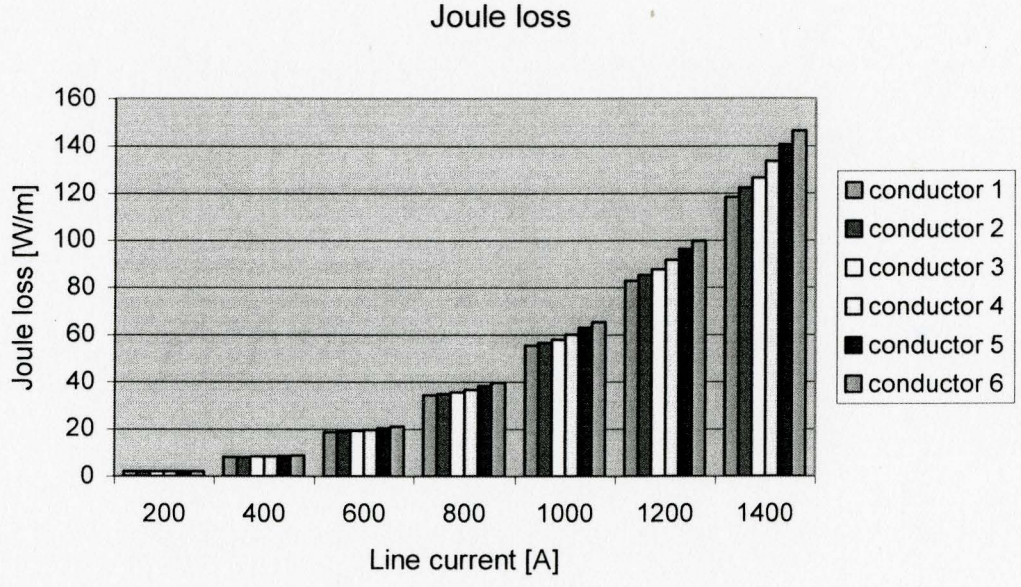

Figure B.5 Variation of Joule losses in six conductors at various line currents

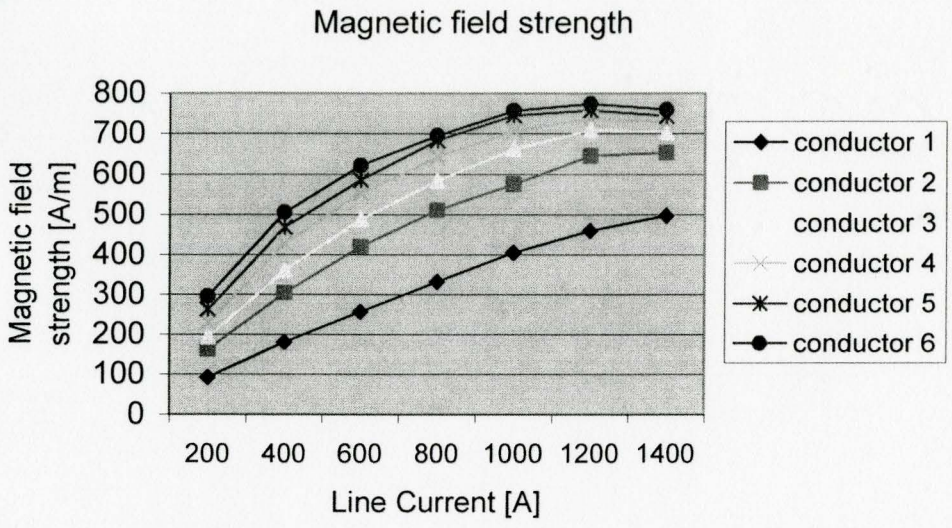

Figure B.6 Variation of six-conductor magnetic field strength at various line currents

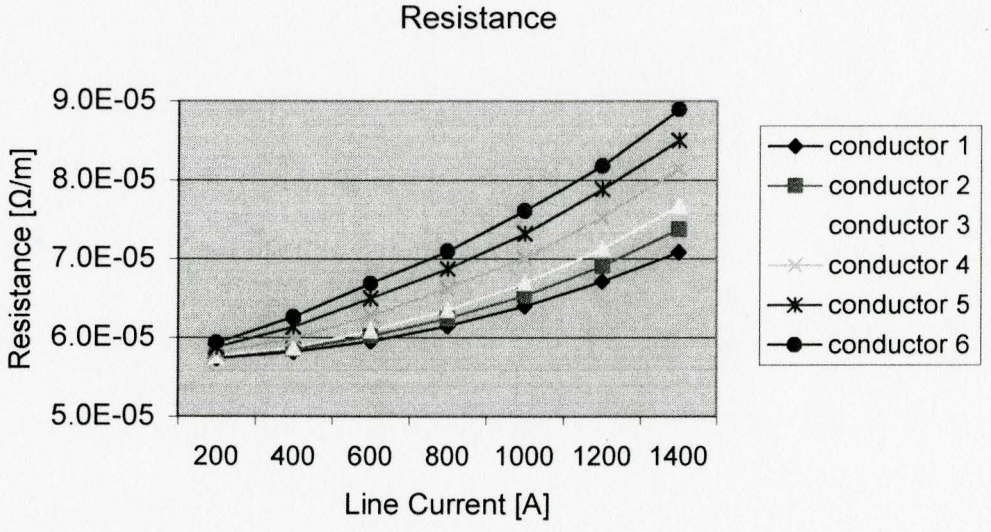

Figure B.7 Variation of resistance in six conductors at various line currents

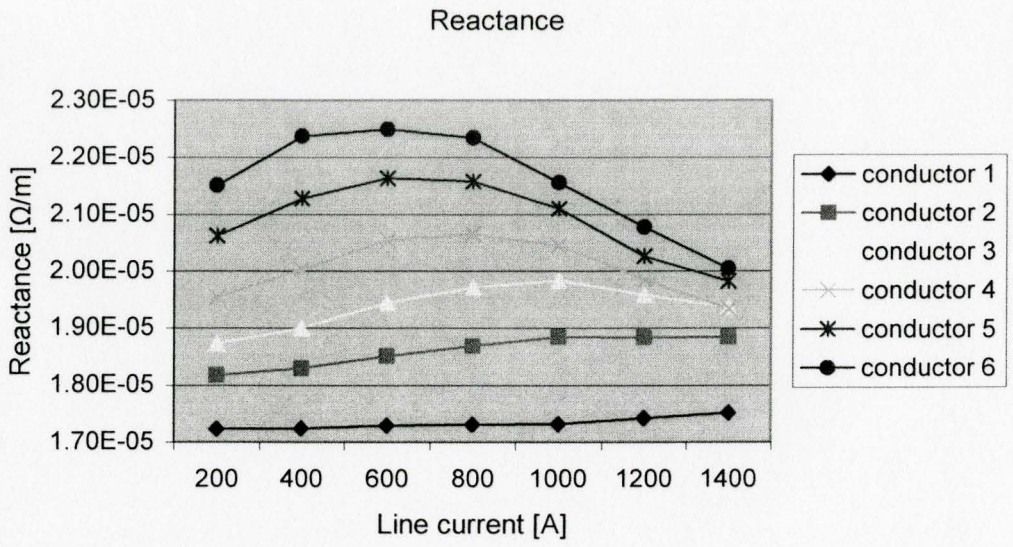

Figure B.8 Variation of reactance in six conductors at various line currents

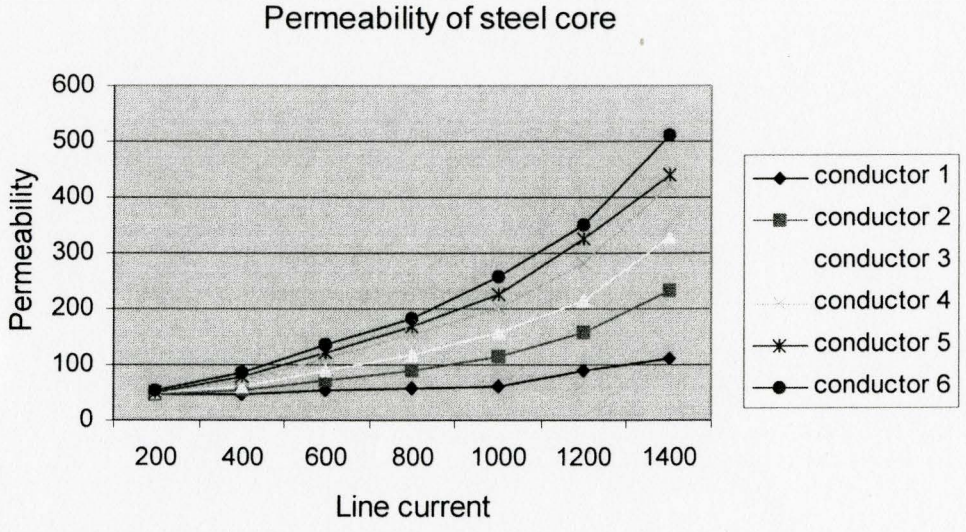

Figure B.9 Variation of the permeability at various line currents

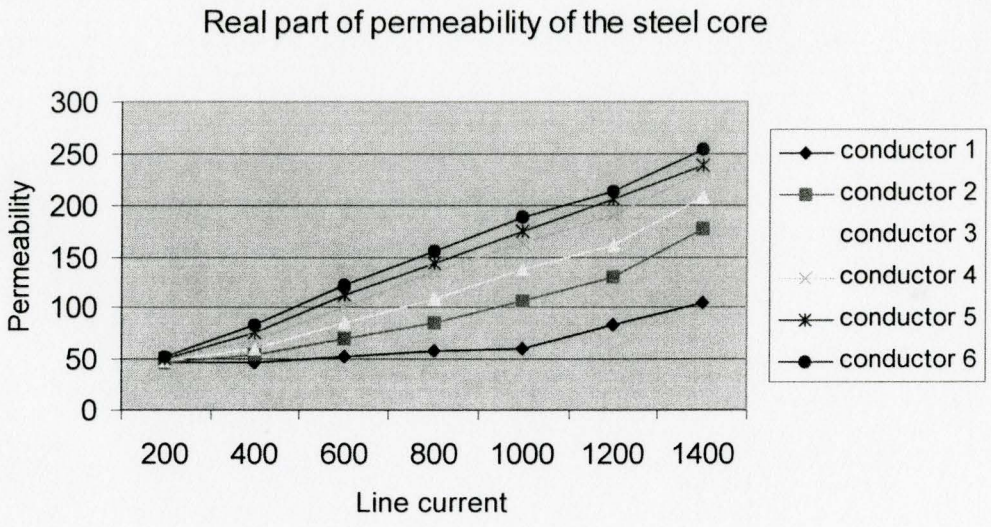

Figure B.10 Variation of real part of the permeability at various line currents

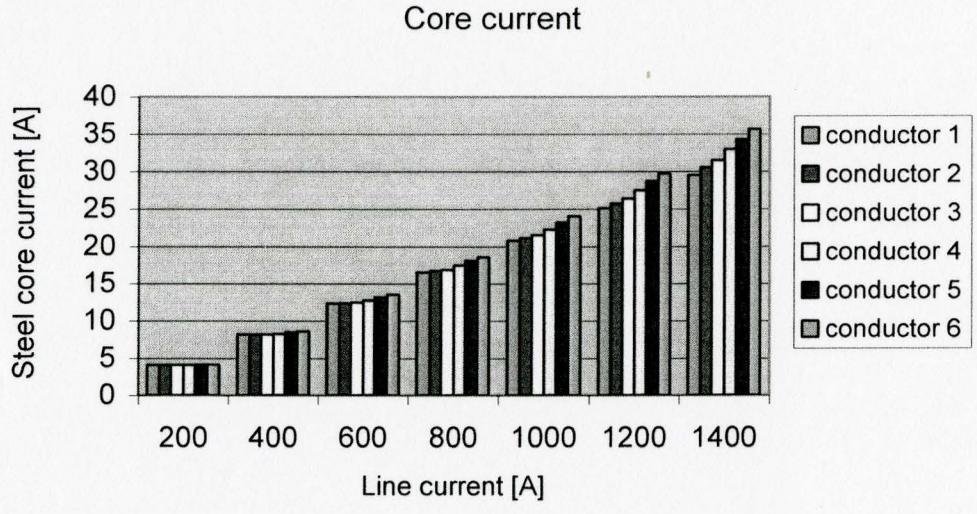

Figure B.11 Variation of steel core current at various line currents

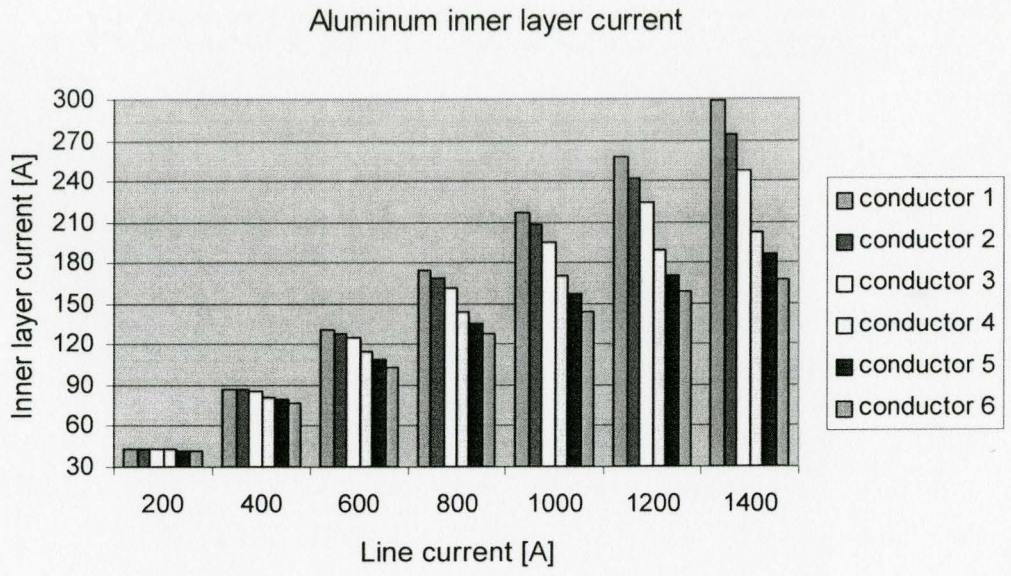

Figure B.12 Variation of aluminum inner layer current at various line currents

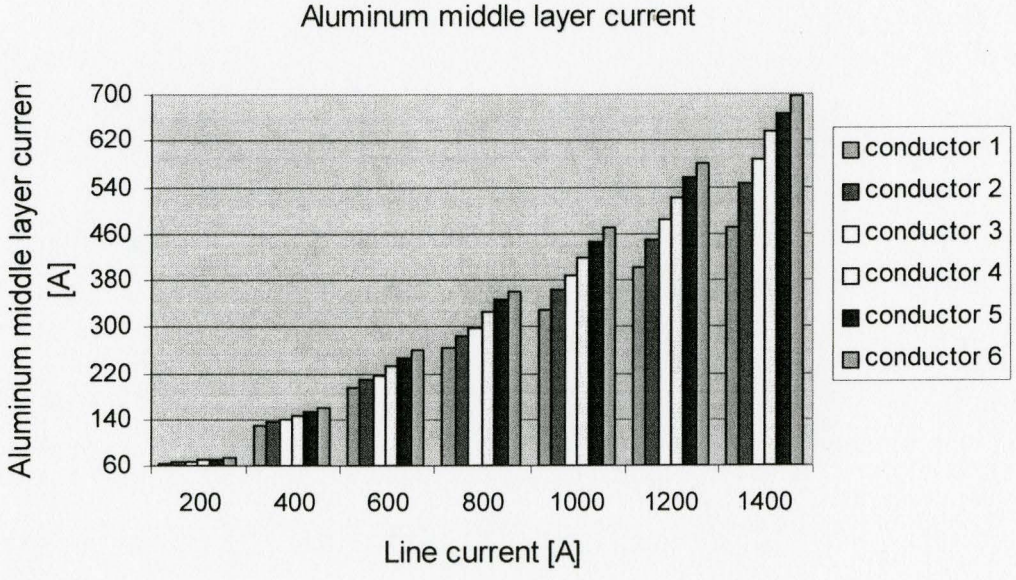

Figure B.13 Variation of aluminum middle layer current at various line currents

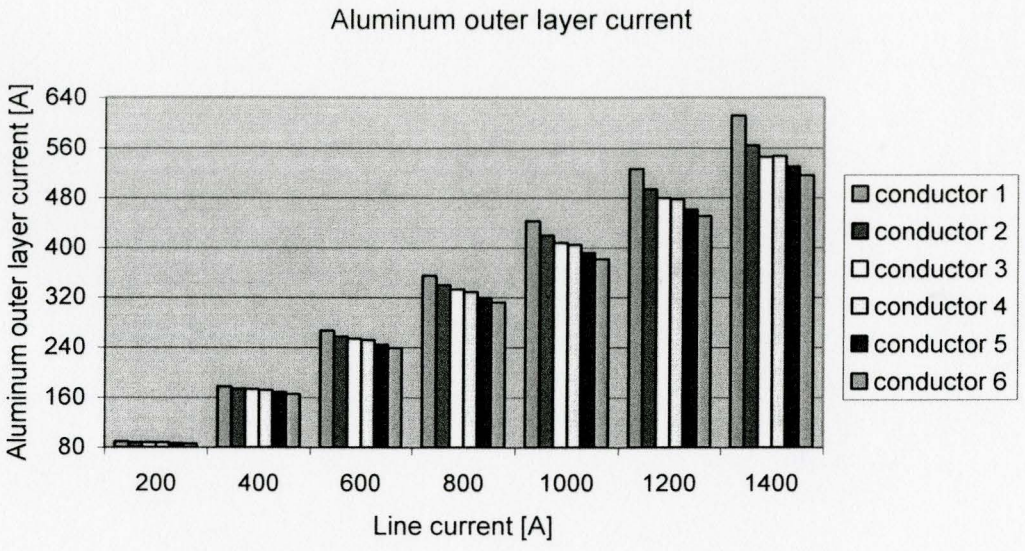

Figure B.14 Variation of aluminum outer layer current at various line currents

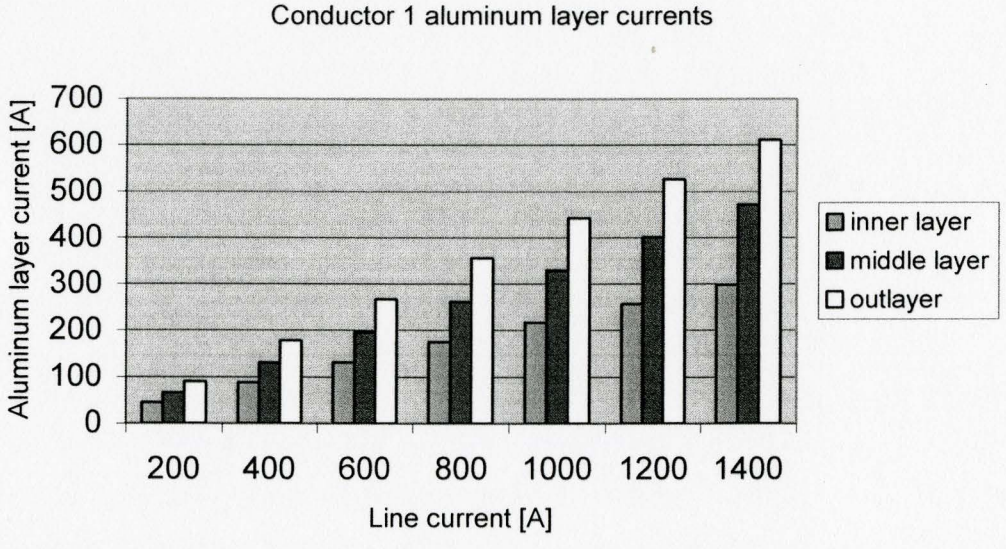

Figure B.15 Variation of three aluminum layer currents in conductor 1 at various line currents

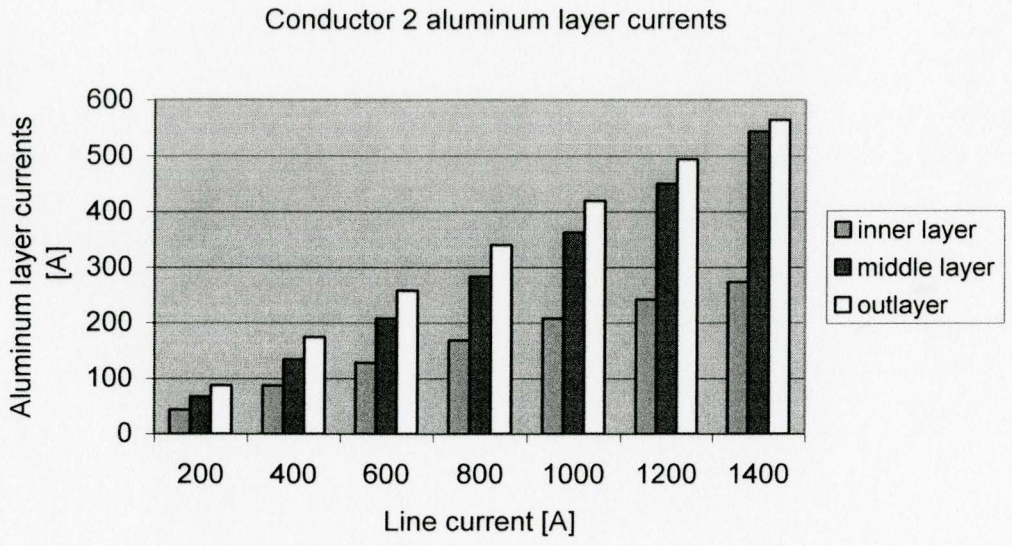

Figure B.16 Variation of aluminum layer currents in conductor 2 at various line currents

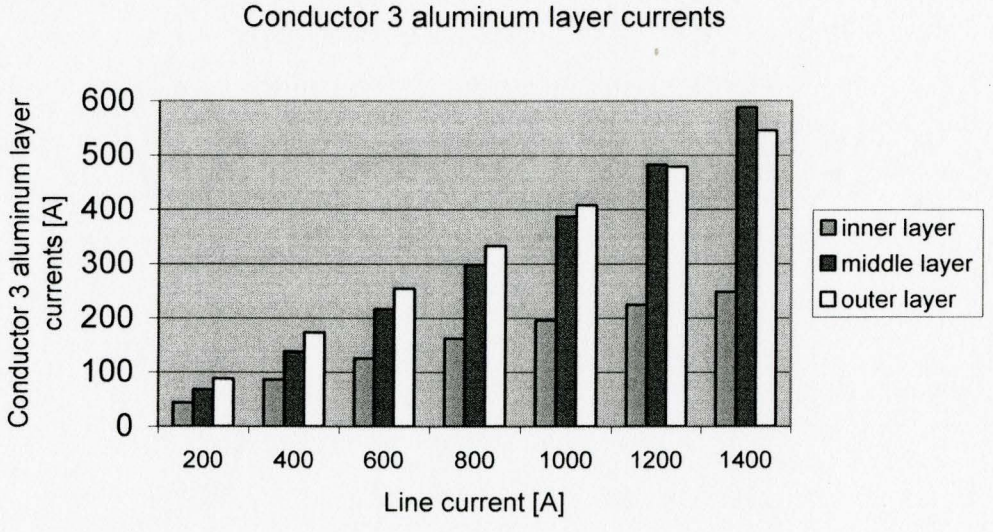

Figure B.17 Variation of aluminum layer currents in conductor 3 at various line currents

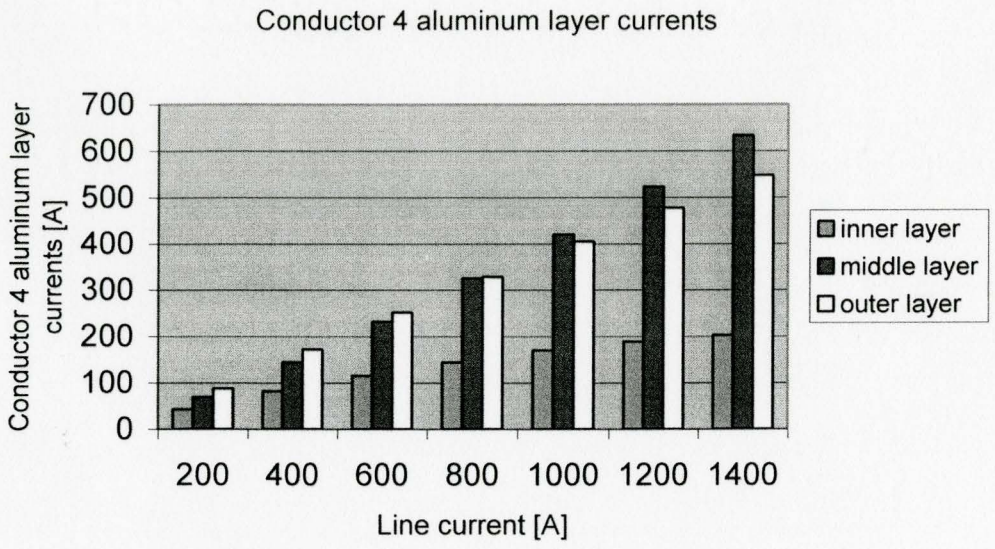

Figure B.18 Variation of three aluminum layer currents in conductor 4 at various line currents

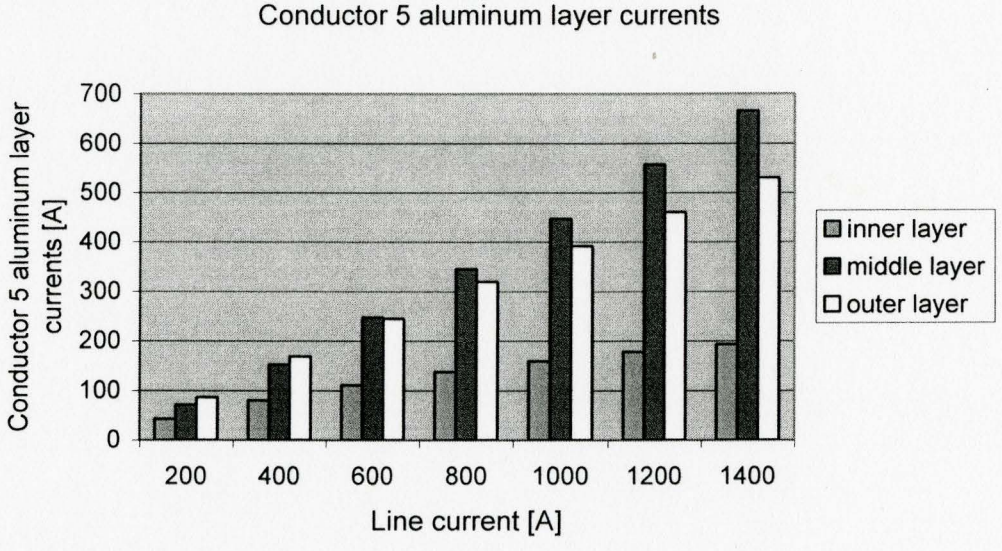

Figure B.19 Variation of aluminum layer currents in conductor 5 at various line currents

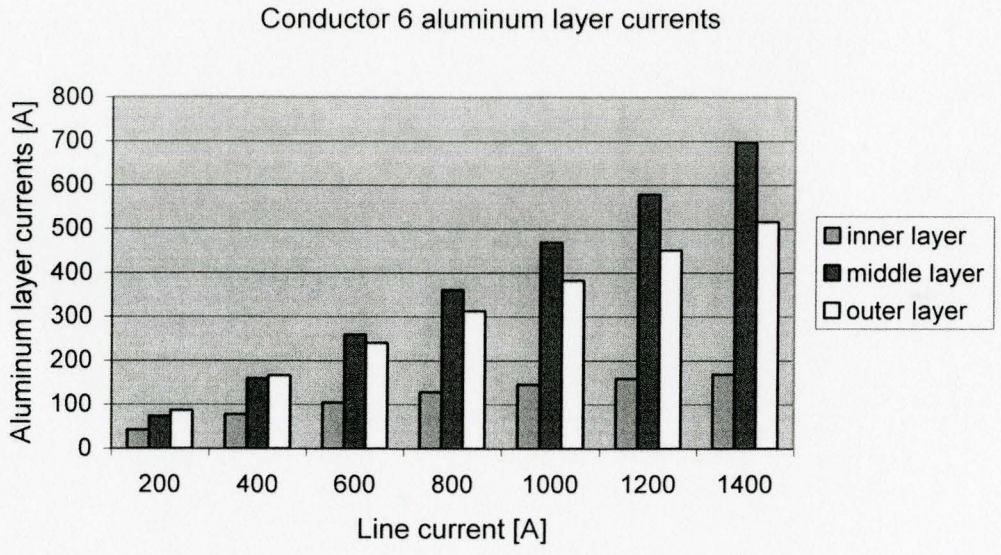

Figure B.20 Variation of aluminum layer currents in conductor 6 at various line currents

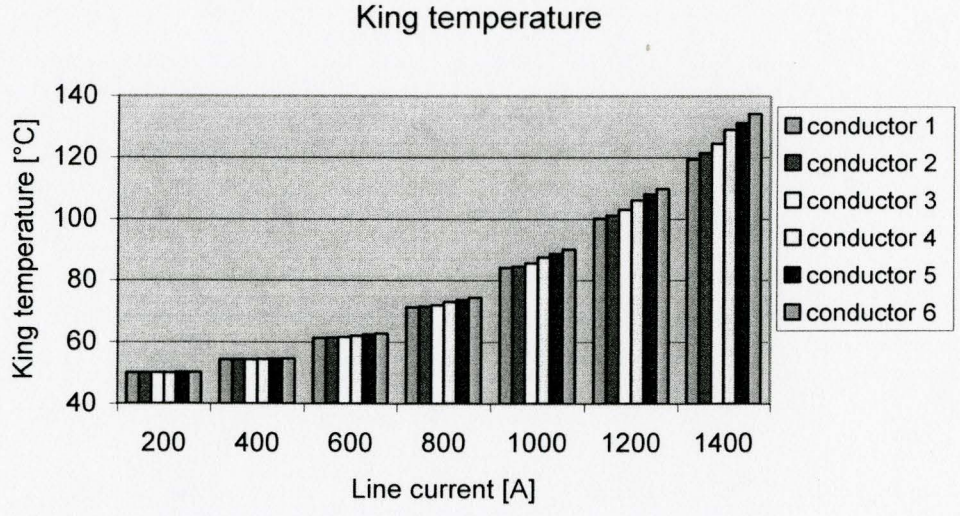

Figure B.21 Variation of steel king layer temperature at various line currents

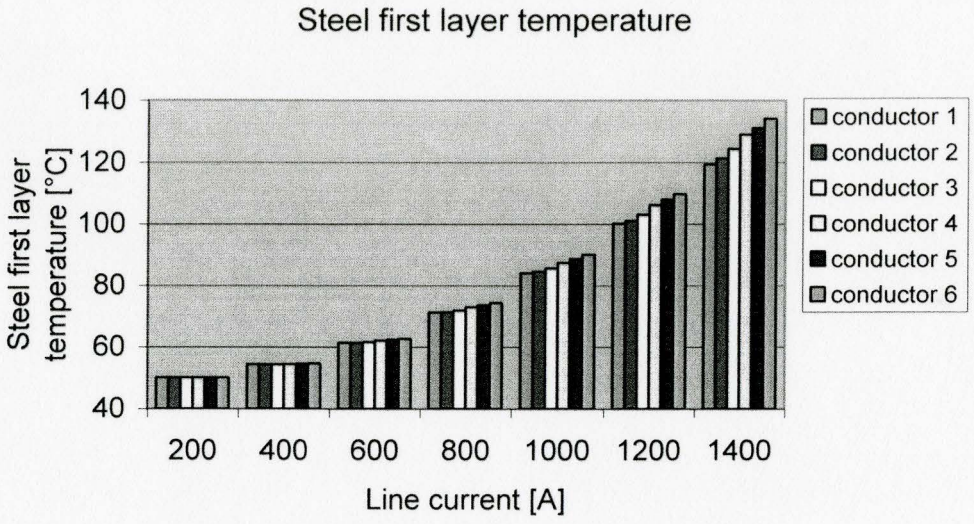

Figure B.22 Variation of steel first layer temperature at various line currents

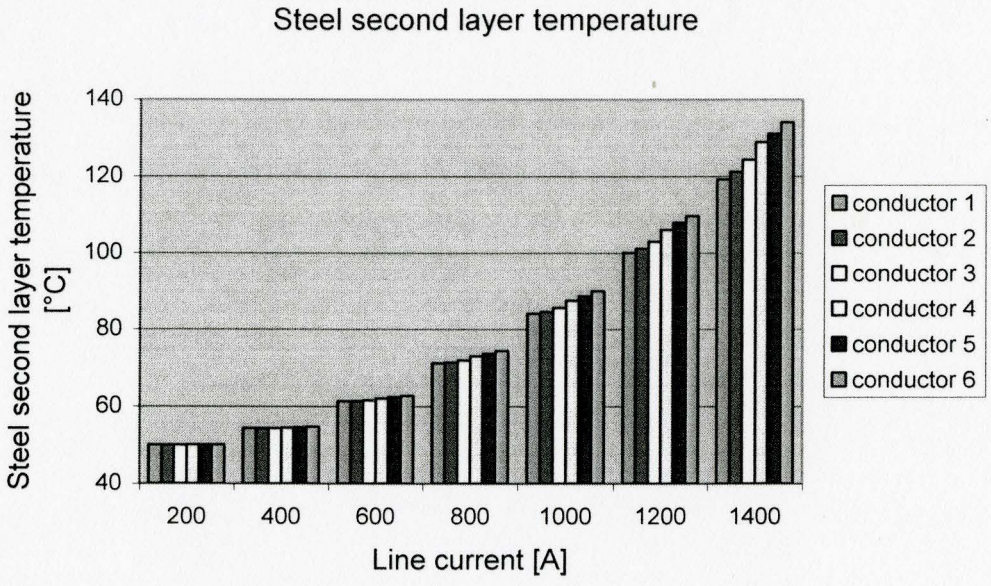

Figure B.23 Variation of steel second layer temperature at various line currents

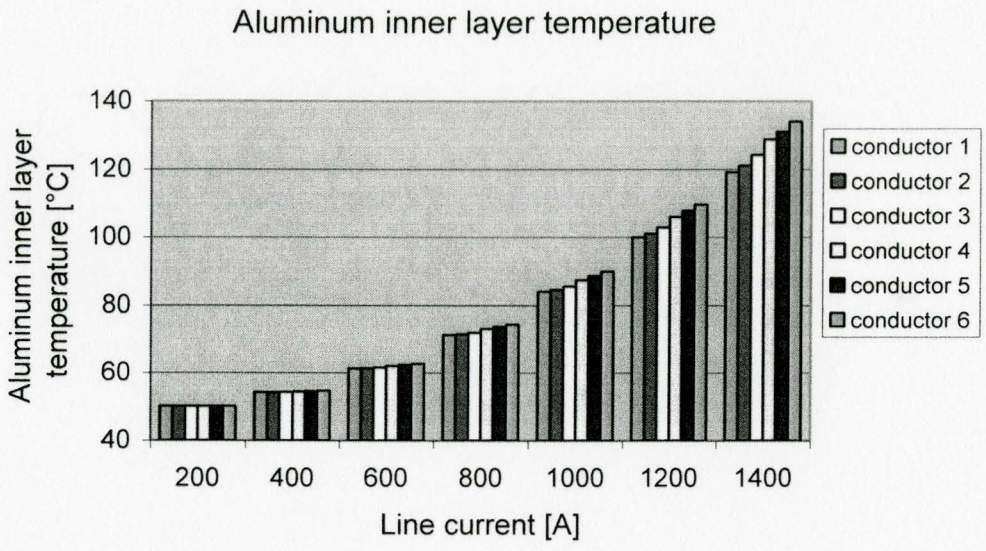

Figure B.24 Variation of aluminum inner layer temperature at various line currents

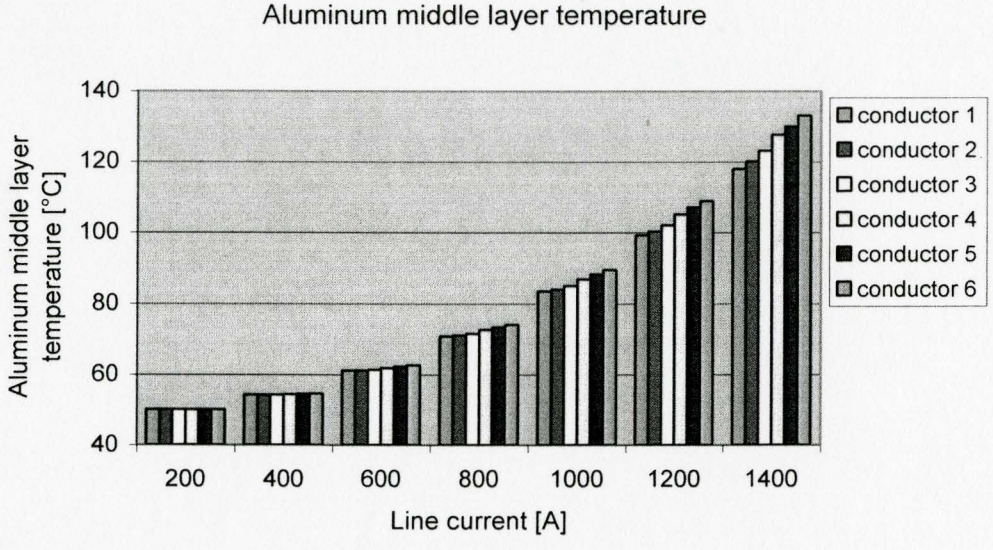

Figure B.25 Variation of aluminum middle layer temperature at various line currents

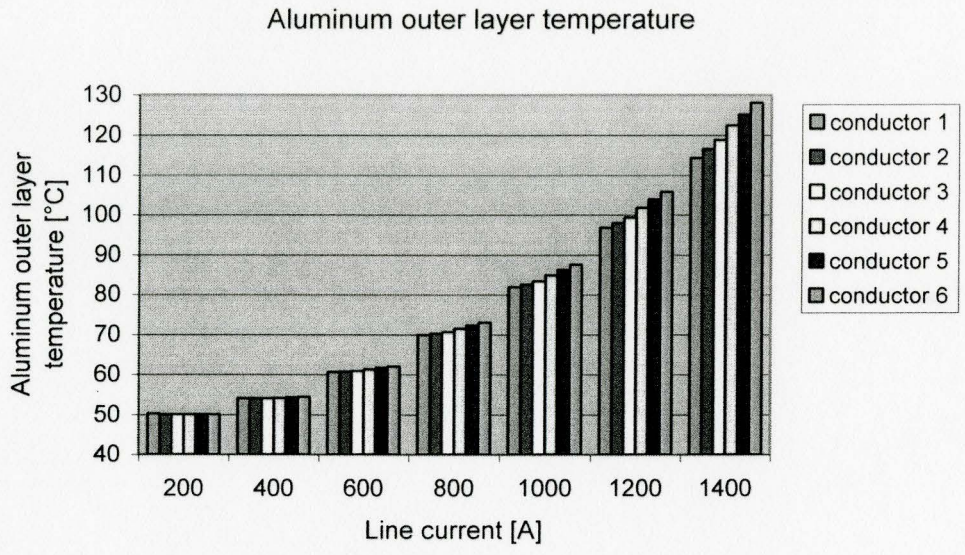

Figure B.26 Variation of aluminum outer layer temperature at various line currents

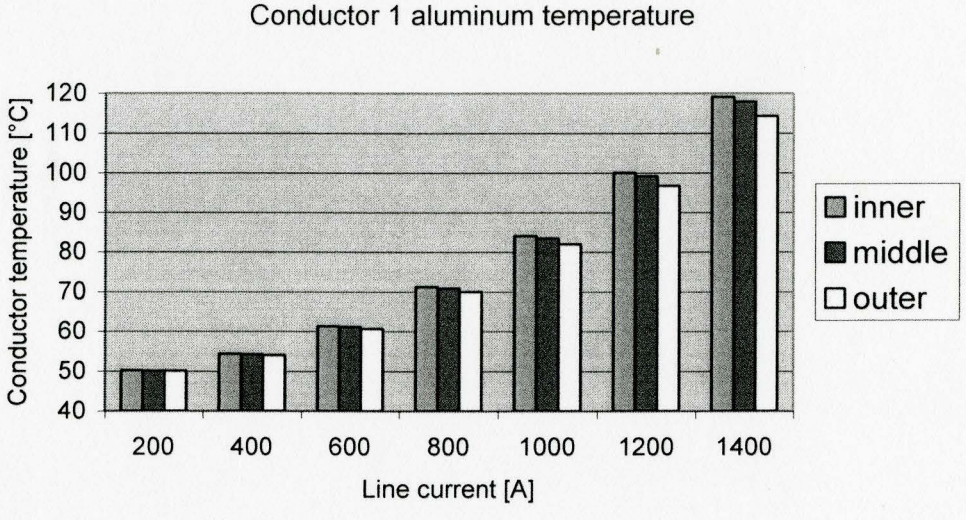

Figure B.27 Variation of aluminum layer temperature in conductor 1 at various line currents

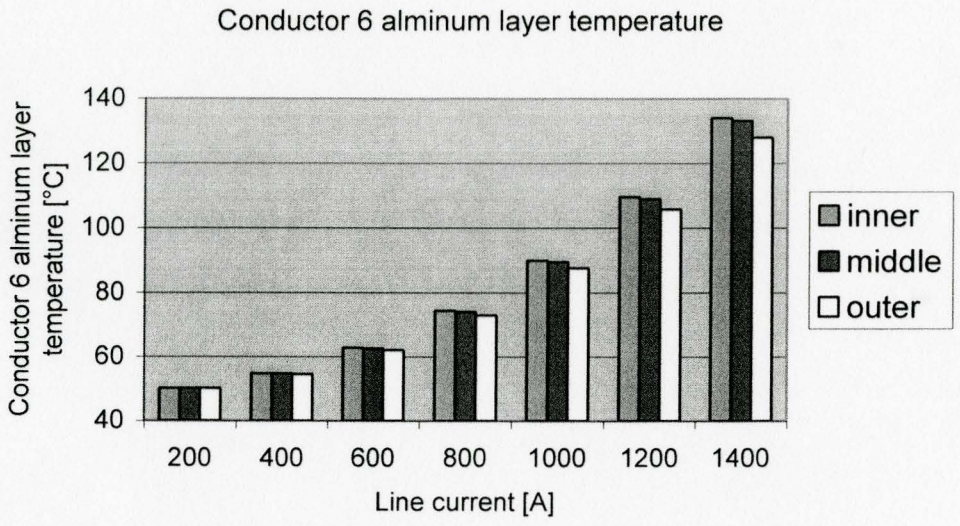

Figure B.28 Variation of aluminum layer temperature in conductor 6 at various line currents

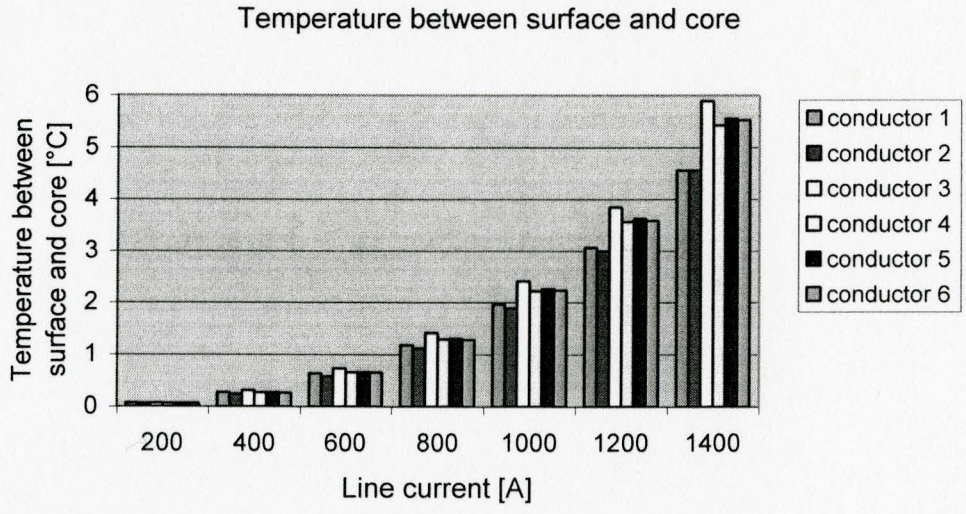

Figure B.29 Temperature differences between steel core and conductor surface

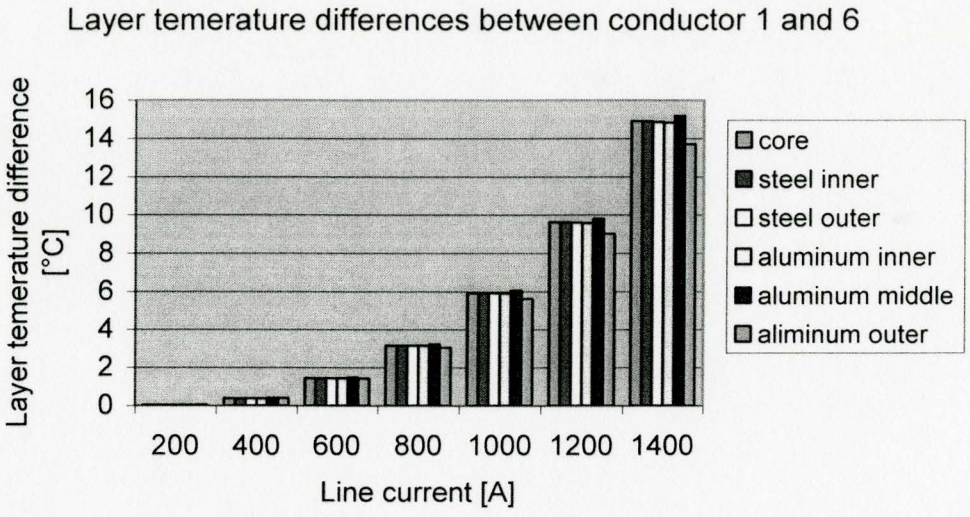

Figure B.30 Temperature differences in layers between conductor 1 and 6

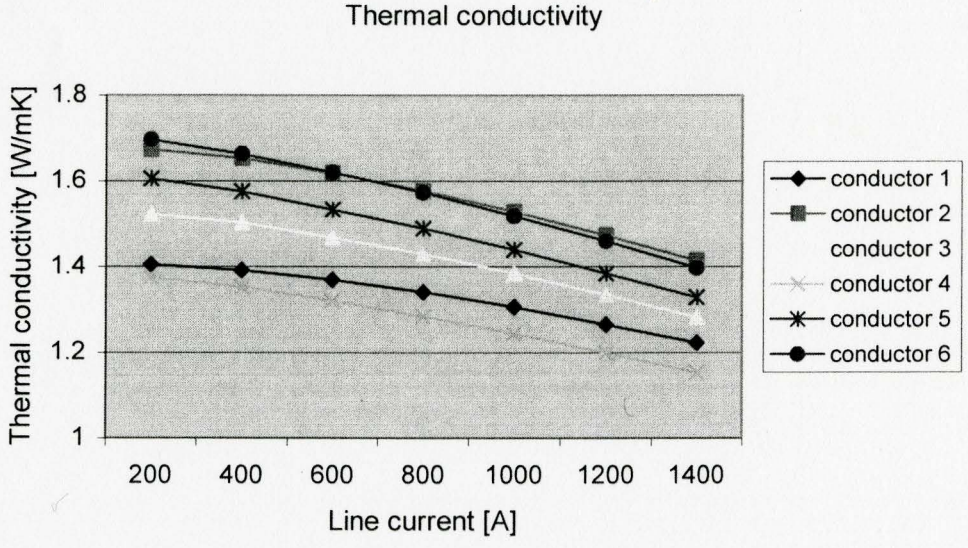

Figure B.31 Variation of thermal conductivity at various line currents

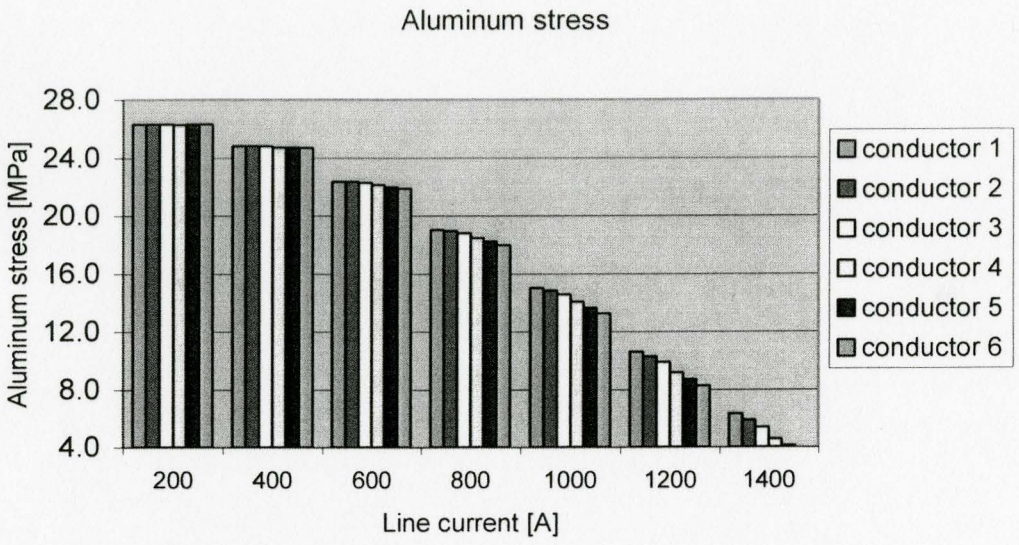

Figure B.32 Variation of aluminum stresses at various line currents

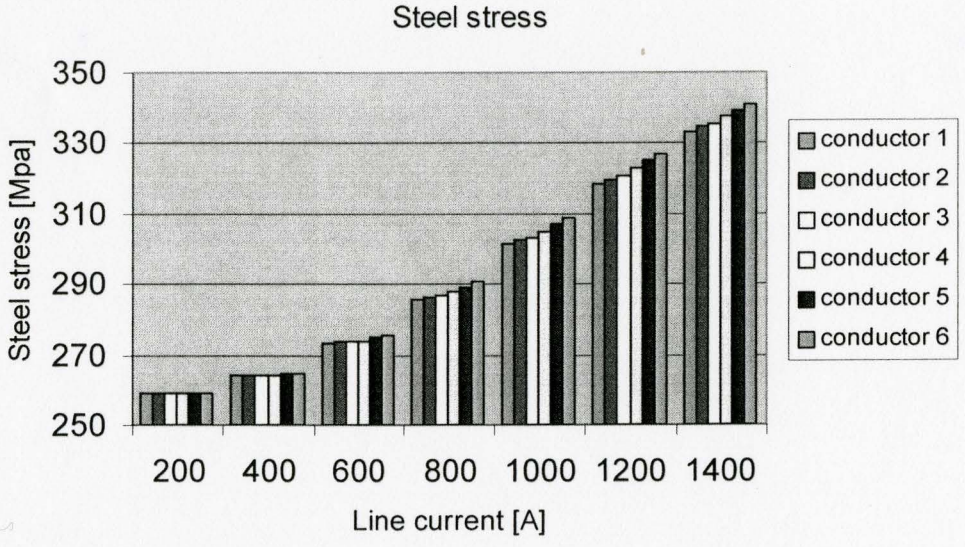

Figure B.33 Variation of steel stresses at various line currents

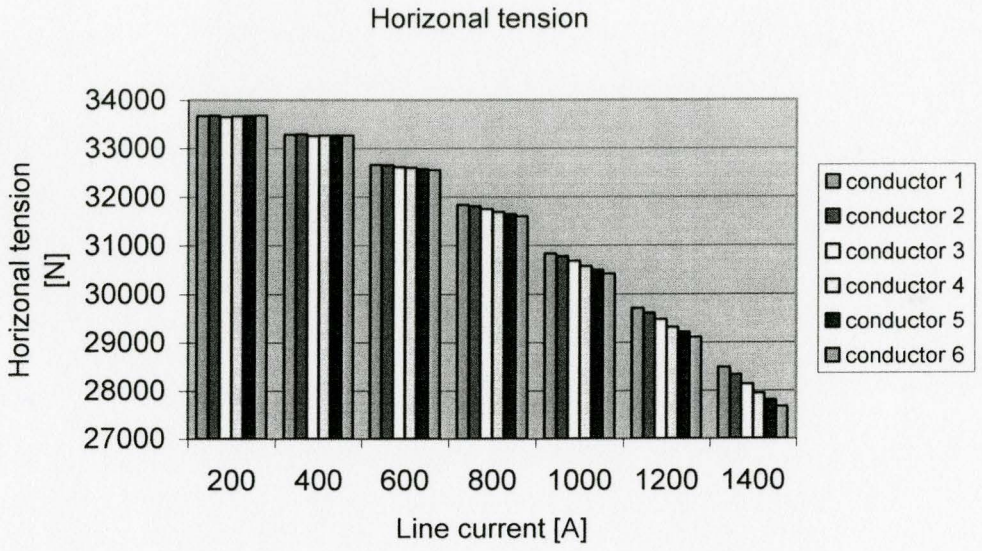

Figure B.34 variation of horizontal tension at various line currents

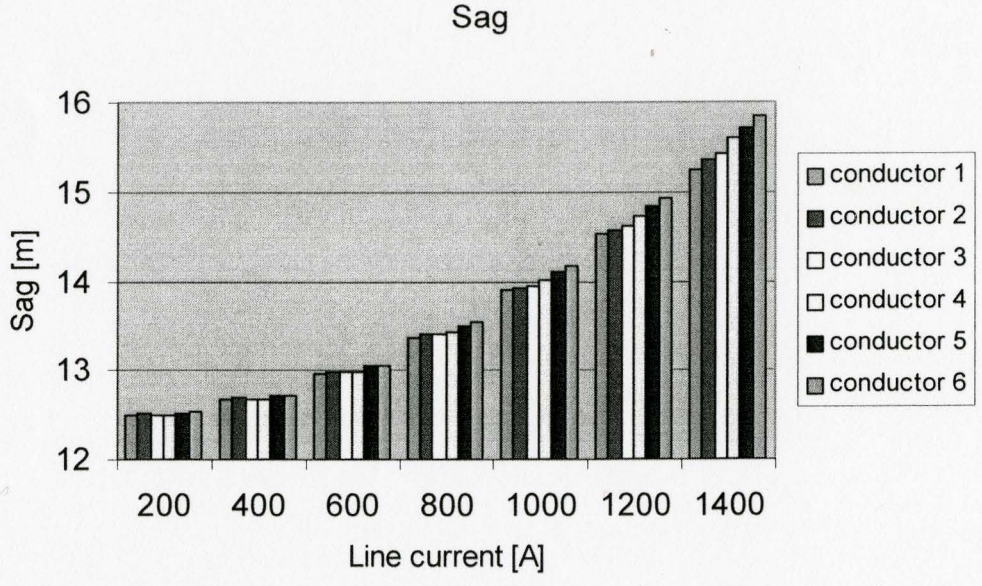

Figure B.35 Variation of sags at various line currents with line length 400 meters

B.3 Fixing wire diameters, changing steel and aluminum lay lengths

Table B.11 Unchanged steel wire and aluminum wire diameters

Steel wire diameter [mm]			Aluminum wire diameter [mm]		
King	Steel lay 1	Steel lay 2	Inner	Middle	Outer
2.189	2.189	2.189	3.647	3.647	3.647
Steel layer's outer diameters [mm]			Aluminum layer's outer diameters [mm]		
Steel lay 1	Steel lay 2	Steel lay 3	Inner	Middle	Outer
2.189	6.567	10.945	18.239	25.533	32.827

Table B.12 Changed steel and aluminum lay lengths

Steel lay length [mm]			Aluminum lay length [mm]		
	Steel lay 1	Steel lay 2	Inner	Middle	Outer
Conductor 1	197.00	262.70	310.1	255.30	426.8
Conductor 2	175.30	248.70	244.10	284.60	347.50
Conductor 3	192.40	241.50	261.30	339.40	369.10
Conductor 4	192.40	182.30	207.80	391.00	394.40
Conductor 5	189.30	231.10	189.20	384.60	346.50
Conductor 6	119.00	177.00	182.00	408.00	328.00
Weight [N/m]					
Conductor 1	Conductor 2	Conductor 3	Conductor 4	Conductor 5	Conductor 6
20.80	20.87	20.80	20.79	20.85	20.90

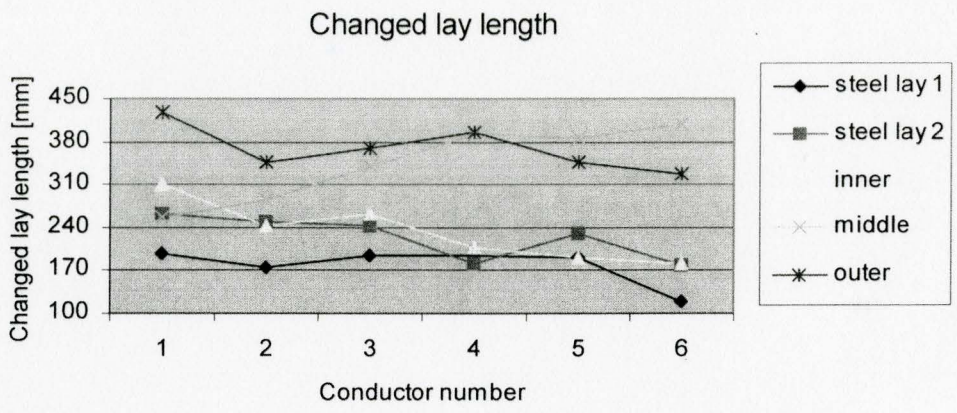

Figure B.36 Variation of lay length for different conductors at 1000 A

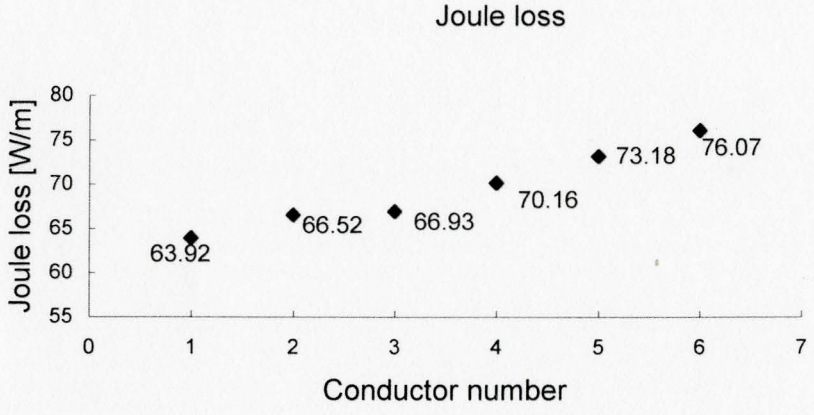

Figure B.37 Variation of Joule losses for different conductors at 1000A

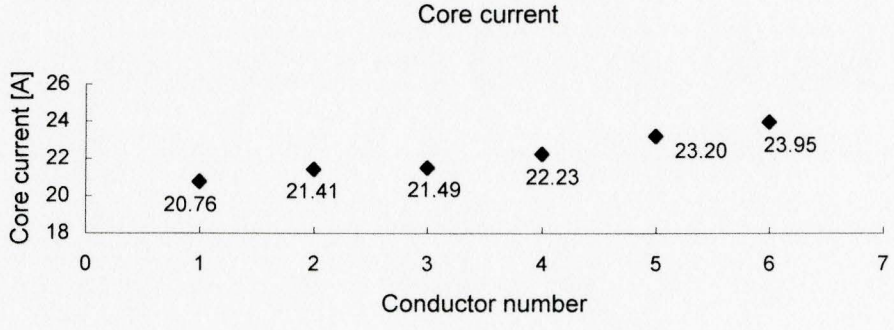

Figure B.38 Variation of core current for different conductors at 1000A

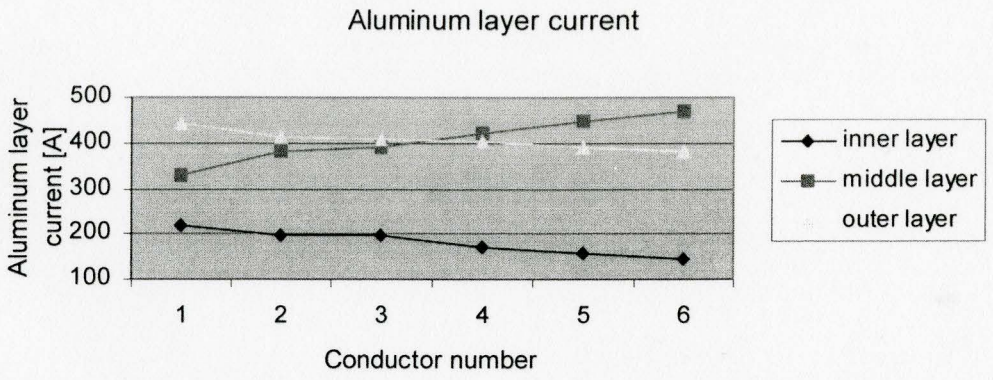

Figure B.39 Variation of aluminum current for different conductors at 1000A

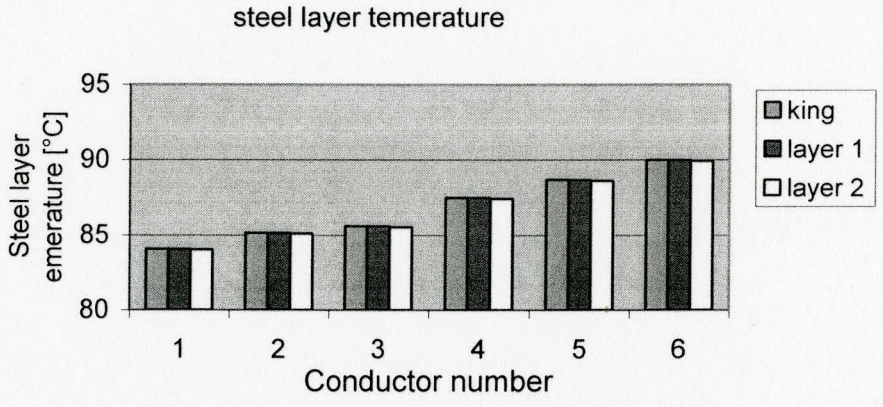

Figure B.40 Variation of steel layer temperature for different conductors at 1000A

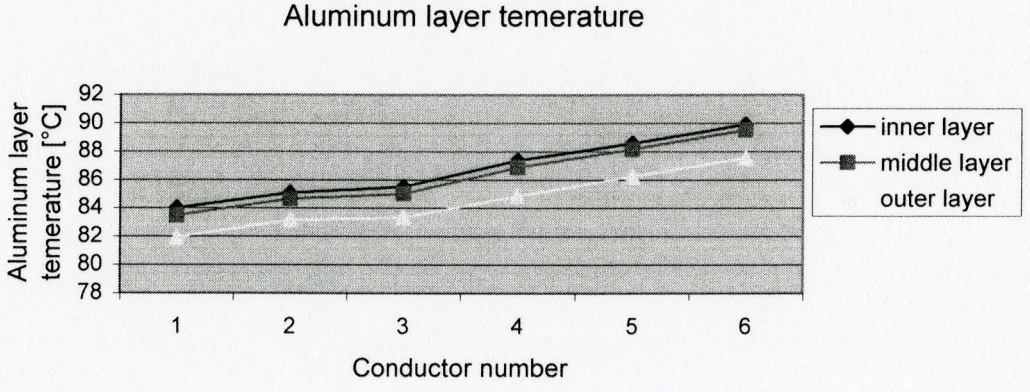

Figure B.41 Variation of aluminum layer temperature for different conductors at 1000A

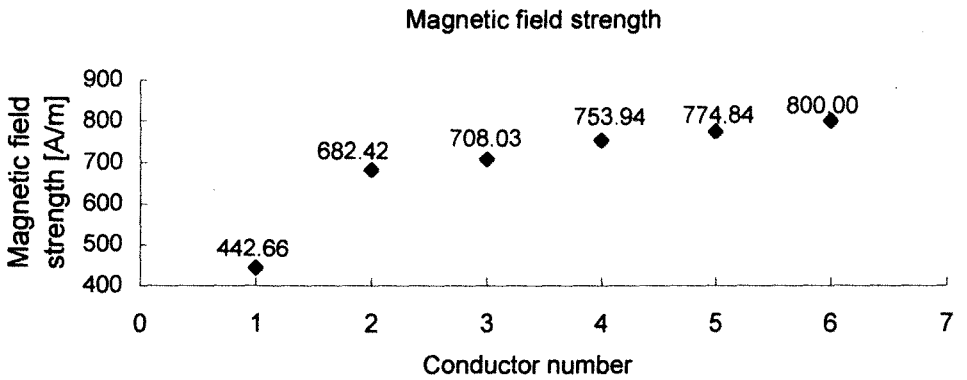

Figure B.42 Variation of magnetic field strength for different conductors at 1000A

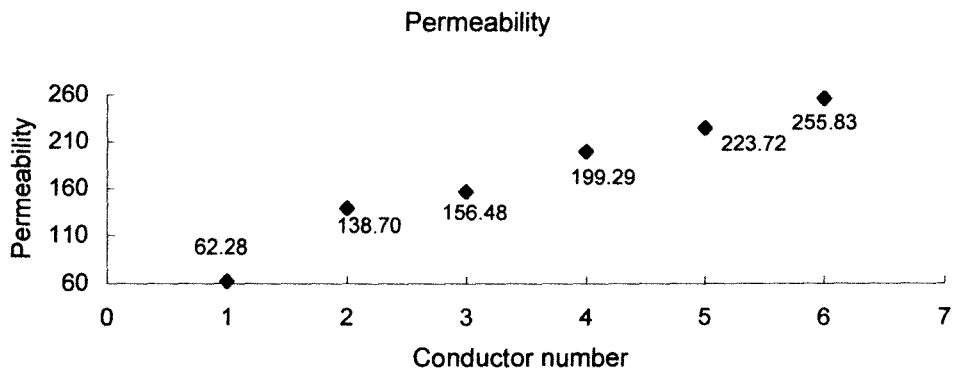

Figure B.43 Variation of permeability for different conductors in 1000A

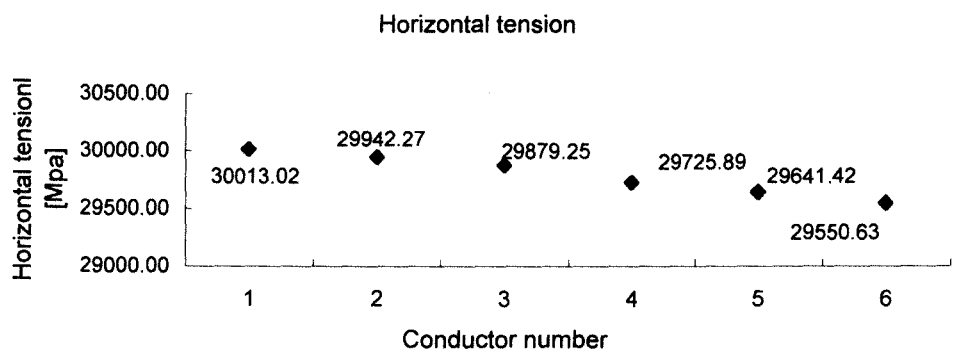

Figure B.44 Variation of horizontal tension for different conductors at 1000A

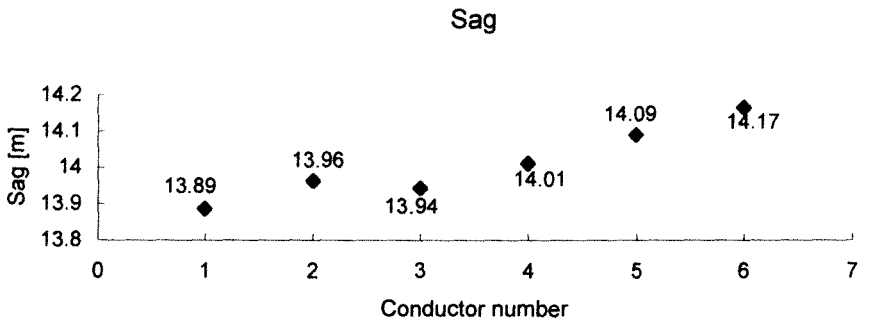

Figure B.45 Variation of sags for different conductors at 1000A

B.4 Fixing steel core size, changing aluminum lay lengths and wire diameters

Table B.13 Changed aluminum wire and layer parameters

Wire diameter [mm]				Aluminum lay length [mm]		
	Inner	Middle	Outer	Inner	Middle	Outer
Conductor 1	3.800	3.800	3.800	310.1	255.30	426.80
Conductor 2	3.695	3.784	3.543	273.8	302.20	405.90
Conductor 3	3.762	3.736	3.518	288.00	397.60	394.10
Conductor 4	3.680	3.559	3.581	267.6	374.30	358.80
Conductor 5	3.724	3.594	3.523	187.30	397.90	329.00
Conductor 6	3.500	3.500	3.500	182.40	408.50	328.30
Outer diameter [mm]						
	Inner	Middle	Outer	Weight [N/m]		
Conductor 1	18.545	26.145	33.745	22.14		
Conductor 2	18.336	25.903	32.988	20.89		
Conductor 3	18.470	25.942	32.978	20.74		
Conductor 4	18.305	25.423	32.585	20.36		
Conductor 5	18.394	25.582	32.627	20.41		
Conductor 6	17.945	24.945	31.945	19.65		

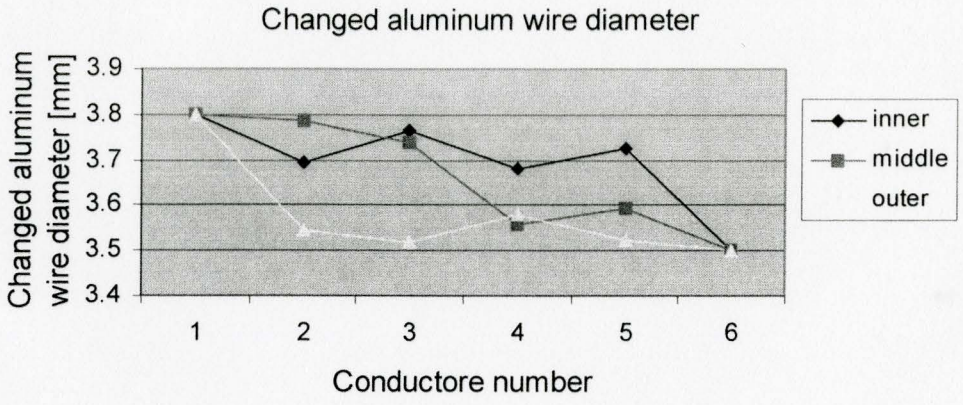

Figure B.46 Changed aluminum diameters at 1000A

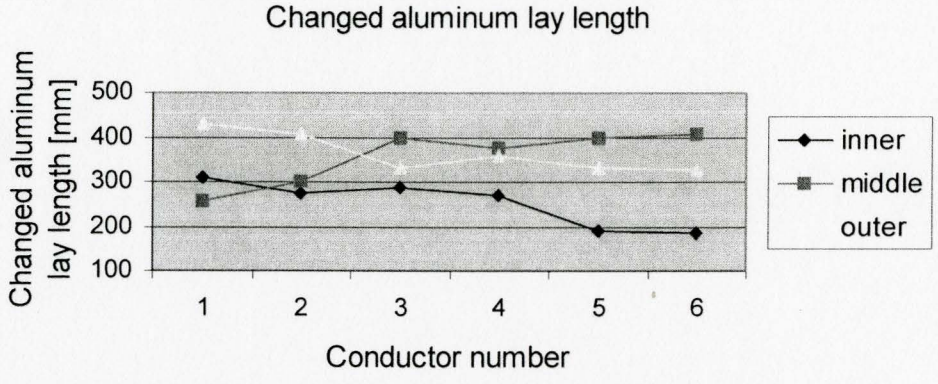

Figure B.47 Changed aluminum lay lengths at 1000A

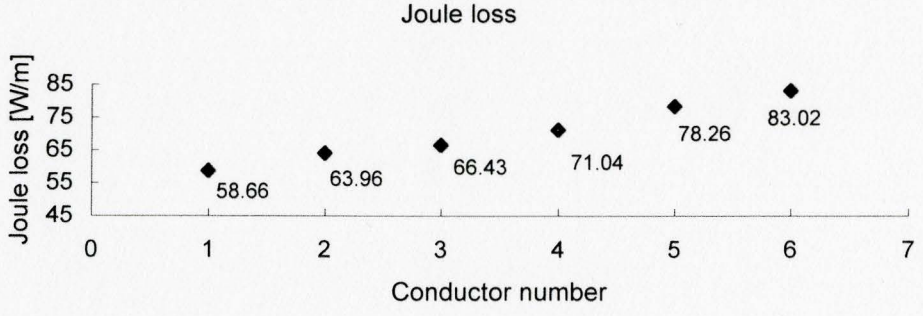

Figure B.48 Variation of Joule losses among conductors at 1000A

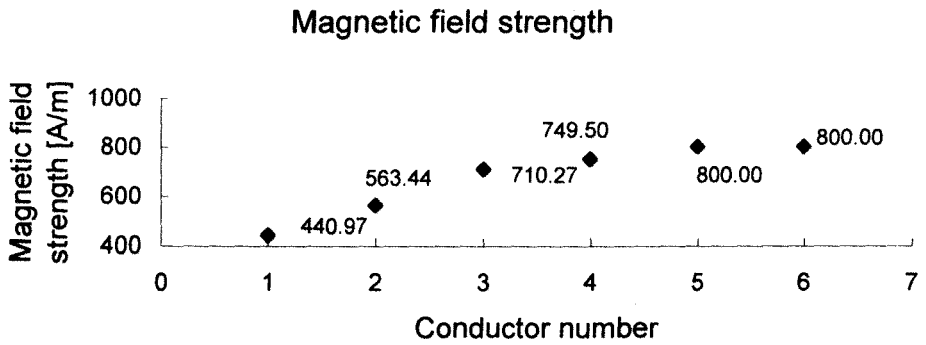

Figure B.49 Variation of magnetic field strength among conductors at 1000A

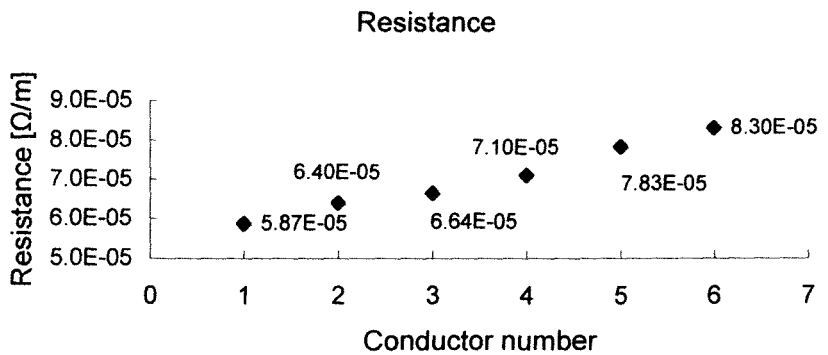

Figure B.50 Variation of resistance among conductors at 1000A

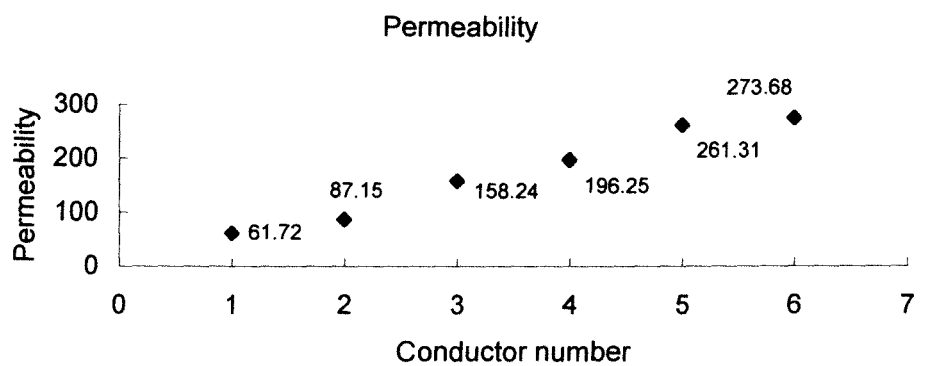

Figure B.51 Variation of permeability among conductors at 1000A

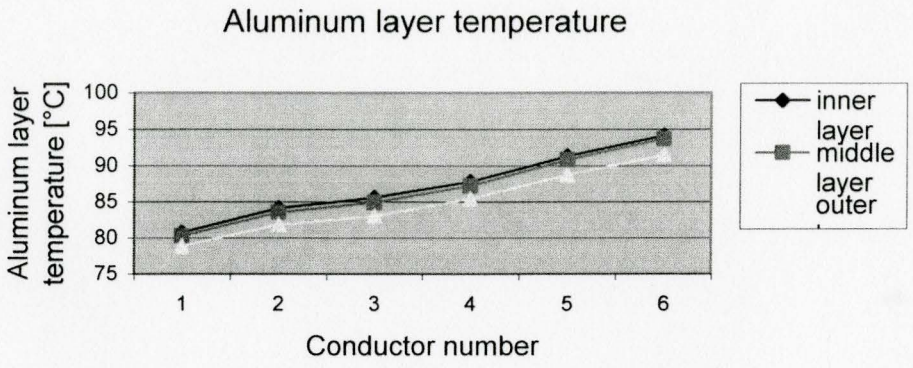

Figure B.52 Variation of aluminum layer temperature among conductors at 1000A

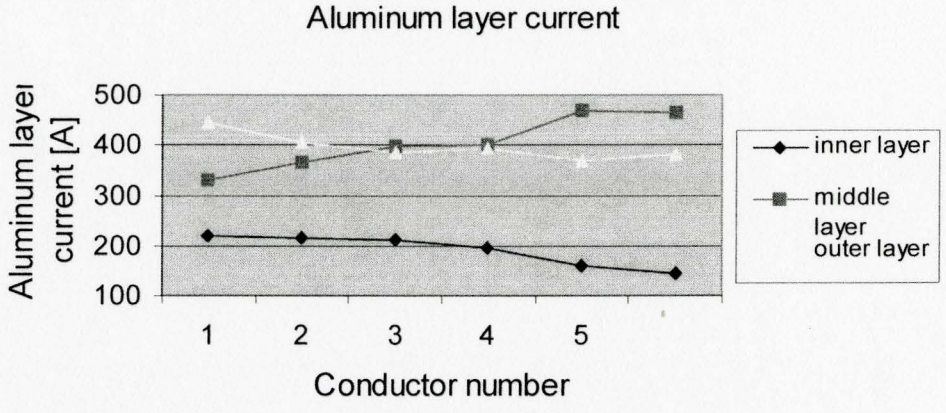

Figure B.53 Variation of aluminum layer current among conductors at 1000A

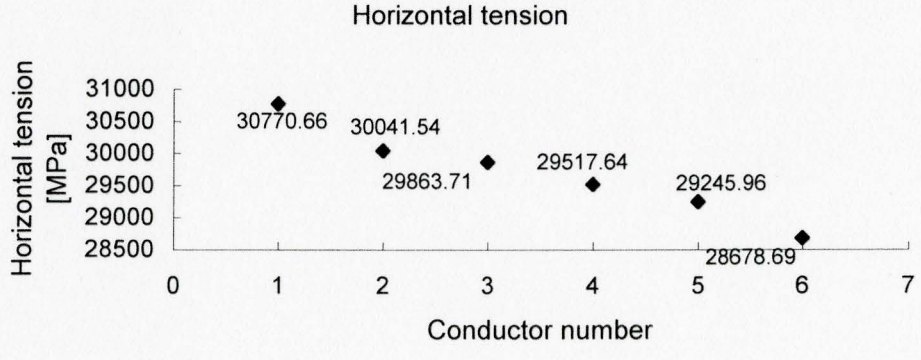

Figure B.54 Variation of horizontal tension among conductors at 1000A

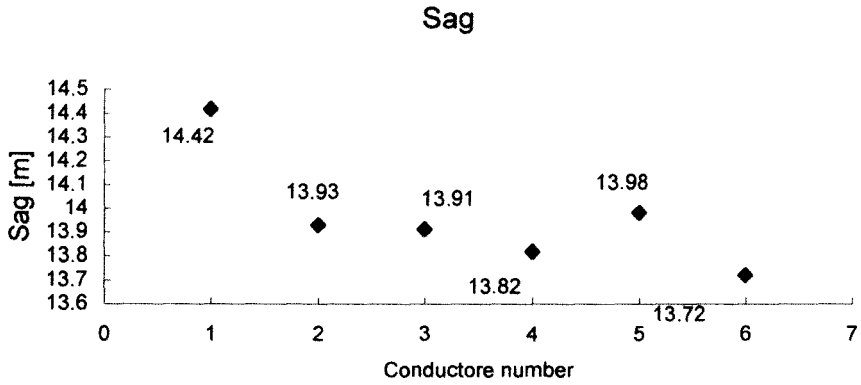

Figure B.55 Variation of sags among conductors at 1000A

Appendix C Results Using Genetic Algorithms in Three-layer Conductor Pheasant

C.1 Results of the application of the Genetic algorithm

Table C.1 Standard in ASTM 232M

Ratio of lay length of a layer to nominal outside diameter of that lay									
Aluminum layer						Steel layer			
Outer		Middle		Inner		Outer		Inner	
Min	Max	Min	Max	Min	Max	Min	Max	Min	Max
10	13	10	16	10	17	16	24	18	30
Conversion of the lay length of Pheasant conductor [mm]									
350.9	456.2	272.9	436.7	194.9	331.4	187.1	280.7	126.3	210.5

Table C.2 Ranges of changed wire diameters and lay lengths

Steel diameter [mm]		Aluminum diameter [mm]	
Lower bound	Upper bound	Lower bound	Upper bound
2.339	2.339	3.75	4.05
Steel lay length [mm]		Aluminum lay length [mm]	
Layer 1		Inner layer	
Lower bound	Upper bound	Lower bound	Upper bound
126.3	210.5	194.9	331.4
Layer 2		Middle layer	
Lower bound	Upper bound	Lower bound	Upper bound
187.1	280.7	272.9	436.7
		Outer layer	
		Lower bound	Upper bound
		350.9	456.2

Table C.3 Min and max losses with changed aluminum lay lengths

Minimum Joule loss [W/m]		Weight [N/m]
55.2475		23.78
Aluminum lay length [mm]		
Inner	Middle	Outer
331.4	272.9	456.2
Maximum Joule loss [W/m]		Weight [N/m]
65.1512		23.85
Aluminum lay length [mm]		
Inner	Middle	Outer
194.9	436.7	350.9

Table C.4 Min and max losses with changed steel and aluminum lay lengths

Minimum Joule loss [W/m]				Weight [N/m]
55.2455				23.77
Layer length [mm]				
Steel lay 1	Steel lay 2	Al inner	Al middle	Al outer
210.5	280.7	331.4	272.9	456.2
Maximum Joule loss [W/m]				Weight [N/m]
65.1574				23.88
Layer length [mm]				
Steel lay 1	Steel lay 2	Al inner	Al middle	Al outer
126.3	187.1	194.9	436.7	350.9

Table C.5 Min and max losses with changed aluminum wire diameters and lay lengths

Minimum Joule loss [W/m]		Weight [N/m]
51.1580		25.18
Aluminum wire diameter [mm]		
Inner	Middle	Outer
4.05	4.05	4.05
Aluminum lay length [mm]		
Inner	Middle	Outer
331.4	272.9	456.2
Maximum Joule loss [W/m]		Weight [N/m]
70.8435		22.52
Aluminum wire diameter [mm]		
Inner	Middle	Outer
3.75	3.75	3.75
Aluminum lay length [mm]		
Inner	Middle	Outer
194.9	436.7	350.9

Table C.6 Min and max losses with changed aluminum wire diameters

Minimum Joule loss [W/m]		Weight [N/m]
53.2105		25.18
Aluminum diameter [mm]		
Inner	Middle	Outer
4.05	4.05	4.05
Maximum Joule loss [W/m]		Weight [N/m]
62.2046		22.45
Aluminum diameter [mm]		
Steel lay 1	Steel lay 2	Inner
3.75	3.75	3.75

Table C.7 Pheasant used as a reference

Aluminum lay length [mm]			Steel lay length [mm]	
Inner	Middle	Outer	First layer	Second layer
175.451	233.934	292.417	354.8	385.991
Aluminum wire diameter [mm]			Steel wire diameter [mm]	
3.899			2.339	
Loss [W/m]		Weight [N/m]	Sag [m]	
57.4298		23.78	15.1273	

Table C.8 Low loss conductors

Results with changed aluminum lay lengths

Aluminum lay [mm]				Weight [N/m]	Loss [W/m]	Sag [m]
Number	Inner	Middle	Outer			
1	280.1	304.0	442.1	23.77	55.8927	15.0976
2	275.0	326.8	446.2	23.75	56.1413	15.0928

Results with changed aluminum lay lengths and wire diameters

Aluminum lay [mm]				Aluminum wire diameter [mm]		
Number	Outer	Middle	Outer	Inner	Middle	Outer
1	313.5	311.1	435.9	3.7725	3.8943	3.8739
2	294.4	277.8	434.9	3.9759	3.7977	3.8445
Number	Weight [N/m]	Loss [W/m]	Sag [m]			
1	23.39	56.6443	14.9284			
2	23.44	57.0540	14.9543			

Results with changed steel and aluminum lay lengths

Steel lay [mm]			Aluminum lay [mm]		
Number	Steel 1	Steel 2	Inner	Middle	Outer
1	194.1	273.6	327.6	273.2	450.7
2	161.7	278.5	317.7	325.6	438.5
Number	Weight [N/m]	Loss [W/m]	Sag [m]		
1	23.78	55.2813	15.0876		
2	23.73	55.7172	15.0756		

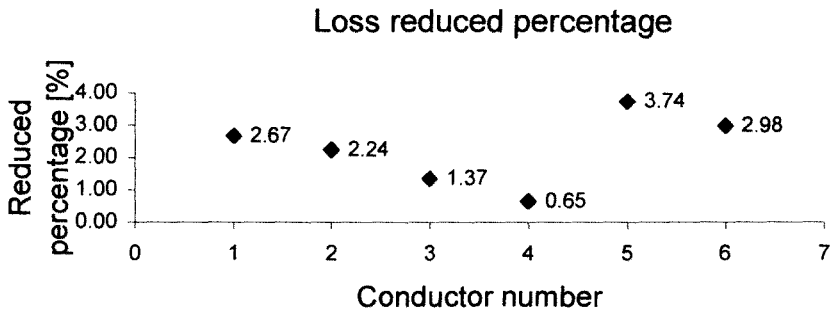

Figure C.1 Percentage of reduced loss compared to the reference

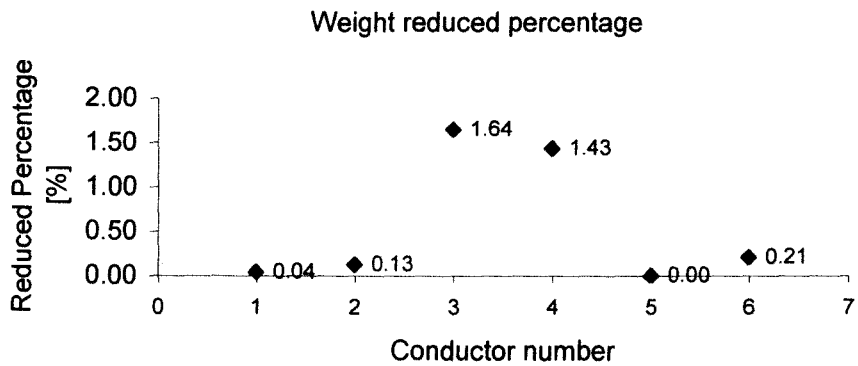

Figure C.2 Percentage of reduced weight compared to the reference

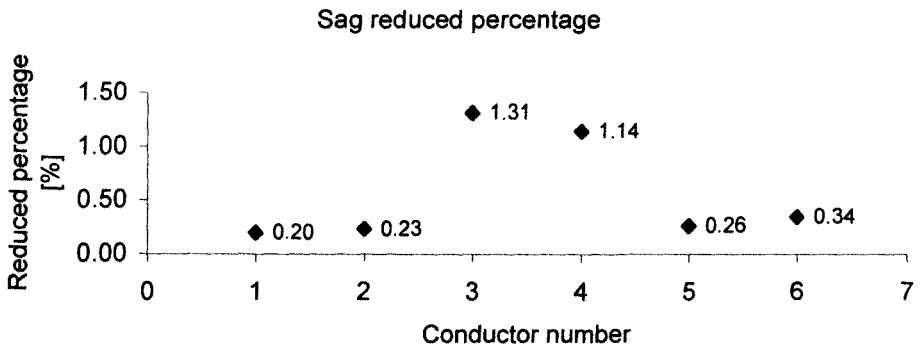

Figure C.3 Percentage of reduced sag compared to the reference

C.2 Fixing wire diameters and steel lay lengths, changing aluminum lay lengths

Table C.9 Unchanged wire and steel lay parameters

Steel wire diameter [mm]			Aluminum wire diameter [mm]		
Steel king	Steel lay 1	Steel lay 2	Inner	Middle	Outer
2.339	2.339	2.339	3.899	3.899	3.899
Steel layer outer diameter [mm]			Aluminum layer outer diameter [mm]		
Steel king	Steel lay 1	Steel lay 2	Inner	Middle	Outer
2.339	7.017	11.695	19.493	27.291	35.089
Steel lay length [mm]			Aluminum lay length [mm]		
Steel king	Steel lay 1	Steel lay 2	Inner	Middle	Outer
1000.0	175.451	233.934	Changed	Changed	Changed

Table C.10 Changed aluminum lay lengths

Conductor number	Inner [mm]	Middle [mm]	Outer [mm]	Weight [N/m]
Conductor 1	331.4	272.9	456.2	23.78
Conductor 2	303.8	302.7	377.5	23.83
Conductor 3	279.3	362.8	394.5	23.77
Conductor 4	252.4	389.5	366.1	23.80
Conductor 5	202.1	411.1	370.4	23.83
Conductor 6	194.9	436.7	350.9	23.85

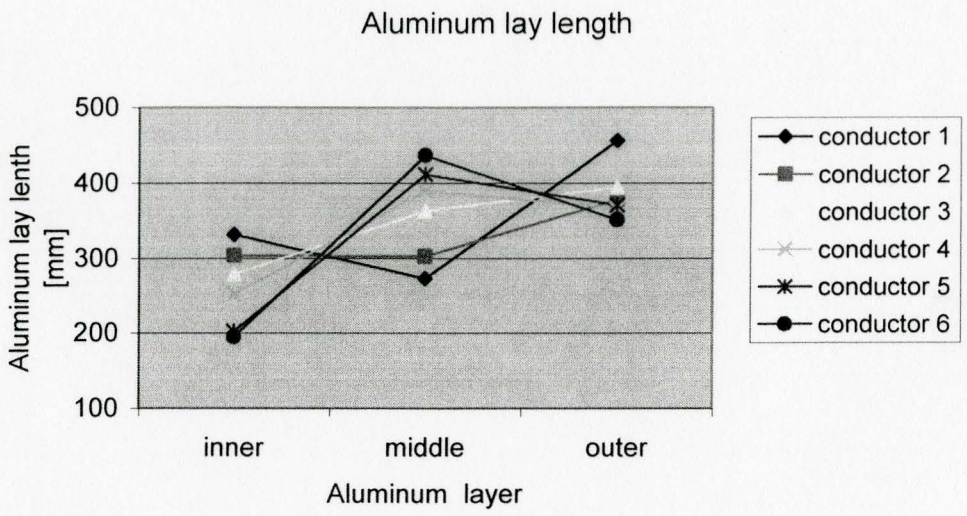

Figure C.4 Changed lay lengths with fixed wire diameters

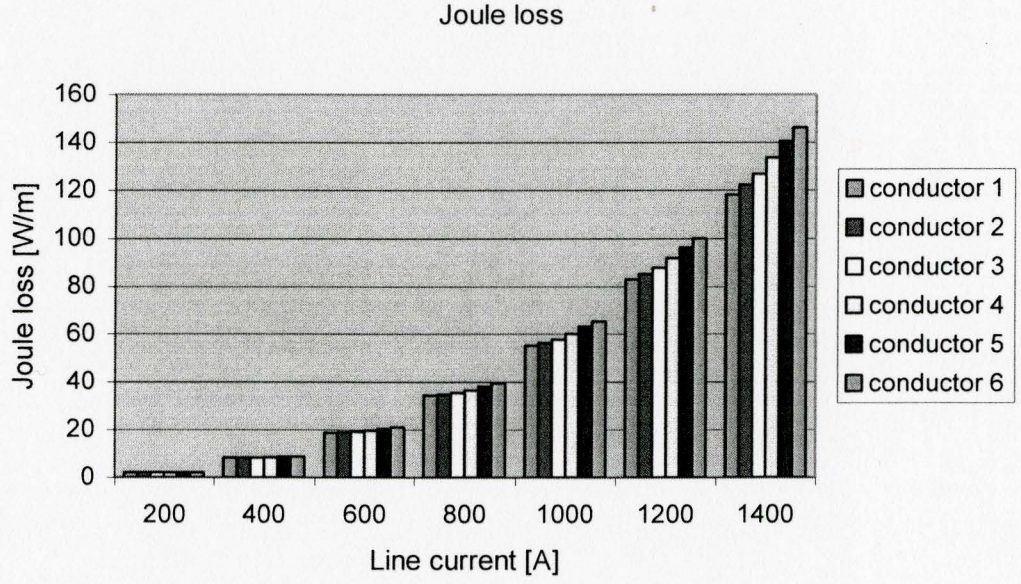

Figure C.5 Variation of Joule losses in six conductors at various line currents

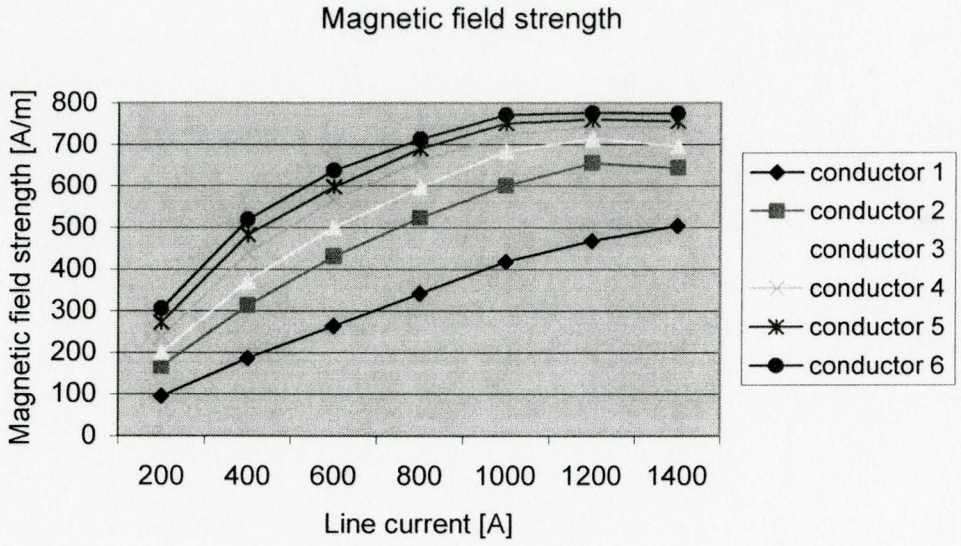

Figure C.6 Variation of six-conductor magnetic field strength at various line currents

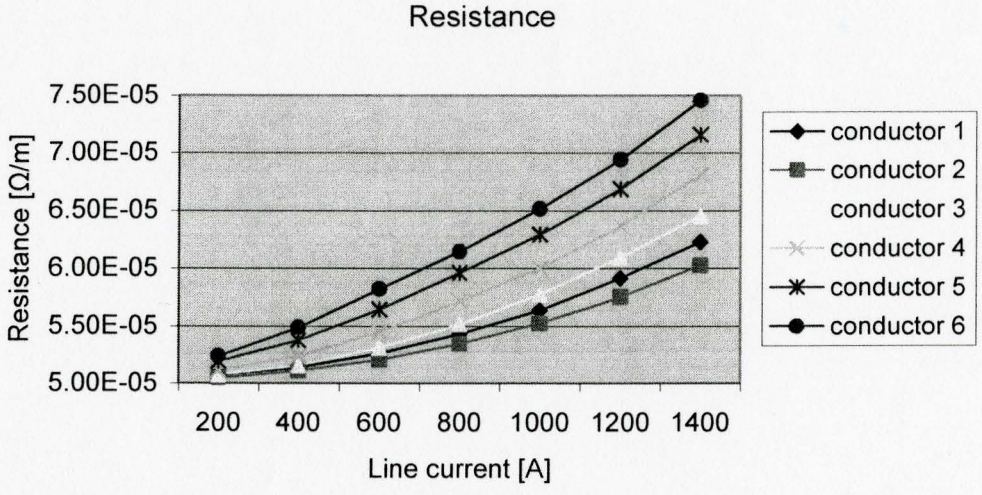

Figure C.7 Variation of resistance in six conductors at various line currents

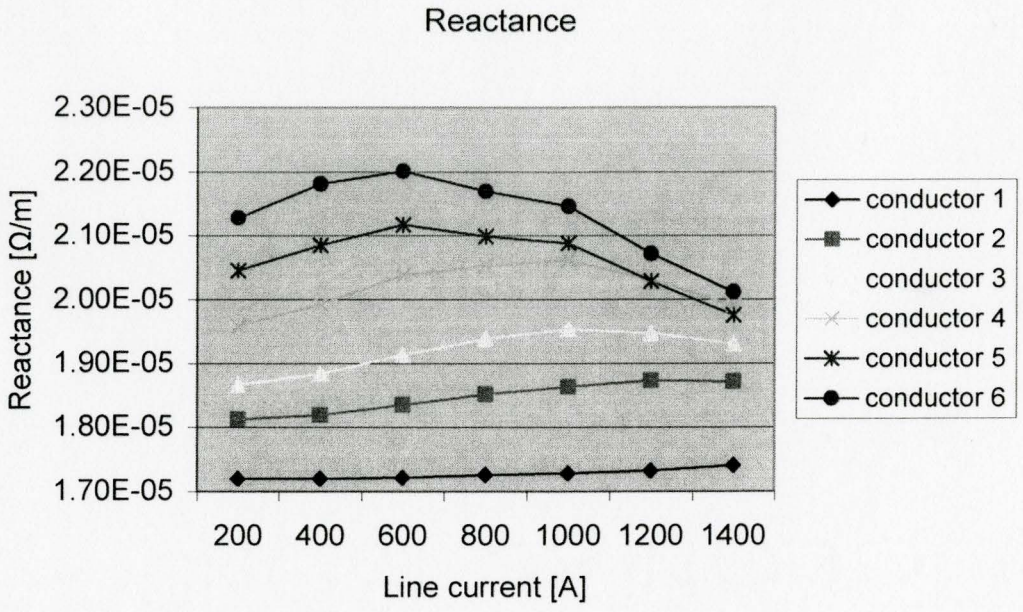

Figure C.8 Variation of reactance in six conductors at various line currents

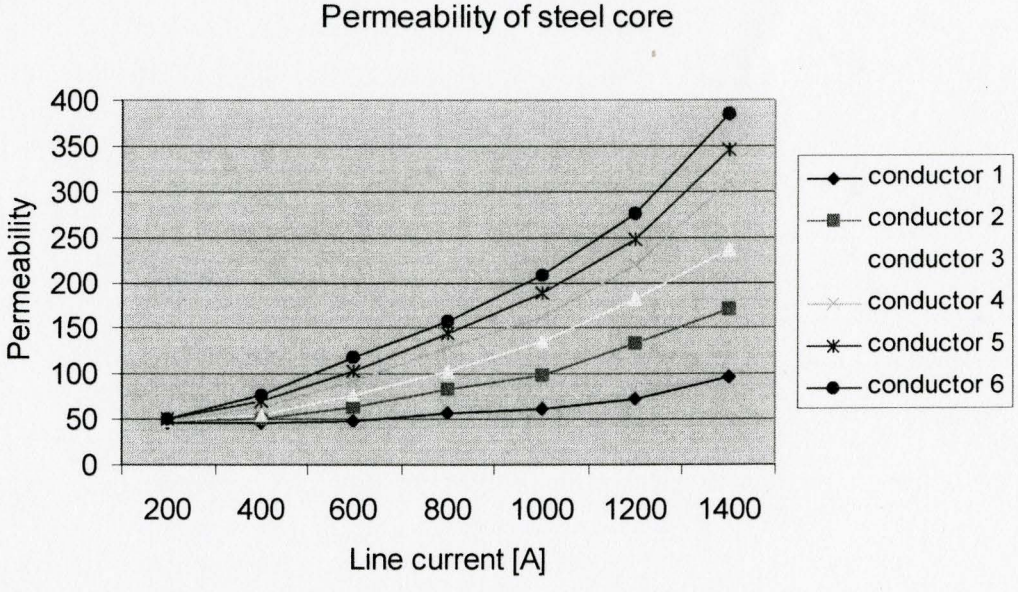

Figure C.9 Variation of the permeability at various line currents

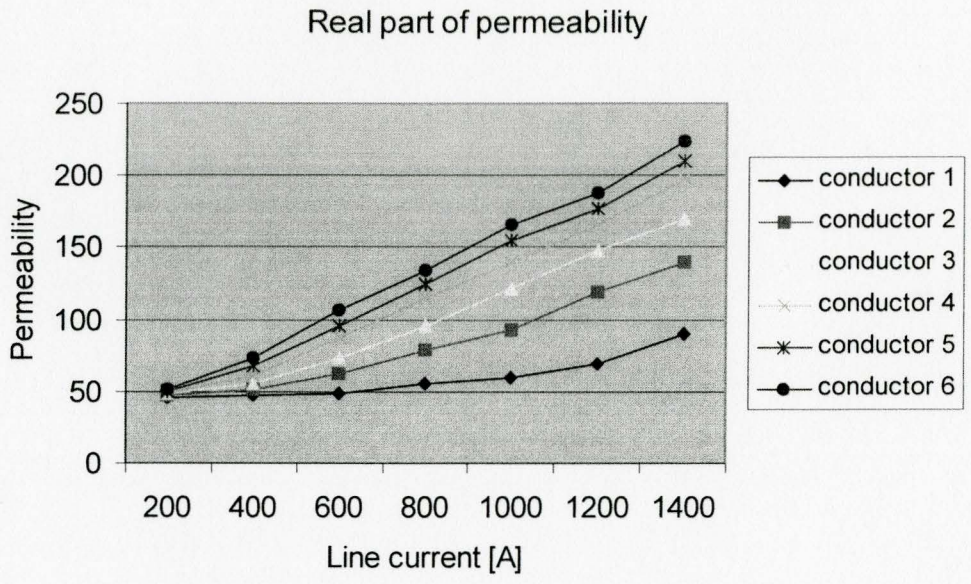

Figure C.10 Variation of real part of the permeability at various line currents

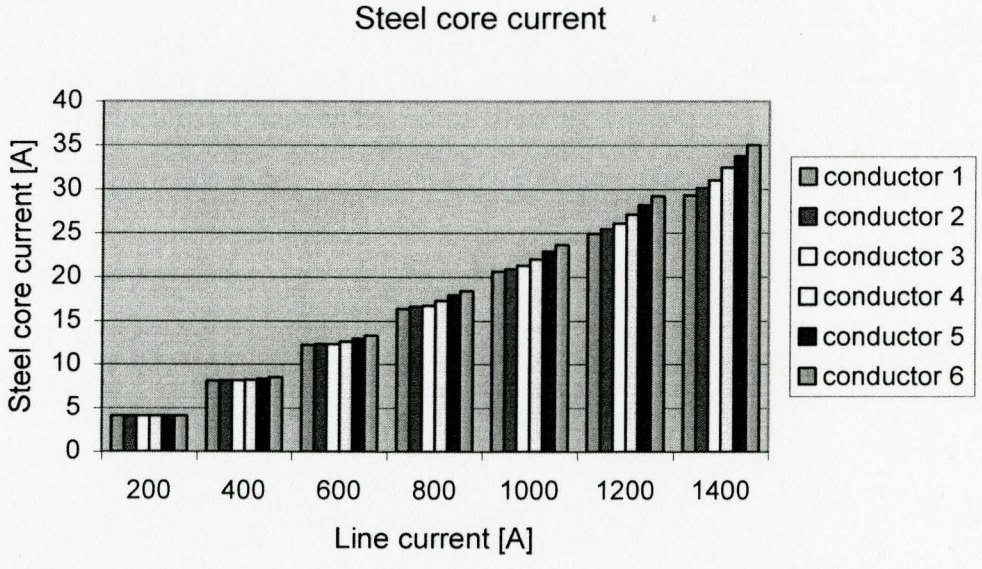

Figure C.11 Variation of steel core current at various line currents

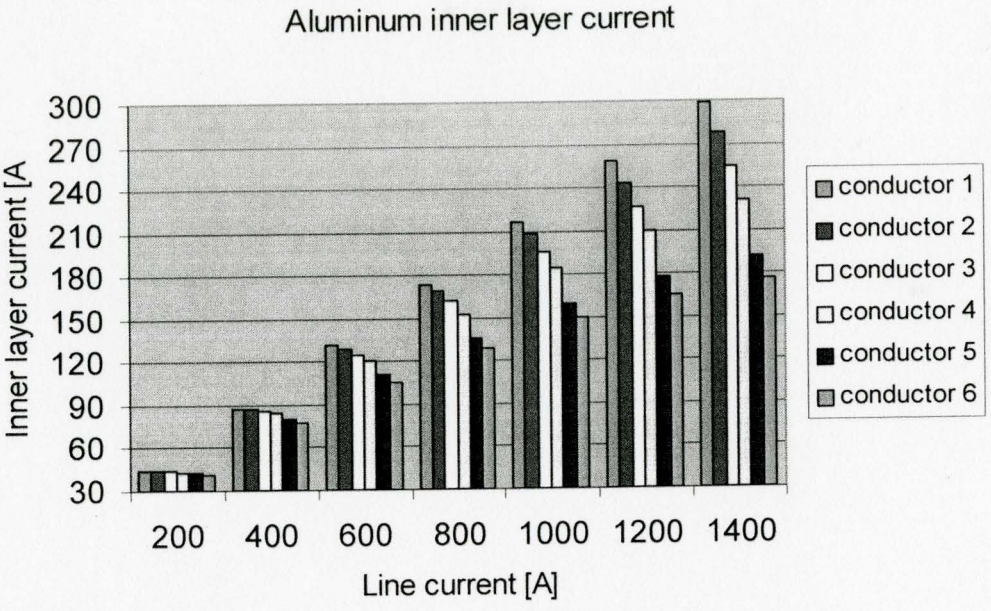

Figure C.12 Variation of aluminum inner layer current at various line currents

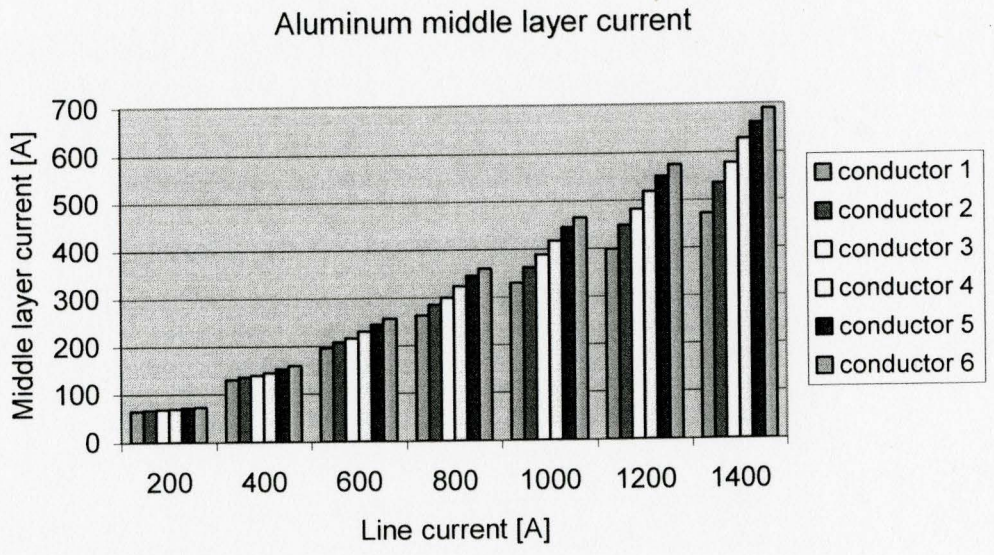

Figure C.13 Variation of aluminum middle layer current at various line currents

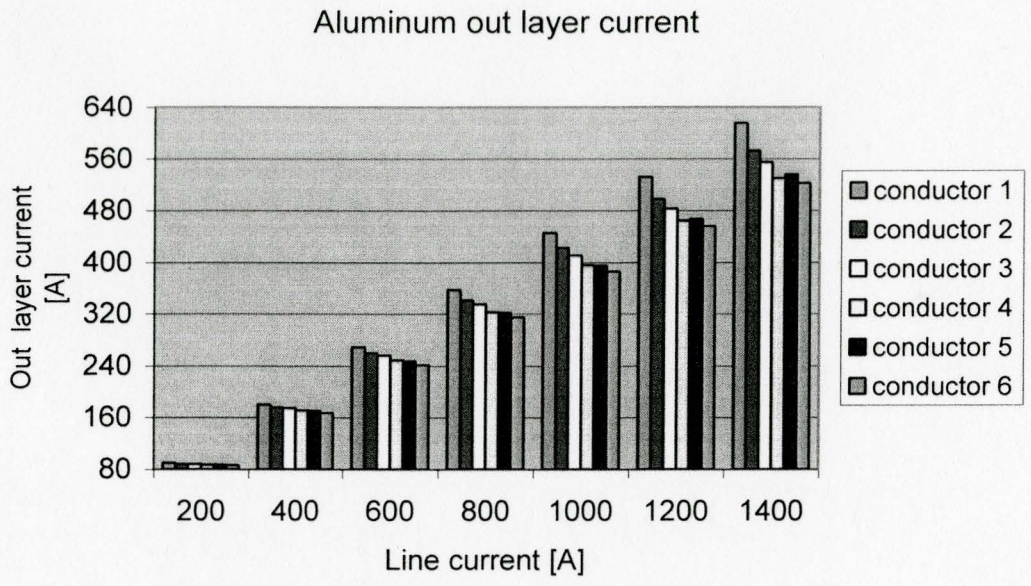

Figure C.14 Variation of aluminum outer layer current at various line currents

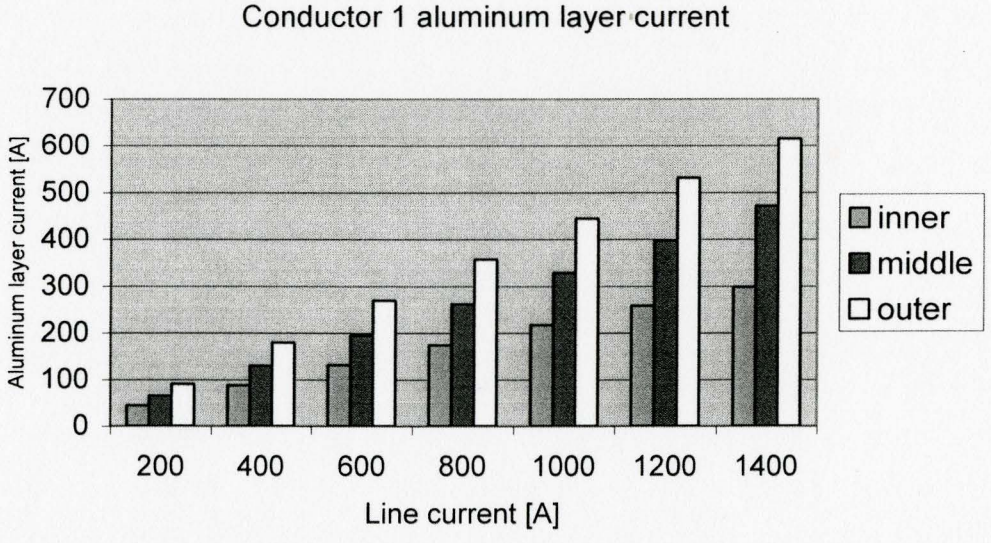

Figure C.15 Variation of three aluminum layer currents in conductor 1 at various line currents

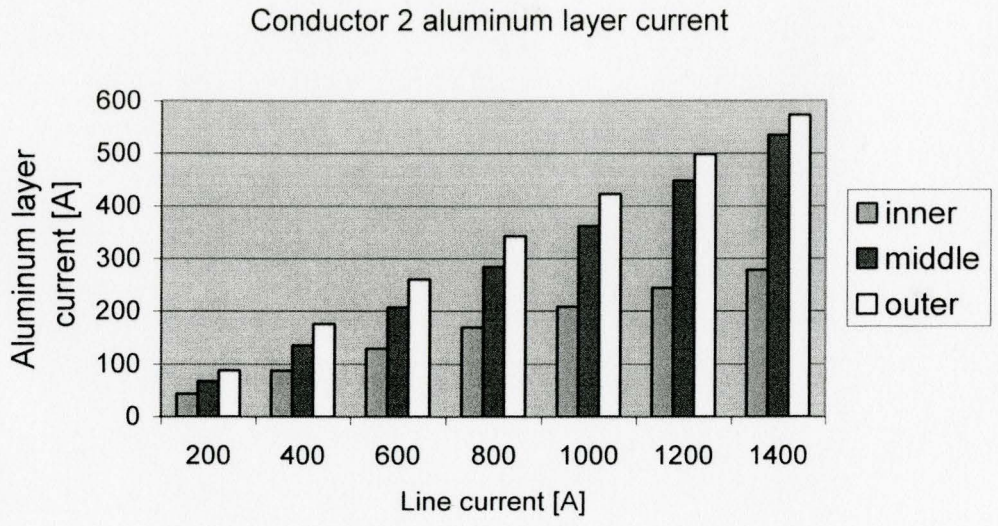

Figure C.16 Variation of aluminum layer currents in conductor 2 at various line currents

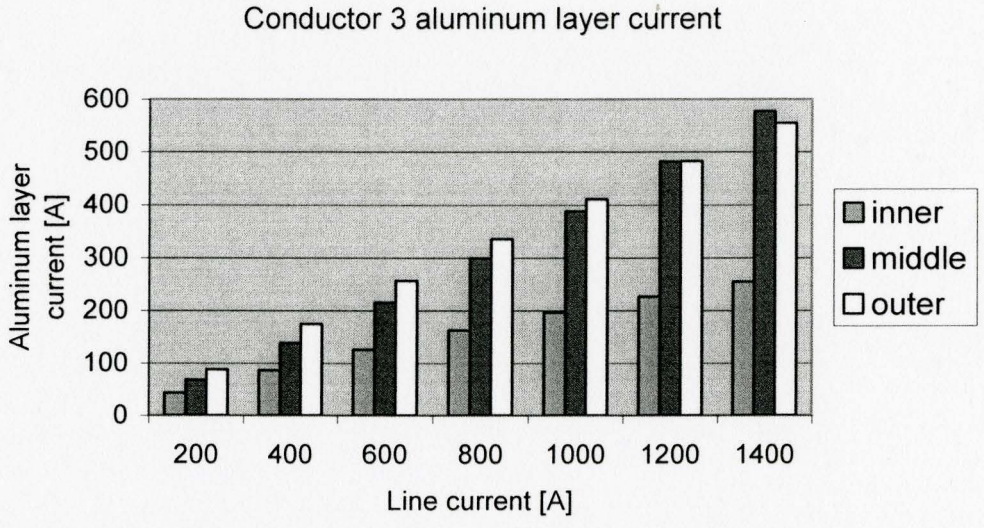

Figure C.17 Variation of aluminum layer currents in conductor 3 at various line currents

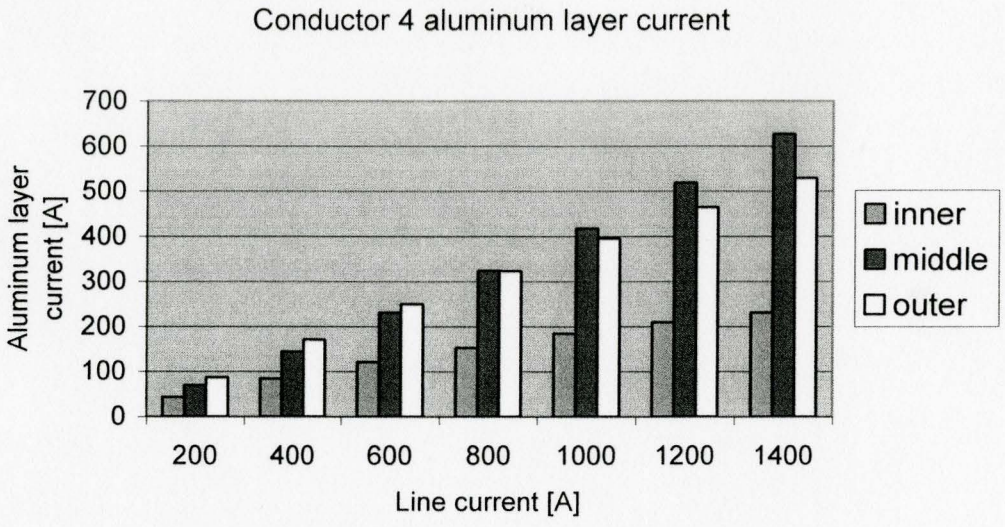

Figure C.18 Variation of three aluminum layer currents in conductor 4 at various line currents

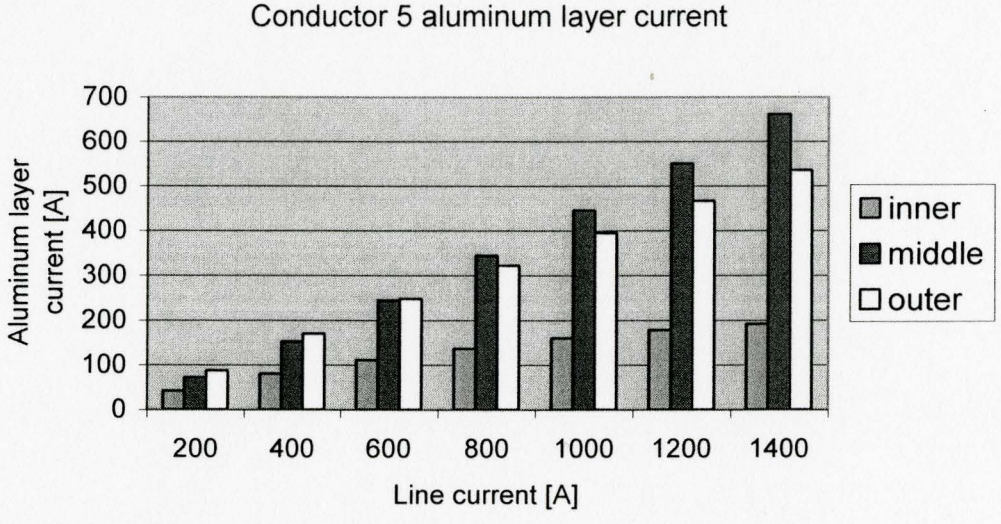

Figure C.19 Variation of aluminum layer currents in conductor 5 at various line currents

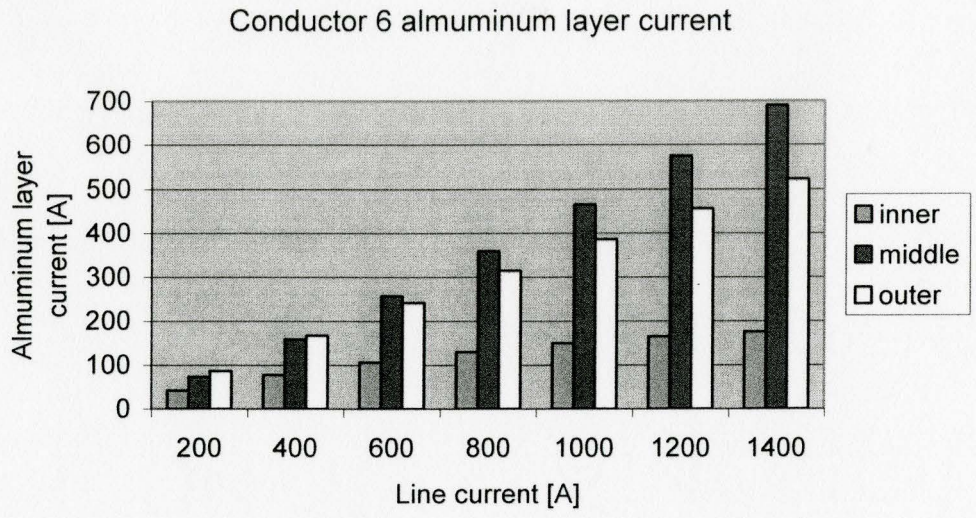

Figure C.20 Variation of aluminum layer currents in conductor 6 at various line currents

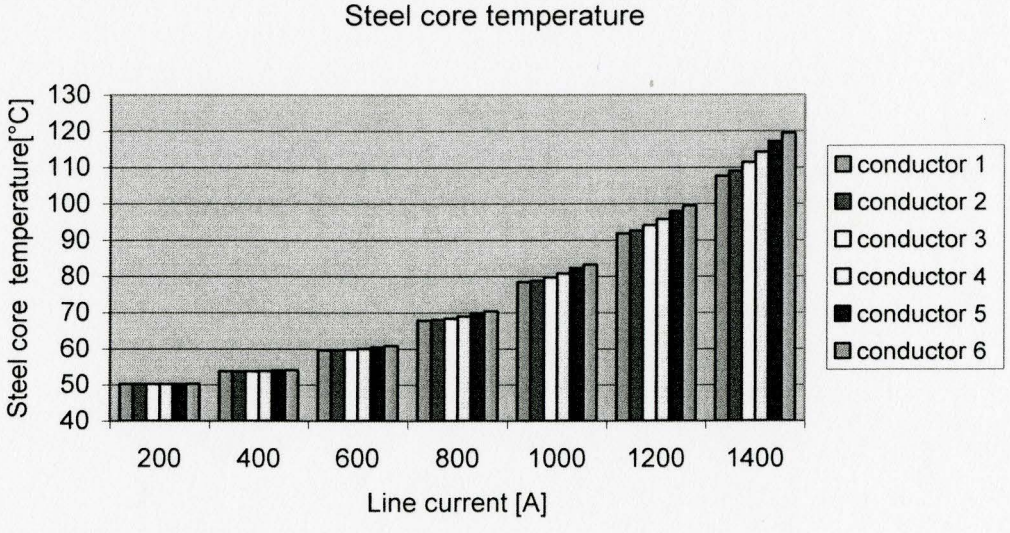

Figure C.21 Variation of steel king layer temperature at various line currents

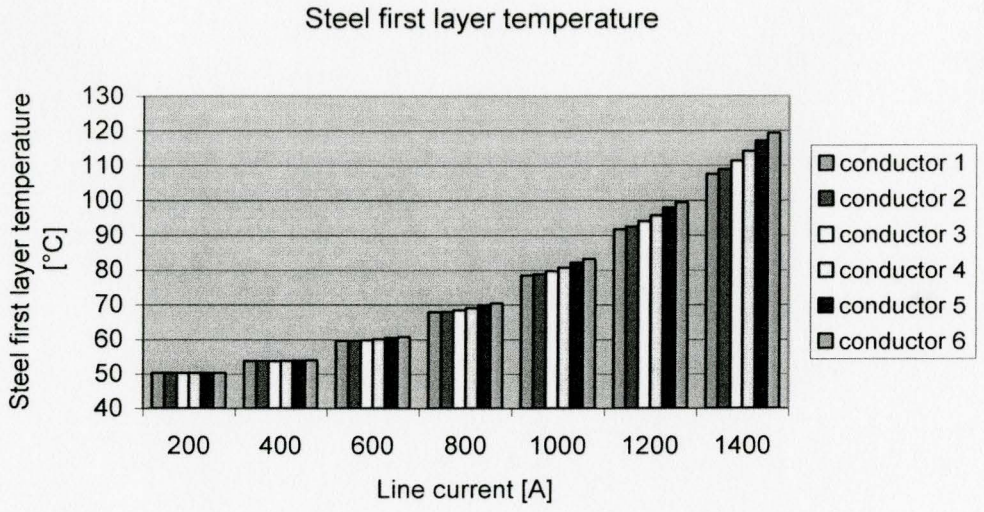

Figure C.22 Variation of steel first layer temperature at various line currents

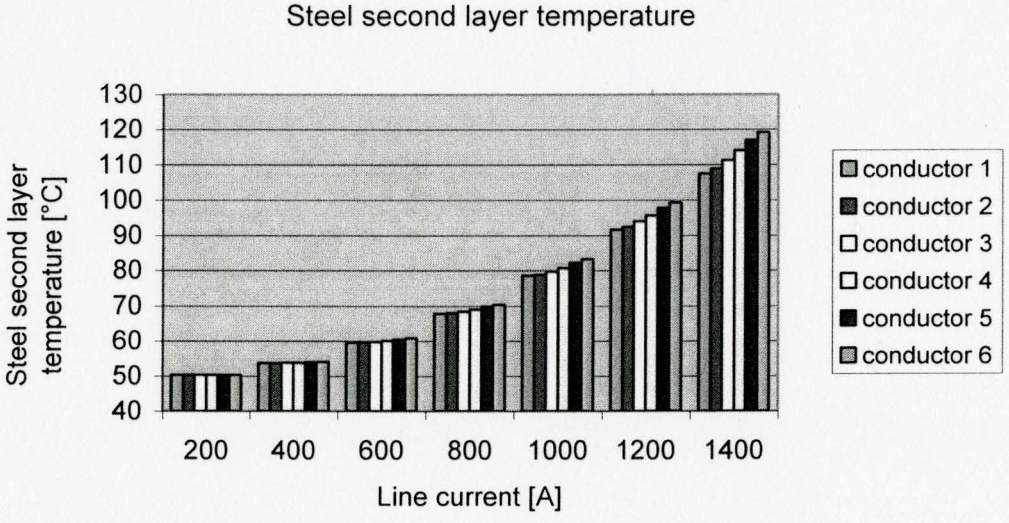

Figure C.23 Variation of steel second layer temperature at various line currents

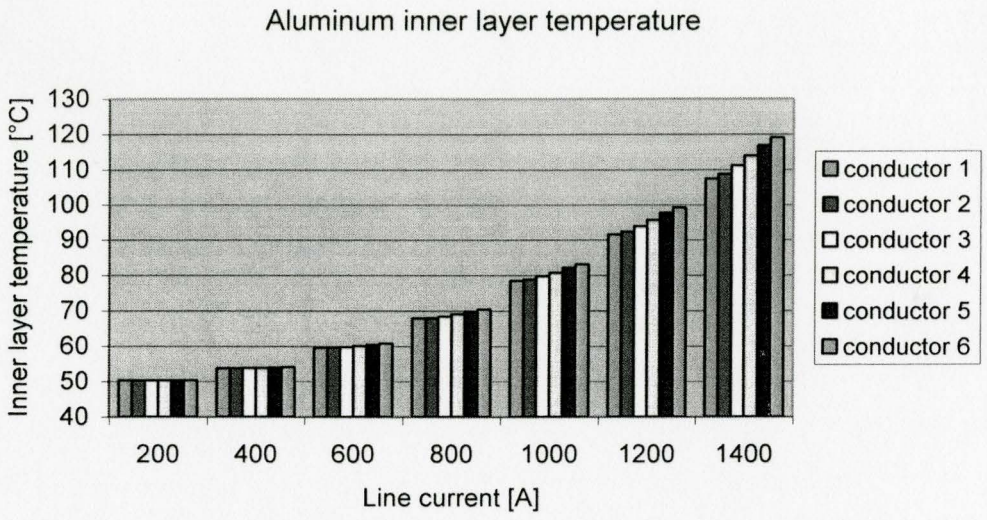

Figure C.24 Variation of aluminum inner layer temperature at various line currents

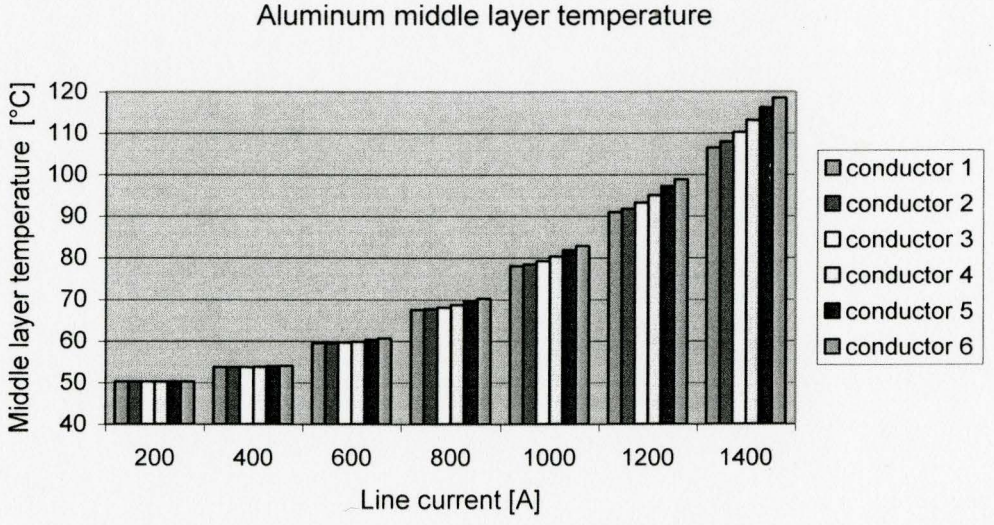

Figure C.25 Variation of aluminum middle layer temperature at various line currents

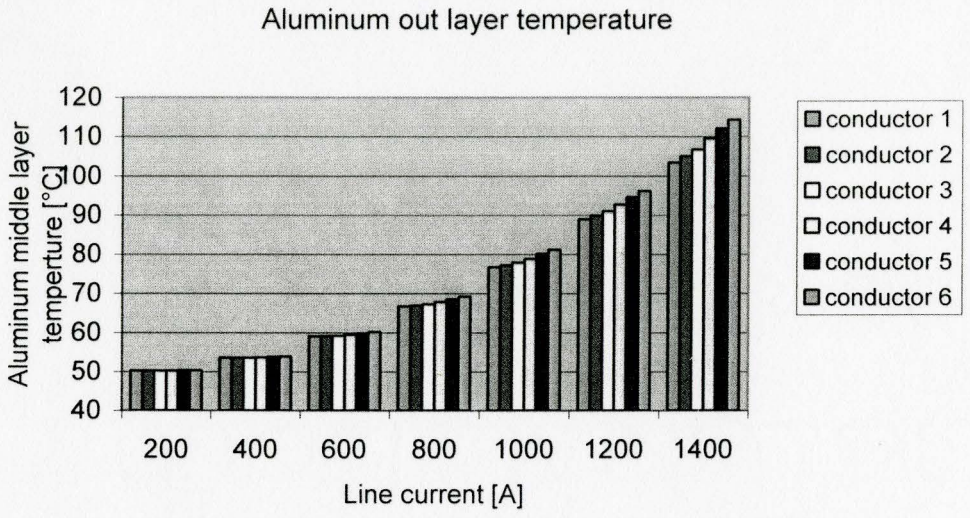

Figure C.26 Variation of aluminum outer layer temperature at various line currents

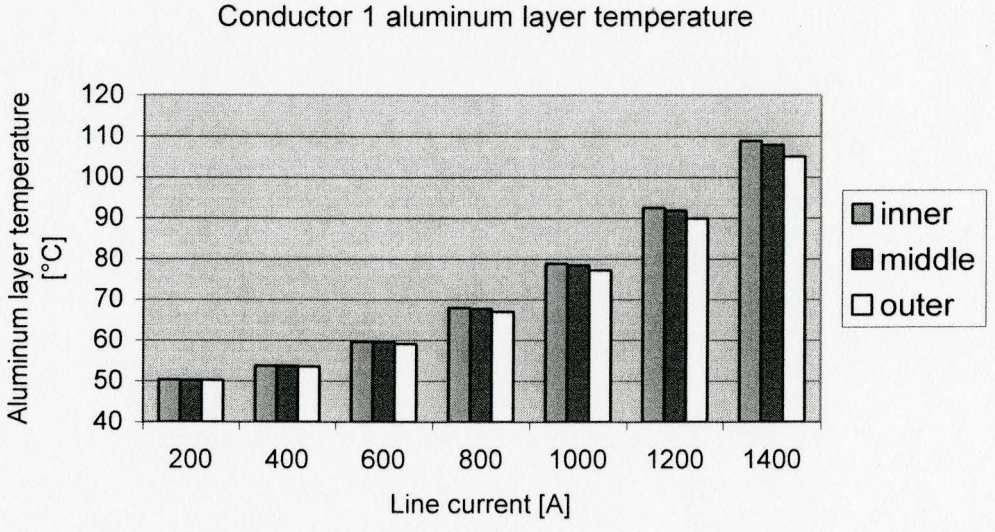

Figure C.27 Variation of aluminum layer temperature in conductor 1 at various line currents

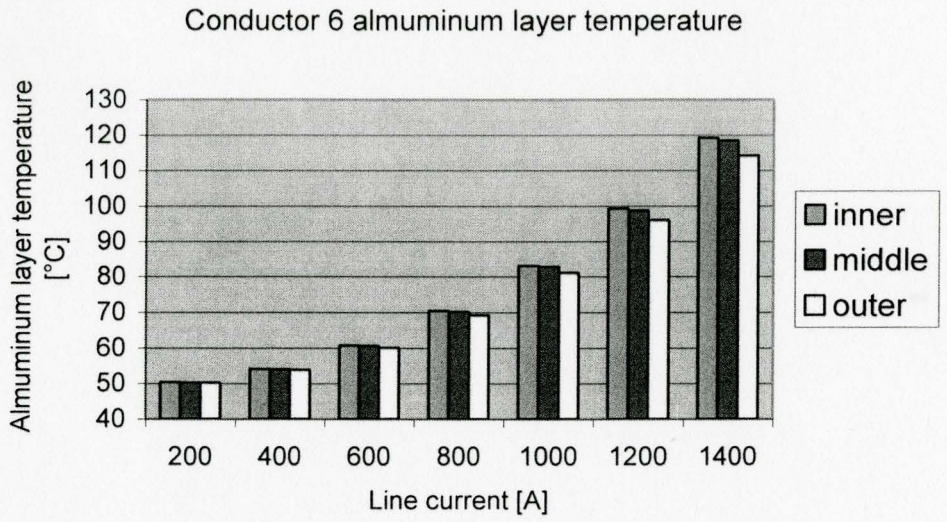

Figure C.28 Variation of aluminum layer temperature in conductor 6 at various line currents

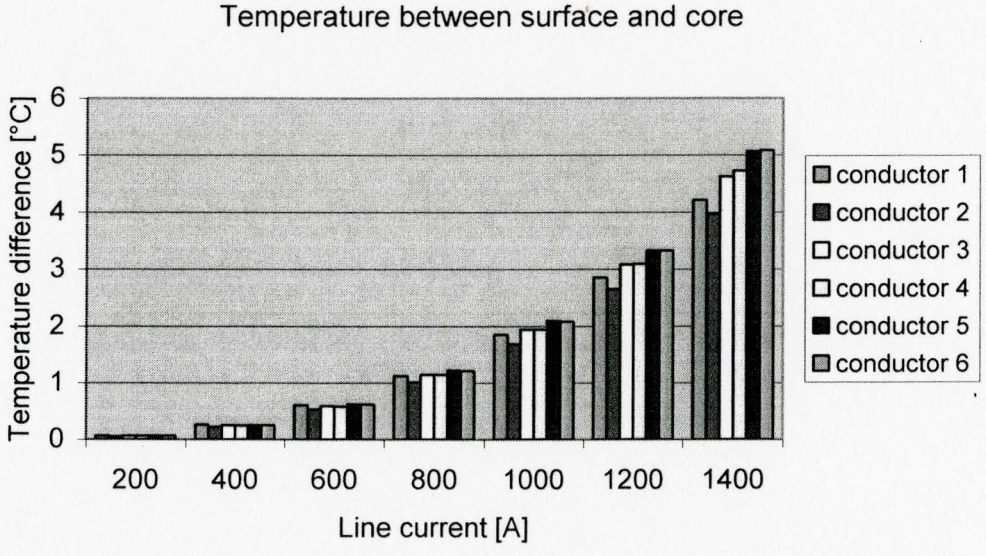

Figure C.29 Temperature differences between steel core and conductor surface

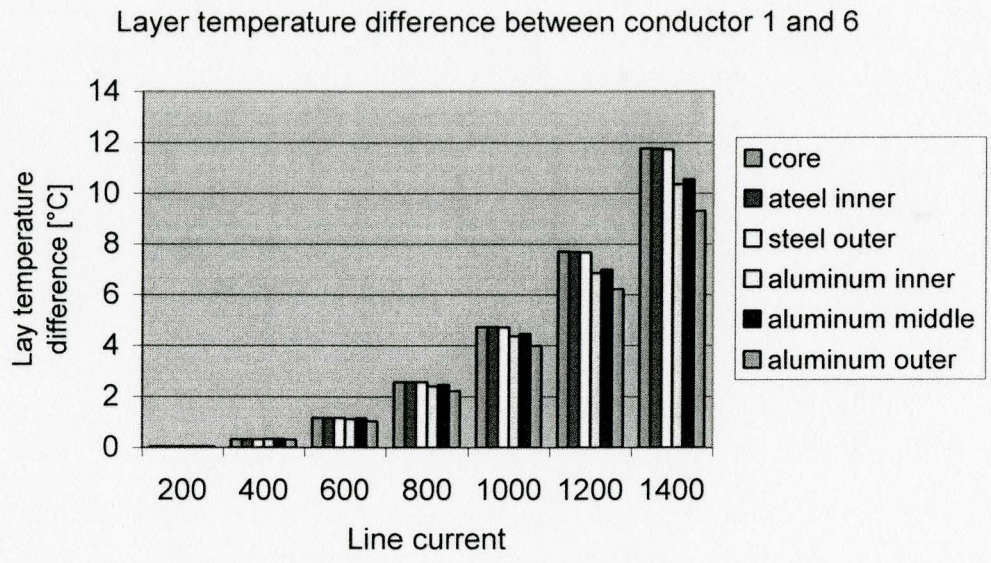

Table C.30 Temperature differences in layers between conductor 1 and 6

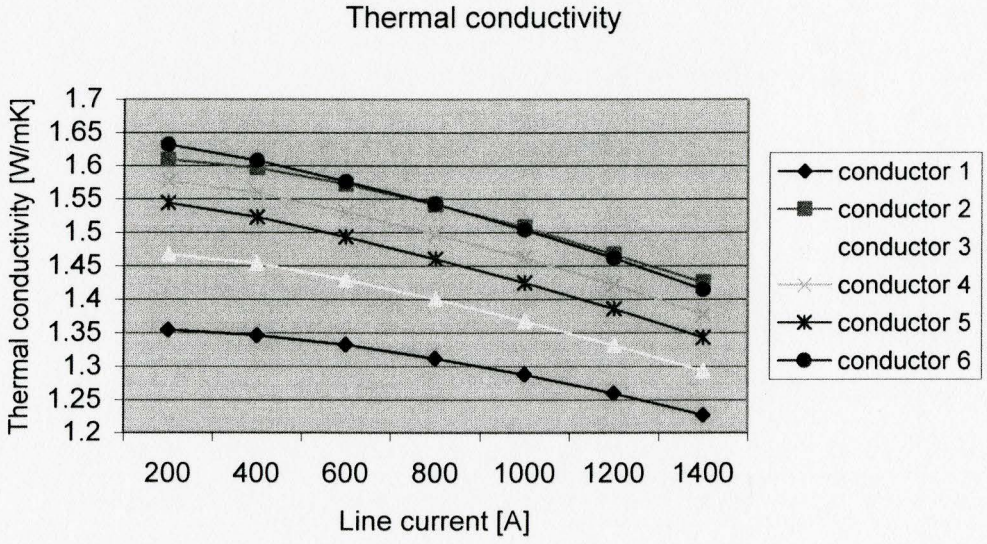

Figure C.31 Variation of the thermal conductivity at various line currents

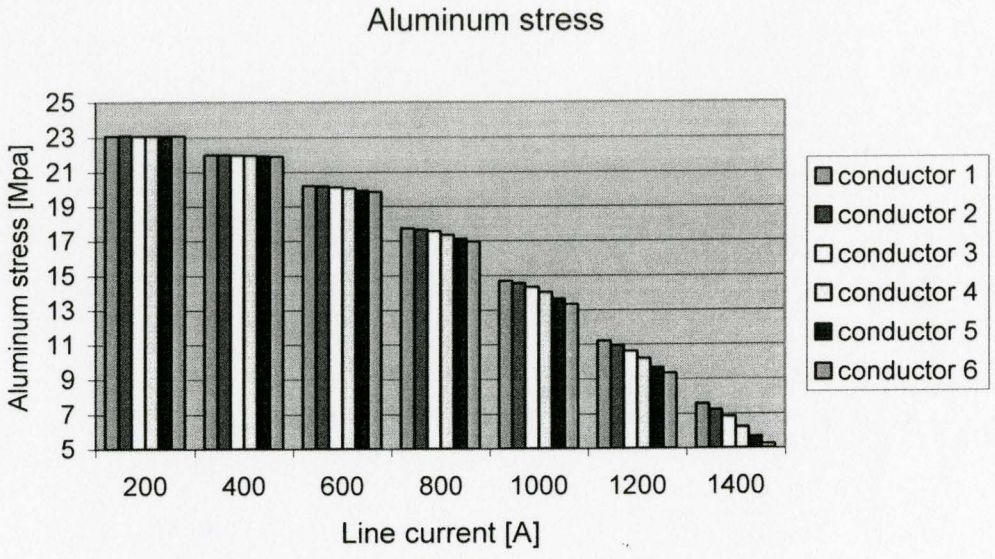

Figure C.32 Variation of aluminum stresses at various line currents

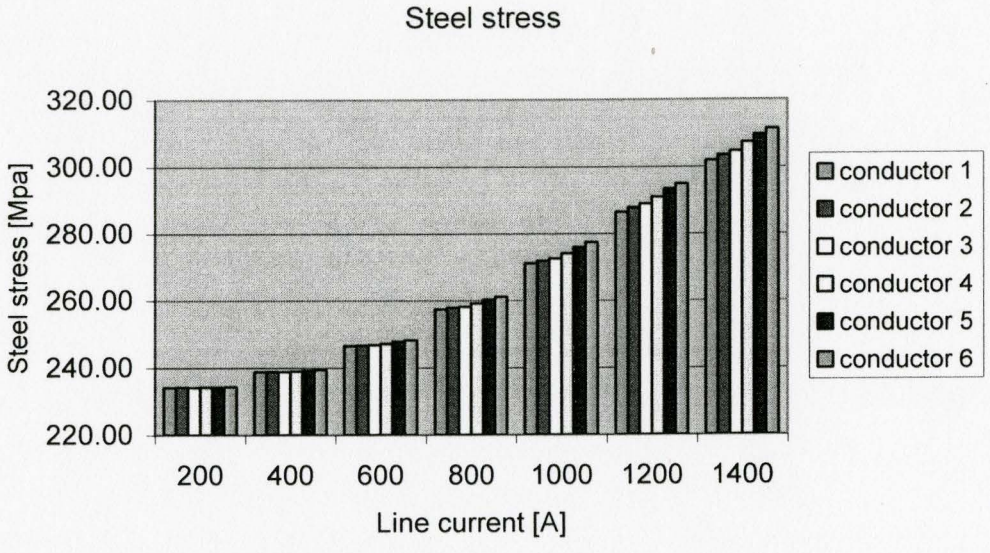

Figure C.33 Variation of steel stresses at various line currents

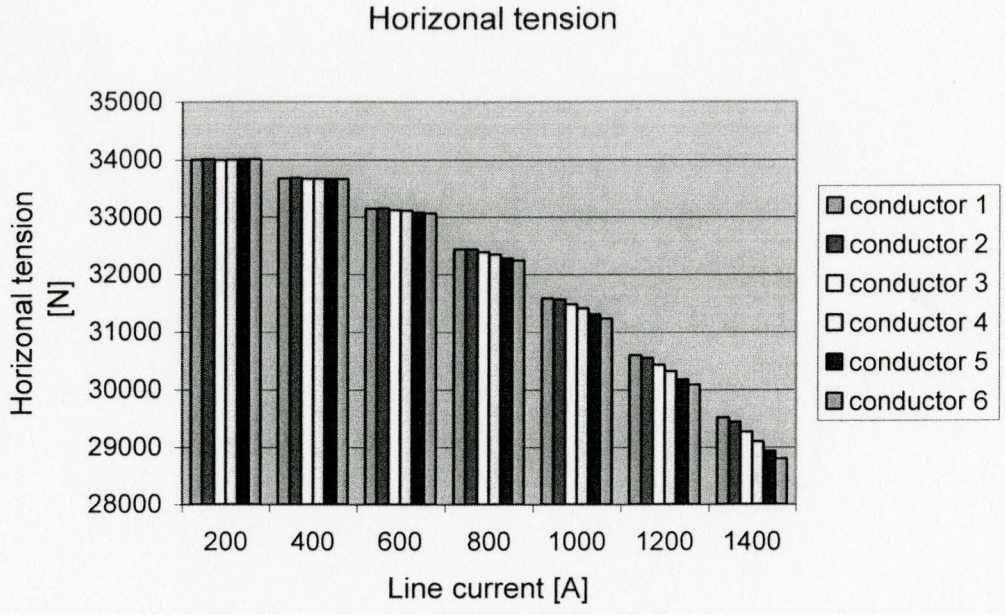

Figure C.34 variation of horizontal tension at various line currents

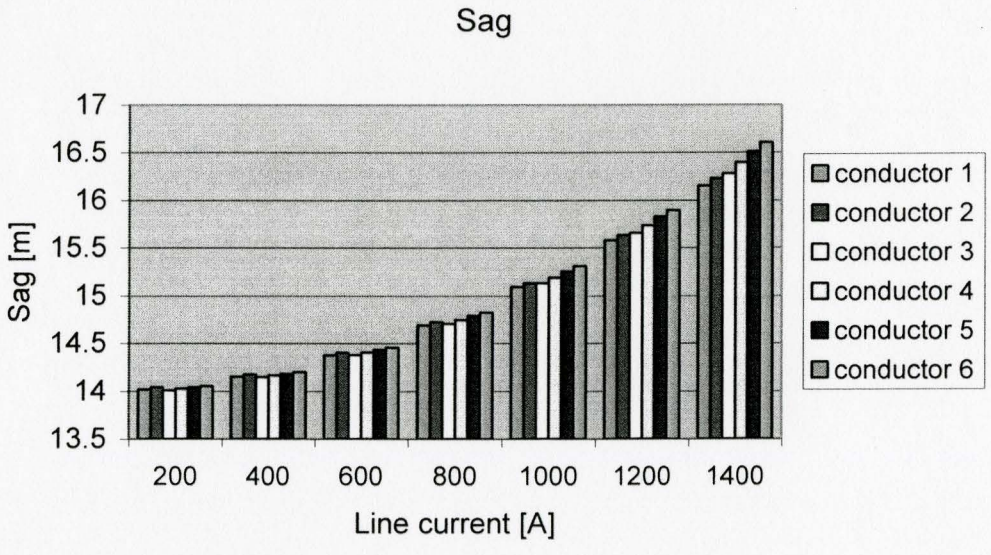

Figure C.35 Variation of sags at various line currents with line length 400 meters

C.3 Fixing wire diameters, changing steel and aluminum lay lengths

Table C.11 Unchanged steel wire and aluminum wire diameters

Steel wire diameter [mm]			Aluminum wire diameter [mm]		
King	Steel lay 1	Steel lay 2	Inner	Middle	Outer
2.339	2.339	2.339	3.899	3.899	3.899
Steel layer's outer diameters [mm]			Aluminum layer's outer diameters [mm]		
Steel lay 1	Steel lay 2	Steel lay 3	Inner	Middle	Outer
2.339	7.017	11.695	19.493	27.291	35.089

Table C.12 Changed steel and aluminum lay lengths

Steel lay length [mm]			Aluminum lay length [mm]		
	Steel lay 1	Steel lay 2	Inner	Middle	Outer
Conductor 1	210.5	280.7	331.4	272.9	456.2
Conductor 2	187.3	265.7	260.8	304.2	371.4
Conductor 3	205.6	258.0	279.3	362.8	394.5
Conductor 4	203.1	264.7	252.4	389.5	366.1
Conductor 5	202.2	246.9	202.1	411.1	370.4
Conductor 6	126.3	187.1	194.9	436.7	350.9
Weight [N/m]					
Conductor 1	Conductor 2	Conductor 3	Conductor 4	Conductor 5	Conductor 6
23.77	23.85	23.76	23.80	23.82	23.88

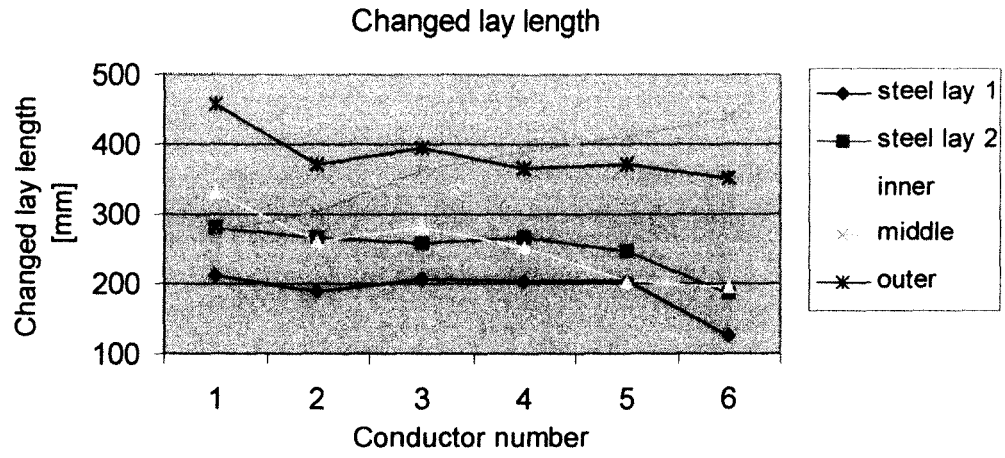

Figure C.36 Variation of lay length for different conductors at 1000 A

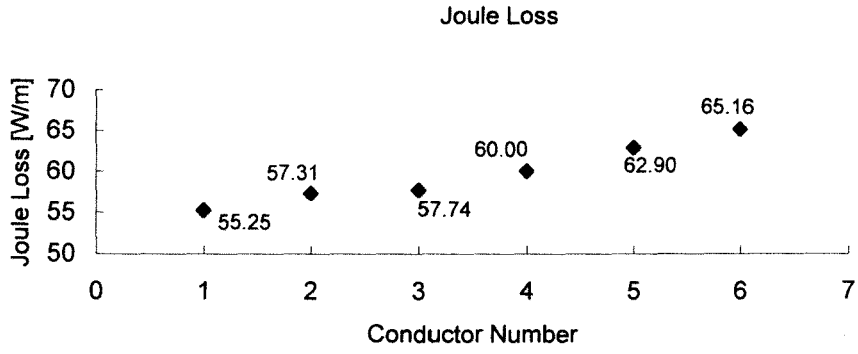

Figure C.37 Variation of Joule losses for different conductors at 1000A

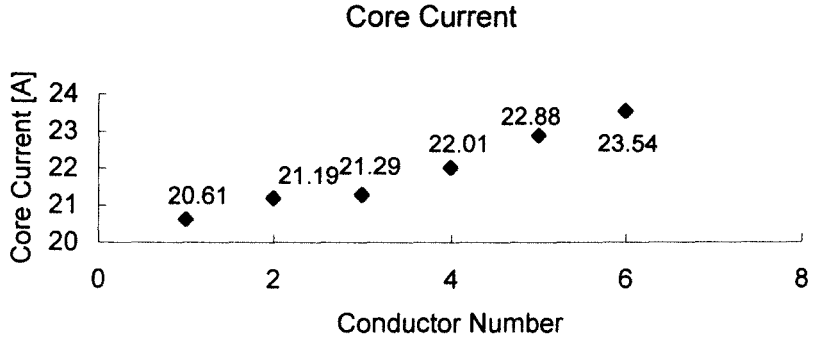

Figure C.38 Variation of core current for different conductors at 1000A

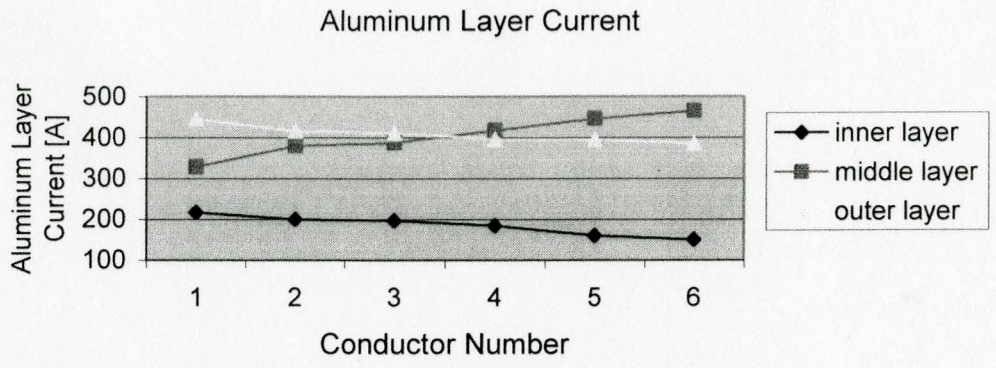

Figure C.39 Variation of aluminum current for different conductors at 1000A

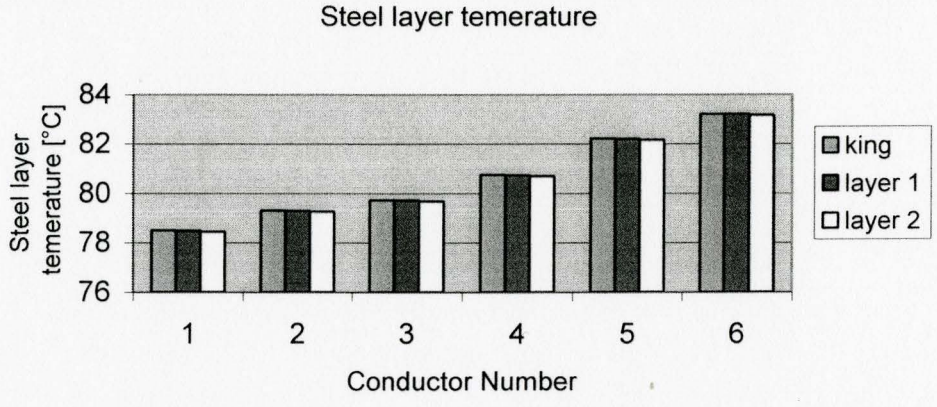

Figure C.40 Variation of steel layer temperature for different conductors at 1000A

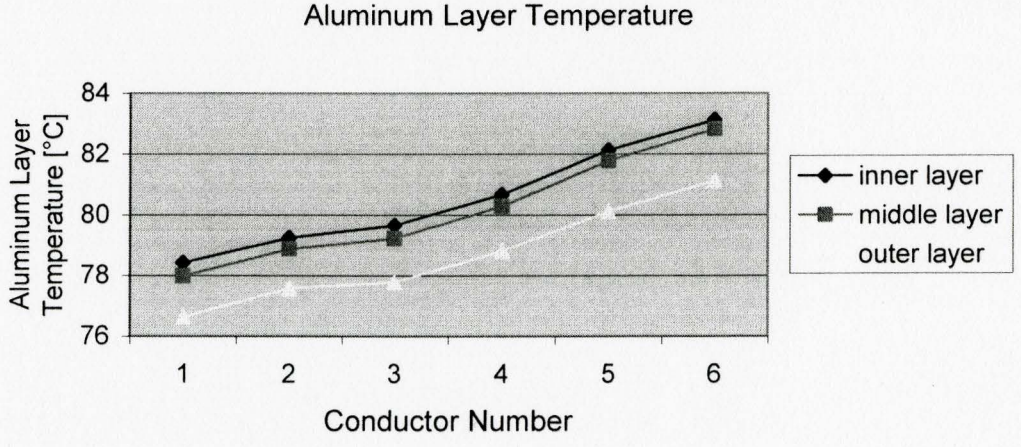

Figure C.41 Variation of aluminum layer temperature for different conductors at 1000A

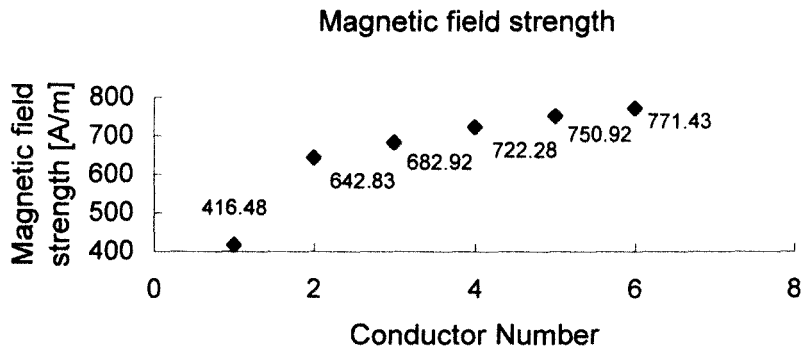

Figure C.42 Variation of magnetic field strength for different conductors at 1000A

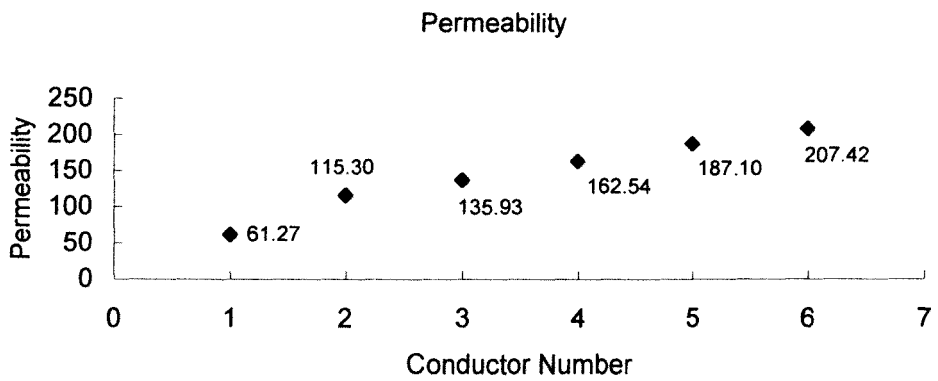

Figure C.43 Variation of permeability for different conductors in 1000A

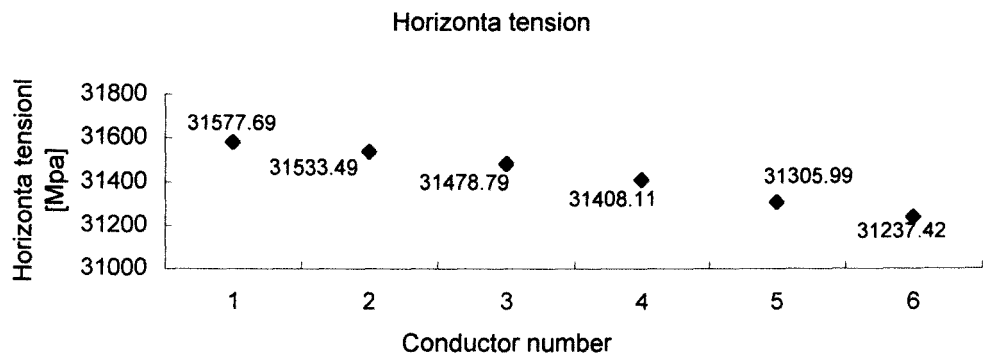

Figure C.44 Variation of horizontal tension for different conductors at 1000A

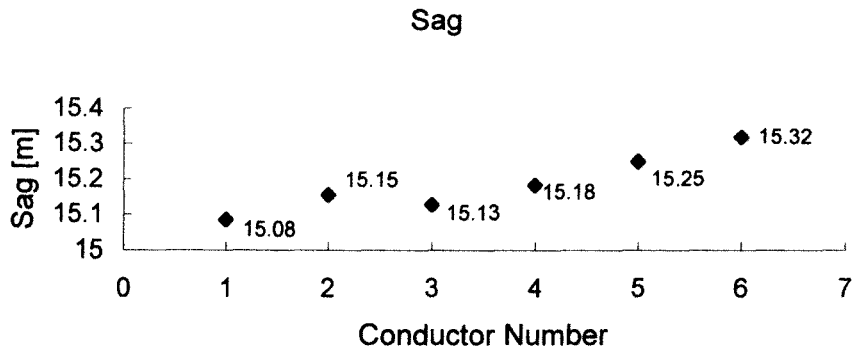

Figure C.45 Variation of sags for different conductors at 1000A

C.4 Fixing steel core size, changing aluminum lay lengths and wire diameters

Table C.13 Changed aluminum wire and layer parameters

	Wire diameter [mm]			Aluminum lay length [mm]		
	Inner	Middle	Outer	Inner	Middle	Outer
Conductor 1	4.05	4.05	4.05	331.4	272.9	456.2
Conductor 2	3.945	4.033	3.793	292.6	323.0	433.9
Conductor 3	3.903	3.782	3.938	258.2	323.4	387.8
Conductor 4	3.909	3.803	3.783	269.7	380.2	381.6
Conductor 5	3.974	3.844	3.772	200.1	425.4	351.6
Conductor 6	3.75	3.75	3.75	194.9	436.7	350.9
	Outer diameter [mm]					
	Inner	Middle	Outer	Weight [N/m]		
Conductor 1	19.795	27.895	35.995	25.18		
Conductor 2	19.586	27.653	35.238	23.84		
Conductor 3	19.502	27.065	34.941	23.63		
Conductor 4	19.512	27.119	34.684	23.05		
Conductor 5	19.644	27.332	34.877	23.34		
Conductor 6	19.195	26.695	34.195	22.52		

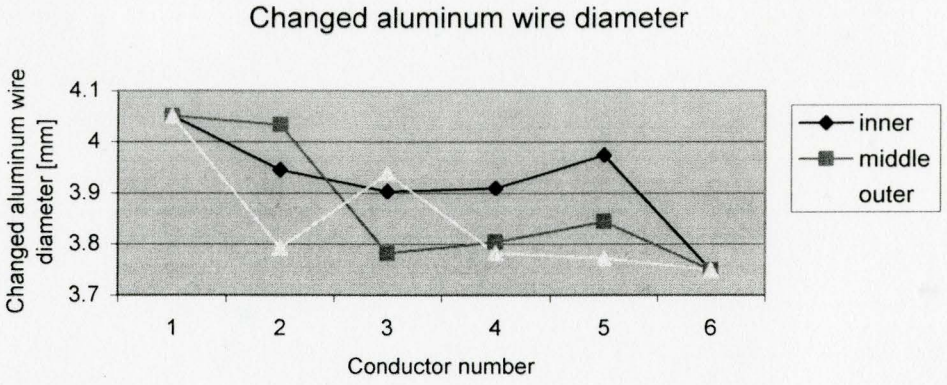

Figure C.46 Changed aluminum diameters at 1000A

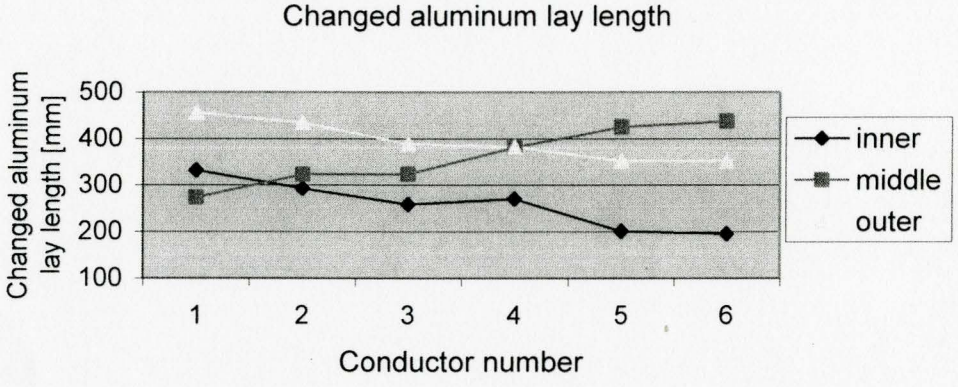

Figure C.47 Changed aluminum lay lengths at 1000A

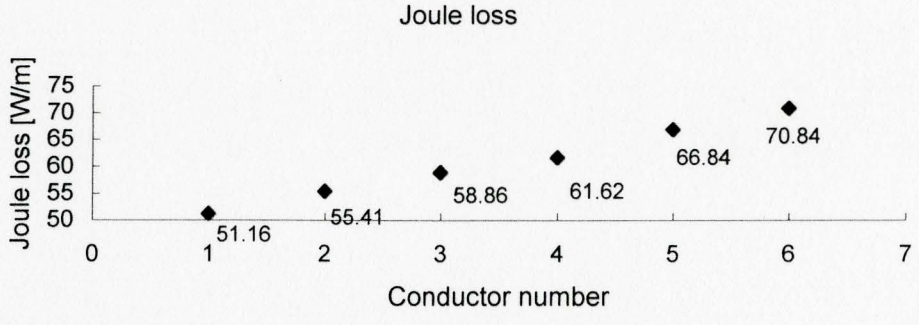

Figure C.48 Variation of Joule losses among conductors at 1000A

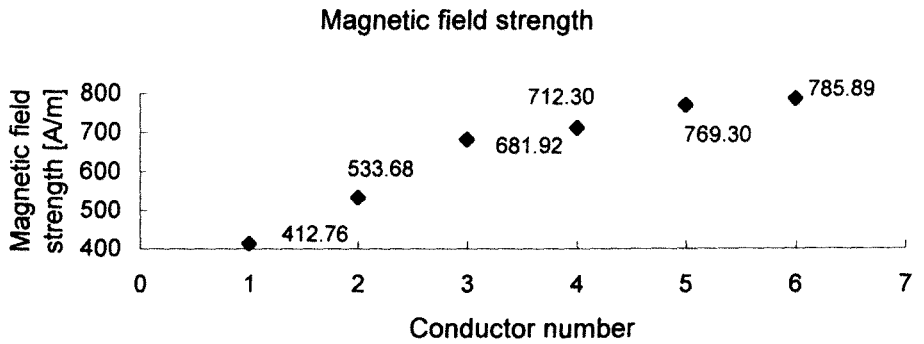

Figure C.49 Variation of magnetic strength among conductors at 1000A

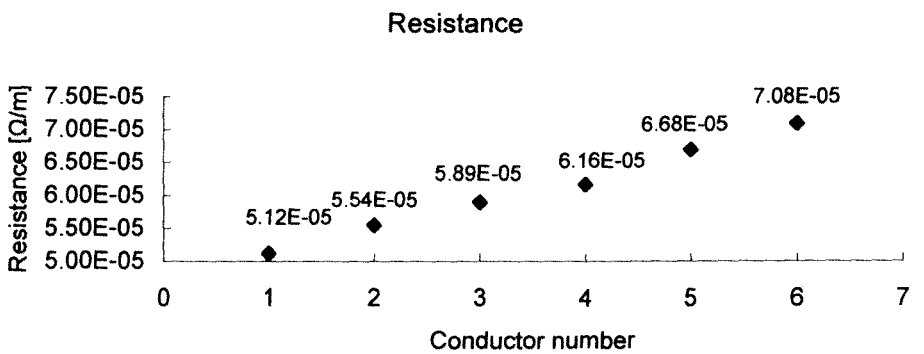

Figure C.50 Variation of resistance among conductors at 1000A

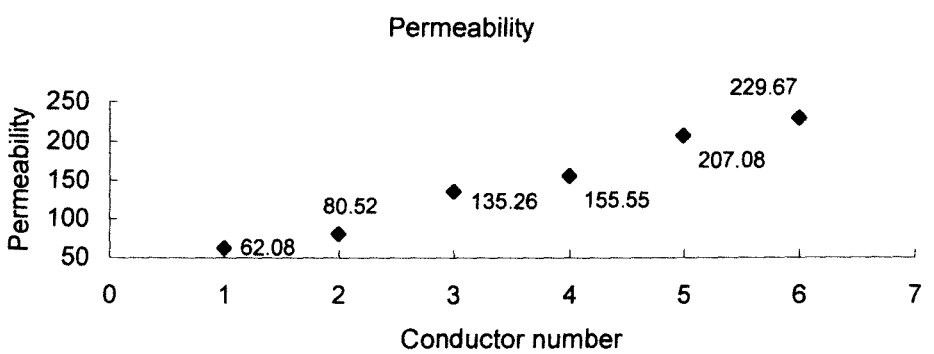

Figure C.51 Variation of permeability among conductors at 1000A

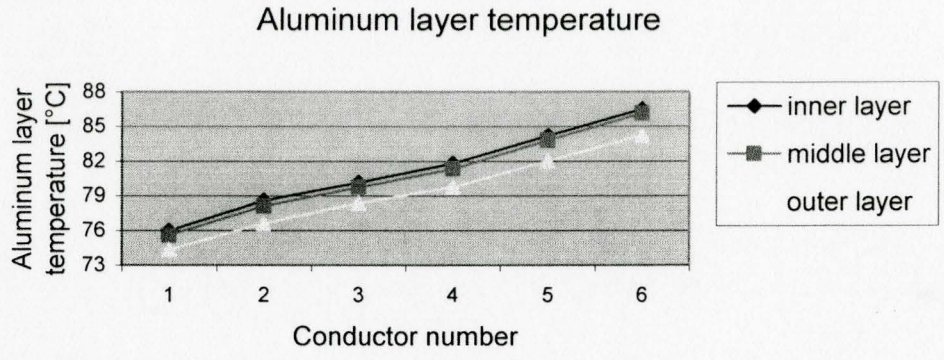

Figure C.52 Variation of aluminum layer temperature among conductors at 1000A

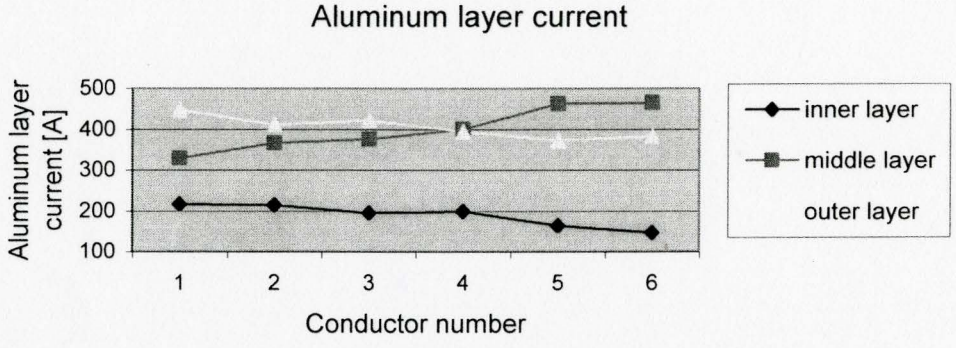

Figure C.53 Variation of aluminum layer current among conductors at 1000A

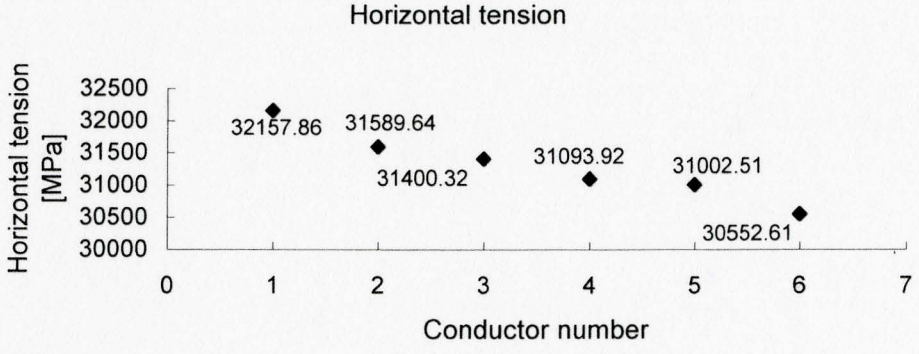

Figure C.54 Variation of horizontal tension among conductors at 1000A

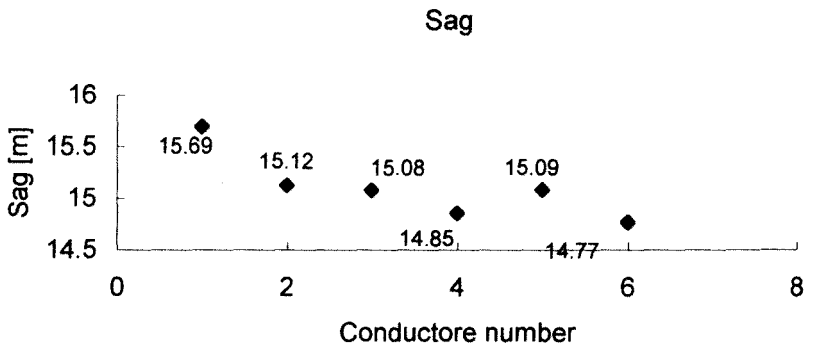

Figure C.55 Variation of sags among conductors at 1000A

Appendix D Results Using Genetic Algorithm in Three-layer Conductor Martin

D.1 Results of the application of the Genetic Algorithm

Table D.1 Standard in ASTM 232M

Ratio of lay length of a layer to nominal outside diameter of that lay									
Aluminum layer						Steel layer			
Outer		Middle		Inner		Outer		Inner	
Min	Max	Min	Max	Min	Max	Min	Max	Min	Max
10	13	10	16	10	17	16	24	18	30
Conversion of the lay length of Martin conductor [mm]									
361.6	470.1	281.2	450.0	200.9	341.5	192.8	289.2	130.1	216.9

Table D.2 Ranges of changed diameters and lay lengths

Steel diameter [mm]		Aluminum diameter [mm]	
Lower bound	Upper bound	Lower bound	Upper bound
		3.95	4.10
Steel lay length [mm]		Aluminum lay length [mm]	
Layer 1		Inner layer	
Lower bound	Upper bound	Lower bound	Upper bound
130.1	216.9	200.9	341.5
Layer 2		Middle layer	
Lower bound	Upper bound	Lower bound	Upper bound
192.8	289.2	281.2	450.0
		Outer layer	
		Lower bound	Upper bound
		361.6	470.1

Table D.3 Min and max losses with changed aluminum lay lengths

Minimum Joule loss [W/m]		Weight [N/m]
51.8173		25.25
Aluminum lay length [mm]		
Inner	Middle	Outer
341.5	281.2	470.1
Maximum Joule loss [W/m]		Weight [N/m]
60.9315		25.33
Aluminum lay length [mm]		
Inner	Middle	Outer
200.9	450.0	361.6

Table D.4 Min and max losses with changed steel and aluminum lay lengths

Minimum Joule loss [W/m]				Weight [N/m]
51.8156				25.24
Layer length [mm]				
Steel lay 1	Steel lay 2	Al inner	Al middle	Al outer
216.9	289.2	341.5	281.2	470.1
Maximum Joule loss [W/m]				Weight [N/m]
60.9372				25.36
Layer length [mm]				
Steel lay 1	Steel lay 2	Al inner	Al middle	Al outer
130.1	192.8	200.9	450.0	361.6

Table D.5 Min and max losses with changed aluminum wire diameters and lay lengths

Minimum Joule loss [W/m]		Weight [N/m]
49.7626		26.03
Aluminum wire diameter [mm]		
Inner	Middle	Outer
4.10	4.10	4.10
Aluminum lay length [mm]		
Inner	Middle	Outer
341.5	281.2	470.1
Maximum Joule loss [W/m]		Weight [N/m]
63.0668		24.69
Aluminum wire diameter [mm]		
Inner	Middle	Outer
3.95	3.95	3.95
Aluminum lay length [mm]		
Inner	Middle	Outer
200.9	450.0	361.6

Table D.6 Min and max losses with changed aluminum wire diameters

Minimum Joule loss [W/m]		Weight [N/m]
51.6904		26.03
Aluminum diameter [mm]		
Inner	Middle	Outer
4.10	4.10	4.10
Maximum Joule loss [W/m]		Weight [N/m]
55.6722		24.62
Aluminum diameter [mm]		
Steel lay 1	Steel lay 2	Inner
3.95	3.95	3.95

Table D.7 Martin used as a reference

Aluminum lay length [mm]			Steel lay length [mm]	
Inner	Middle	Outer	First layer	Second layer
301.333	365.633	397.782	180.784	241.046

Aluminum wire diameter [mm]	Steel wire diameter [mm]
4.018	2.410

Loss [W/m]	Weight [N/m]	Sag [m]
53.8037	25.25	15.7532

Table D.8 Low loss conductors

Results with changed aluminum lay lengths

Aluminum lay [mm]				Weight [N/m]	Loss [W/m]	Sag [m]
Number	Inner	Middle	Outer			
1	276.4	392.1	464.6	25.18	53.6048	15.7211
2	283.4	336.7	459.8	25.22	52.6881	15.7214

Results with changed aluminum lay length and wire diameters

Aluminum lay [mm]				Aluminum wire diameter [mm]		
Number	Inner	Middle	Outer	Inner	Middle	Outer
1	241	285.8	300.6	3.9713	4.0033	4.0148
2	303.4	286.3	448.2	4.0629	3.9739	3.9973
Number	Weight [N/m]	Loss [W/m]	Sag [m]			
1	25.11	52.8419	15.6704			
2	25.15	52.6244	15.6815			

Results with changed steel and aluminum lay lengths

Steel lay [mm]			Aluminum wire diameter [mm]		
Number	Steel 1	Steel 2	Inner	Middle	Outer
1	166.6	287.0	327.4	335.6	451.9
2	186.8	283.2	330.7	281.5	469.0
Number	Weight [N/m]	Loss [W/m]	Sag [m]		
1	25.20	52.2329	15.7041		
2	25.25	51.8598	15.7187		

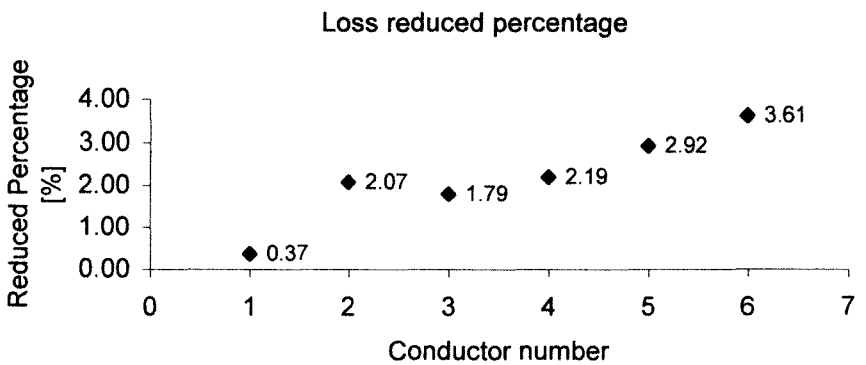

Figure D.1 Percentage of reduced loss compared to the reference

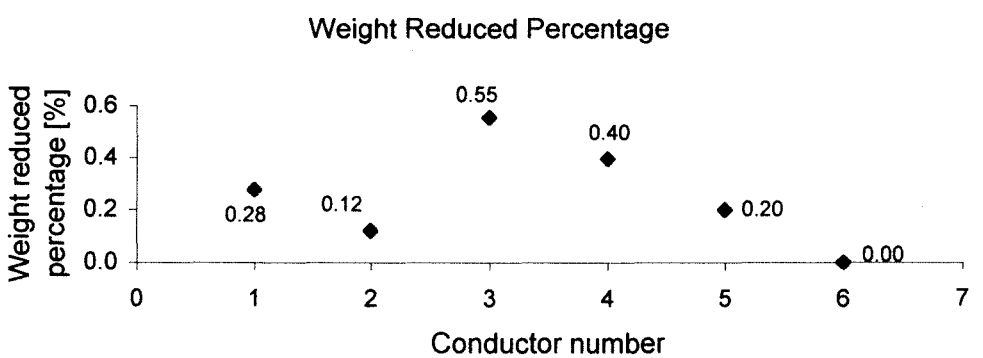

Figure D.2 Percentage of reduced weight compared to the reference

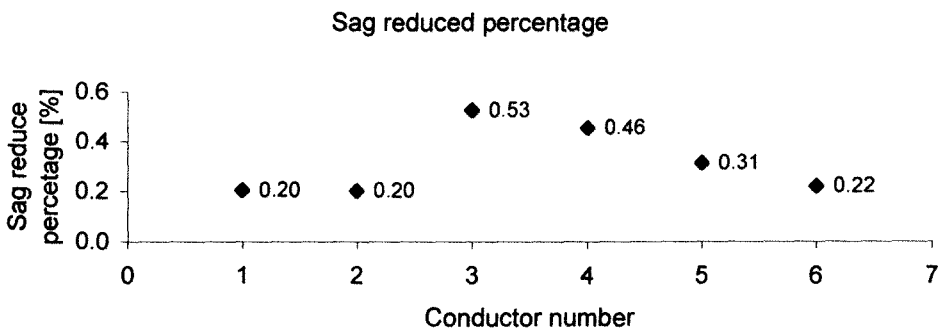

Figure D.3 Percentage of reduced sag compared to the reference

D.2 Fixing wire diameters and steel lay length, changing aluminum lay lengths

Table D.9 Unchanged wire and steel lay parameters

Steel wire diameter [mm]			Aluminum wire diameter [mm]		
Steel king	Steel lay 1	Steel lay 2	Inner	Middle	Outer
2.410	2.410	2.410	4.018	4.018	4.018
Steel layer outer diameter [mm]			Aluminum layer outer diameter [mm]		
Steel king	Steel lay 1	Steel lay 2	Inner	Middle	Outer
2.410	7.230	12.050	20.086	28.122	36.158
Steel lay length [mm]			Aluminum lay length [mm]		
Steel king	Steel lay 1	Steel lay 2	Inner	Middle	Outer
1000.0	180.8	241.0	Changed	Changed	Changed

Table D.10 Changed aluminum lay lengths

Conductor number	Inner [mm]	Middle [mm]	Outer [mm]	Weight [N/m]
Conductor 1	341.5	281.2	470.1	25.25
Conductor 2	313.1	311.9	389.1	25.31
Conductor 3	287.8	373.9	406.5	25.24
Conductor 4	260.1	401.4	377.2	25.28
Conductor 5	208.4	423.7	381.7	25.30
Conductor 6	200.9	450.0	361.6	25.33

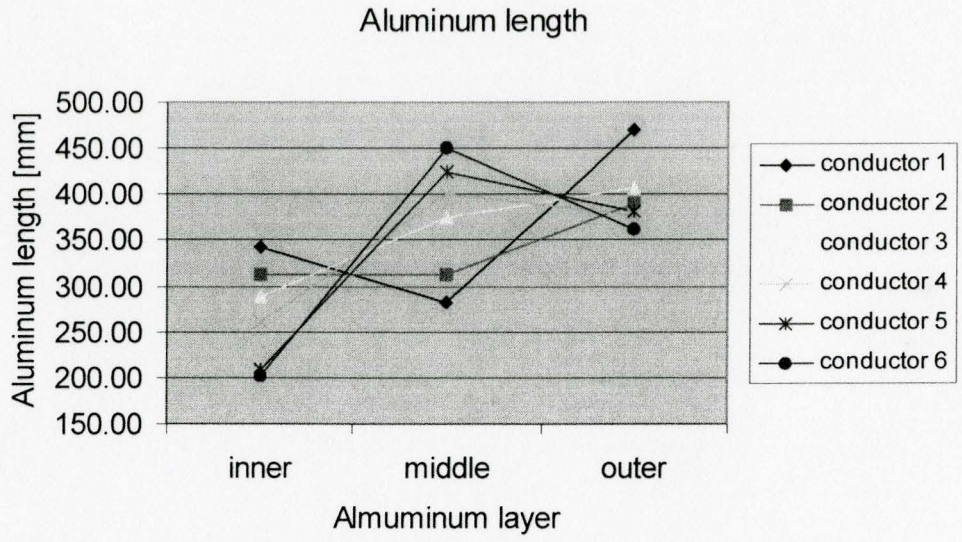

Figure D.4 Changed lay lengths with fixed wire diameters

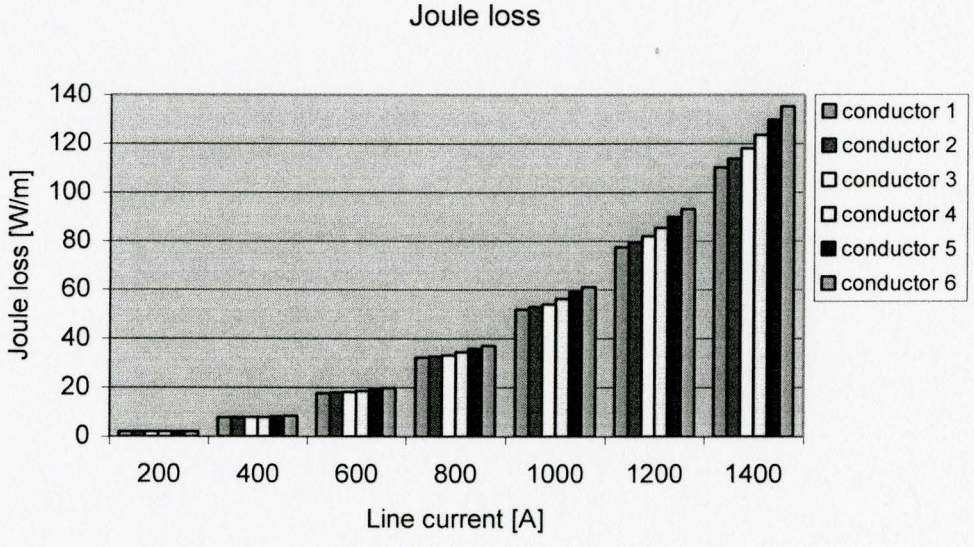

Figure D.5 Variation of Joule losses in six conductors at various line currents

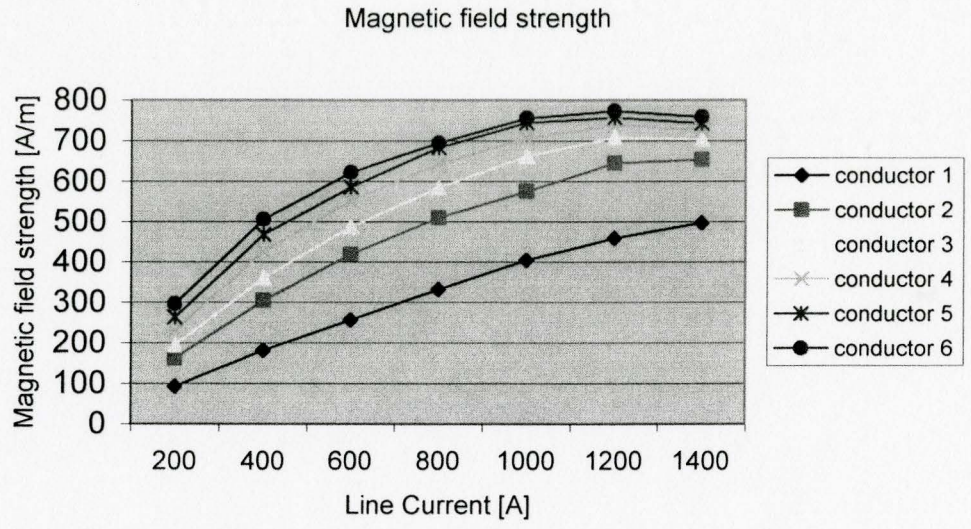

Figure D.6 Variation of six-conductor magnetic field strength at various line currents

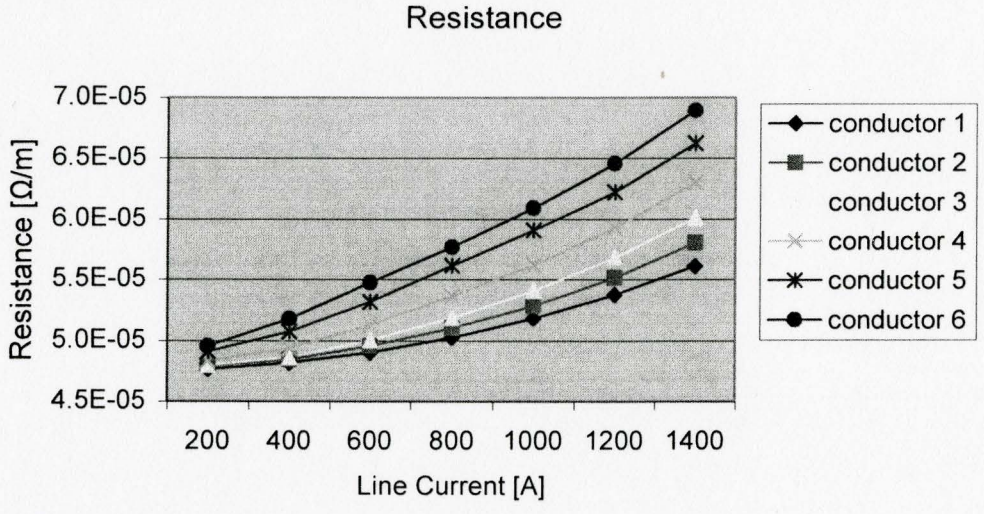

Figure D.7 Variation of resistance in six conductors at various line currents

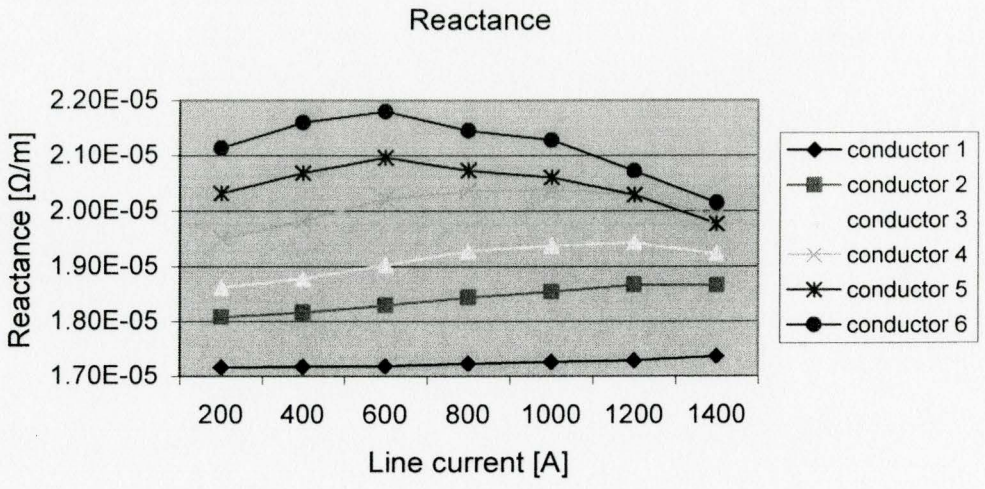

Figure D.8 Variation of reactance in six conductors at various line currents

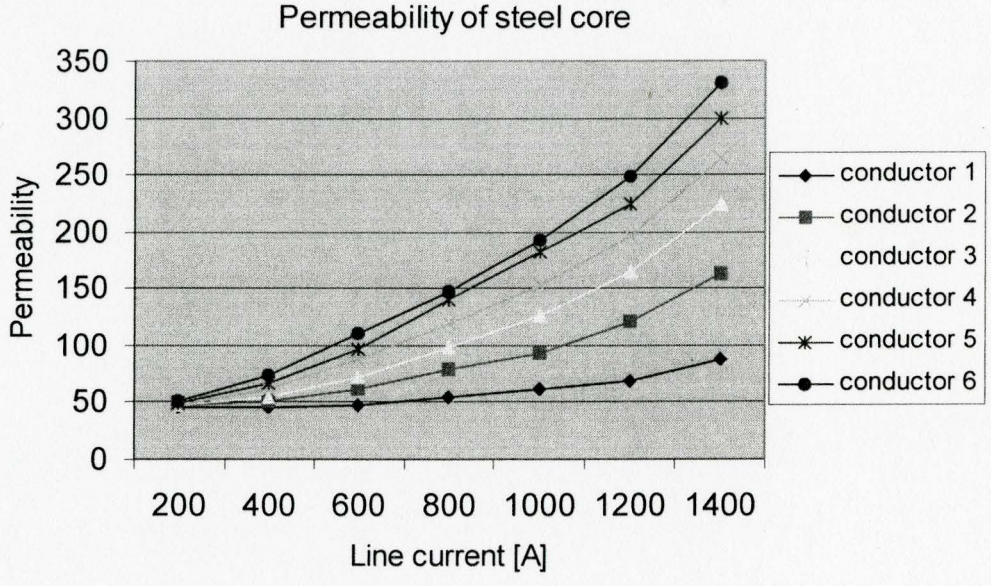

Figure D.9 Variation of permeability at various line currents

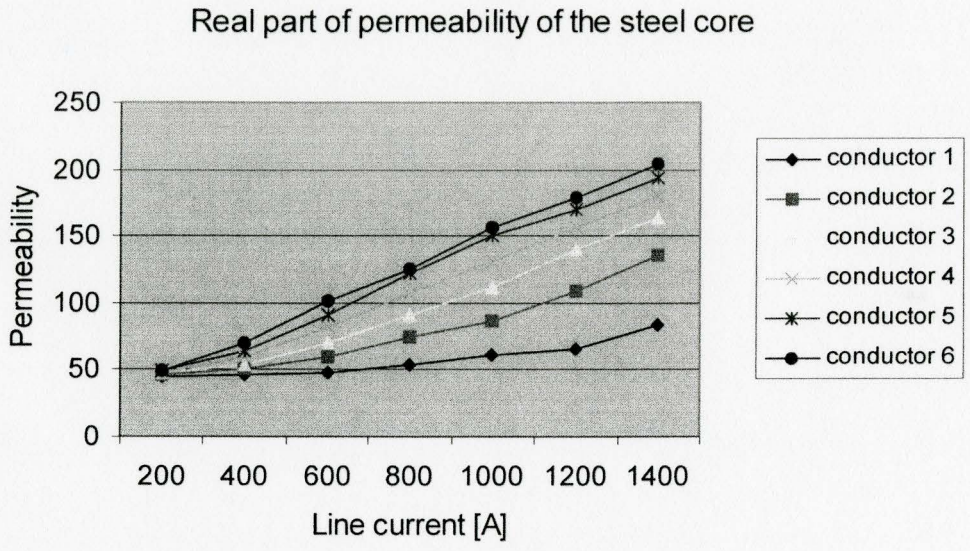

Figure D.10 Variation of real part of the permeability at various line currents

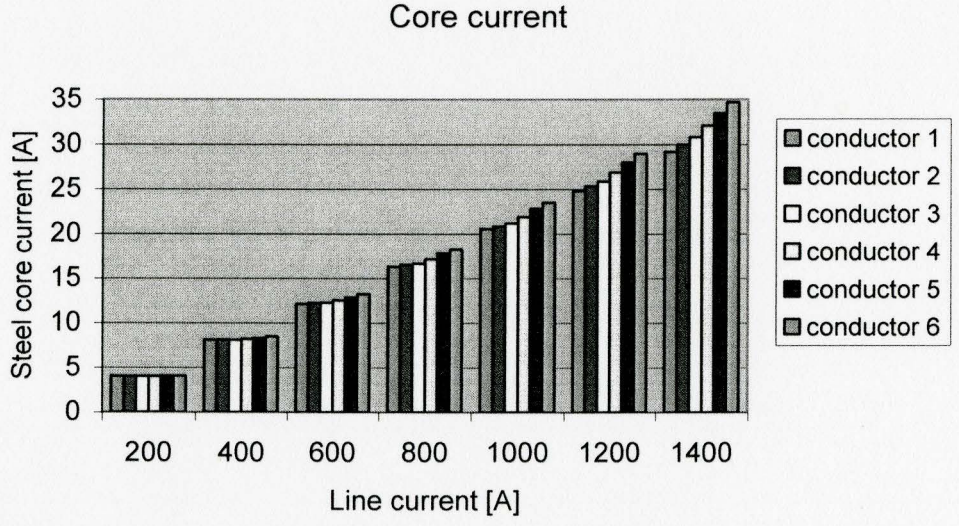

Figure D.11 Variation of steel core current at various line currents

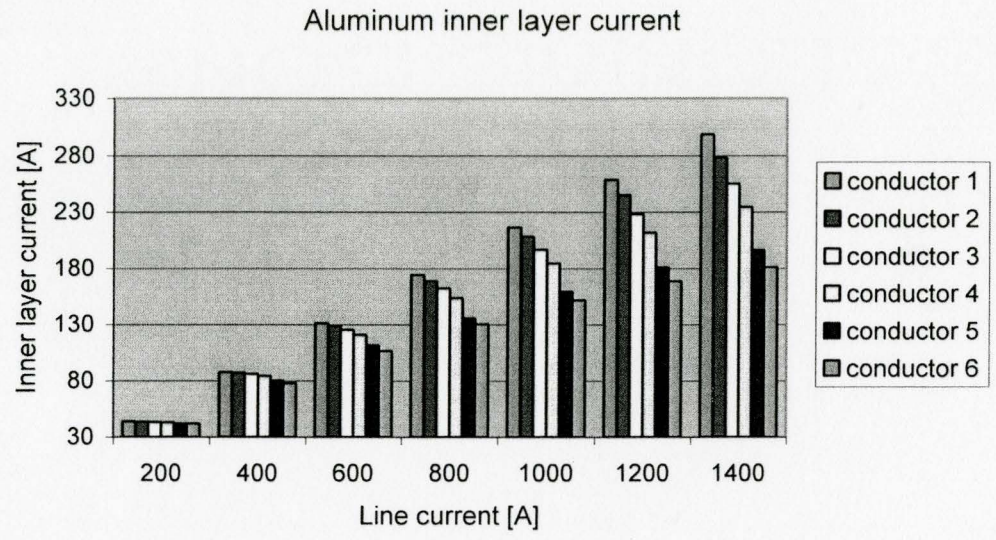

Figure D.12 Variation of aluminum inner layer current at various line currents

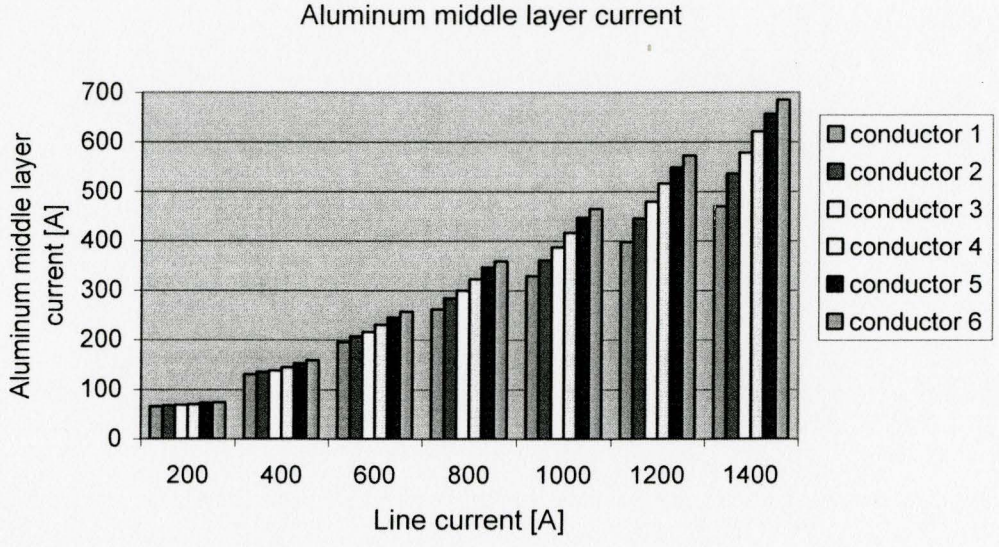

Figure D.13 Variation of aluminum middle layer current at various line currents

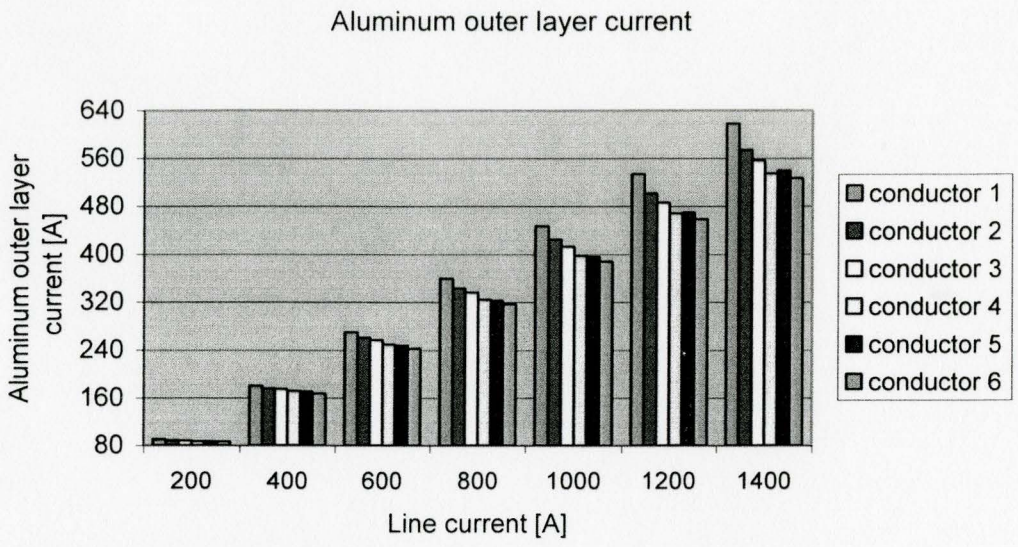

Figure D.14 Variation of aluminum outer layer current at various line currents

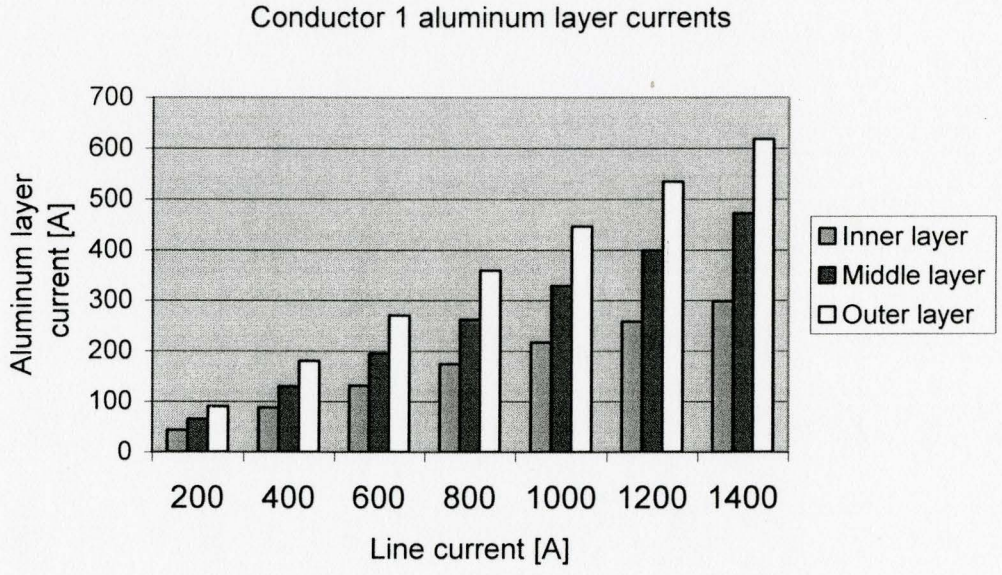

Figure D.15 Variation of three aluminum layer currents in conductor 1 at various line currents

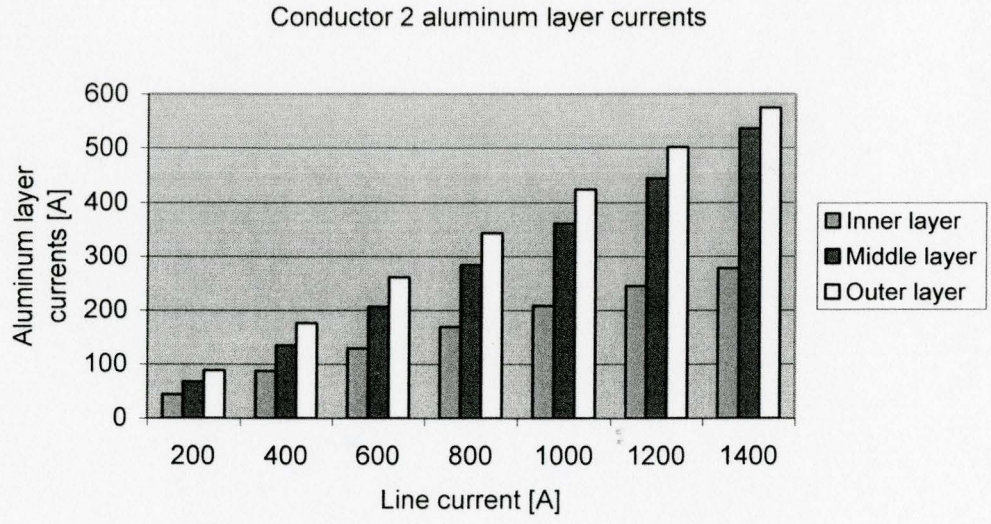

Figure D.16 Variation of aluminum layer currents in conductor 2 at various line currents

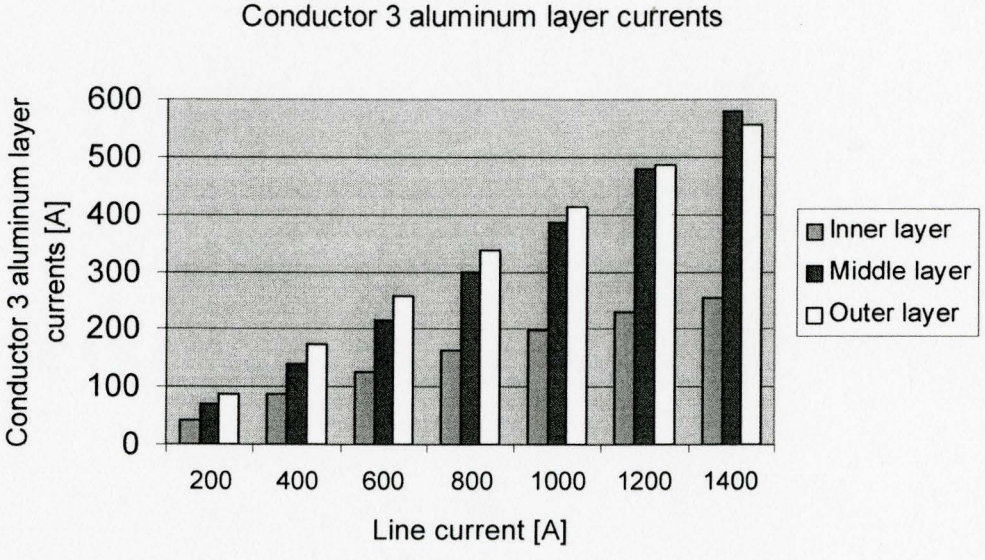

Figure D.17 Variation of aluminum layer currents in conductor 3 at various line currents

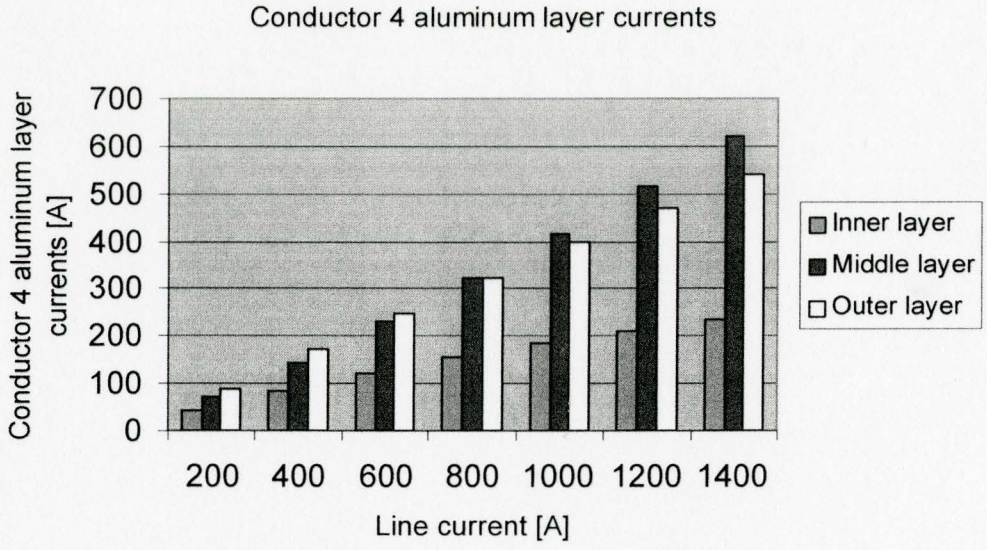

Figure D.18 Variation of three aluminum layer currents in conductor 4 at various line currents

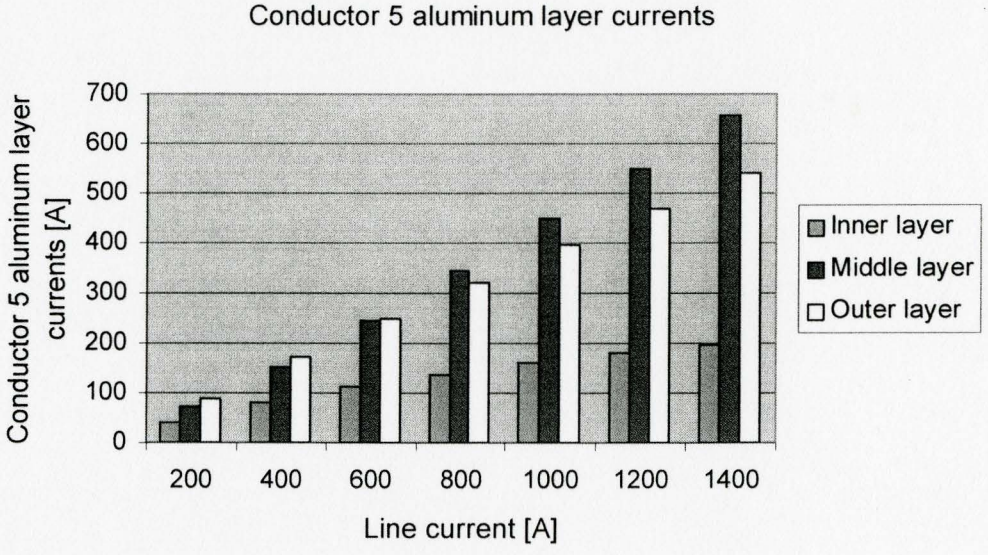

Figure D.19 Variation of aluminum layer currents in conductor 5 at various line currents

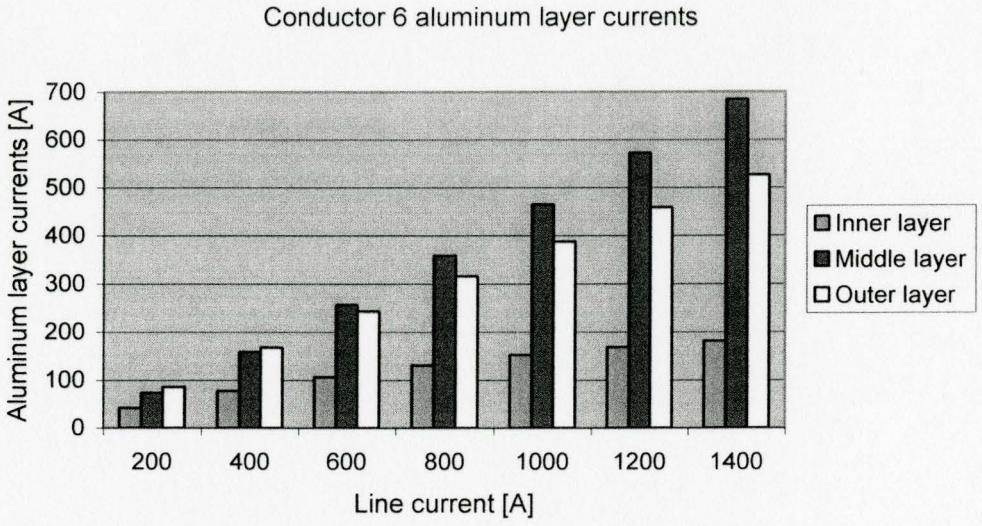

Figure D.20 Variation of aluminum layer currents in conductor 6 at various line currents

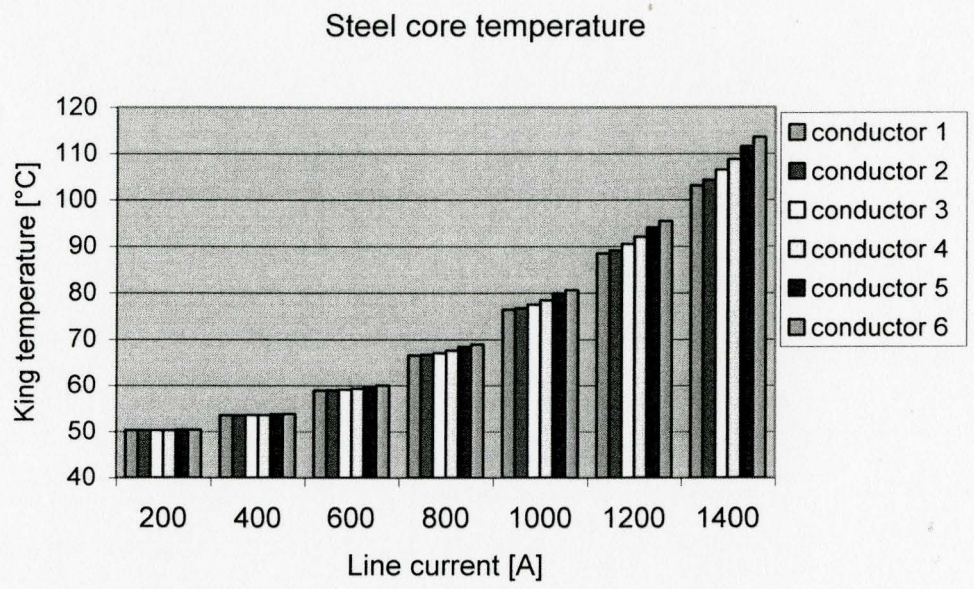

Figure D.21 Variation of steel king layer temperature at various line currents

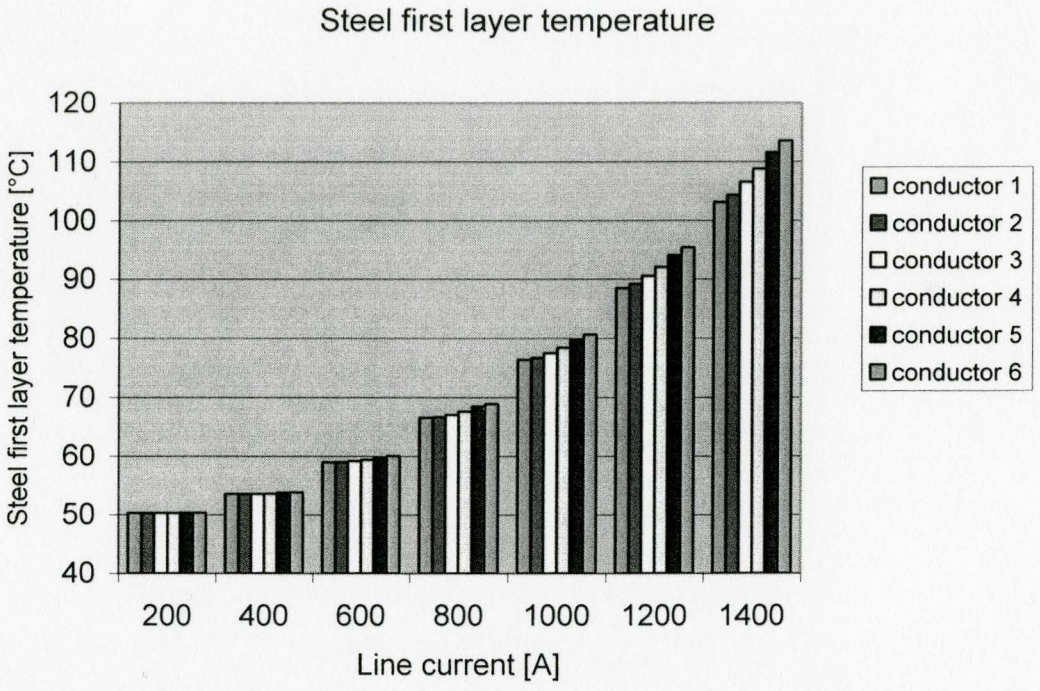

Figure D.22 Variation of steel first layer temperature at various line currents

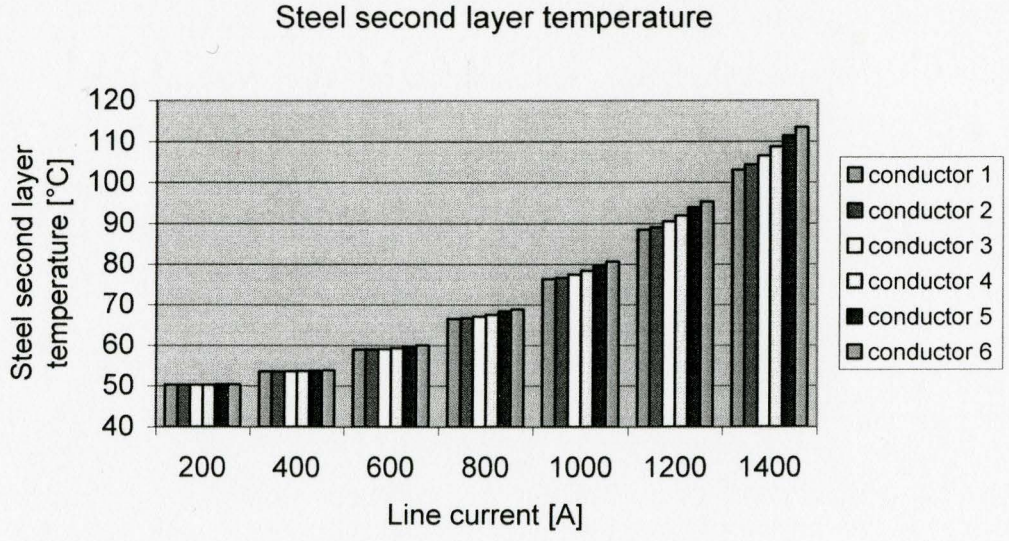

Figure D.23 Variation of steel second layer temperature at various line currents

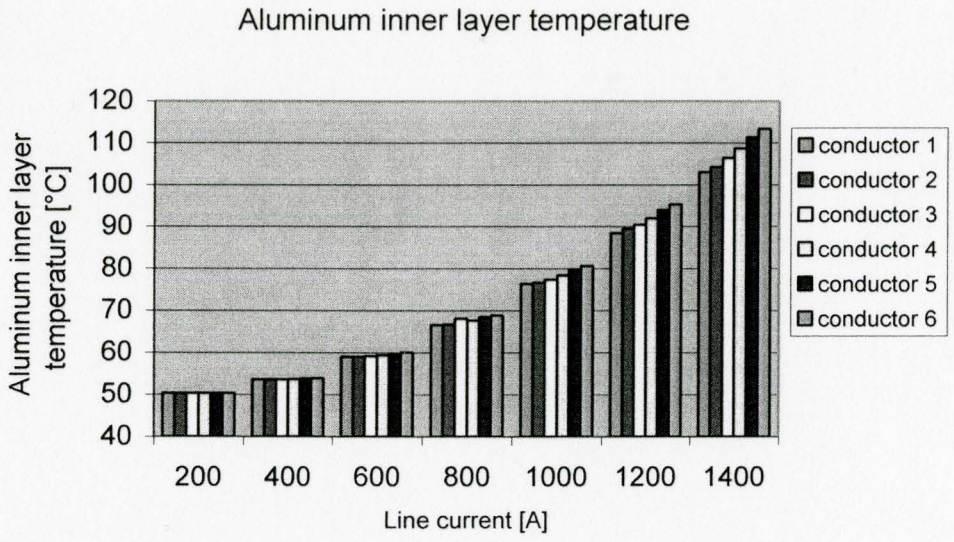

Figure D.24 Variation of aluminum inner layer temperature at various line currents

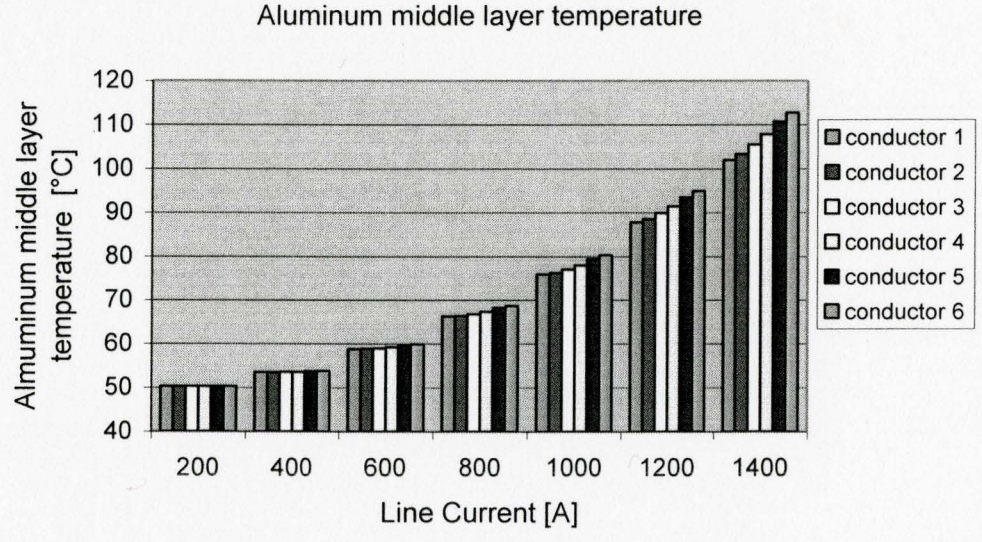

Figure D.25 Variation of aluminum middle layer temperature at various line currents

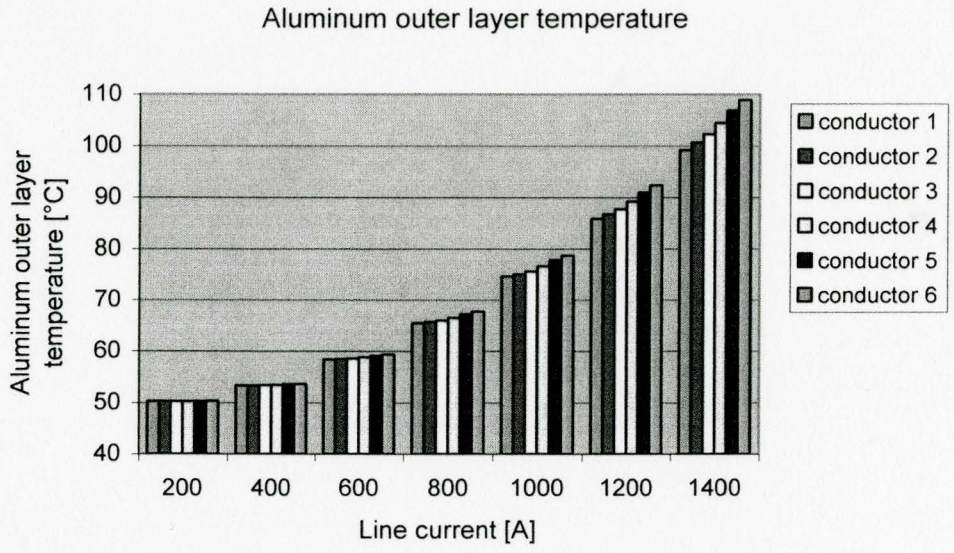

Figure D.26 Variation of aluminum outer layer temperature at various line currents

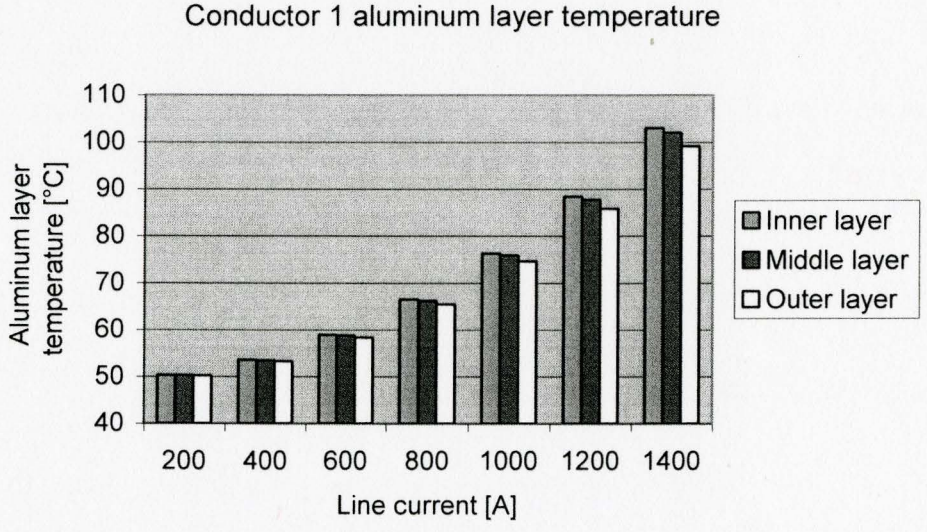

Figure D.27 Variation of aluminum layer temperature in conductor 1 at various line currents

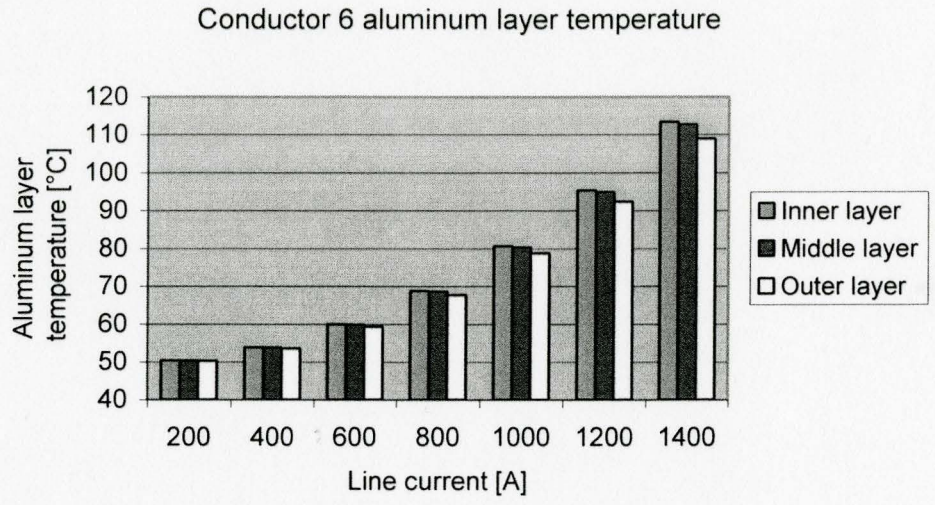

Figure D.28 Variation of aluminum layer temperature in conductor 6 at various line currents

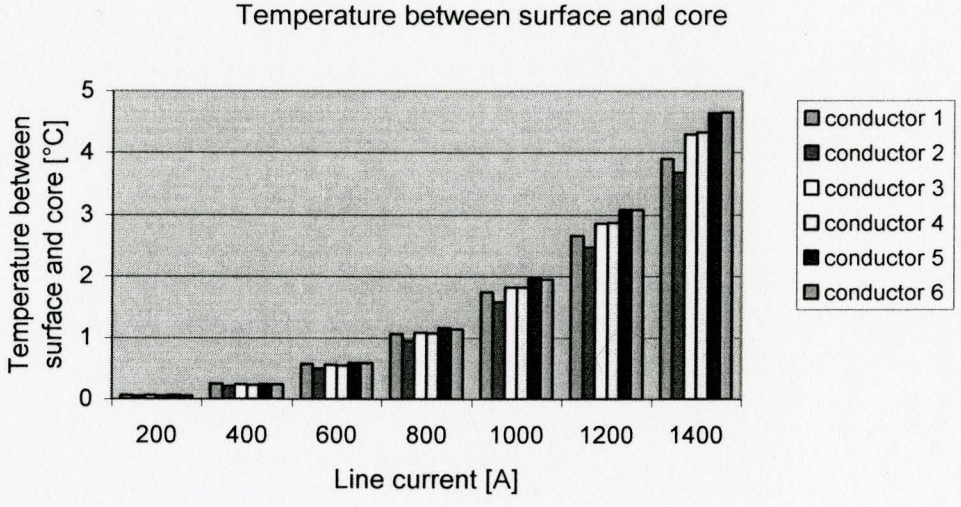

Figure D.29 Temperature differences between steel core and conductor surface

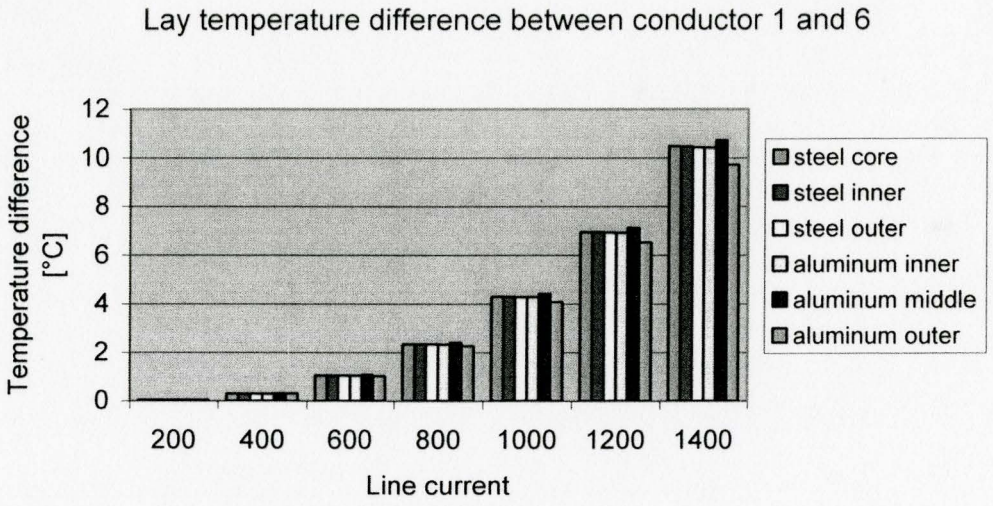

Figure D.30 Temperature differences in layers between conductor 1 and 6

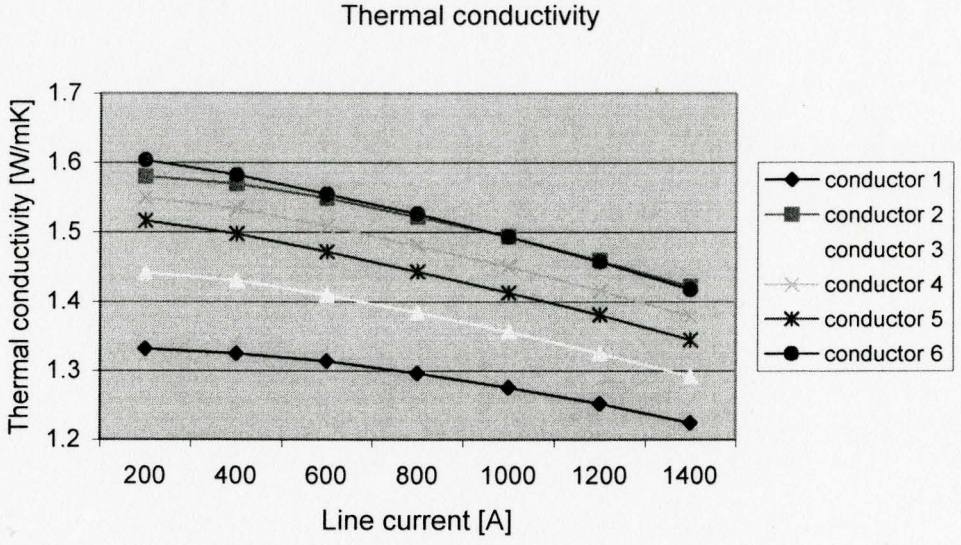

Figure D.31 Variation of thermal conductivity at various line currents

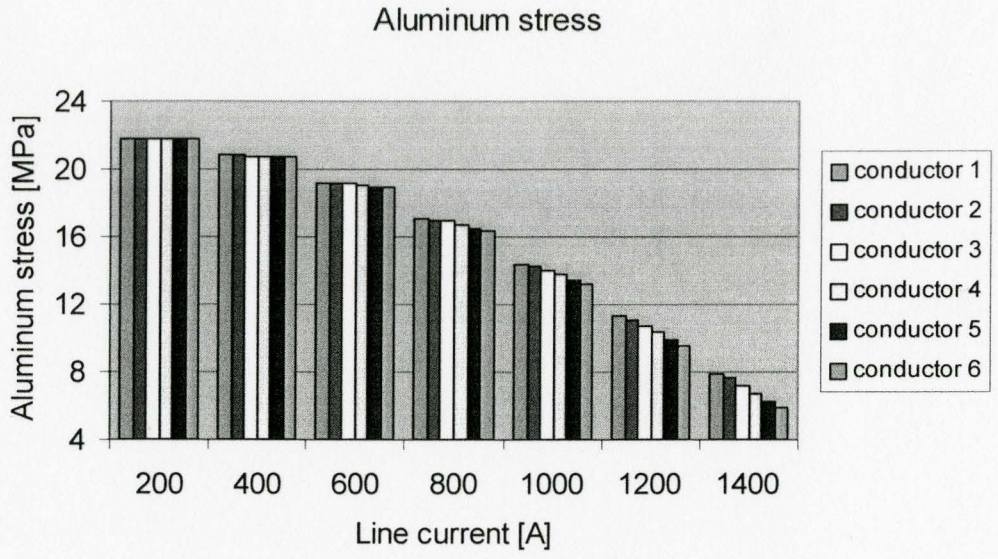

Figure D.32 Variation of aluminum stresses at various line currents

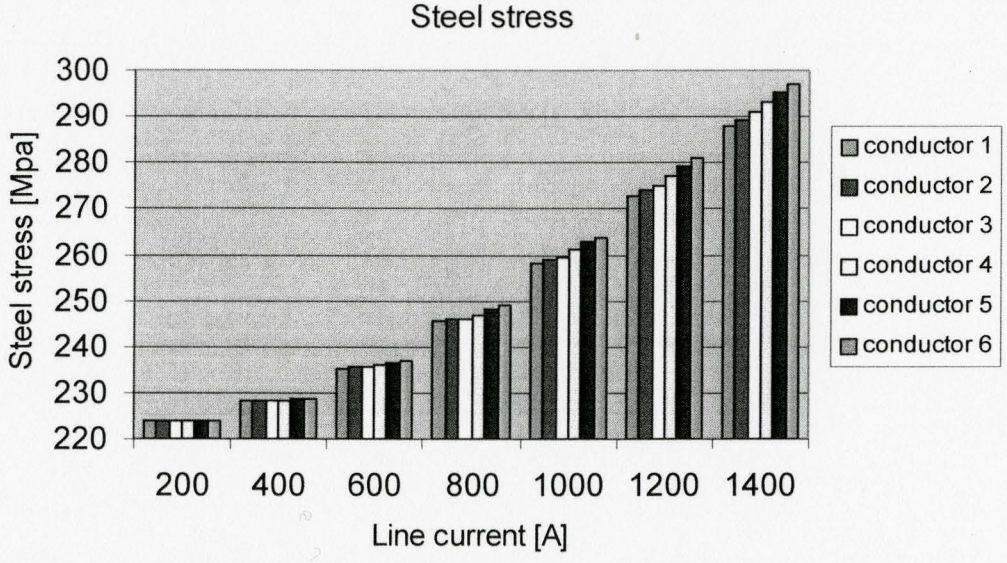

Figure D.33 Variation of steel stresses at various line currents

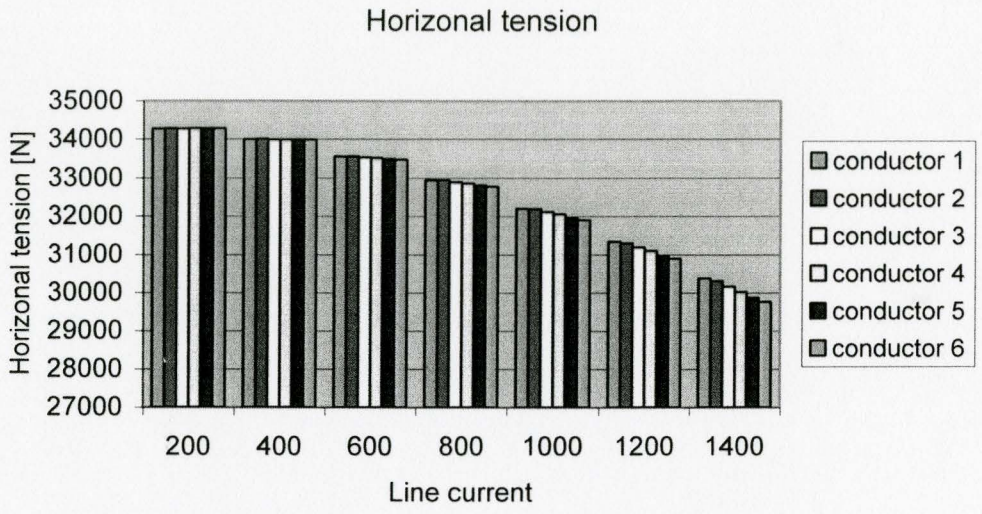

Figure D.34 variation of horizontal tension at various line currents

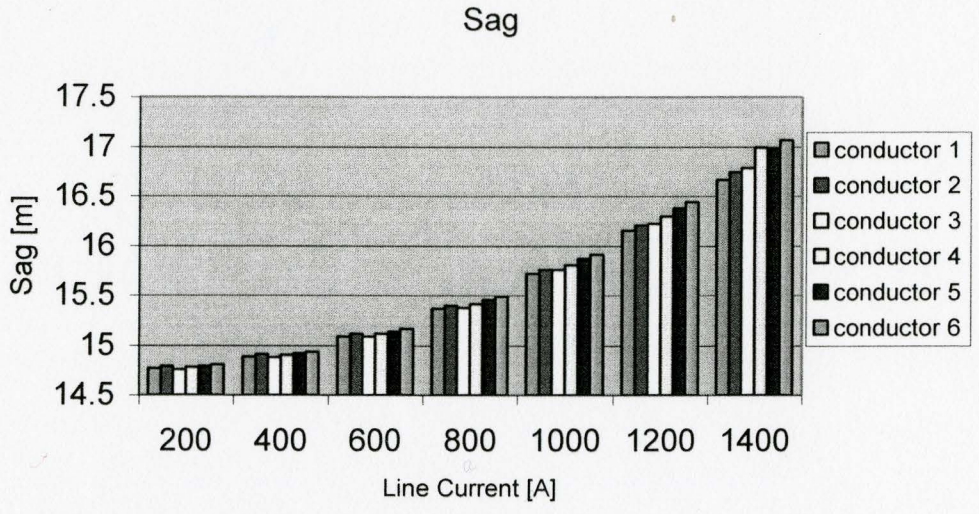

Figure D.35 Variation of sags at various line currents with line length 400 meters

D.3 Fixing wire diameters, changing steel and aluminum lay lengths

Table D.11 Unchanged steel wire and aluminum wire diameters

Steel wire diameter [mm]			Aluminum wire diameter [mm]		
King	Steel lay 1	Steel lay 2	Inner	Middle	Outer
2.410	2.410	2.410	4.018	4.018	4.018
Steel layer's outer diameters [mm]			Aluminum layer's outer diameters [mm]		
Steel lay 1	Steel lay 2	Steel lay 3	Inner	Middle	Outer
2.410	7.230	12.050	200.860	28.122	36.158

Table D.12 Changed steel and aluminum lay lengths

Steel lay length [mm]			Aluminum lay length [mm]		
	Steel lay 1	Steel lay 2	Inner	Middle	Outer
Conductor 1	216.9	289.2	341.5	281.2	470.1
Conductor 2	152.1	195.8	313.1	311.9	389.1
Conductor 3	211.9	265.9	287.8	373.9	406.5
Conductor 4	209.3	272.7	260.1	401.4	377.2
Conductor 5	208.4	254.4	208.4	423.7	381.7
Conductor 6	130.1	192.8	200.9	450.0	361.6
Weight [N/m]					
Conductor 1	Conductor 2	Conductor 3	Conductor 4	Conductor 5	Conductor 6
25.24	25.33	25.23	25.27	25.30	25.36

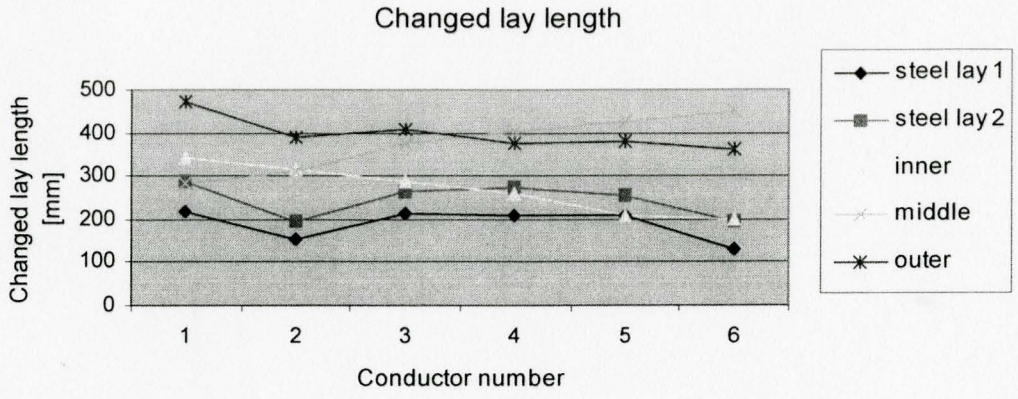

Figure D.36 Variation of lay length for different conductors at 1000 A

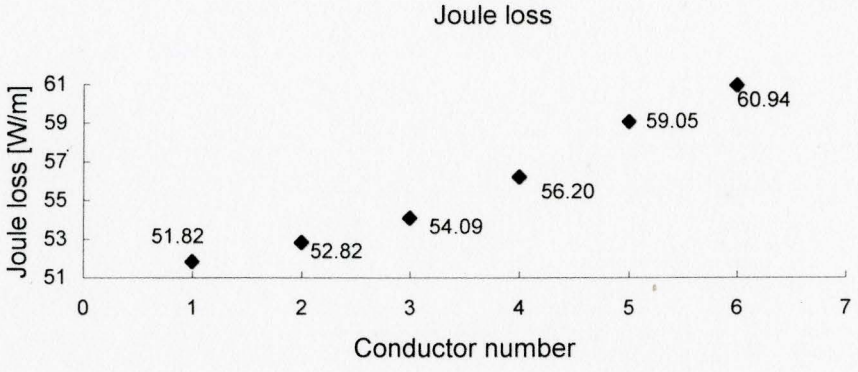

Figure D.37 Variation of Joule losses for different conductors at 1000A

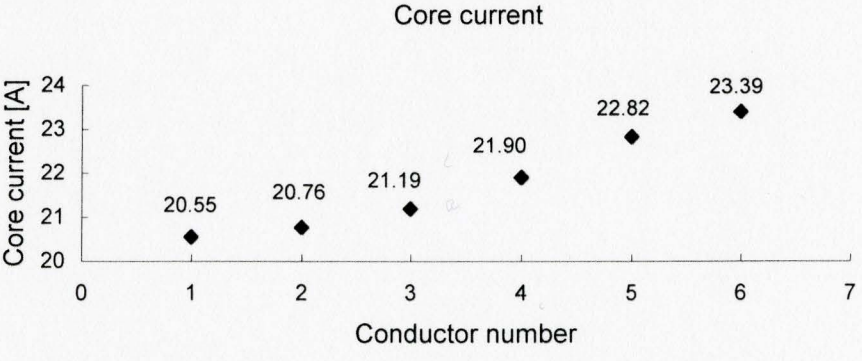

Figure D.38 Variation of core current for different conductors at 1000A

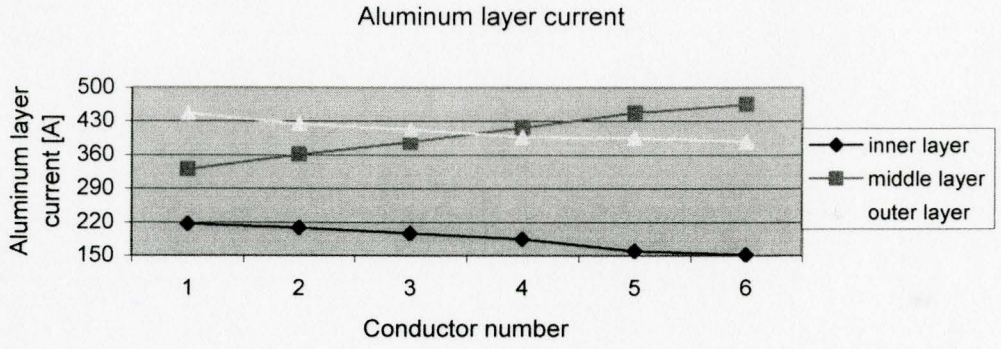

Figure D.39 Variation of aluminum current for different conductors at 1000A

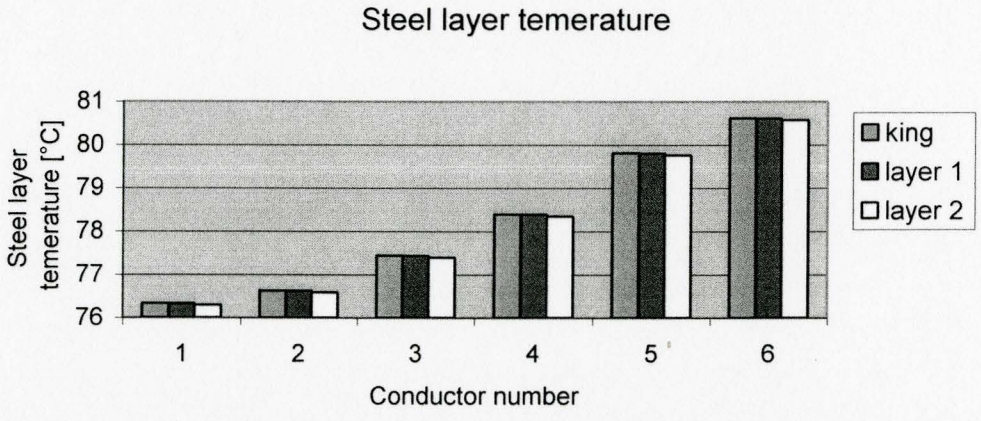

Figure D.40 Variation of steel layer temperature for different conductors at 1000A

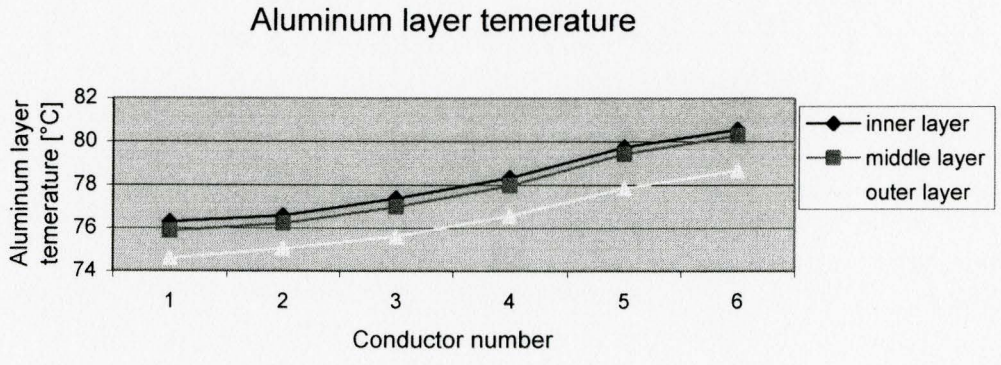

Figure D.41 Variation of aluminum layer temperatures for different conductors at 1000A

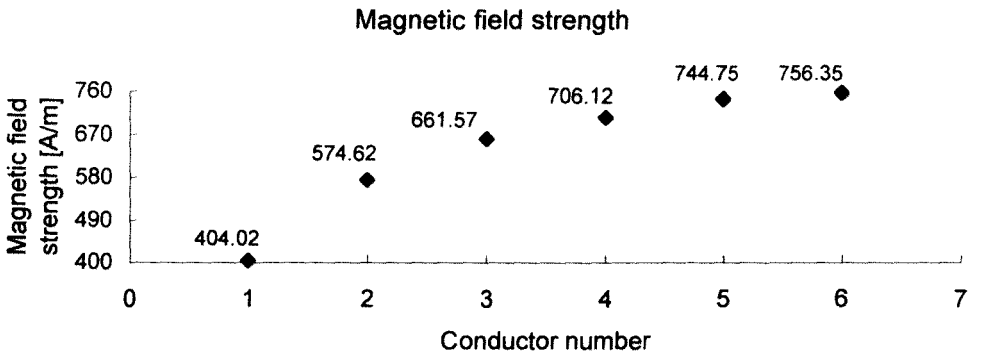

Figure D.42 Variation of magnetic field strength for different conductors at 1000A

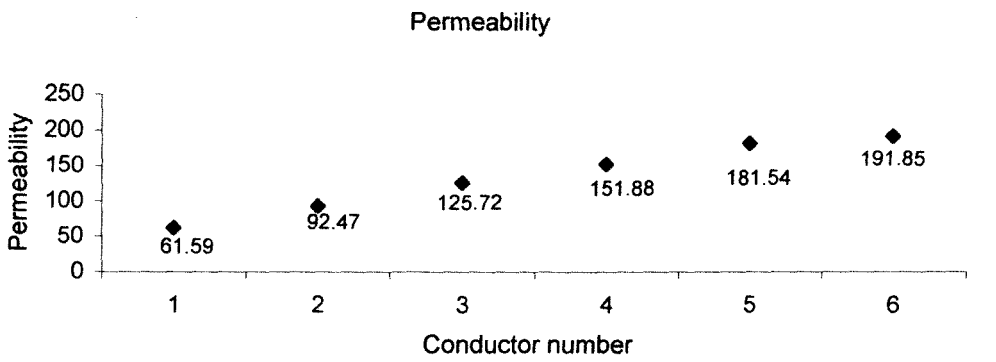

Figure D.43 Variation of permeability for different conductors in 1000A

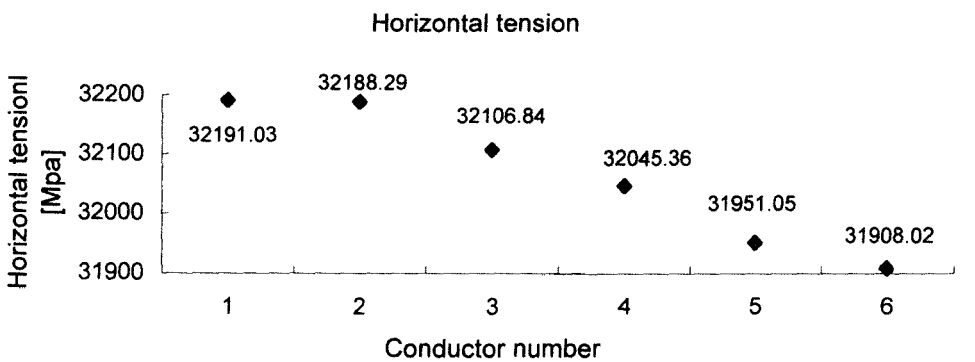

Figure D.44 Variation of horizontal tension for different conductors at 1000A

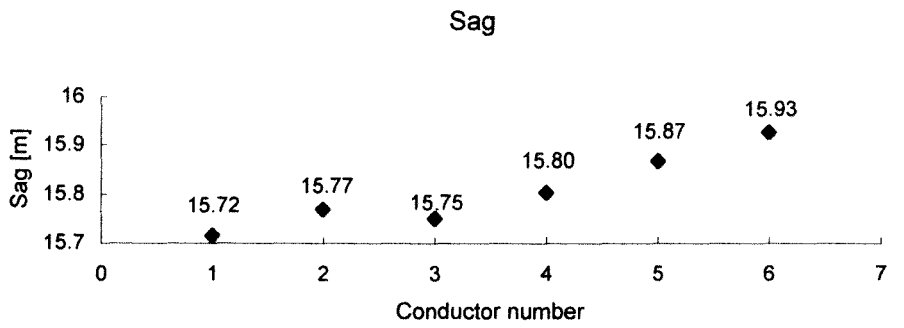

Figure D.45 Variation of sags for different conductors at 1000A

D.4 Fixing steel core size, changing aluminum lay lengths and wire diameters

Table D.13 Changed aluminum wire and layer parameters

	Wire diameter [mm]			Aluminum lay length [mm]		
	Inner	Middle	Outer	Inner	Middle	Outer
Conductor 1	4.1	4.1	4.1	341.5	281.2	470.1
Conductor 2	4.048	4.092	3.971	301.6	332.9	447.1
Conductor 3	3.972	4.001	3.952	263.6	352.4	448.2
Conductor 4	3.950	3.994	3.971	220.7	391.8	417.9
Conductor 5	3.969	4.031	3.977	205.8	438.4	362.4
Conductor 6	3.95	3.95	3.95	200.9	450.0	361.6
	Outer diameter [mm]					
	Inner	Middle	Outer	Weight [N/m]		
Conductor 1	20.250	28.450	36.650	26.03		
Conductor 2	20.145	28.329	36.271	25.33		
Conductor 3	19.994	27.994	35.897	24.80		
Conductor 4	19.951	27.938	35.880	24.85		
Conductor 5	19.988	28.050	36.004	25.09		
Conductor 6	19.952	27.852	35.752	24.70		

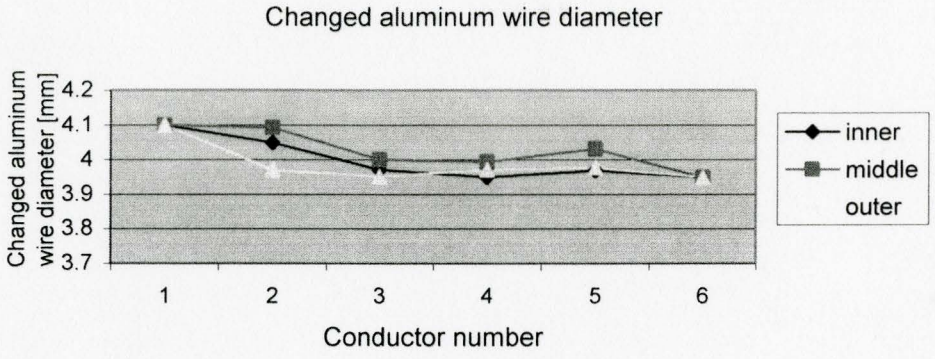

Figure D.46 Changed aluminum diameters at 1000A

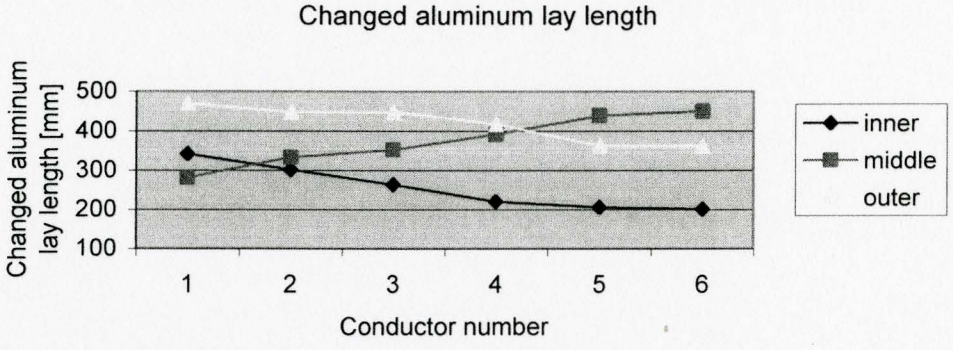

Figure D.47 Changed aluminum lay lengths at 1000A

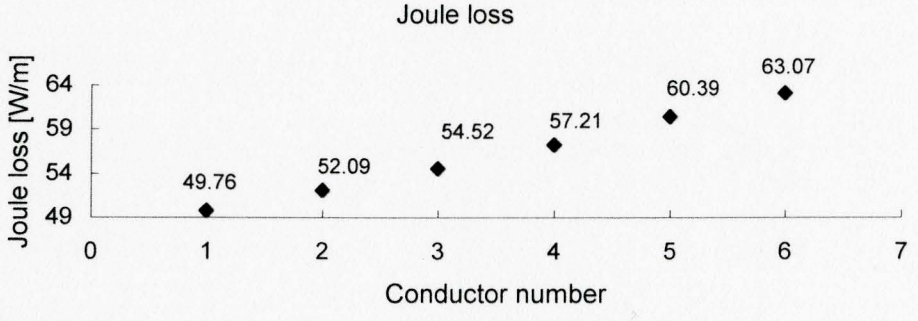

Figure D.48 Variation of Joule loss among conductors at 1000A

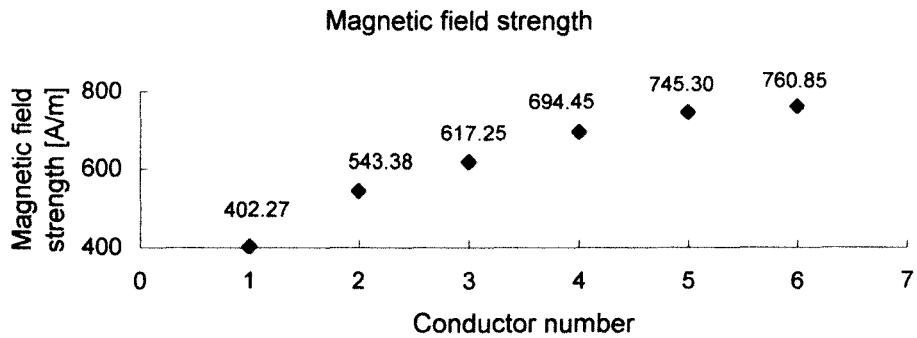

Figure D.49 Variation of magnetic field strength among conductors at 1000A

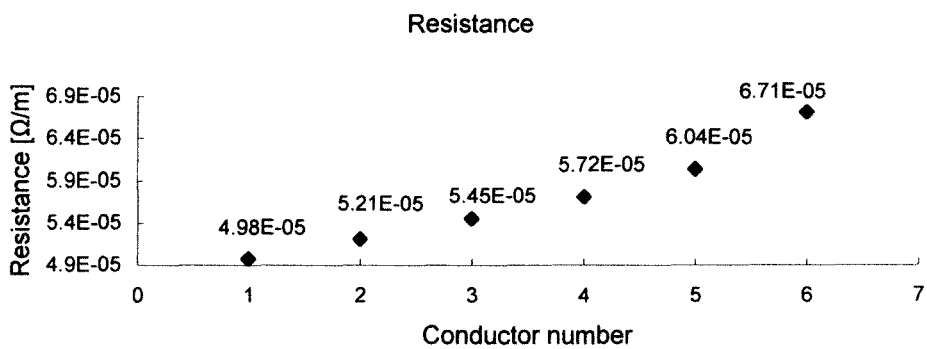

Figure D.50 Variation of resistance among conductors at 1000A

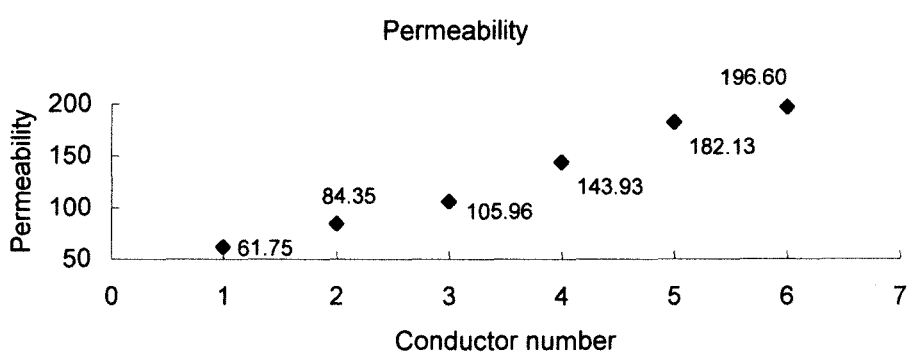

Figure D.51 Variation of permeability among conductors at 1000A

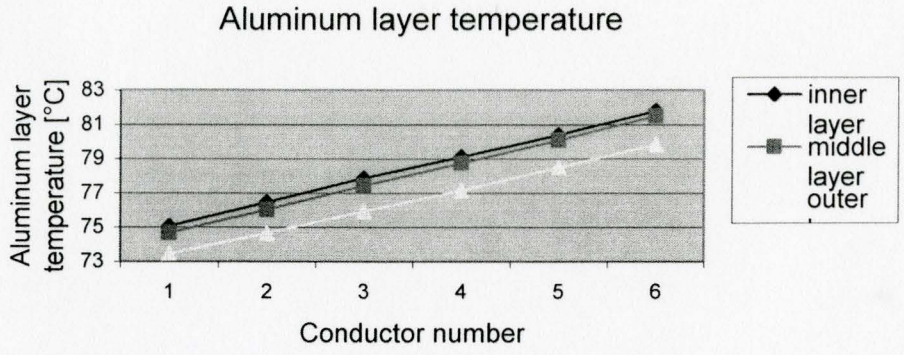

Figure D.52 Variation of aluminum layer temperature among conductors at 1000A

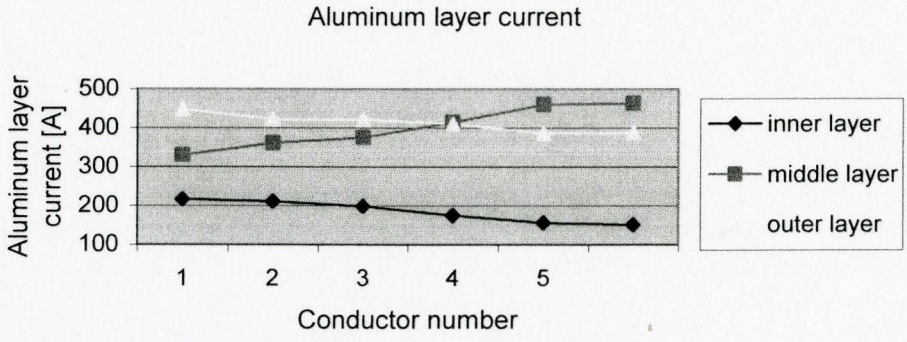

Figure D.53 Variation of aluminum layer current among conductors at 1000A

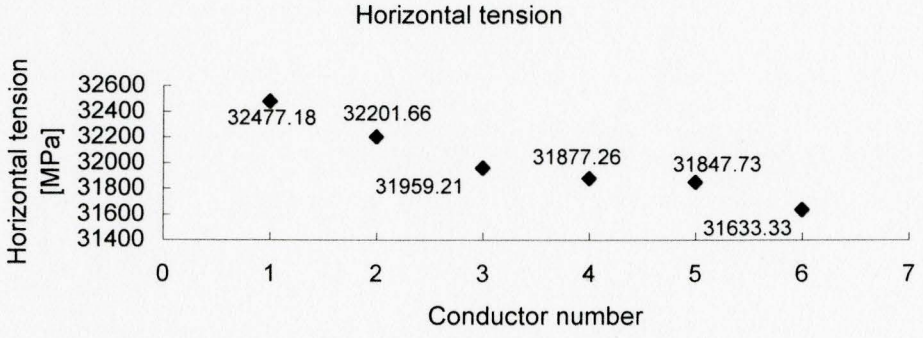

Figure D.54 Variation of horizontal tension among conductors at 1000A

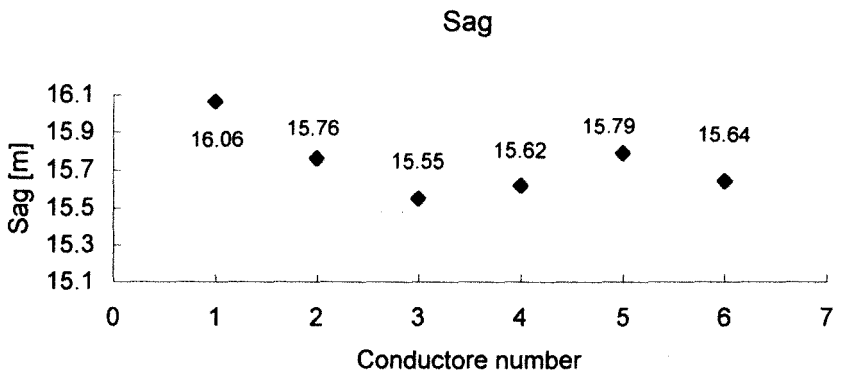

Figure D.55 Variation of sags among conductors at 1000A

Appendix E Results Using GA in Three-layer Conductor Plover

E.1 Results of the application of the Genetic Algorithm

Table E.1 Standard in ASTM 232M

Ratio of lay length of a layer to nominal outside diameter of that lay									
Aluminum layer						Steel layer			
Outer		Middle		Inner		Outer		Inner	
Min	Max	Min	Max	Min	Max	Min	Max	Min	Max
10	13	10	16	10	17	16	24	18	30
Conversion of the lay length of Plover conductor [mm]									
372.2	483.9	289.5	463.2	206.8	351.6	198.6	297.8	134.0	223.4

Table E.2 Ranges of changed wire diameters and lay lengths

Steel diameter [mm]		Aluminum diameter [mm]	
Lower bound	Upper bound	Lower bound	Upper bound
2.482	2.482	4.0	4.2
Steel lay length [mm]		Aluminum lay length [mm]	
Layer 1		Inner layer	
Lower bound	Upper bound	Lower bound	Upper bound
134.0	223.4	206.8	351.6
Layer 2		Middle layer	
Lower bound	Upper bound	Lower bound	Upper bound
198.6	297.8	289.5	463.2
		Outer layer	
		Lower bound	Upper bound
		372.2	483.9

Table E.3 Min and max losses with changed aluminum lay lengths

Minimum Joule loss [W/m]		Weight [N/m]
48.7728		26.76
Aluminum lay length [mm]		
Inner	Middle	Outer
351.6	289.5	483.9
Maximum Joule loss [W/m]		Weight [N/m]
57.2164		26.84
Aluminum lay length [mm]		
Inner	Middle	Outer
206.8	463.2	372.2

Table E.4 Min and max losses with changed steel and aluminum lay lengths

Minimum Joule loss [W/m]				Weight [N/m]
48.7712				26.74
Layer length [mm]				
Steel lay 1	Steel lay 2	Al inner	Al middle	Al outer
223.4	297.8	351.6	289.5	483.9
Maximum Joule loss [W/m]				Weight [N/m]
57.2217				26.86
Layer length [mm]				
Steel lay 1	Steel lay 2	Al inner	Al middle	Al outer
134.0	198.6	206.8	463.2	372.2

Table E.5 Min and max losses with changed aluminum wire diameters and lay lengths

Minimum Joule loss [W/m]		Weight [N/m]
47.2974		27.39
Aluminum wire diameter [mm]		
Inner	Middle	Outer
4.2	4.2	4.2
Aluminum lay length [mm]		
Inner	Middle	Outer
351.6	289.5	483.9
Maximum Joule loss [W/m]		Weight [N/m]
61.3672		25.55
Aluminum wire diameter [mm]		
Inner	Middle	Outer
4.0	4.0	4.0
Aluminum lay length [mm]		
Inner	Middle	Outer
206.8	463.2	372.2

Table E.6 Min and max values with changed aluminum wire diameters

Minimum Joule loss [W/m]		Weight [N/m]
49.0844		27.39
Aluminum diameter [mm]		
Inner	Middle	Outer
4.2	4.2	4.2
Maximum Joule loss [W/m]		Weight [N/m]
54.0417		25.47
Aluminum diameter [mm]		
Steel lay 1	Steel lay 2	Inner
4.0	4.0	4.0

Table E.7 Plover used as reference

Aluminum lay length [mm]			Steel lay length [mm]	
Inner	Middle	Outer	First layer	Second layer
310.02	376.33	409.41	186.12	248.16
Aluminum wire diameter [mm]			Steel wire diameter [mm]	
4.135			2.482	
Loss [W/m]		Weight [N/m]		Sag [m]
50.6066		26.75		16.4142

Table E.8 Low loss conductors

Results with changed aluminum lay lengths

Aluminum lay [mm]				Weight [N/m]	Loss [W/m]	Sag [m]
Number	Inner	Middle	Outer			
1	320.9	402.6	477.8	26.66	49.7690	16.3607
2	336.1	372.2	434.5	26.72	49.7275	16.3833

Results with changed aluminum lay length and wire diameters

Aluminum lay [mm]				Aluminum wire diameter [mm]		
Number	Inner	Middle	Outer	Inner	Middle	Outer
1	311.9	418.9	471.9	4.0952	4.1116	4.18
2	324.2	339.9	441.0	4.1376	4.09	4.152
Number	Weight [N/m]	Loss [W/m]	Sag [m]			
1	26.69	50.2063	16.3841			
2	26.68	49.7629	16.3624			

Results with changed steel and aluminum lay lengths

Steel lay [mm]			Aluminum lay [mm]		
Number	Steel 1	Steel 2	Inner	Middle	Outer
1	168.2	290.9	342.6	462.9	462.5
2	171.6	295.5	337.1	345.4	465.1
Number	Weight [N/m]	Loss [W/m]	Sag [m]		
1	26.63	50.4667	16.3583		
2	26.70	49.1728	16.3667		

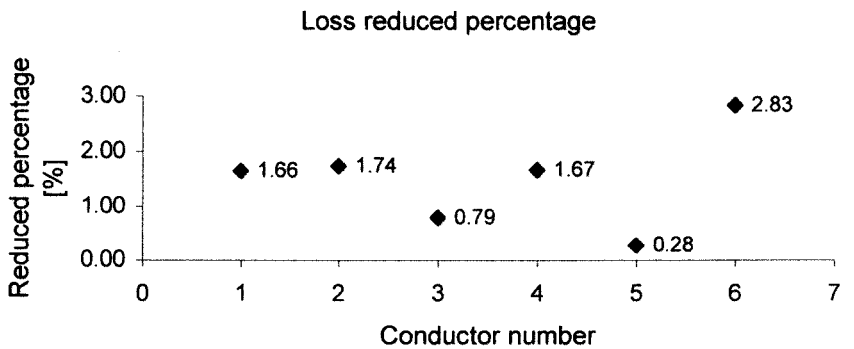

Figure E.1 Percentage of reduced loss compared to the reference

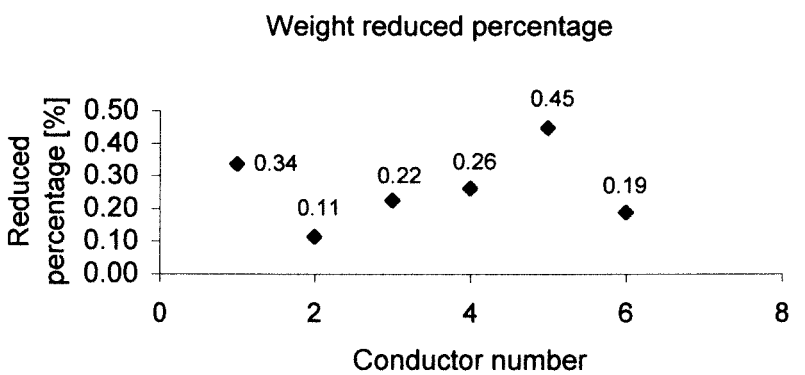

Figure E.2 Percentage of reduced weight compared to the reference

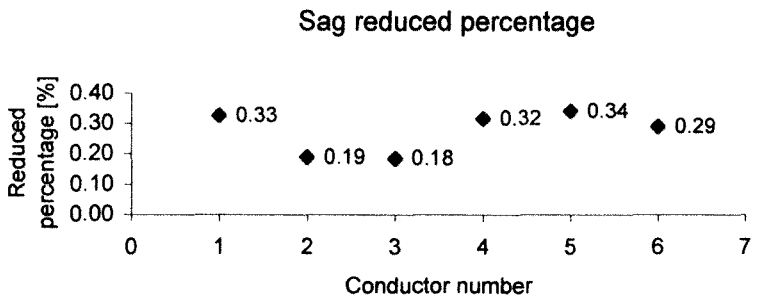

Figure E.3 Percentage of reduced sag compared to the reference

E.2 Fixing wire diameters and steel lay lengths, changing aluminum lay lengths

Table E.9 Unchanged wire and steel lay parameters

Steel wire diameter [mm]			Aluminum wire diameter [mm]		
Steel king	Steel lay 1	Steel lay 2	Inner	Middle	Outer
2.482	2.482	2.482	4.135	4.135	4.135
Steel layer outer diameter [mm]			Aluminum layer outer diameter [mm]		
Steel king	Steel lay 1	Steel lay 2	Inner	Middle	Outer
2.482	7.446	12.410	20.680	28.950	37.220
Steel lay length [mm]			Aluminum lay length [mm]		
Steel king	Steel lay 1	Steel lay 2	Inner	Middle	Outer
1000.0	186.10	248.20	Changed	Changed	Changed

Table E.10 Changed aluminum lay lengths

Conductor number	Inner [mm]	Middle [mm]	Outer [mm]	Weight [N/m]
Conductor 1	351.6	289.5	483.9	26.76
Conductor 2	322.4	321.1	400.5	26.81
Conductor 3	296.1	378.1	397.0	26.78
Conductor 4	267.8	413.2	388.3	26.78
Conductor 5	214.5	436.1	392.9	26.81
Conductor 6	206.8	463.2	372.2	26.84

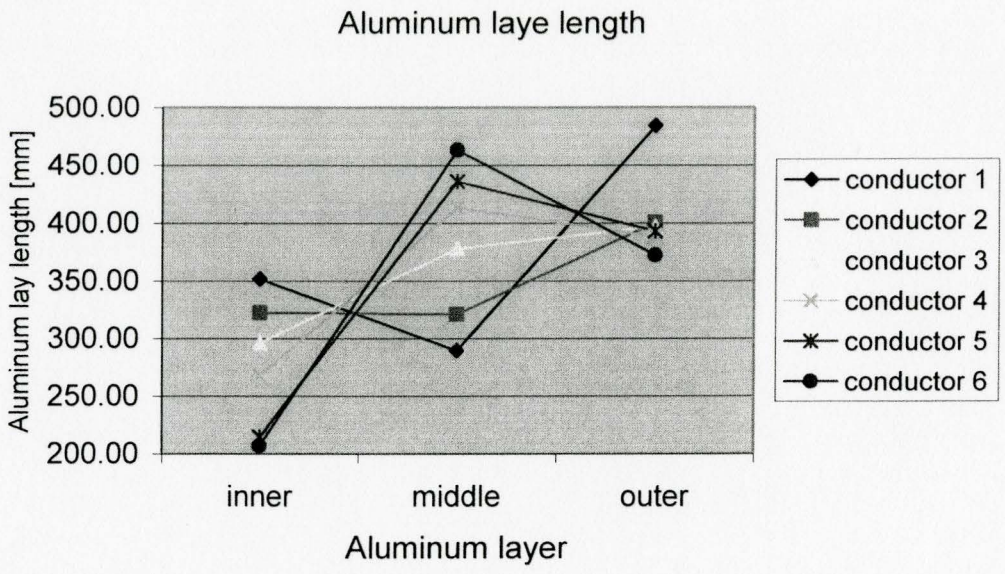

Figure E.4 Changed lay lengths with fixed wire diameters

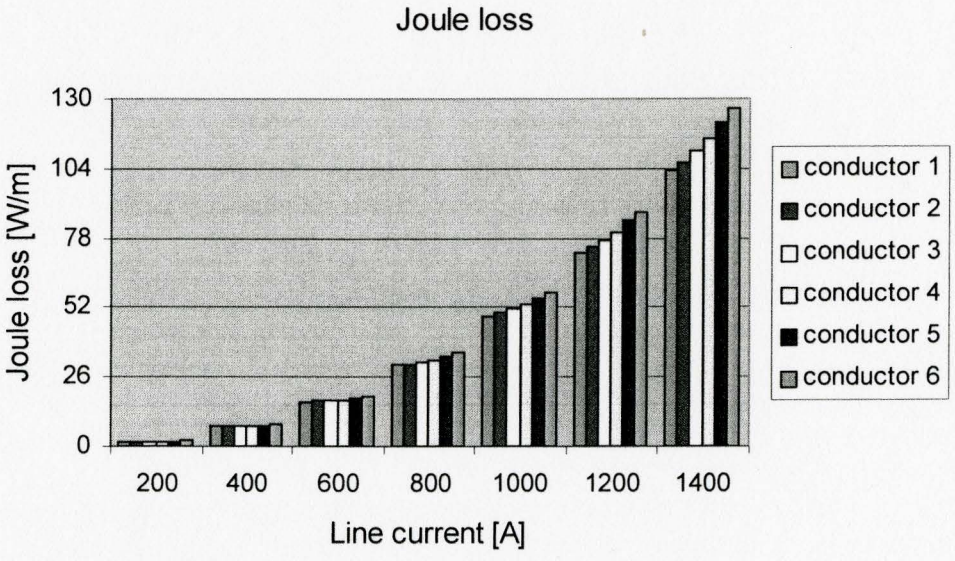

Figure E.5 Variation of Joule losses in six conductors at various line currents

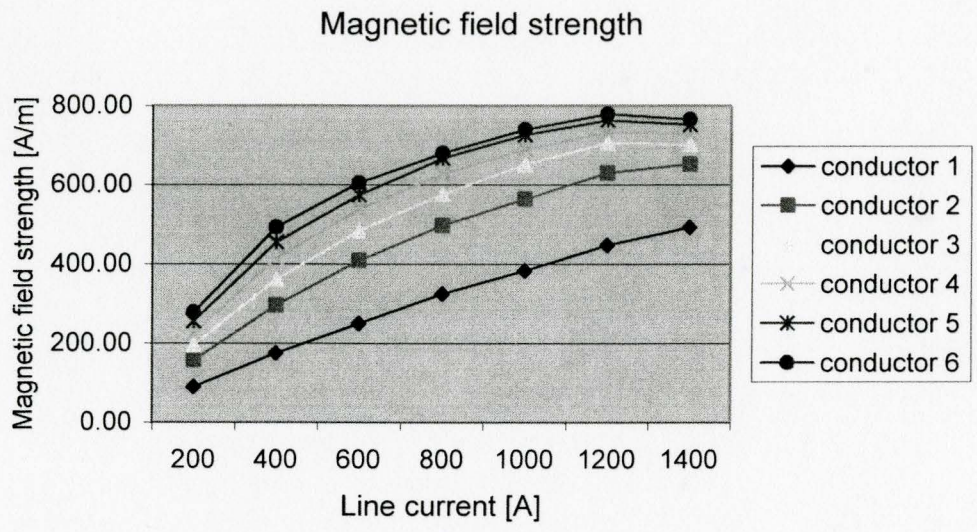

Figure E.6 Variation of six conductor magnetic strength at various line currents

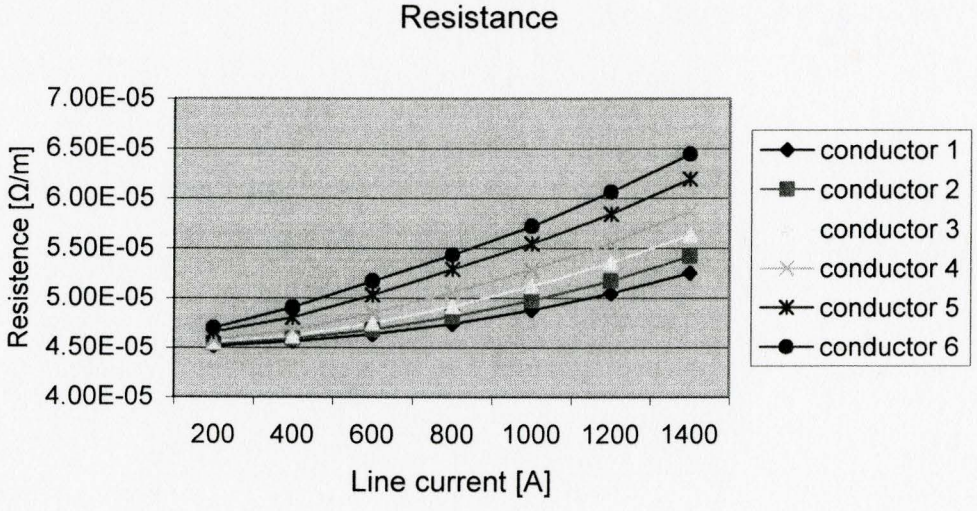

Figure E.7 Variation of resistance in six conductors at various line currents

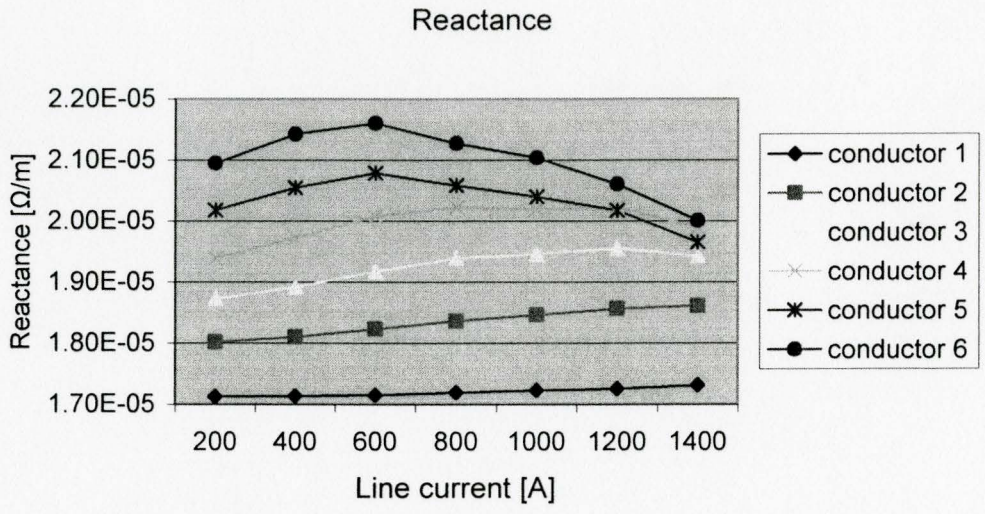

Figure E.8 Variation of reactance in six conductors at various line currents

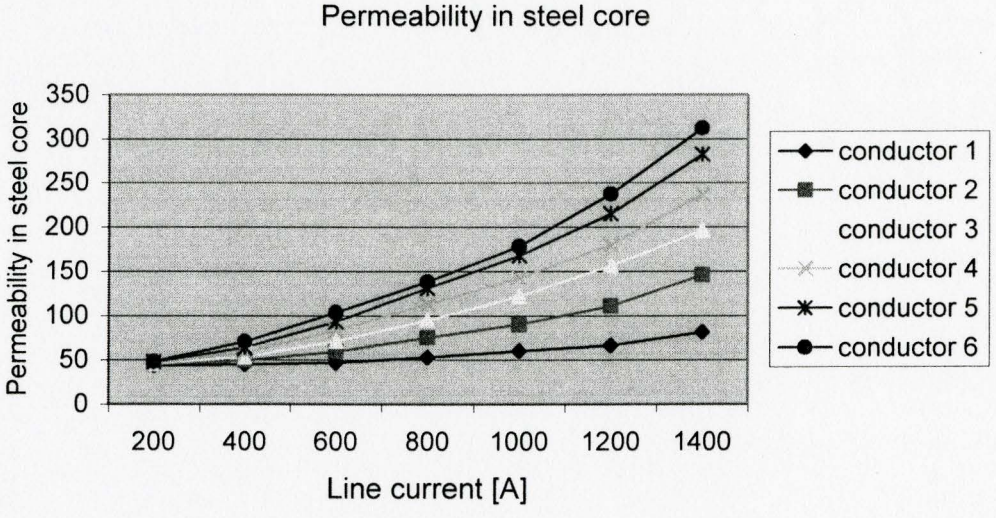

Figure E.9 Variation of the permeability at various line currents

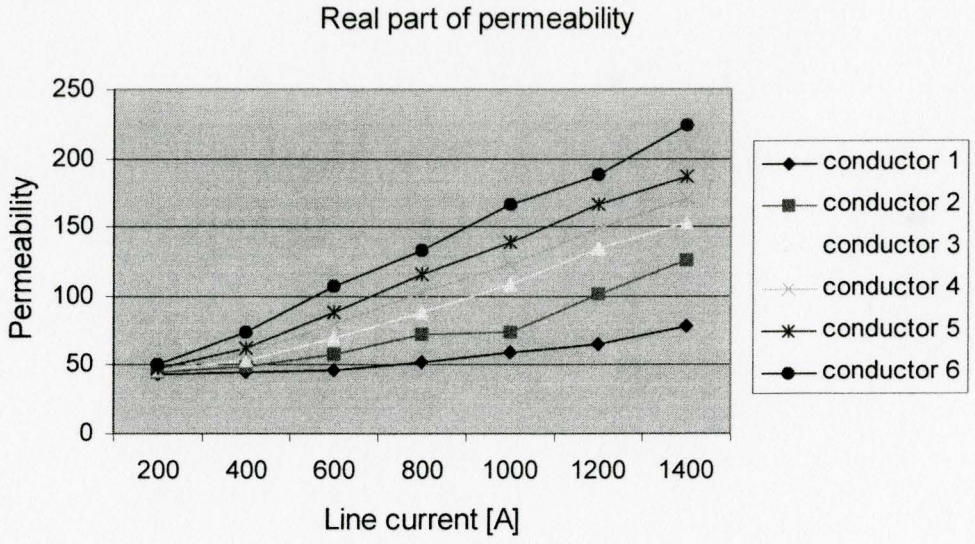

Figure E.10 Variation of real part of the permeability at various line currents

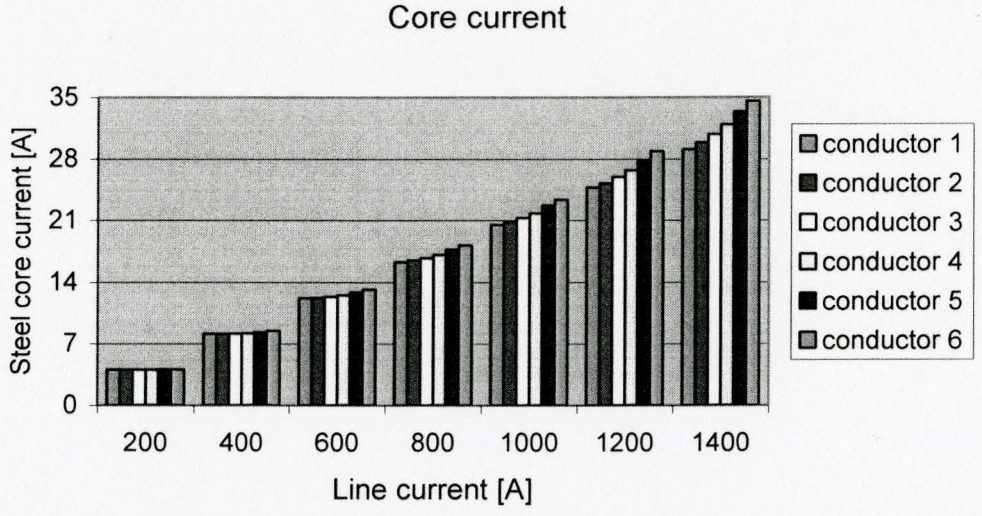

Figure E.11 Variation of steel core current at various line currents

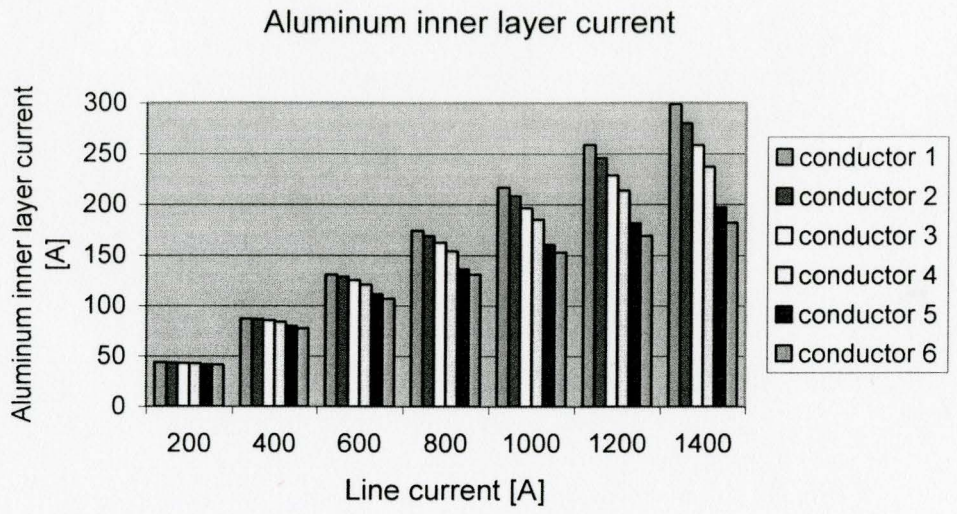

Figure E.12 Variation of aluminum inner layer current at various line currents

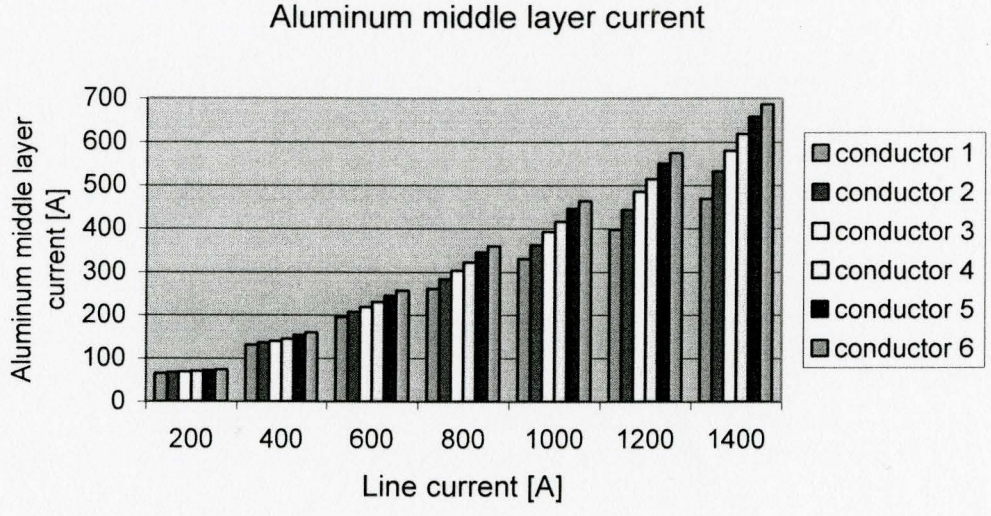

Figure E.13 Variation of aluminum middle layer current at various line currents

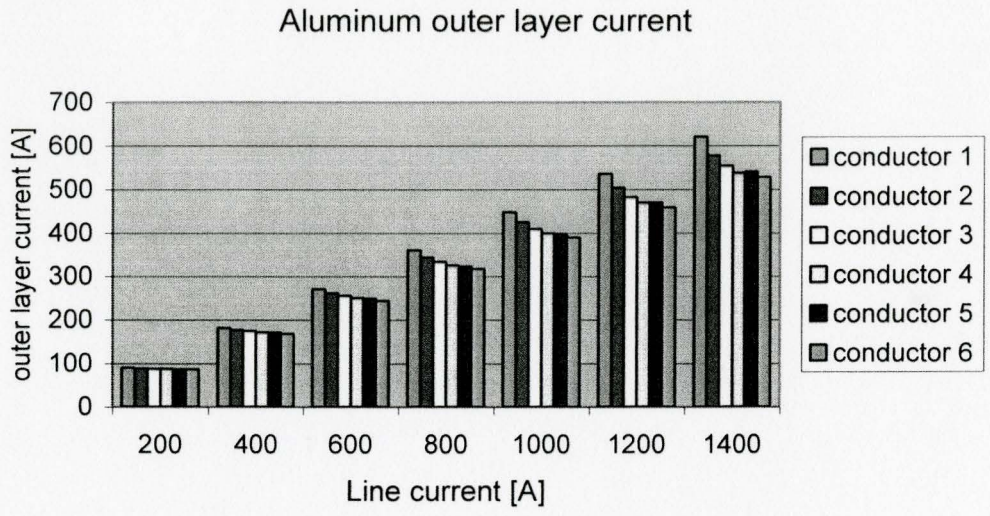

Figure E.14 Variation of aluminum outer layer current at various line currents

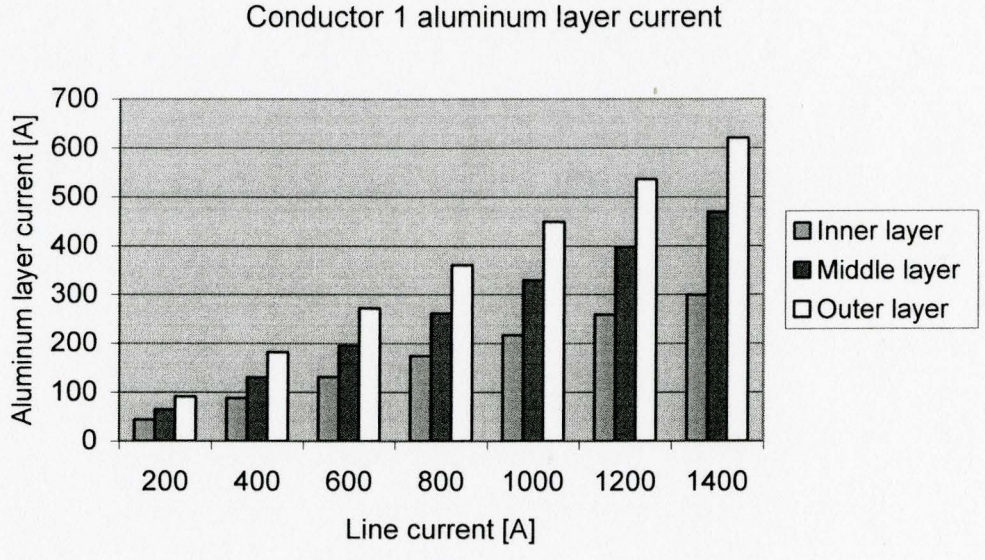

Figure E.15 Variation of three aluminum layer currents in conductor 1 at various line currents

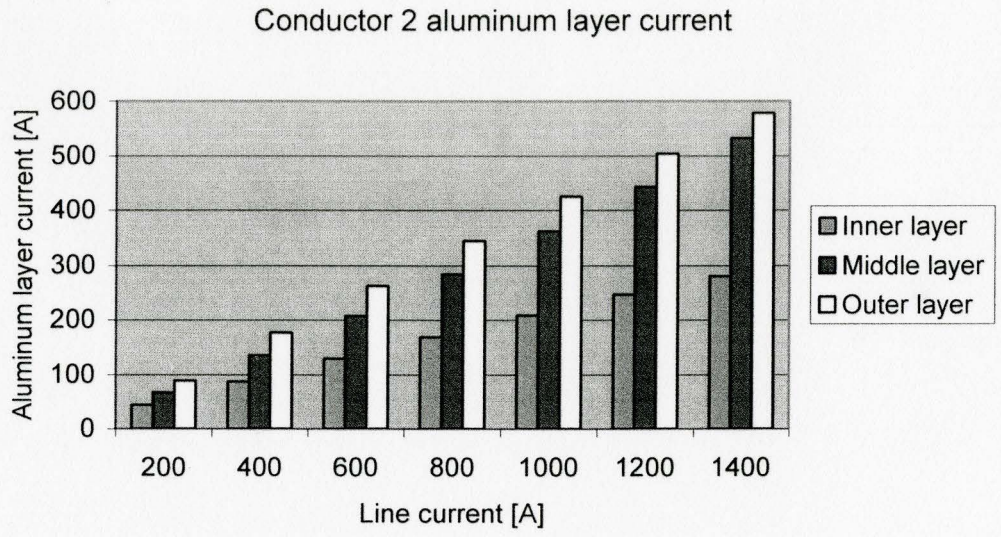

Figure E.16 Variation of aluminum layer currents in conductor 2 at various line currents

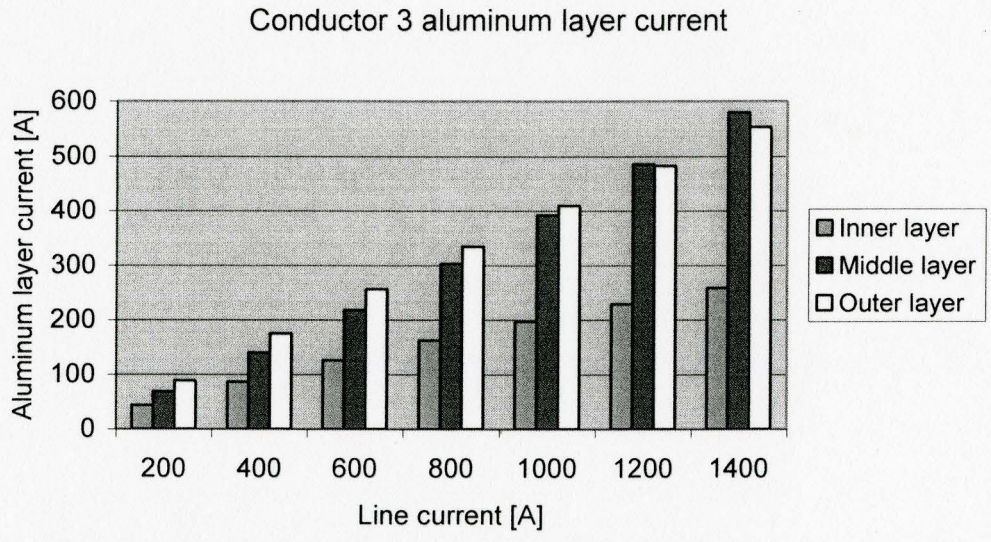

Figure E.17 Variation of aluminum layer currents in conductor 3 at various line currents

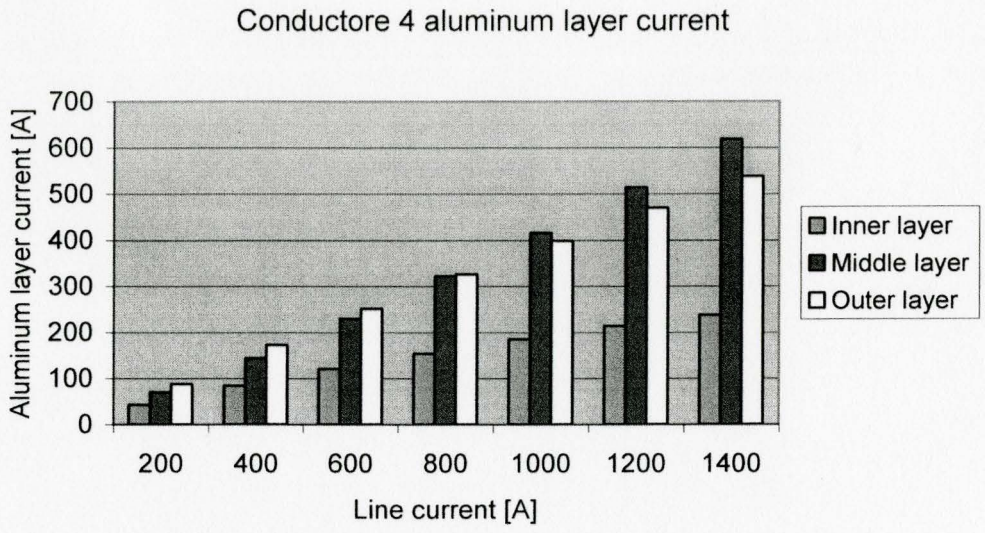

Figure E.18 Variation of three aluminum layer currents in conductor 4 at various line currents

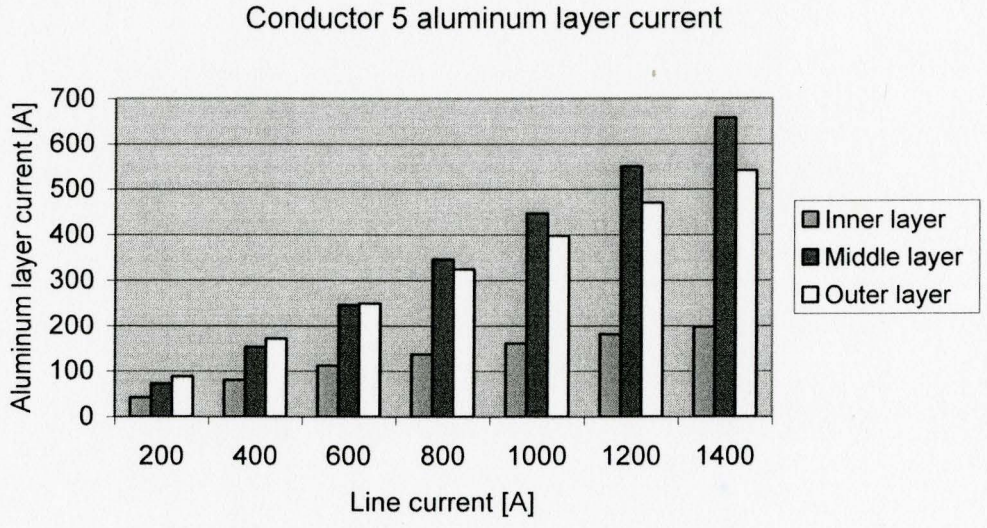

Figure E.19 Variation of aluminum layer currents in conductor 5 at various line currents

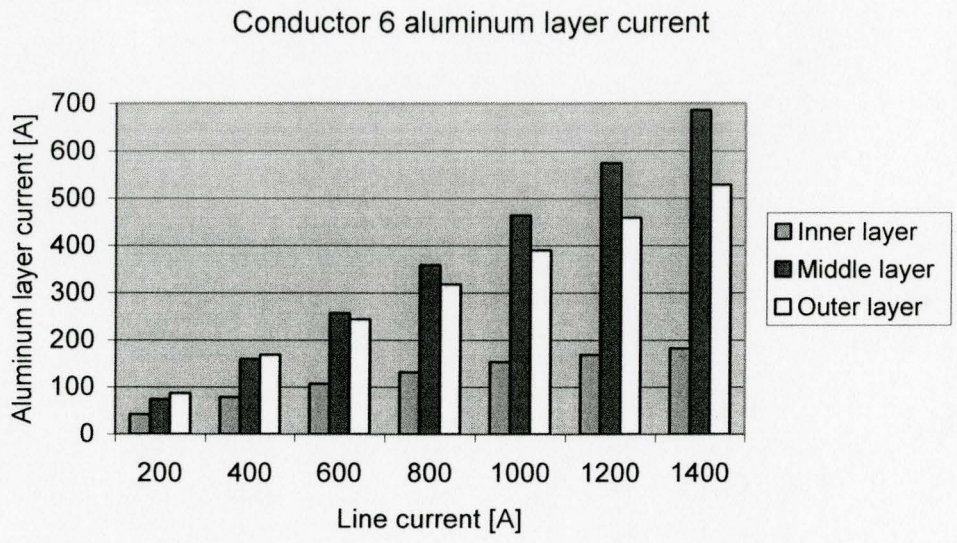

Figure E.20 Variation of aluminum layer currents in conductor 6 at various line currents

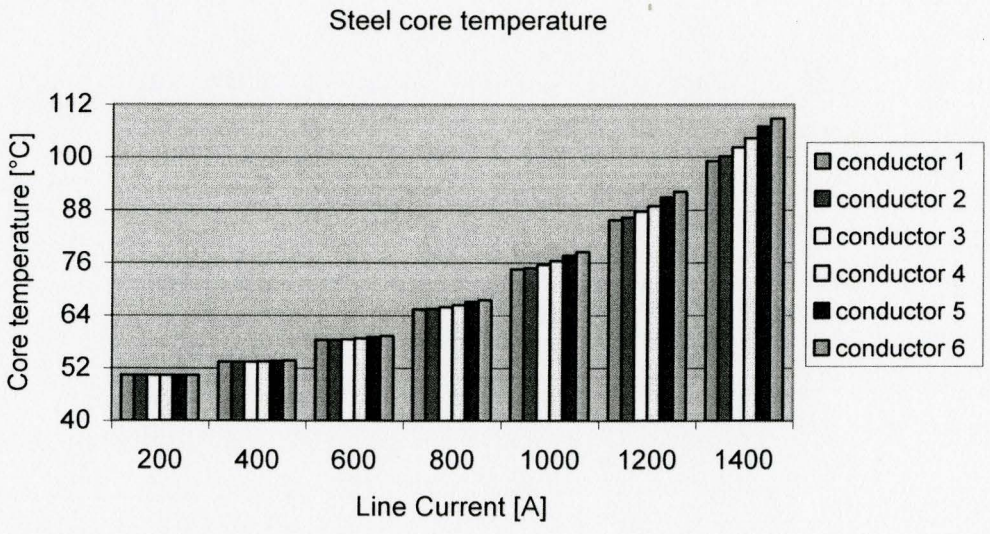

Figure E.21 Variation of steel king layer temperature at various line currents

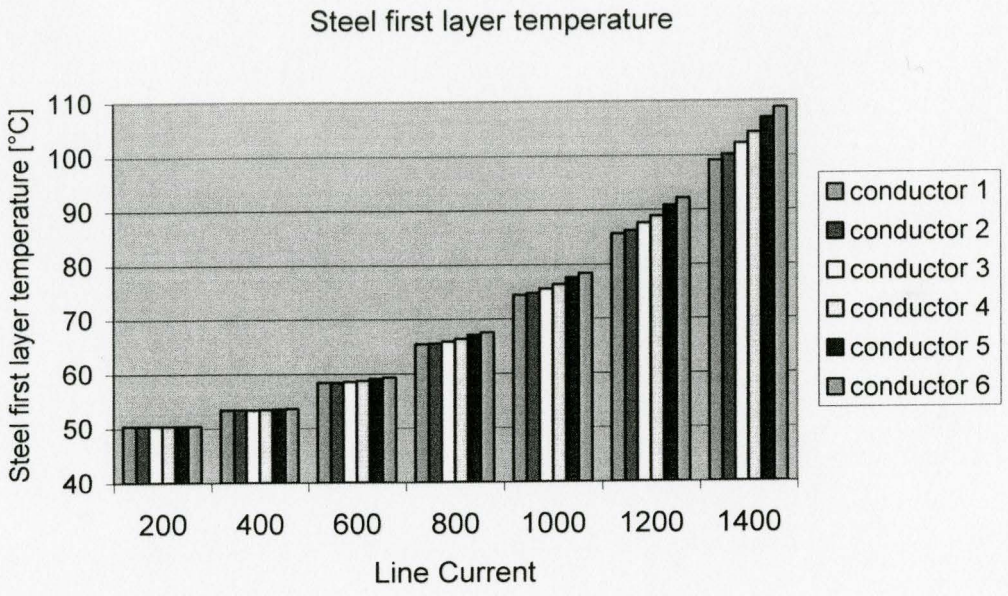

Figure E.22 Variation of steel first layer temperature at various line currents

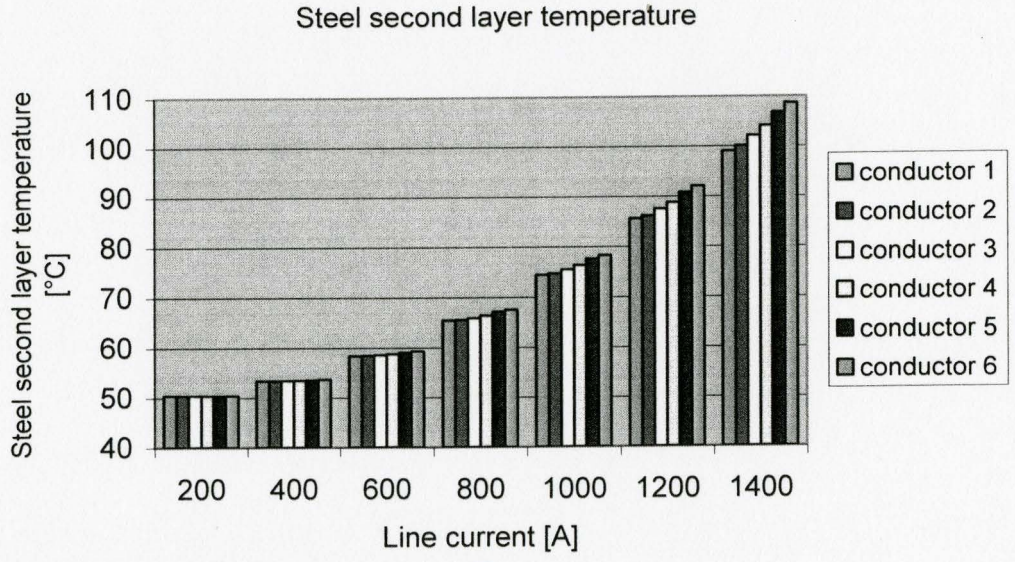

Figure E.23 Variation of steel second layer temperature at various line currents

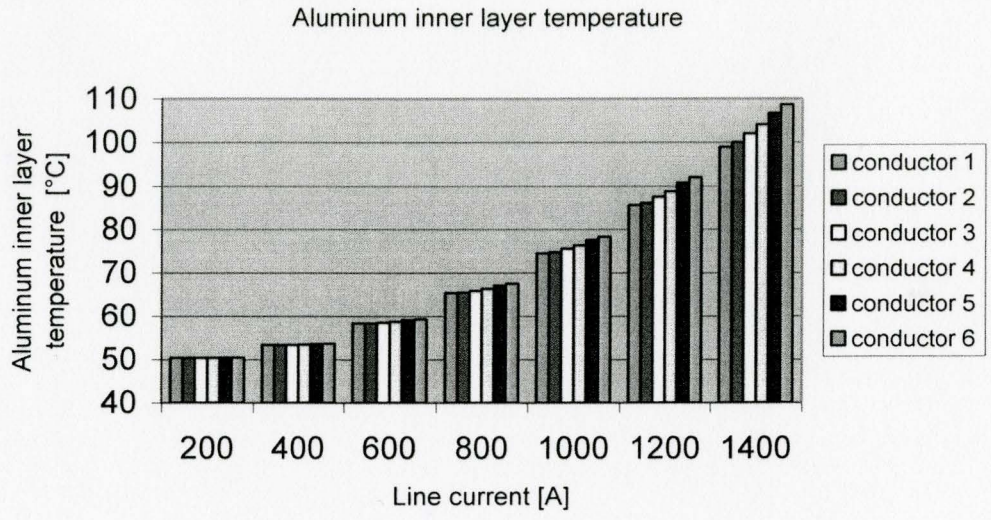

Figure E.24 Variation of aluminum inner layer temperature at various line currents

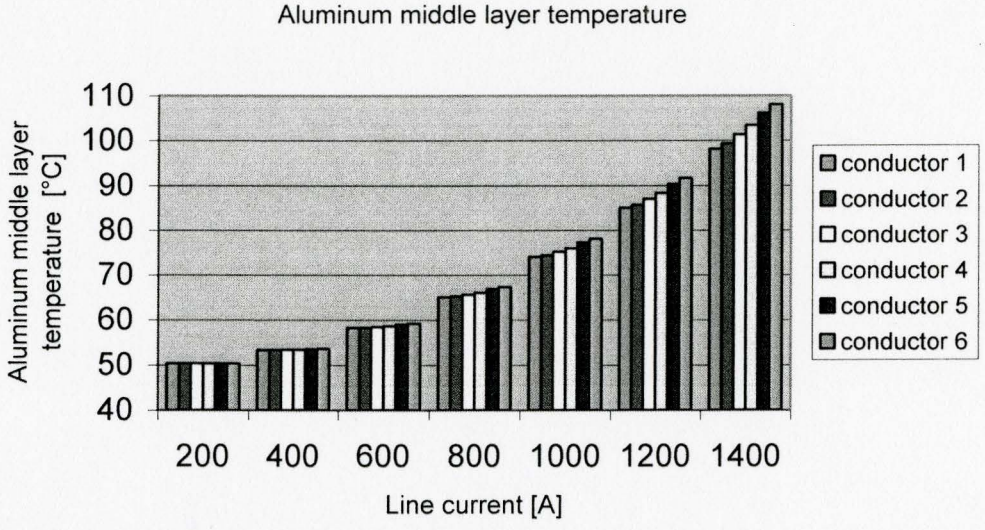

Figure E.25 Variation of aluminum middle layer temperature at various line currents

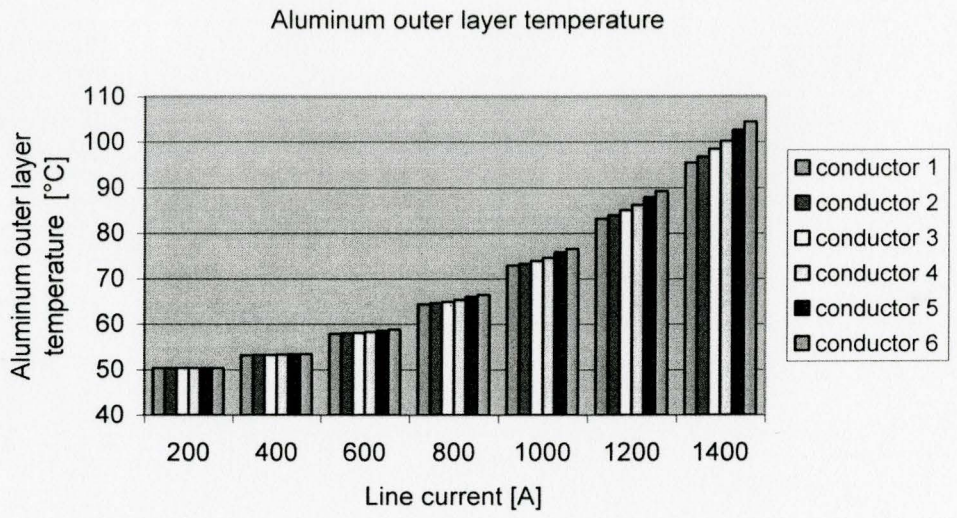

Figure E.26 Variation of aluminum outer layer temperature at various line currents

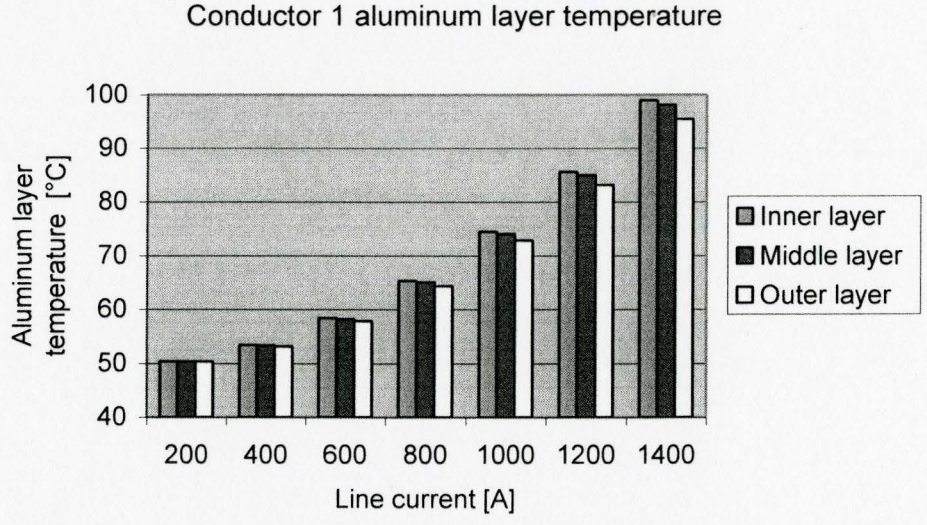

Figure E.27 Variation of aluminum layer temperature in conductor 1 at various line currents

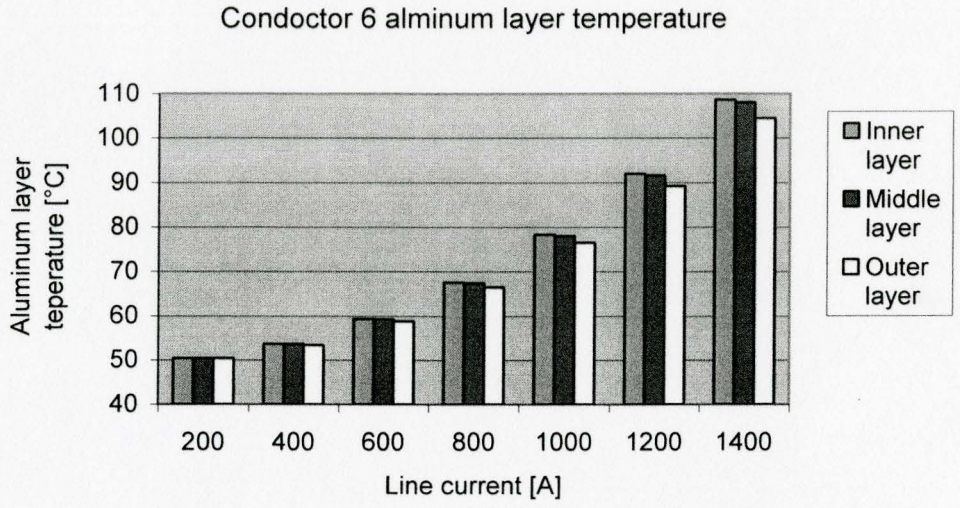

Figure E.28 Variation of aluminum layer temperature in conductor 6 at various line currents

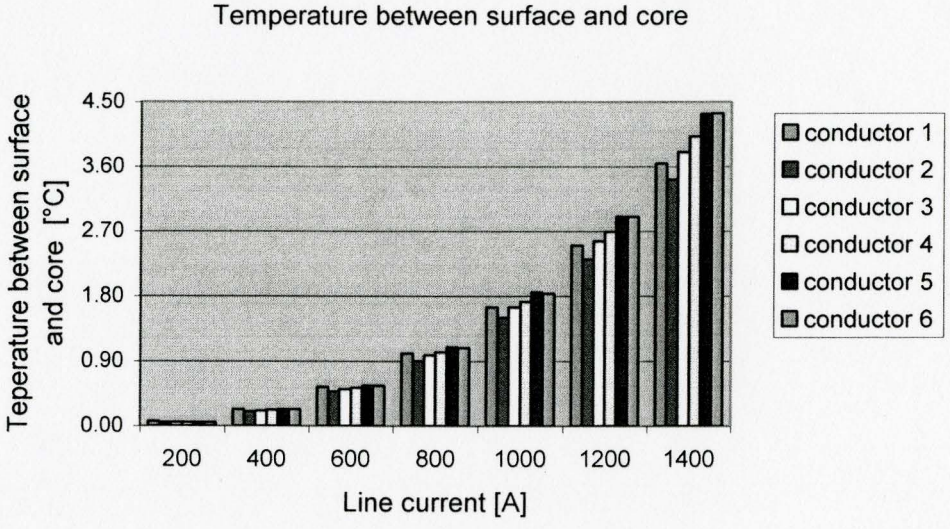

Figure E.29 Temperature differences between steel core and conductor surface

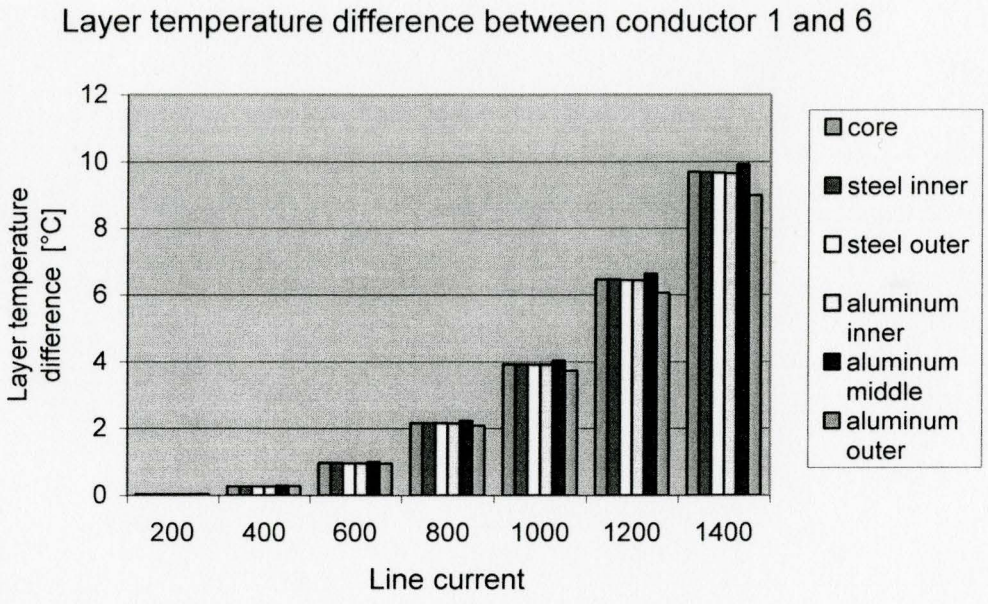

Figure E.30 Temperature differences in layers between conductor 1 and 6

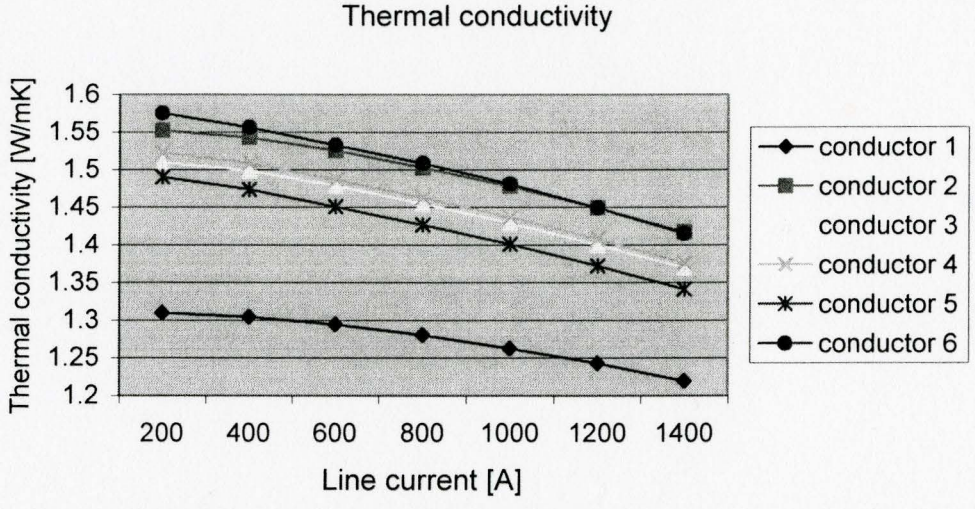

Figure E.31 Variation of thermal conductivity at various line currents

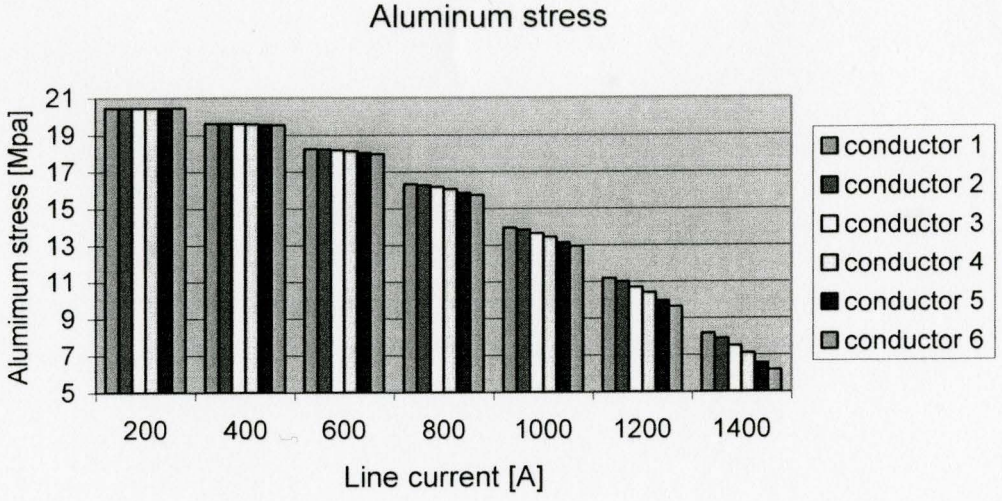

Figure E.32 Variation of aluminum stresses at various line currents

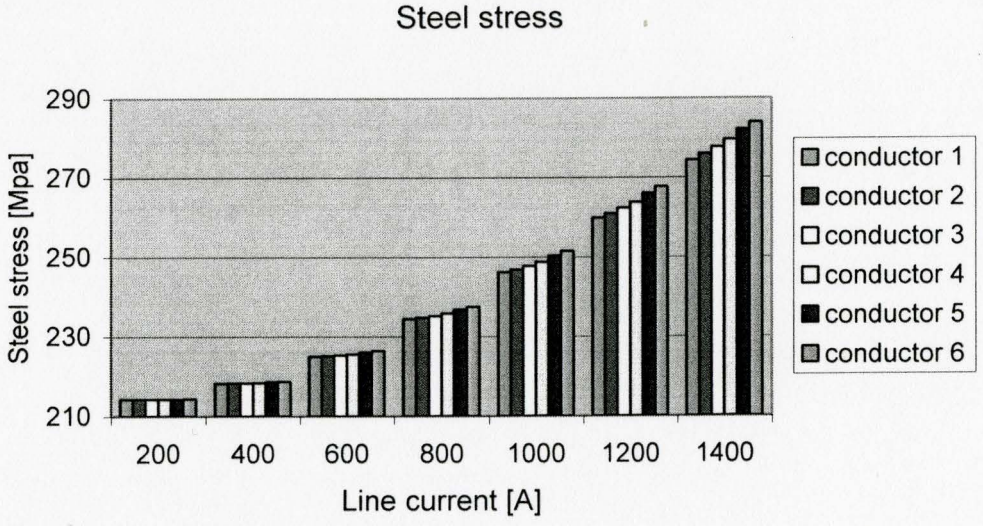

Figure E.33 Variation of steel stresses at various line currents

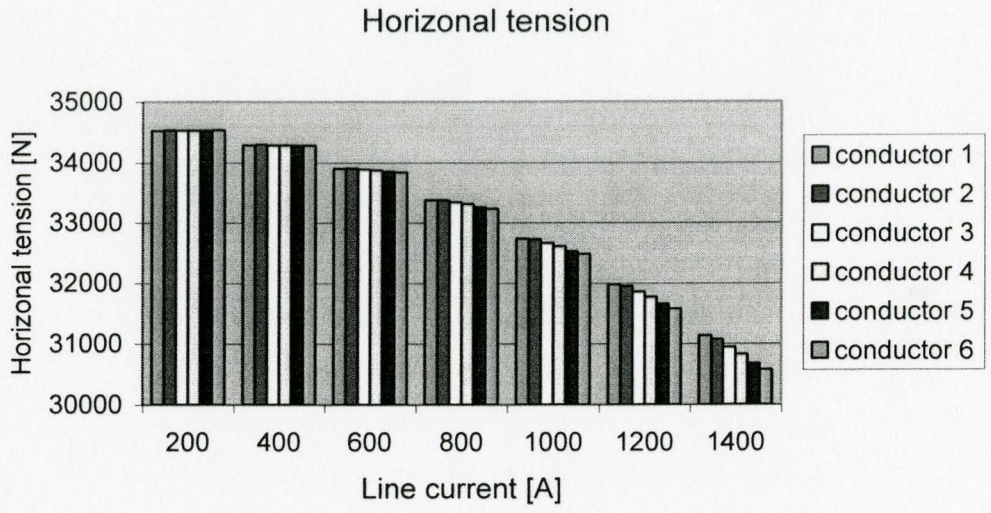

Figure E.34 variation of horizontal tension at various line currents

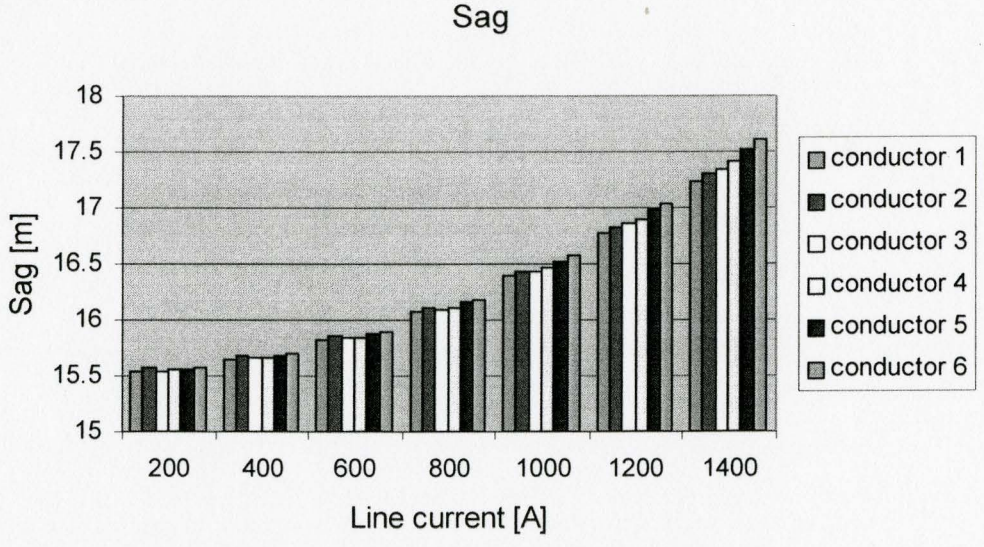

Figure E.35 Variation of sags at various line currents with line length 400 meters

E.3 Fixing wire diameters, changing steel and aluminum lay lengths

Table E.11 Unchanged steel wire and aluminum wire diameters

Steel wire diameter [mm]			Aluminum wire diameter [mm]		
King	Steel lay 1	Steel lay 2	Inner	Middle	Outer
2.482	2.482	2.482	4.135	4.135	4.135
Steel layer's outer diameters [mm]			Aluminum layer's outer diameters [mm]		
Steel lay 1	Steel lay 2	Steel lay 3	Inner	Middle	Outer
2.482	7.446	12.410	20.680	28.950	37.220

Table E.12 Changed steel and aluminum lay lengths

Steel lay length [mm]			Aluminum lay length [mm]		
	Steel lay 1	Steel lay 2	Inner	Middle	Outer
Conductor 1	223.4	297.8	351.6	289.5	483.9
Conductor 2	156.6	201.7	322.4	321.1	400.5
Conductor 3	160.7	255.4	296.1	378.1	397.0
Conductor 4	215.5	280.8	267.8	413.2	388.3
Conductor 5	214.6	262.0	214.5	436.1	392.9
Conductor 6	134.0	198.6	206.8	463.2	372.2
Weight [N/m]					
Conductor 1	Conductor 2	Conductor 3	Conductor 4	Conductor 5	Conductor 6
26.74	26.83	26.78	26.77	26.80	26.80

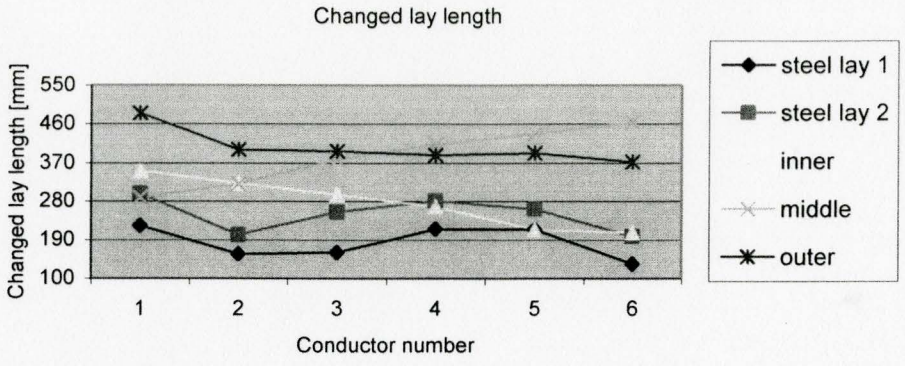

Figure E.36 Variation of lay lengths for different conductors at 1000 A

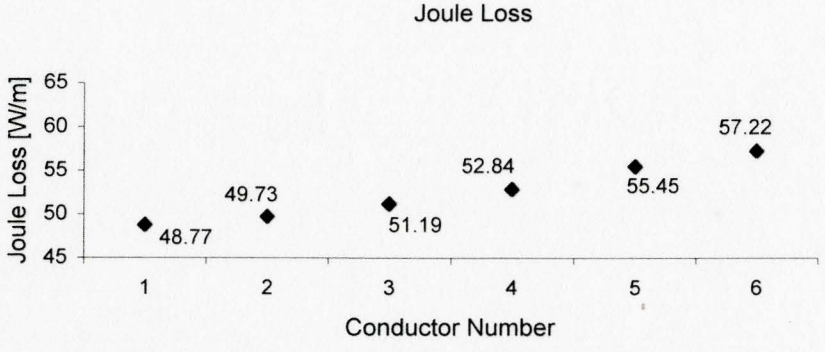

Figure E.37 Variation of Joule losses for different conductors at 1000A

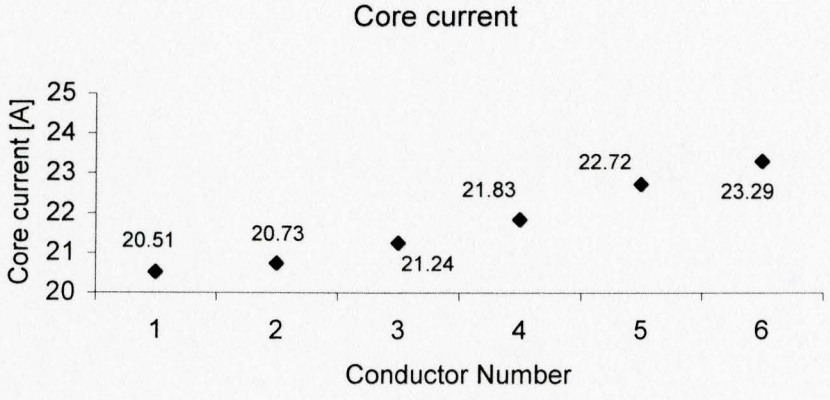

Figure E.38 Variation of core current for different conductors at 1000A

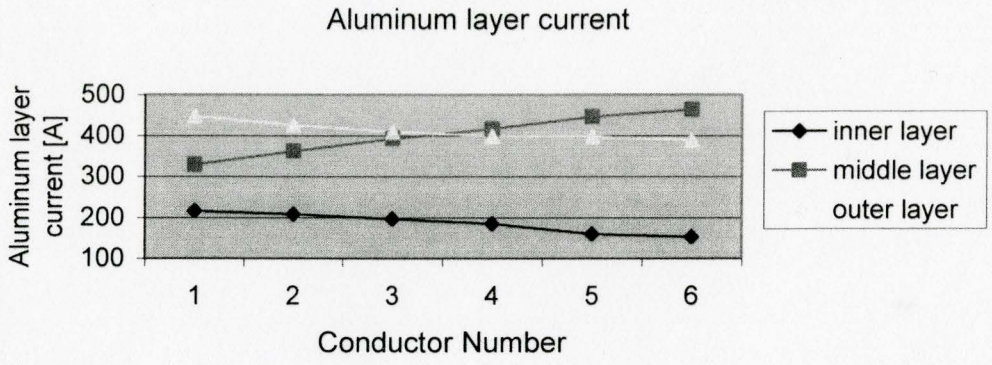

Figure E.39 Variation of aluminum current for different conductors at 1000A

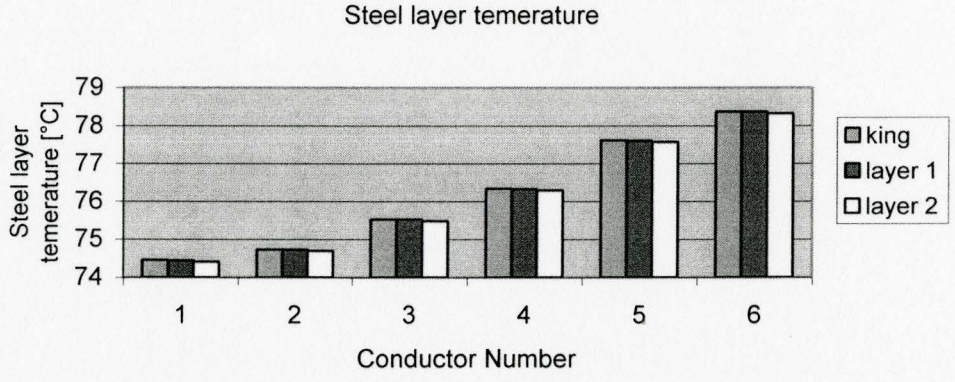

Figure E.40 Variation of steel layer temperature for different conductors at 1000A

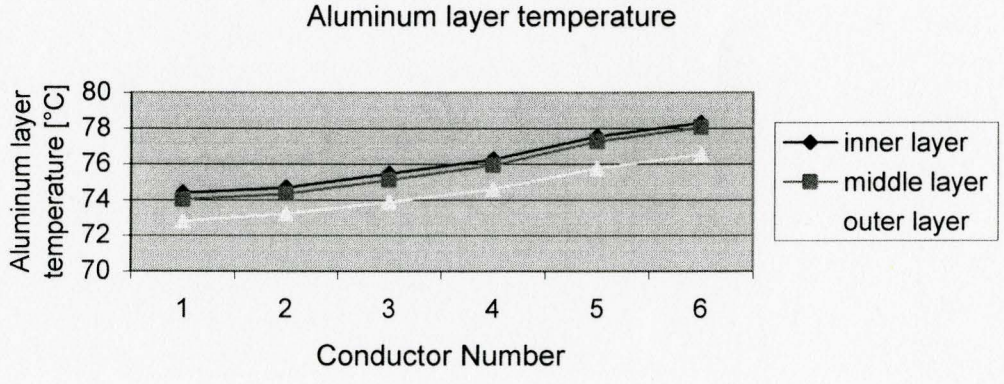

Figure E.41 Variation of aluminum layer temperature for different conductors at 1000A

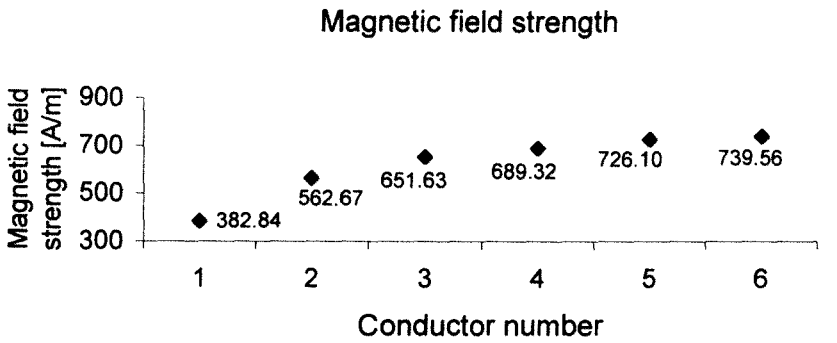

Figure E.42 Variation of magnetic field strength for different conductors at 1000A

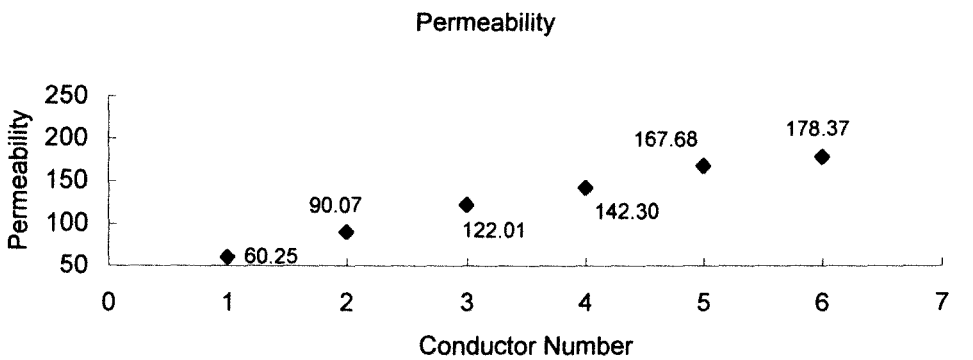

Figure E.43 Variation of permeability for different conductors in 1000A

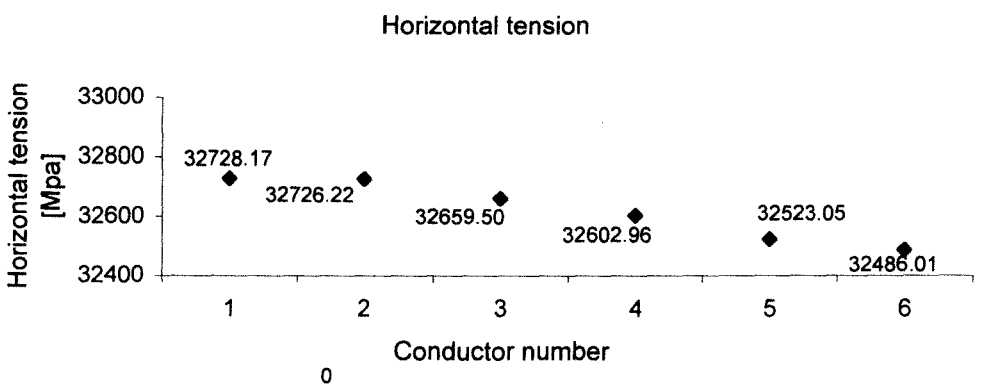

Figure E.44 Variation of horizontal tension for different conductors at 1000A

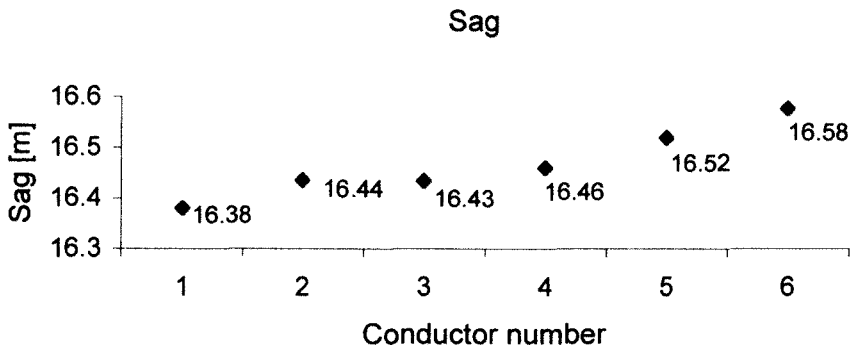

Figure E.45 Variation of sags for different conductors at 1000A

E.4 Fixing steel core size, changing aluminum lay lengths and wire diameters

Table E.13 Changed aluminum wire and layer parameters

	Wire diameter [mm]			Aluminum lay length [mm]		
	Inner	Middle	Outer	Inner	Middle	Outer
Conductor 1	4.20	4.20	4.20	351.6	289.5	483.9
Conductor 2	4.13	4.189	4.028	310.5	342.7	460.2
Conductor 3	4.029	4.067	4.002	271.4	362.8	461.3
Conductor 4	4.004	4.058	4.028	227.2	403.3	430.2
Conductor 5	4.025	4.108	4.036	211.9	451.2	373.0
Conductor 6	4.000	4.000	4.000	206.8	463.2	372.2

	Outer diameter [mm]			
	Inner	Middle	Outer	Weight [N/m]
Conductor 1	20.810	29.210	37.610	27.39
Conductor 2	20.670	29.048	37.105	26.44
Conductor 3	20.468	28.602	36.606	25.73
Conductor 4	20.418	28.535	36.591	25.79
Conductor 5	20.461	28.676	36.749	26.09
Conductor 6	20.410	28.410	36.410	25.55

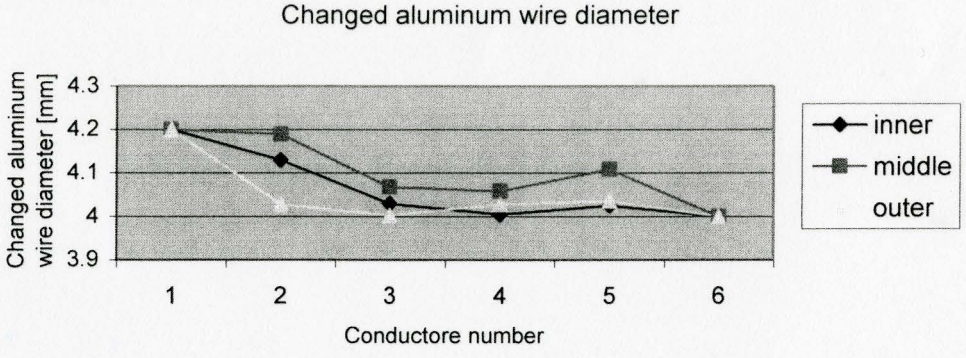

Figure E.46 Changed aluminum diameters at 1000A

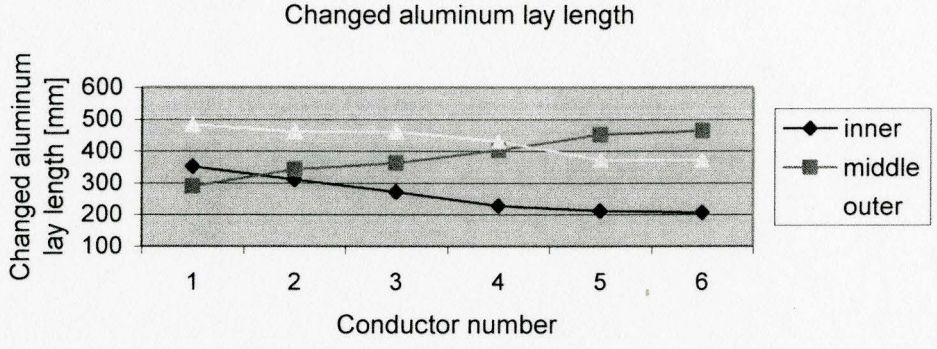

Figure E.47 Changed aluminum lay lengths at 1000A

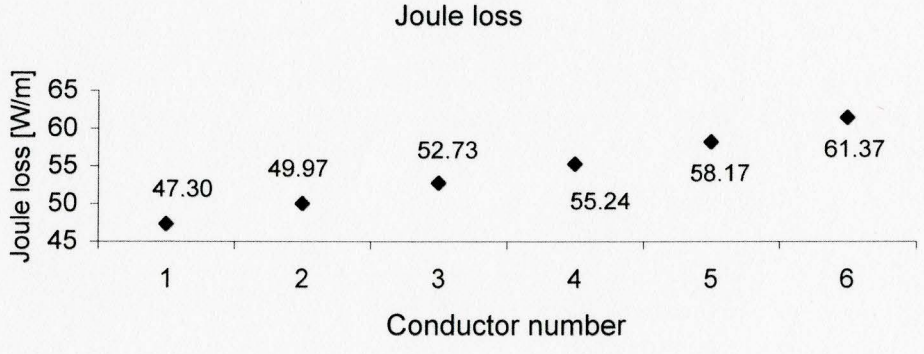

Figure E.48 Variation of Joule losses among conductors at 1000A

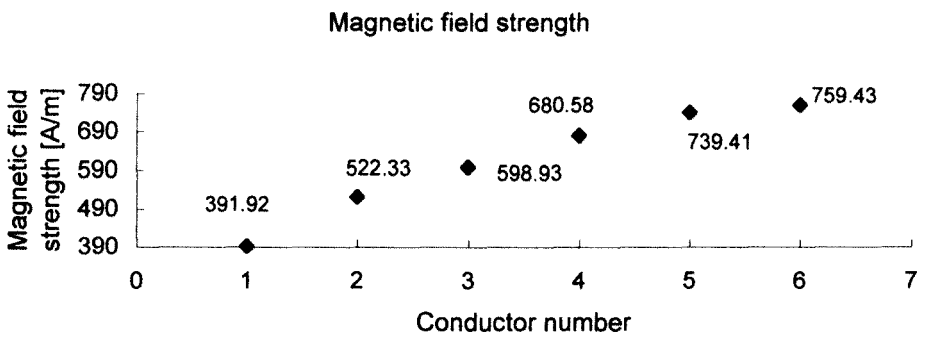

Figure E.49 Variation of magnetic strength among conductors at 1000A

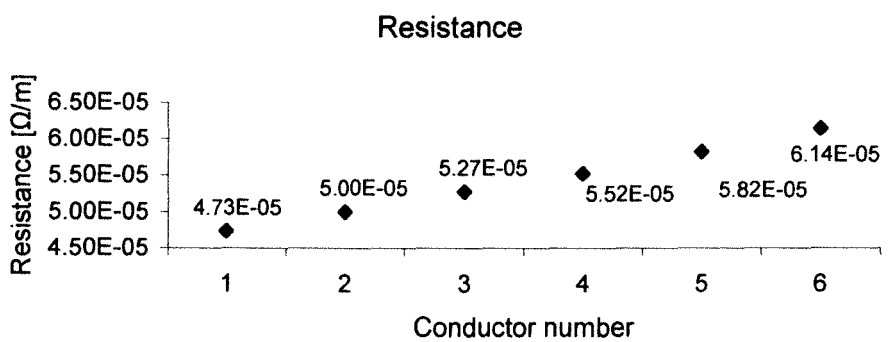

Figure E.50 Variation of resistance among conductors at 1000A

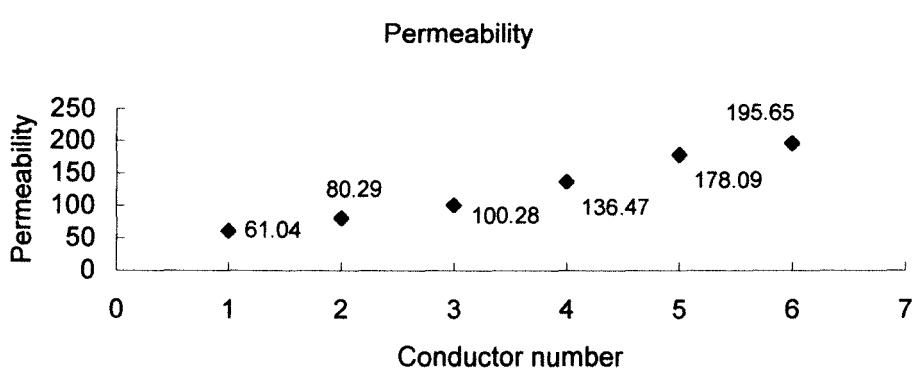

Figure E.51 Variation of permeability among conductors at 1000A

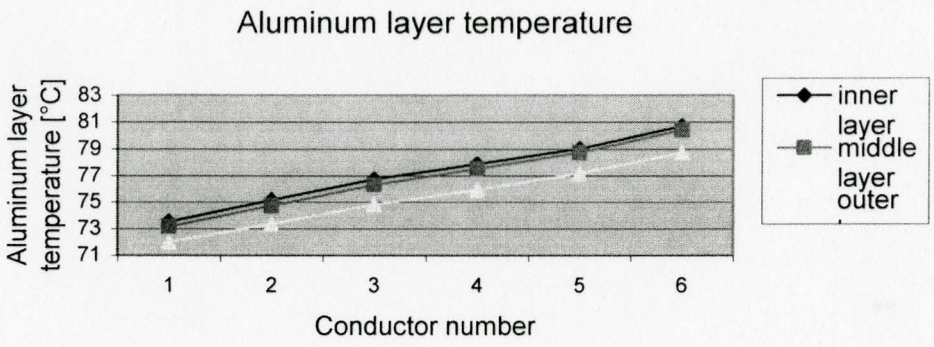

Figure E.52 Variation of aluminum layer temperature among conductors at 1000A

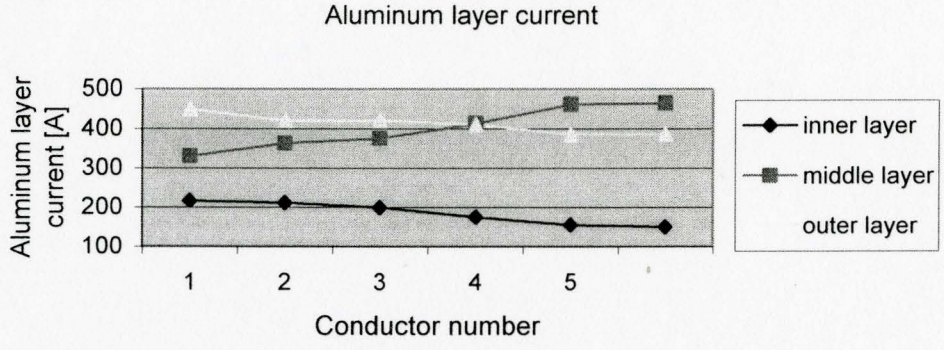

Figure E.53 Variation of aluminum layer current among conductors at 1000A

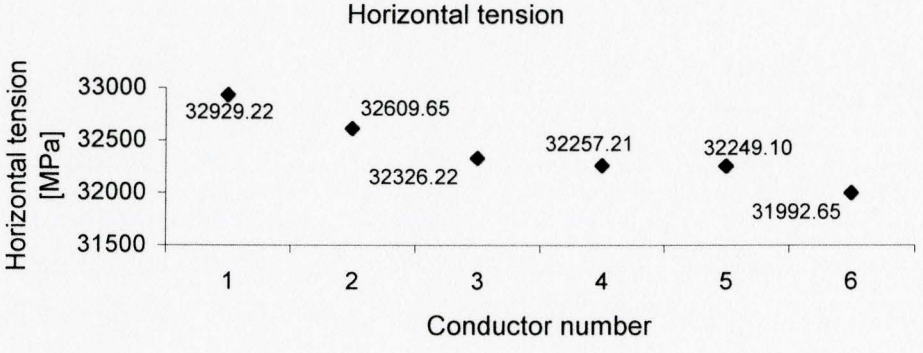

Figure E.54 Variation of horizontal tension among conductors at 1000A

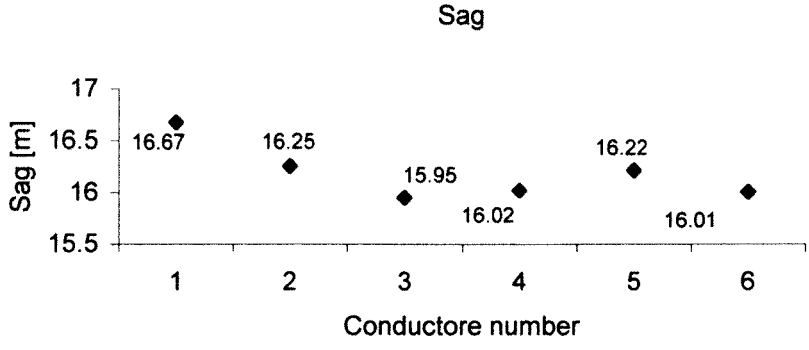

Figure E.55 Variation of sags among conductors at 1000A

Appendix F Results Using Genetic Algorithms in Three-layer Conductor Cardinal

F.1 Results of the application of the Genetic Algorithm

Table F.1 Standard in ASTM 232M

Ratio of lay length of a layer to nominal outside diameter of that lay							
Aluminum layer						Steel layer	
Outer		Middle		Inner		Outer	
Min	Max	Min	Max	Min	Max	Min	Max
10	13	10	16	10	17	18	30
Conversion of the lay length of Cardinal conductor [mm]							
303.8	394.9	236.3	378.1	168.8	286.9	182.3	303.8

Ranges of changed lay lengths in this project is the same as that of table F.1

Table F.2 Min and max losses with changed aluminum lay lengths

Minimum Joule loss [W/m]		Weight [N/m]
76.7966		17.92
Aluminum lay length [mm]		
Inner	Middle	Outer
286.9	236.3	394.9
Maximum Joule loss [W/m]		Weight [N/m]
80.6103		17.98
Aluminum lay length [mm]		
Inner	Middle	Outer
168.8	378.1	303.8

Table F.3 Min and max losses with changed steel and aluminum lay lengths

Minimum Joule loss [W/m]		Weight [N/m]	
76.7951		17.92	
Layer length [mm]			
Steel lay 1	Al inner	Al middle	Al outer
303.8	286.9	236.3	394.9
Maximum Joule loss [W/m]		Weight [N/m]	
80.6167		17.99	
Layer length [mm]			
Steel lay 1	Al inner	Al middle	Al outer
182.3	168.8	378.1	303.8

Table F.4 Cardinal used as a reference

Aluminum lay length [mm]			Steel lay length [mm]
Inner	Middle	Outer	First layer
253.2	307.2	334.2	253.2
Aluminum wire diameter [mm]		Steel wire diameter [mm]	
3.376		3.376	
Loss [W/m]	Weight [N/m]		Sag [m]
77.2778	17.92		12.8740

Table F.5 Low loss conductors

Results with changed aluminum lay lengths

Aluminum lay [mm]				Weight [N/m]	Loss [W/m]	Sag [m]
Number	Inner	Middle	Outer			
1	279.6	377.8	377.4	17.84	76.6676	12.8374
2	261.9	328.6	389.9	17.86	77.0309	12.8536

Results with changed steel and aluminum lay lengths

Steel lay [mm]		Aluminum lay [mm]		
Number	Steel 1	Inner	Middle	Outer
1	168.2	342.6	462.9	462.5
2	171.6	337.1	345.4	465.1

Number	Weight [N/m]	Loss [W/m]	Sag [m]
1	26.63	50.4667	16.3583
2	26.70	49.1728	16.3667

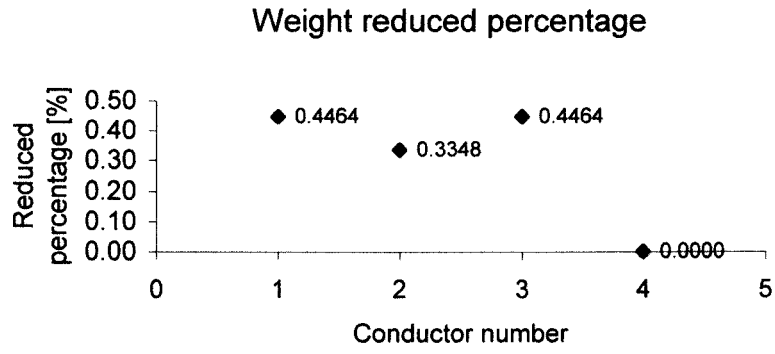

Figure F.1 Percentage of reduced loss compared to the reference

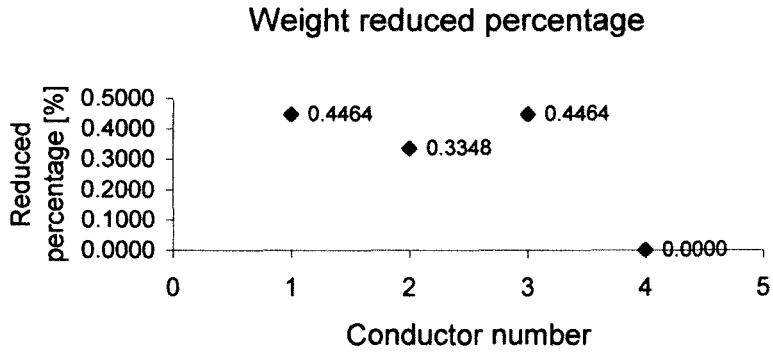

Figure F.2 Percentage of reduced weight compared to the reference

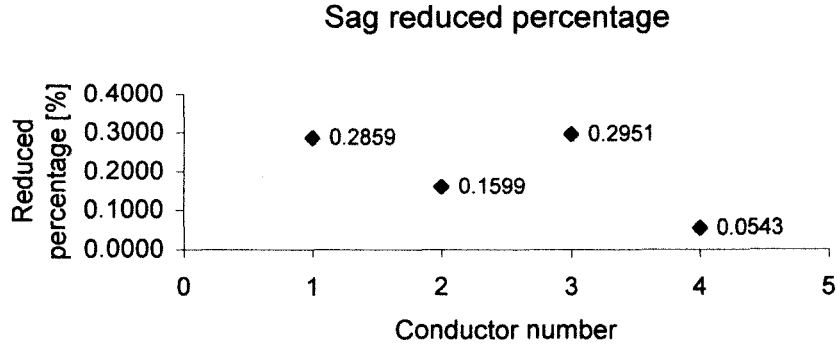

Figure F.3 Percentage of reduced sag compared to the reference

F.2 Fixing wire diameters and steel lay lengths, changing aluminum lay lengths

Table F.6 Unchanged wire and steel lay parameters

Steel wire diameter [mm]		Aluminum wire diameter [mm]		
Steel king	Steel lay 1	Inner	Middle	Outer
3.376	3.376	3.376	3.376	3.376
Steel layer outer diameter [mm]		Aluminum layer outer diameter [mm]		
Steel king	Steel lay 1	Inner	Middle	Outer
3.376	10.127	16.878	23.629	30.380
Steel lay length [mm]		Aluminum lay length [mm]		
Steel king	Steel lay 1	Inner	Middle	Outer
1000.0	253.2	Changed	Changed	Changed

Table F.7 Changed aluminum lay lengths

Conductor number	Inner [mm]	Middle [mm]	Outer [mm]	Weight [N/m]
Conductor 1	286.9	236.3	394.9	17.92
Conductor 2	263.0	262.1	326.8	17.96
Conductor 3	241.8	314.1	341.5	17.91
Conductor 4	192.3	361.9	364.9	17.90
Conductor 5	175.1	356.00	320.7	17.96
Conductor 6	168.8	378.1	303.8	17.98

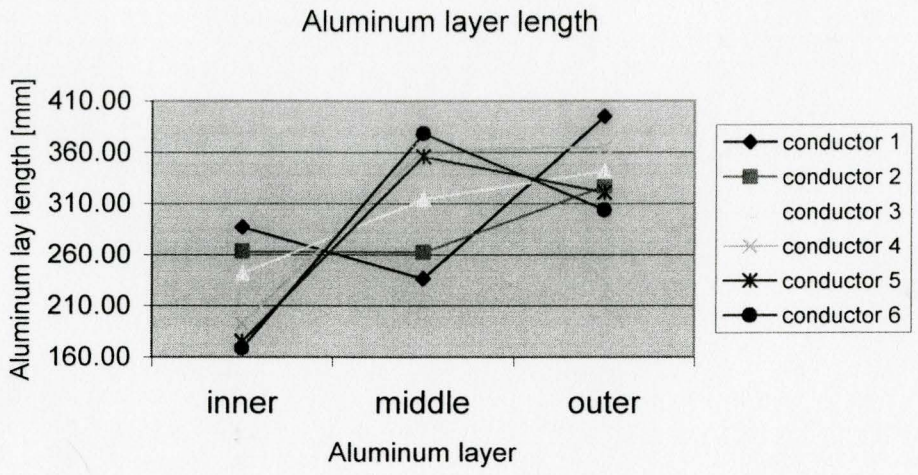

Figure F.4 Changed lay lengths with fixed wire diameters

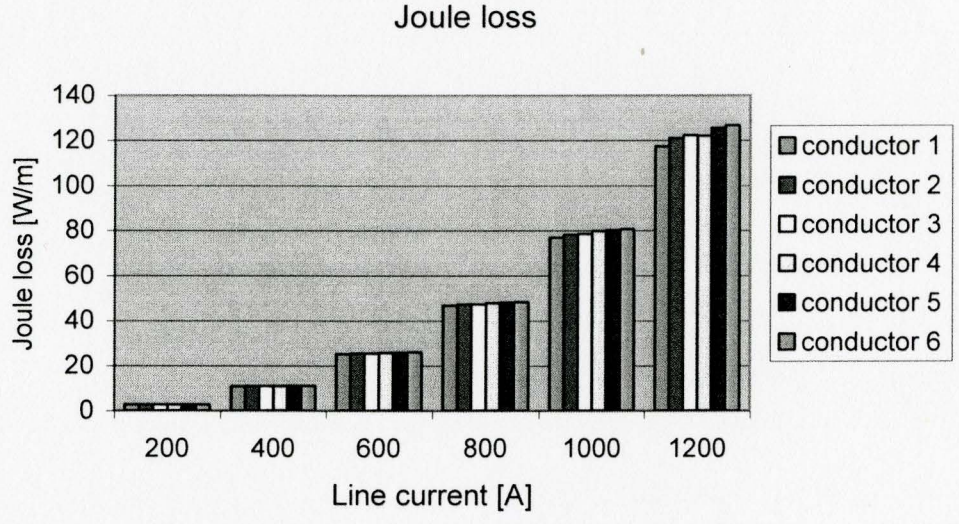

Figure F.5 Variation of Joule losses in six conductors at various line currents

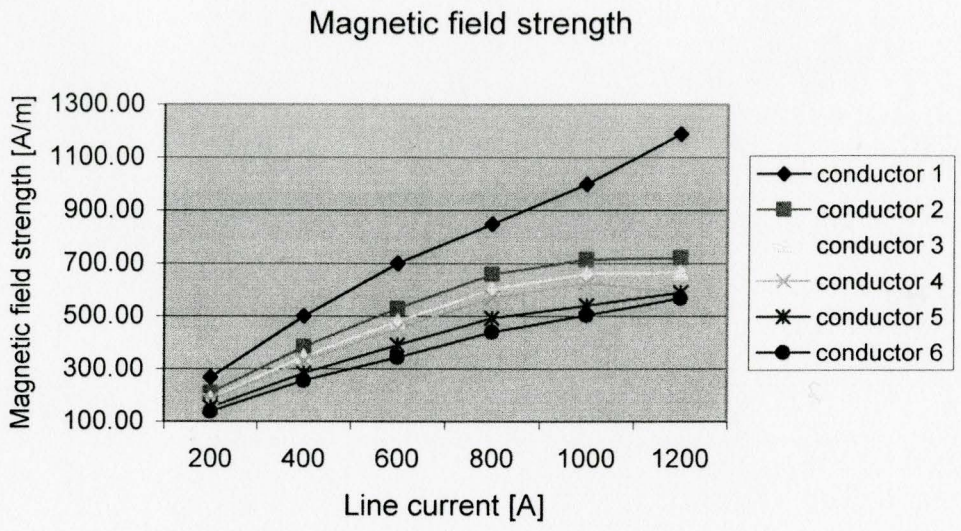

Figure F.6 Variation of six-conductor magnetic field strength at various line currents

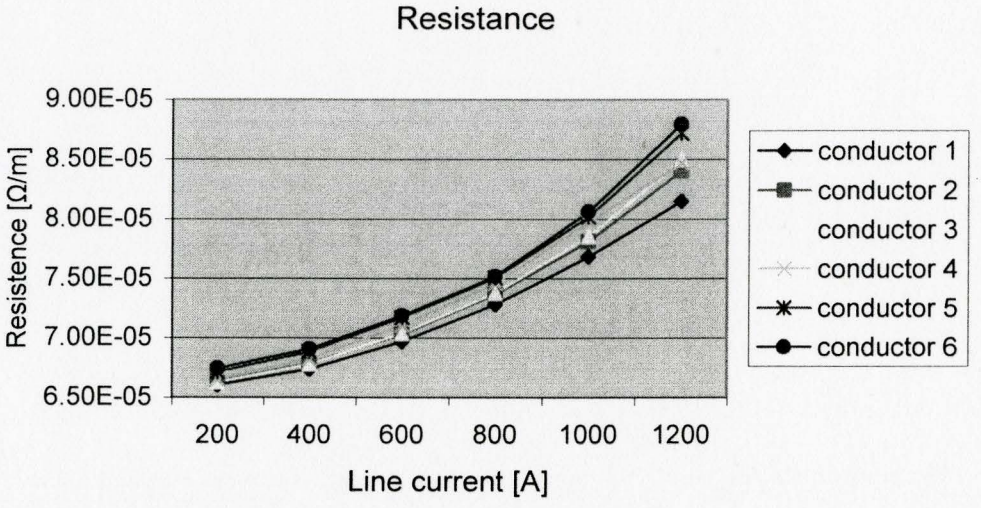

Figure F.7 Variation of resistance in six conductors at various line currents

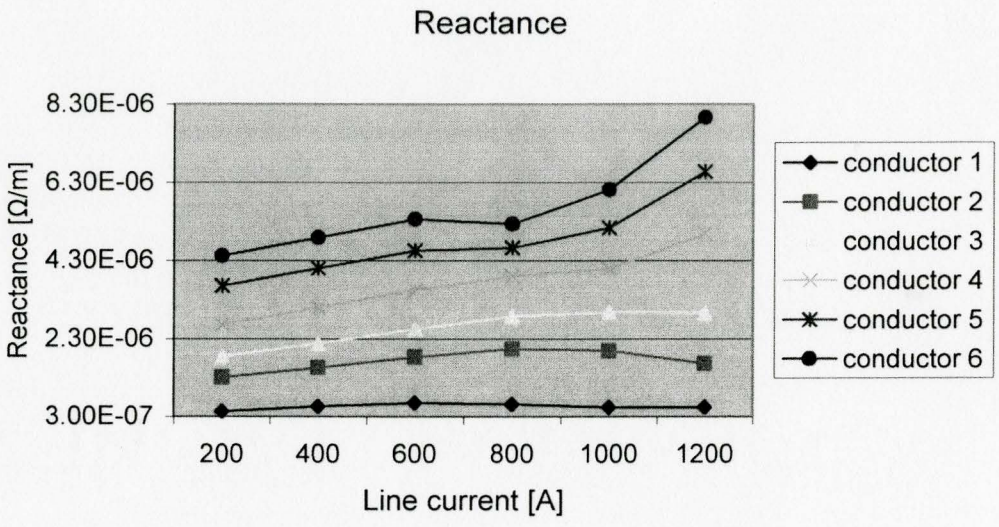

Figure F.8 Variation of reactance in six conductors at various line currents

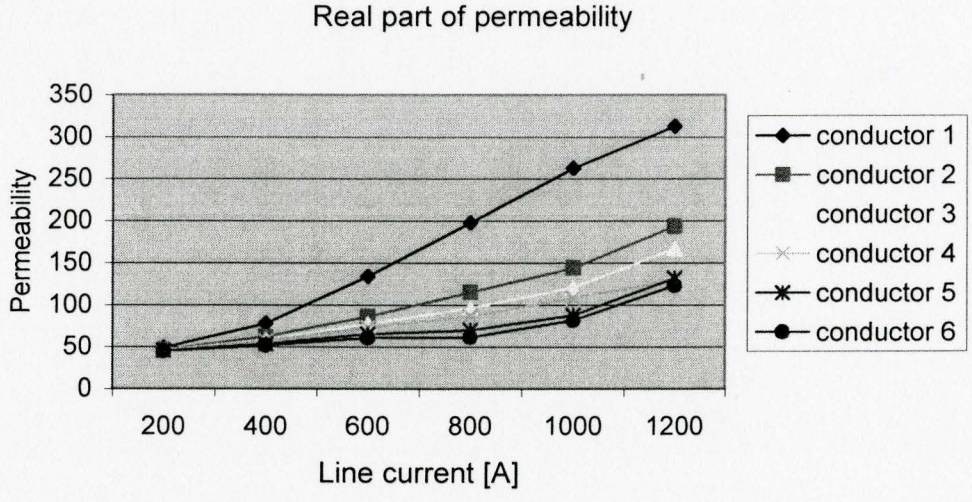

Figure F.9 Variation of real part of the permeability at various line currents

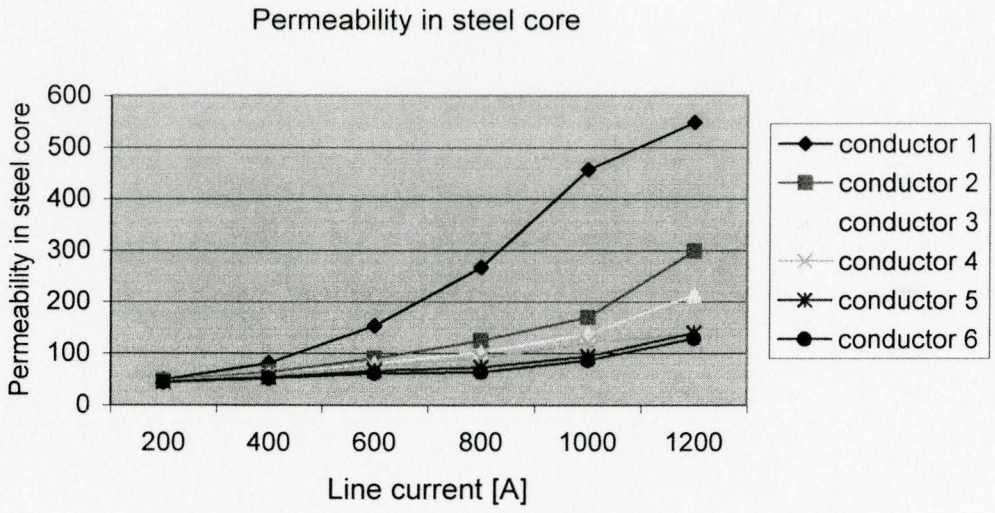

Figure F.10 Variation of the permeability at various line currents

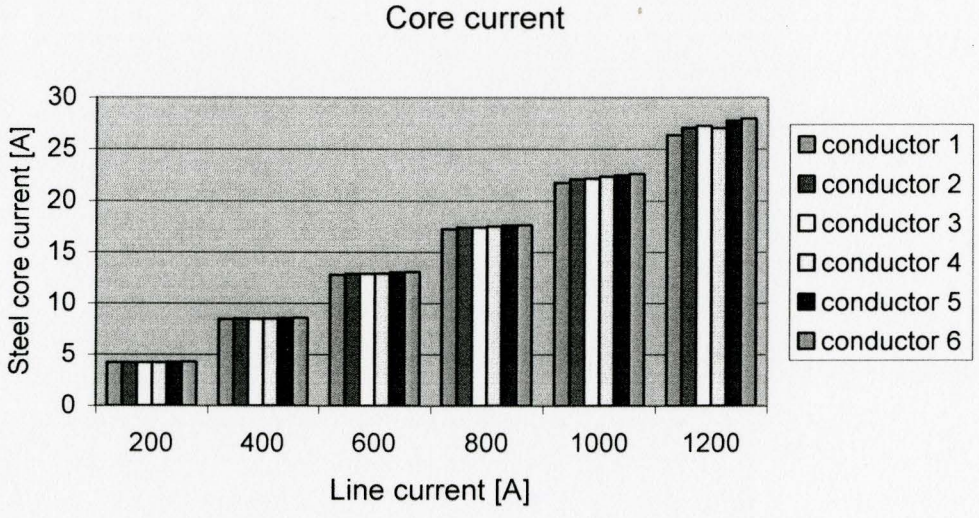

Figure F.11 Variation of steel core current at various line currents

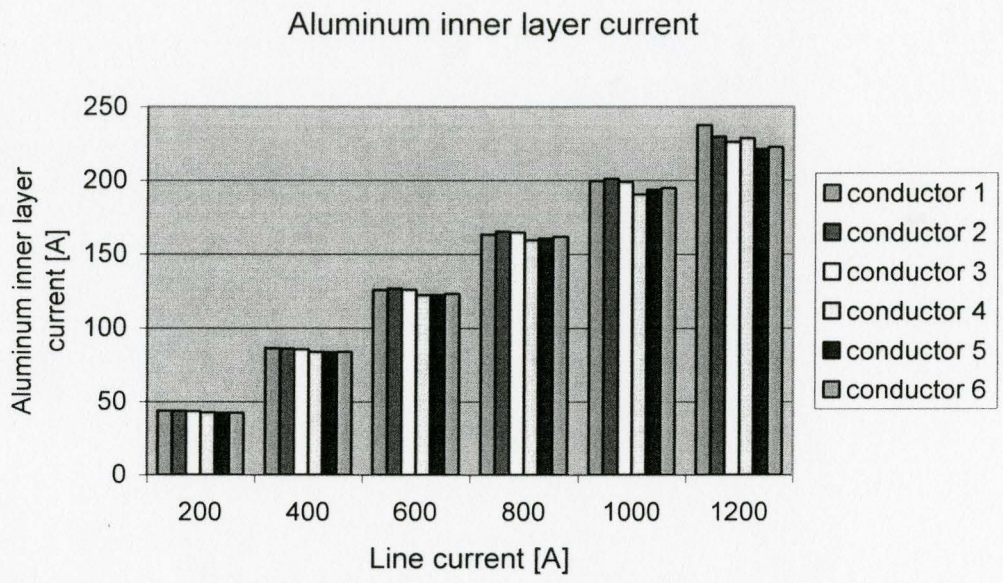

Figure F.12 Variation of aluminum inner layer current at various line currents

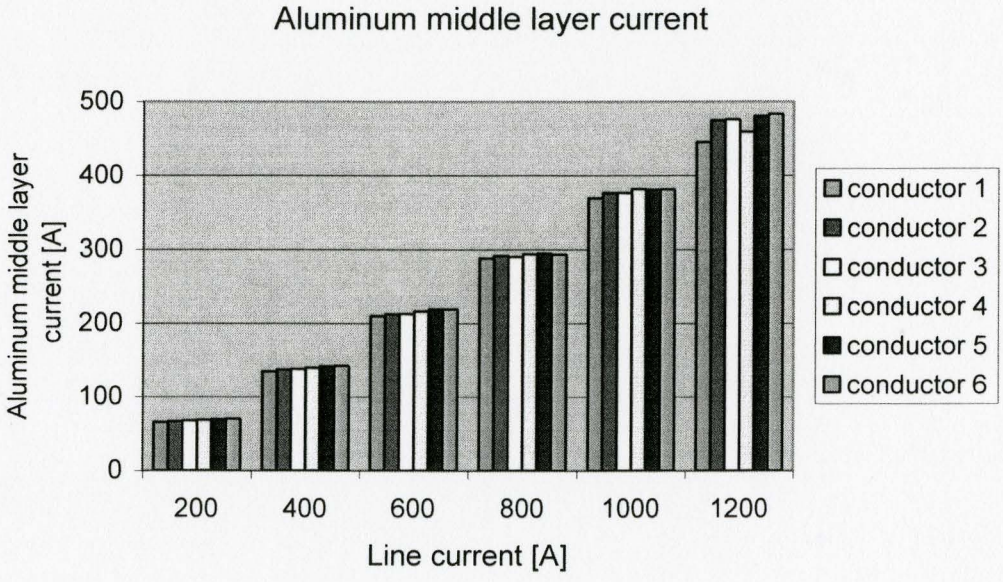

Figure F.13 Variation of aluminum middle layer current at various line currents

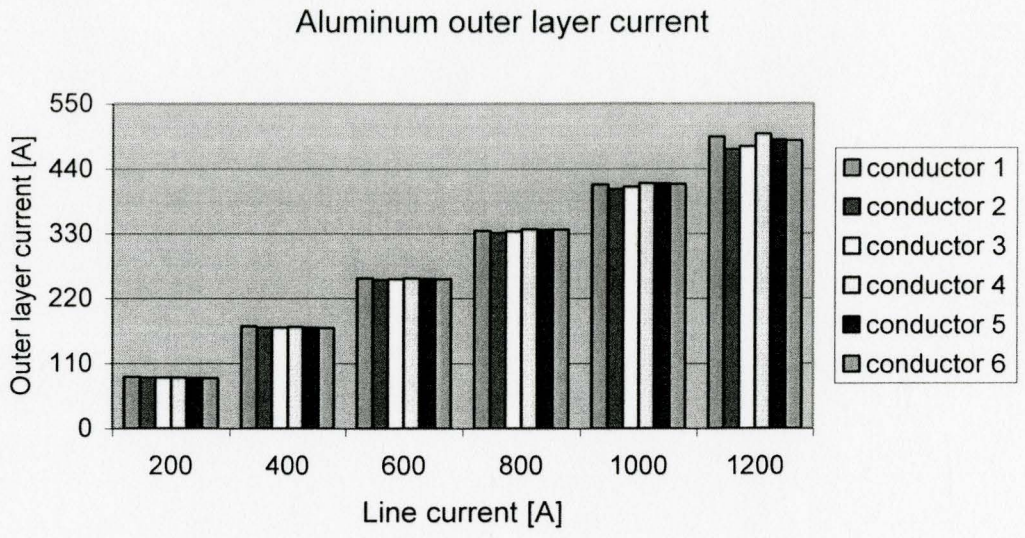

Figure F.14 Variation of aluminum outer layer current at various line currents

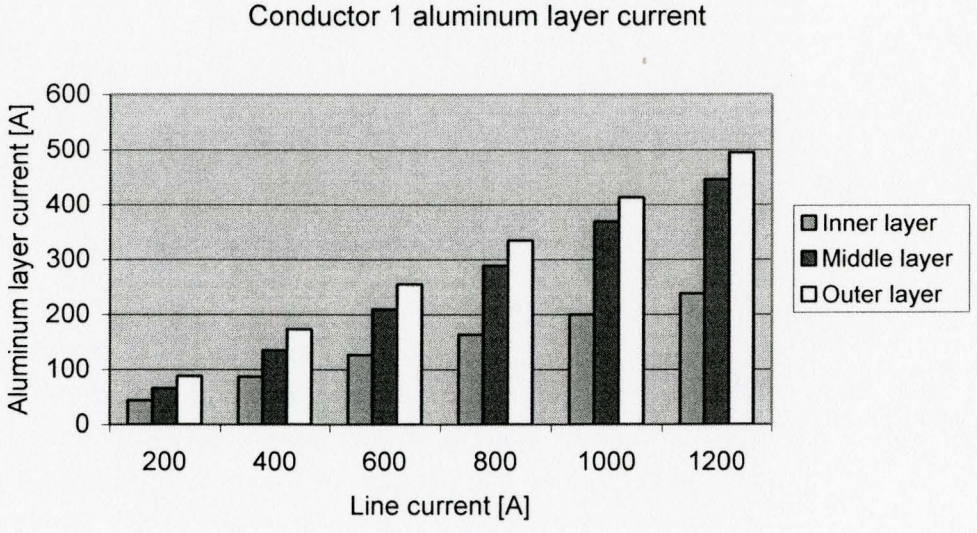

Figure F.15 Variation of three aluminum layer currents in conductor 1 at various line currents

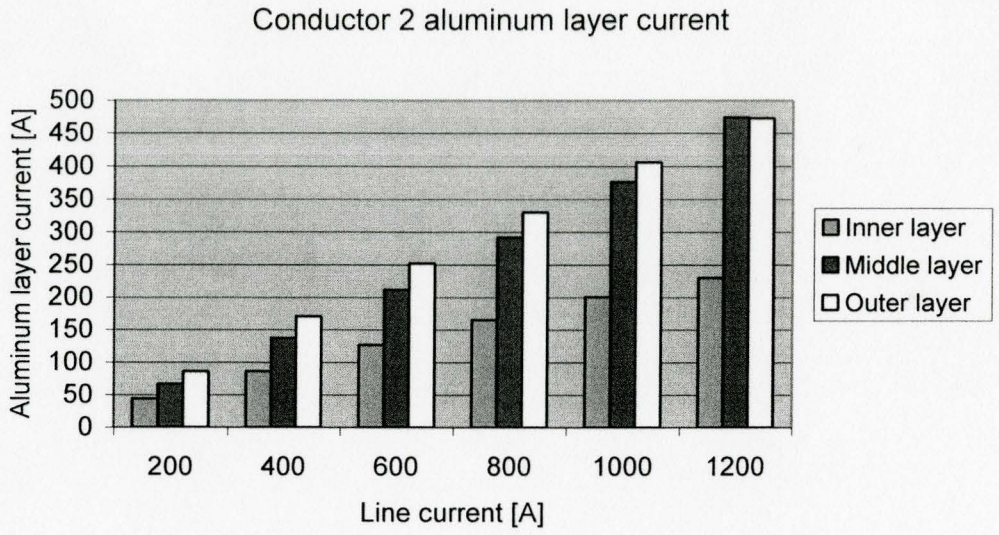

Figure F.16 Variation of aluminum layer currents in conductor 2 at various line currents

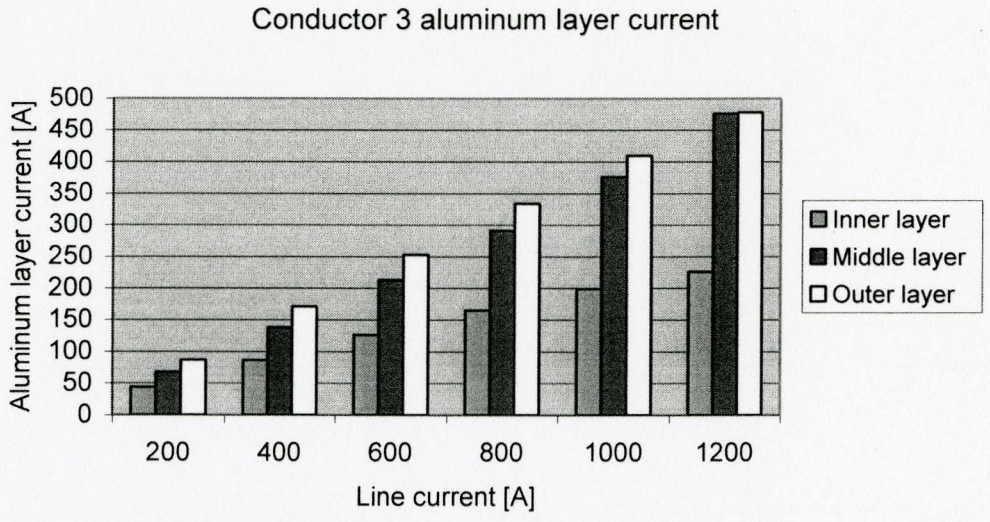

Figure F.17 Variation of aluminum layer currents in conductor 3 at various line currents

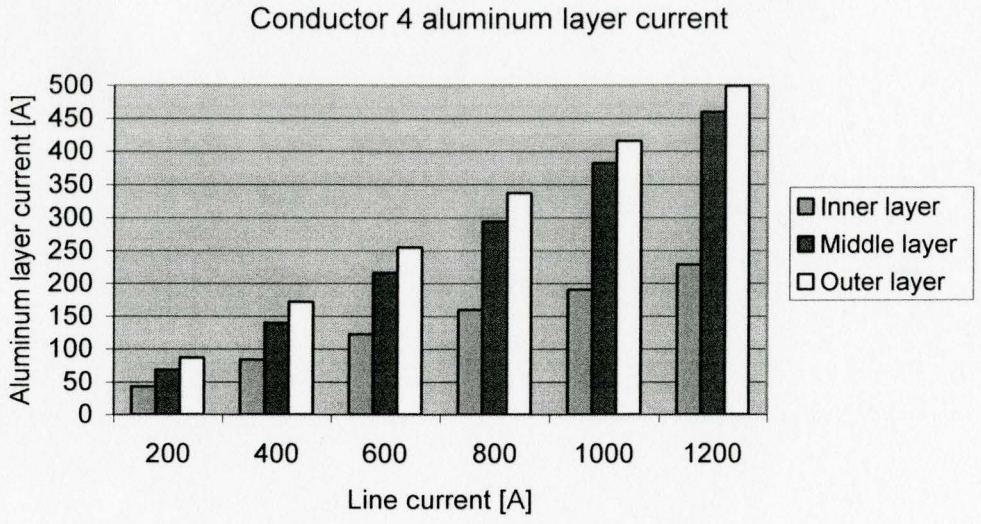

Figure F.18 Variation of three aluminum layer currents in conductor 4 at various line currents

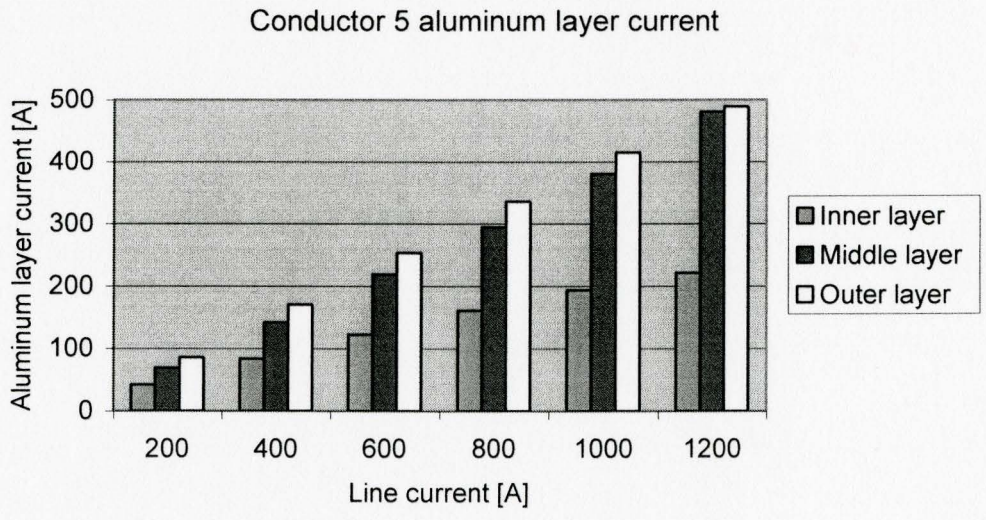

Figure F.19 Variation of aluminum layer currents in conductor 5 at various line currents

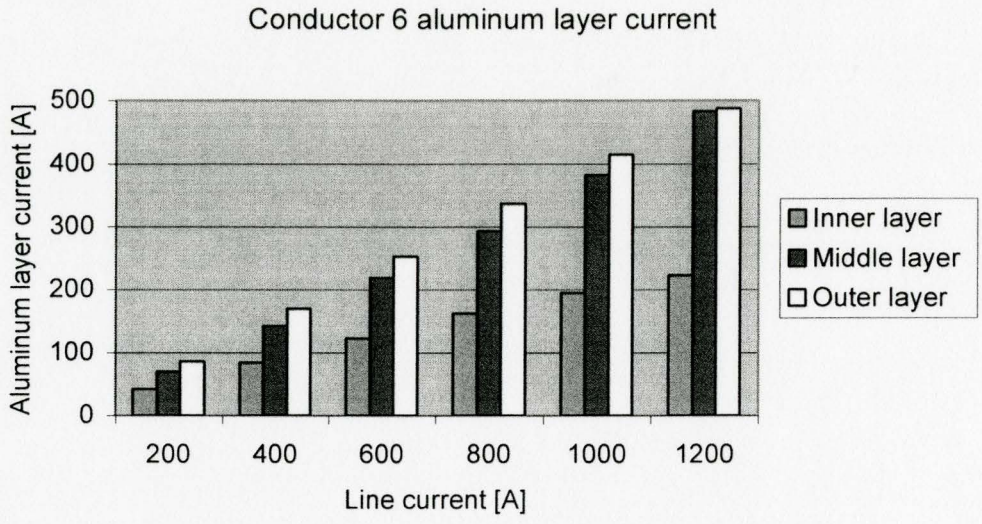

Figure F.20 Variation of aluminum layer currents in conductor 6 at various line currents

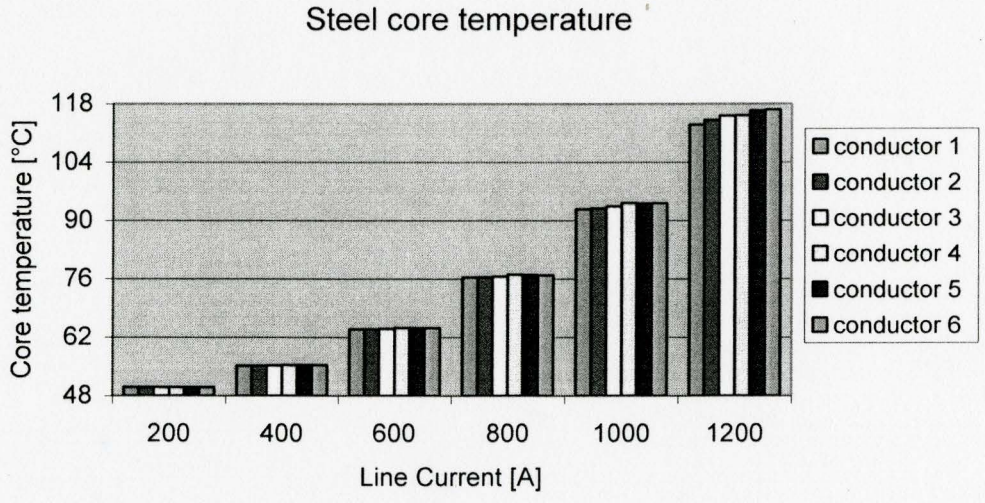

Figure F.21 Variation of steel king layer temperature at various line currents

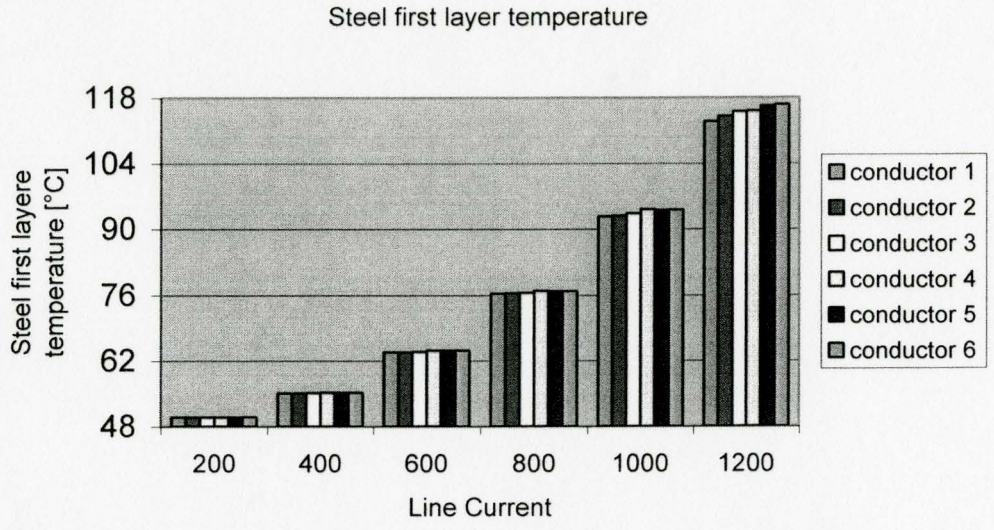

Figure F.22 Variation of steel first layer temperature at various line currents

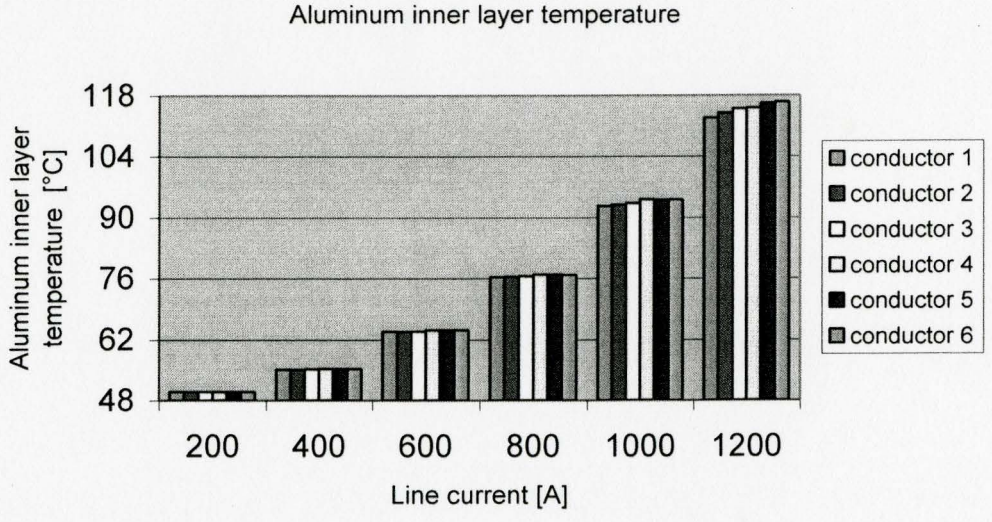

Figure F.23 Variation of aluminum inner layer temperature at various line currents

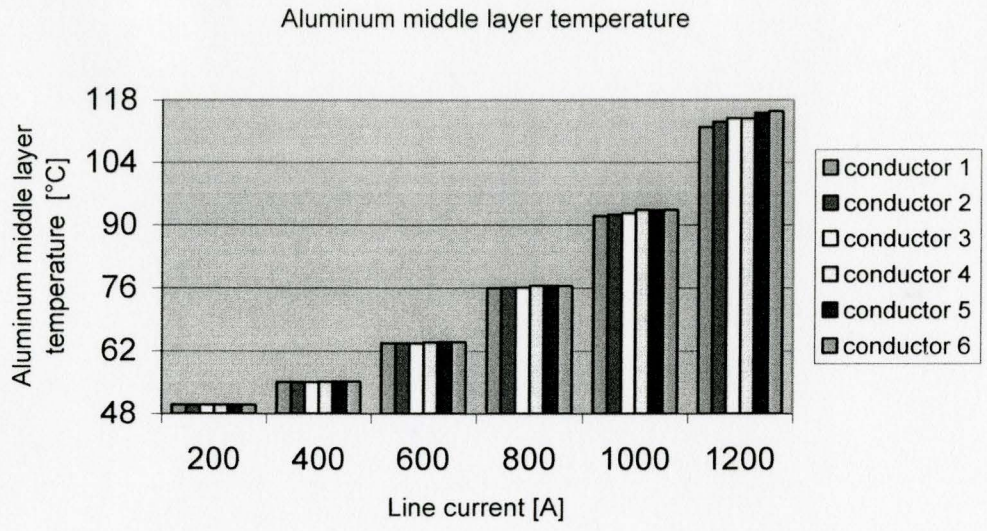

Figure F.24 Variation of aluminum middle layer temperature at various line currents

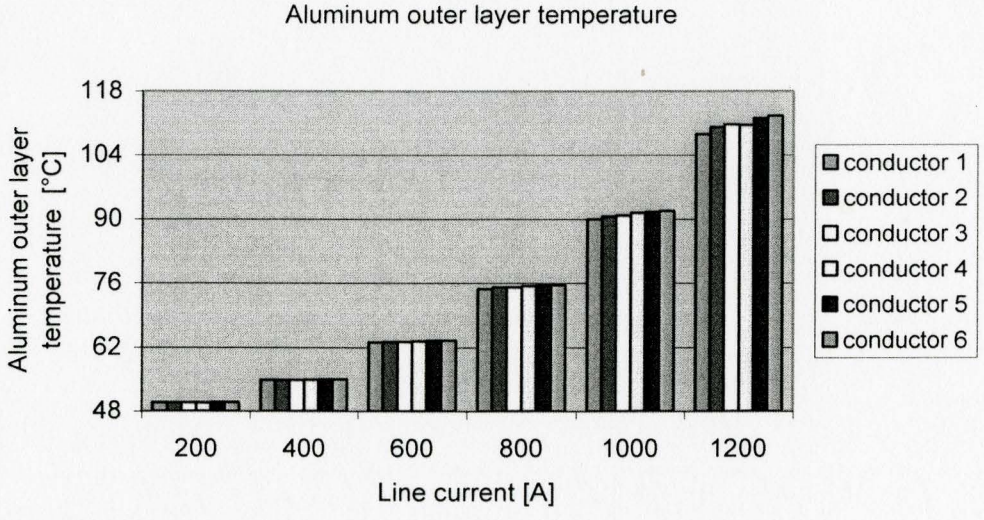

Figure F.25 Variation of aluminum outer layer temperature at various line currents

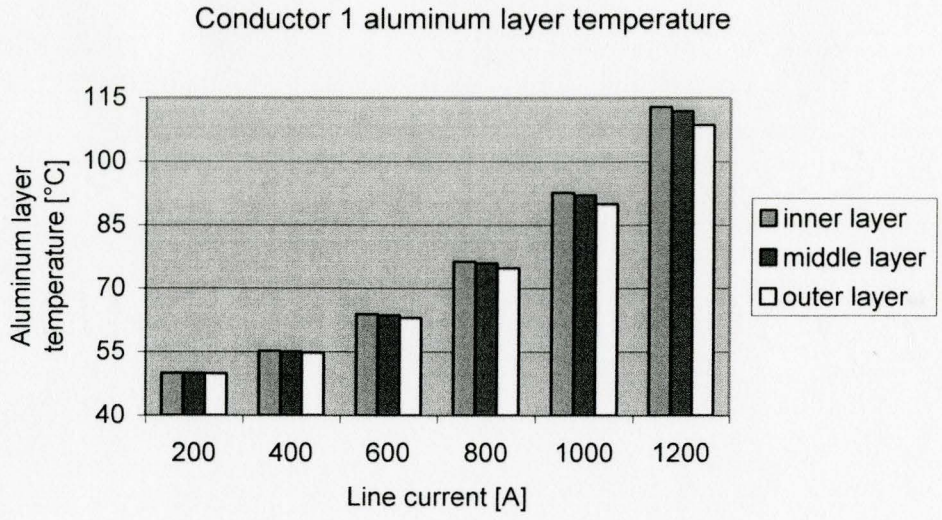

Figure F.26 Variation of aluminum layer temperature in conductor 1 at various line currents

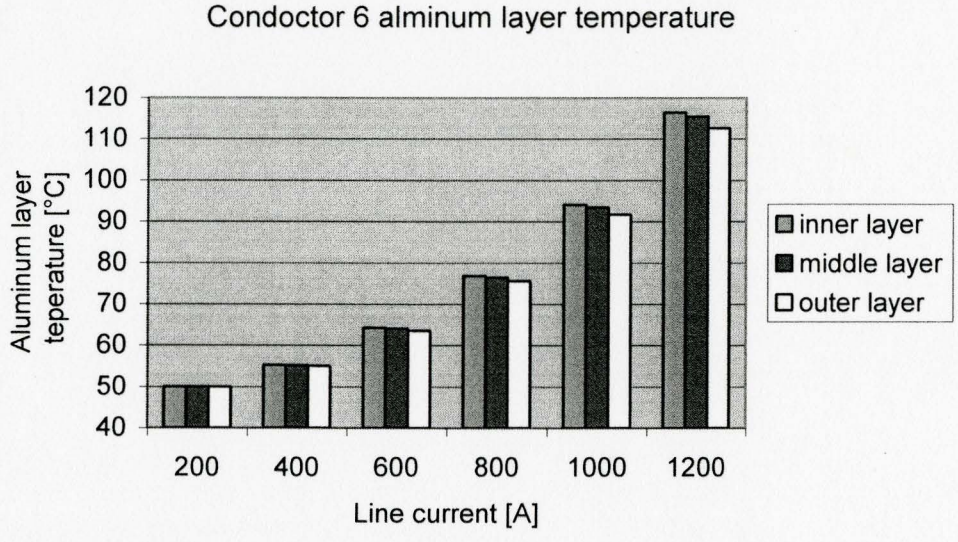

Figure F.27 Variation of aluminum layer temperature in conductor 6 at various line currents

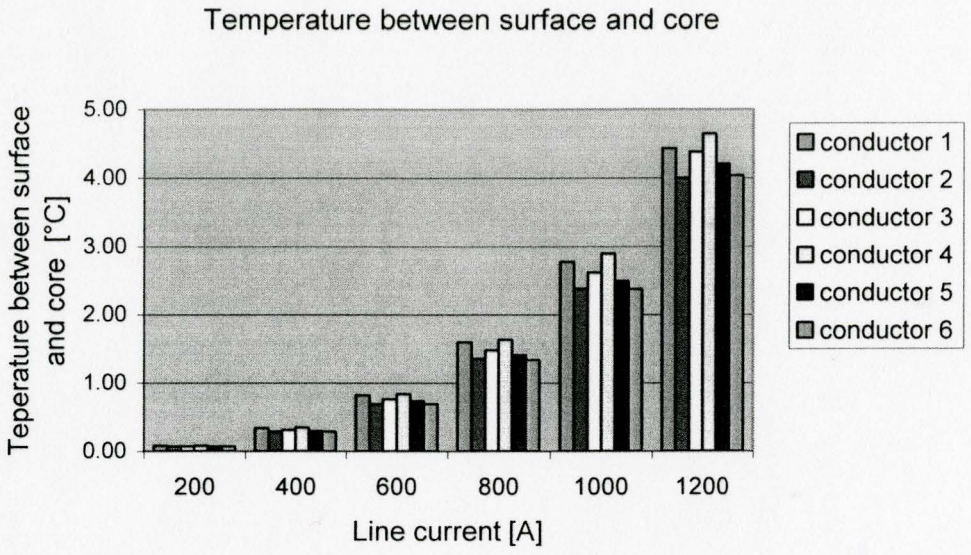

Figure F.28 Temperature differences between steel core and conductor surface

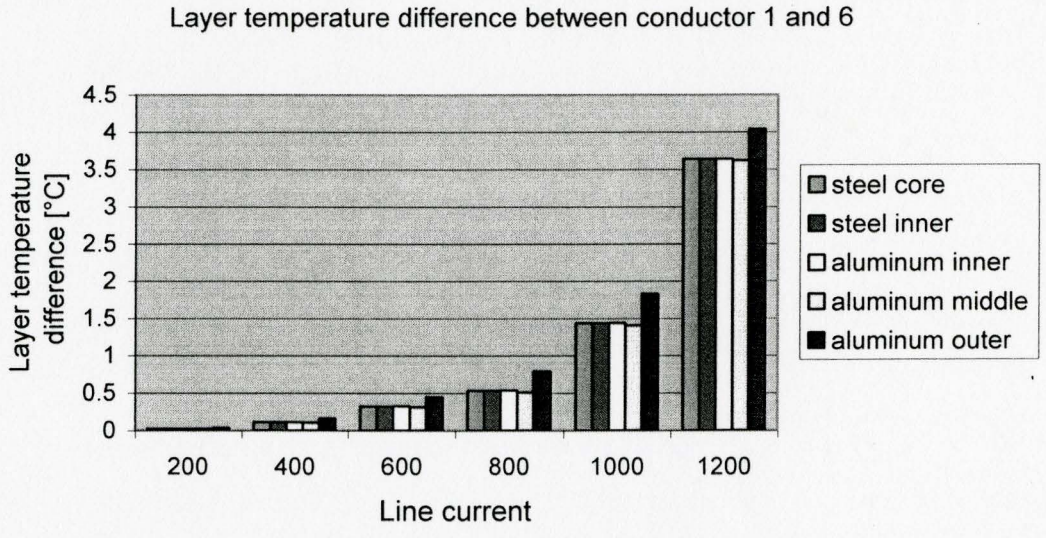

Figure F.29 Temperature differences in layers between conductor 1 and 6

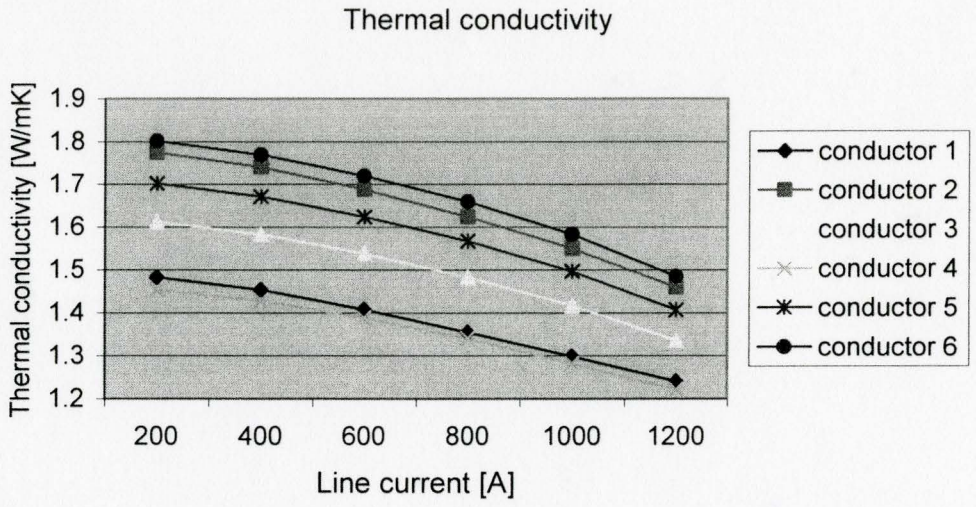

Figure F.30 Variation of the thermal conductivity at various line currents

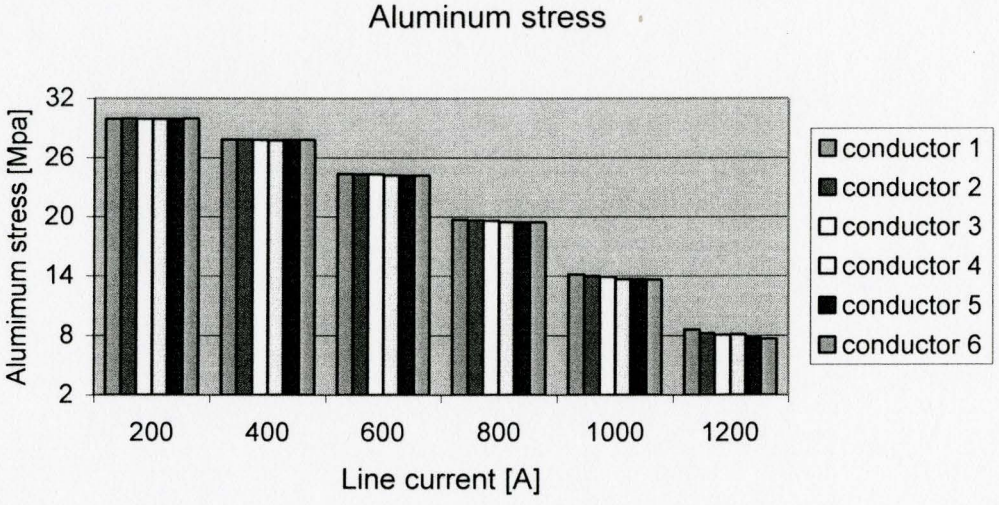

Figure F.31 Variation of aluminum stresses at various line currents

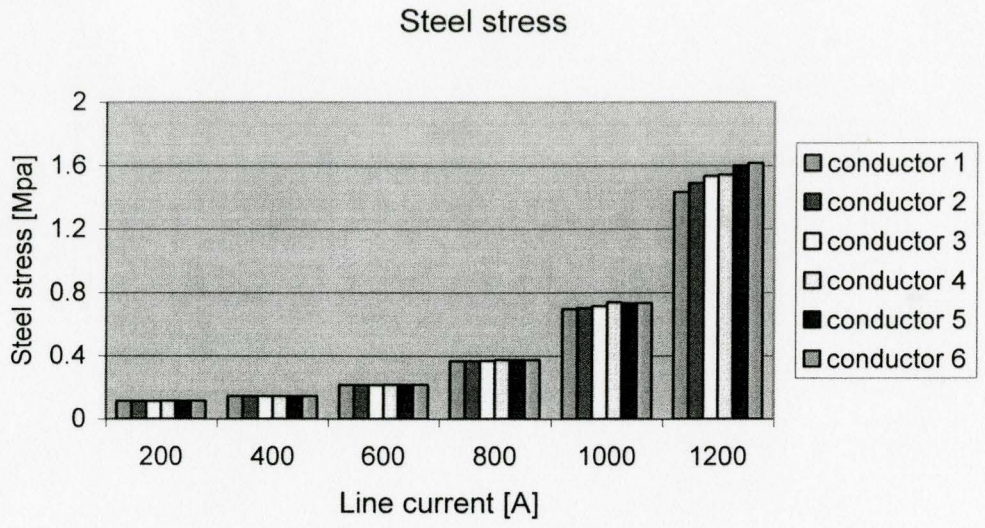

Figure F.32 Variation of steel stresses at various line currents

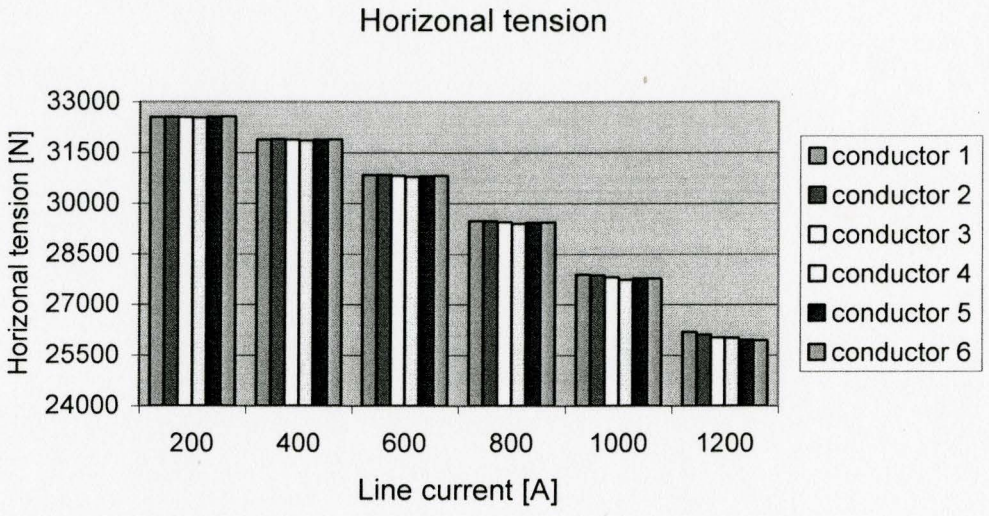

Figure F.33 variation of horizontal tension at various line currents

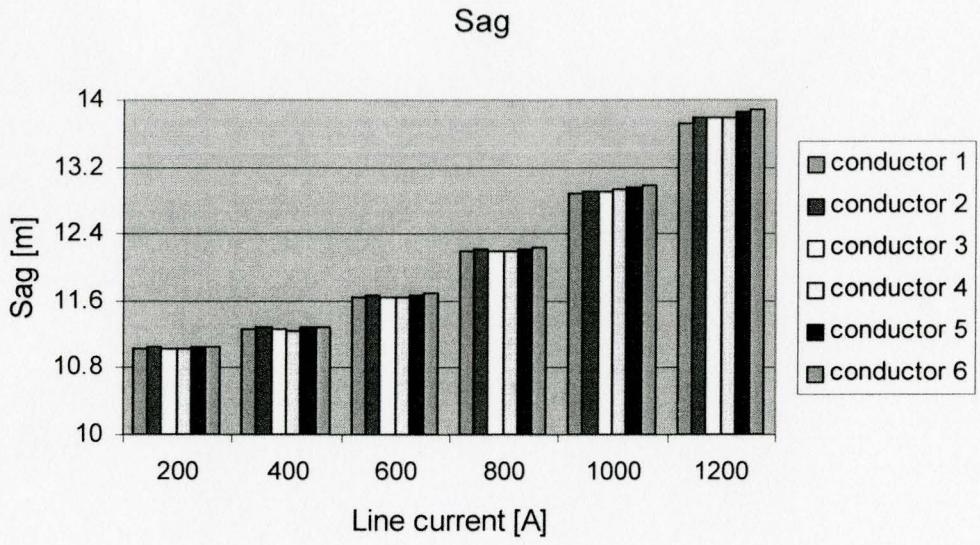

Figure F.34 Variation of sags at various line currents with line length 400 meters

F.3 Fixing wire diameters, changing steel and aluminum lay lengths

Table F.8 Unchanged steel wire and aluminum wire diameters

Steel wire diameter [mm]		Aluminum wire diameter [mm]		
King	Steel lay 1	Inner	Middle	Outer
3.376	3.376	3.376	3.376	3.376
Outer diameters [mm]		Aluminum layer's outer diameters [mm]		
Steel lay 1	Steel lay 2	Inner	Middle	Outer
3.376	10.127	16.878	23.629	30.380

Table F.9 Changed steel and aluminum lay lengths

Steel lay length [mm]			Aluminum lay length [mm]		
	Steel lay 1	Steel lay 2	Inner	Middle	Outer
Conductor 1	303.8	286.9	236.3	394.9	303.8
Conductor 2	213	263	262.1	326.8	213
Conductor 3	296.8	241.8	314.1	341.5	296.8
Conductor 4	296.8	192.3	361.9	364.9	296.8
Conductor 5	291.9	175.1	356	320.7	291.9
Conductor 6	182.3	168.8	378.1	303.8	182.3
Weight [N/m]					
Conductor 1	Conductor 2	Conductor 3	Conductor 4	Conductor 5	Conductor 6
17.92	17.97	17.91	17.89	17.99	17.99

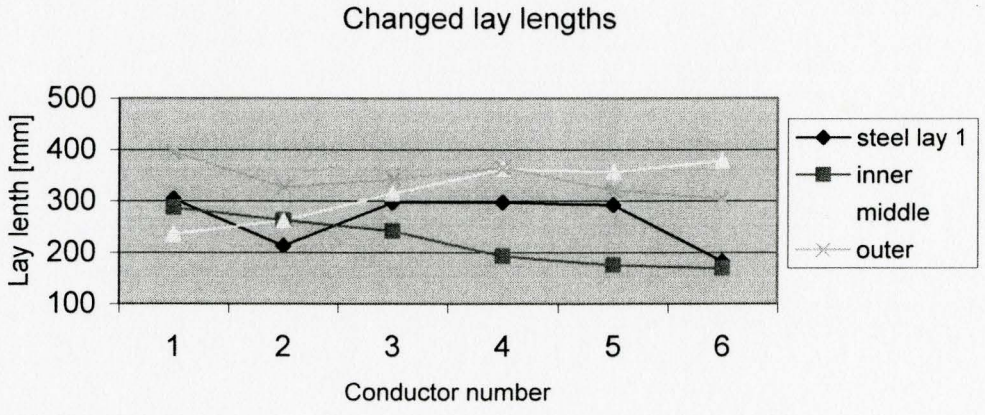

Figure F.35 Variation of lay length for different conductors at 1000 A

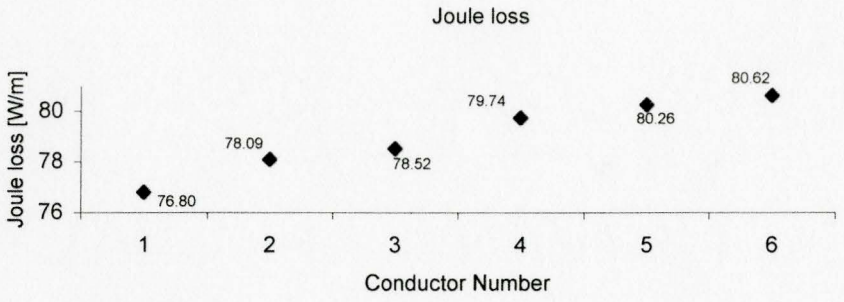

Figure F.36 Variation of Joule losses for different conductors at 1000A

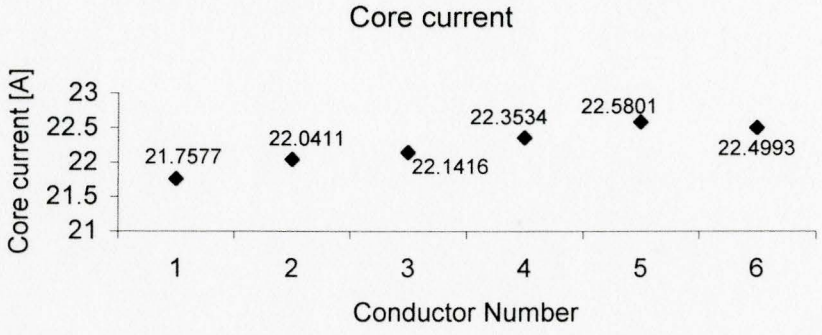

Figure F.37 Variation of core current for different conductors at 1000A

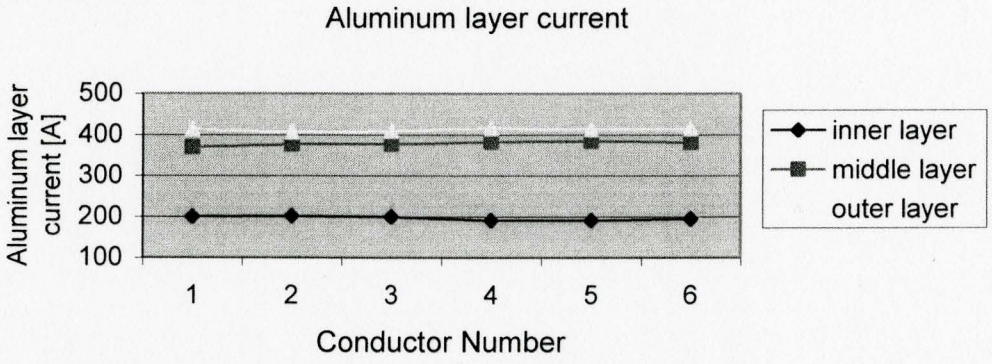

Figure F.38 Variation of aluminum current for different conductors at 1000A

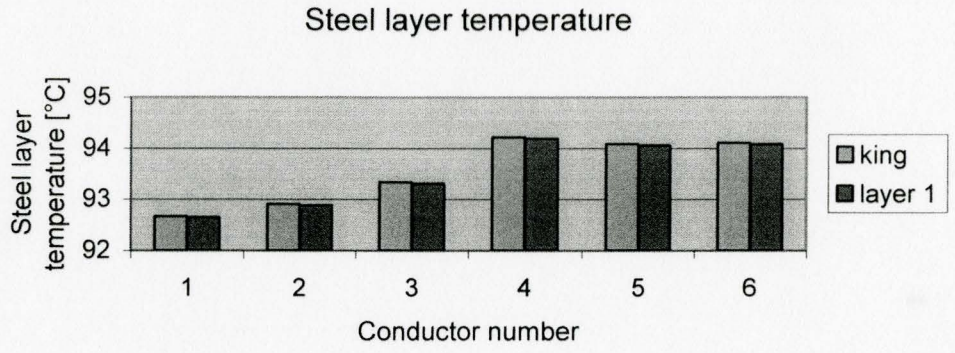

Figure F.39 Variation of steel layer temperature for different conductors at 1000A

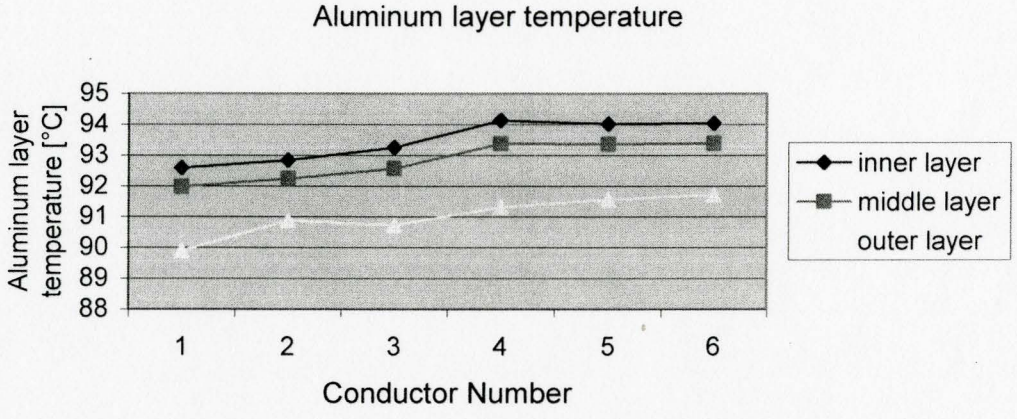

Figure F.40 Variation of aluminum layer temperature for different conductors at 1000A

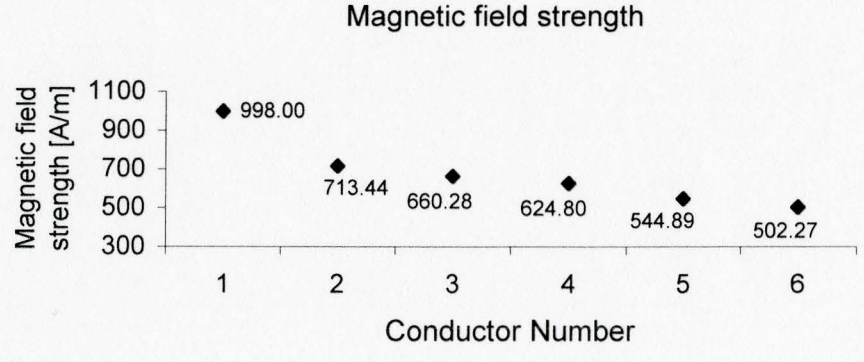

Figure F.41 Variation of magnetic field strength for different conductors at 1000A

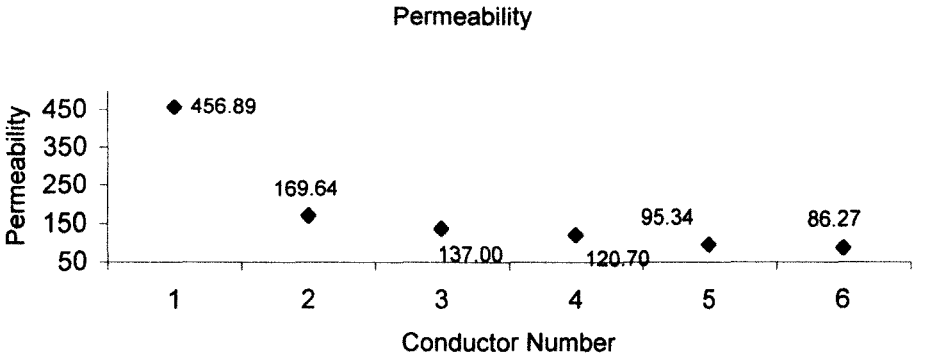

Figure F.42 Variation of the permeability for different conductors in 1000A

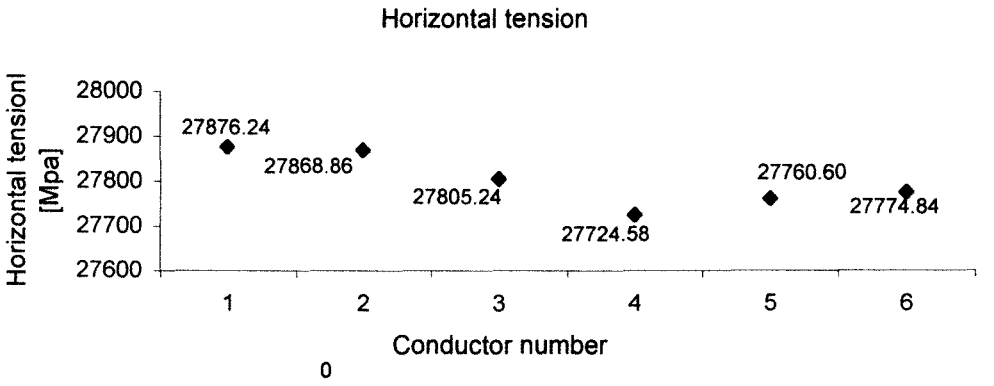

Figure F.43 Variation of horizontal tension for different conductors at 1000A

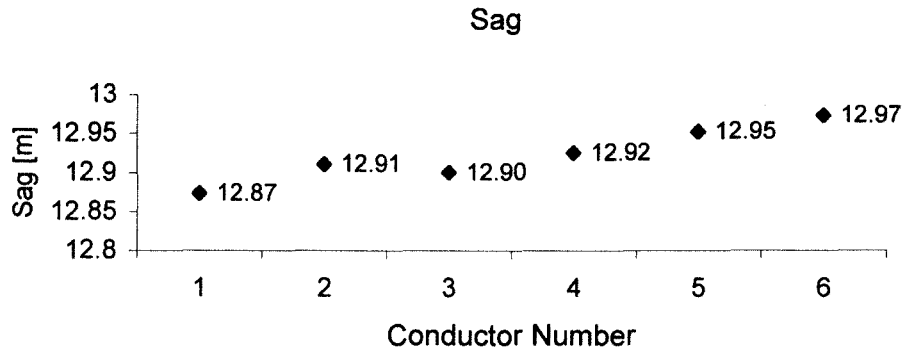

Figure F.44 Variation of sags for different conductors at 1000A

Reference

[1] V. Filipovic Gledja, V. T. Morgan, R. D. Findlay

"A Probability Based Unified Model for Predicting the Electrical and Thermal Characteristics of Stranded Overhead-Line Conductors"

Proceedings of the 1994 Canadian Conference on the Electrical and Computer Engineering, Vol. 1, Sept 1994, pp 182-185

[2] W. A. Lewis, L. W. Matsch

"Magnetic Properties of ACSR Core Wire"

AIEE Transactions, Vol. 77, part III, 1958, pp. 1178-1189

[3] W. A. Lewis and P. D. Tuttle

"The Resistance and Reactance of Aluminum Conductors, Steel Reinforced"

Tran. A.I.E.E, Vol. 77, part III, Feb. 1959, p1189-1215

[4] V. T. Morgan and C. F. Price

" Magnetic Properties in Axial 50Hz Fields of Steel Core Wire for Overhead-Line Conductors"

Proc. IEE (London), Vol. 116, No. 10, October 1969, pp.1681-1694

[5] J. S. Barrett, O. Nigol, C. J. Fehervari, R. D. Findlay

"A New Model of AC Resistance in ACSR Conductors"

IEEE Transactions on Power Delivery, Vol. 1, No. 2, 1986, pp. 198-208

[6] V. T. Morgan, R. D. Findlay and Bo Zhang

"Distribution of Current Density in ACSR Conductors"

Proceedings of the 1994 Canadian Conference on the Electrical and Computer Engineering, Vol. 1, 1994, pp. 165-168

[7] T. Varney

"ACSR, Graphic method for Sag-Tension Calculations"

Aluminum Company of America, June 1927

[8] C. A. Jordan

"A Simplified Sag Tension Method for Steel-Reinforced Aluminum Conductors"

AIEE Transactions on Power Apparatus and Systems, Vol. 71, pt. III, 1952, pp. 1108-1118

[9] CIGRE WG 22-05

"Permanent Elongation of Conductors. Predictor Equation and Evaluation Methods"

Electra, No. 75, 1981, pp. 63-98

[10] O. Nigol and J. S. Barret

"Characteristics of ACSR Conductors at High Temperatures and Stresses"

IEEE Trans. on Power Apparatus and Systems, Vol. PAS-100, 1981, pp.485-493

[11] J. S. Barrett, S. Dutta and O. Nigol

"A New Computer Model of ACSR Conductors"

IEEE Trans. on Power Apparatus and Systems, Vol. PAS-102, 1983, pp.614-621

[12] J. S. Barret

"Optimization of Conductor Design"

IEEE Transactions on Power Delivery, Vol. 4, No. 1, 1989, pp. 453-463

[13] V. T. Morgan and R. D. Findlay

"Effects of Axial Tension and Reduced Air Pressure on the Radial Thermal Conductivity of a Stranded Conductor"

IEEE Transactions on Power Delivery, Vol. 8, No. 2, 1993, pp. 553-558

[14] V. T. Morgan

"The Heat Transfer from Bare Stranded Conductors By Natural and Forced Convection in Air"

Heat Mass Transfer, Vol. 16, 1973, pp. 2023-2034

[15] V. T. Morgan

"Thermal Behaviour of Electrical Conductors"

John Wiley & Sons Inc., 1991(ISBN 0 471 93071 7)

[16] Bo Zhang

"A Study of the Magnetic Properties of ACSR Core Wire with the Objective of Reducing Transmission Losses"

Master Thesis, McMaster University, 1986

[17] Visnja Filipovic-Gledja

A probability Based Unified Model For Predicting Electrical, Mechanical and Thermal Characteristics of Stranded Overhead-Line Conductors"

Ph.D. Thesis, McMaster University, 1997

[18] ASTM Designation: B232M-01

"Standard Specification for Concentric-Lay Stranded Aluminum Conductors"

Annual Book of ASTM standard, Vol.02.03

[19] Drazena Brocilo

"Modifications of COOLTEMP Program, an Analysis and Prediction Program for Aluminum Conductor, Steel Reinforced (ACSR)"

Master Thesis, McMaster University, 1999

[20] Libin Xue

"An improved Unified Model of ACSR"

Master Thesis, McMaster University, 1998

[21] Hongjuan Wang

"Some Aspects of Two layer ASCR "

Master Thesis, McMaster University, 2004

[22] Thomas B$\ddot{a}$ck, David B Fogel, Zbigniew Michalewocz,

"Evolutionary Computation 1"

Institute of Physics Publishing, 2000

[23] David B. Fogel

"Evolutionary Computation"

Second Edition, IEEE Press, 2000

[24] Lance Chapmans

"The Practical Handbook of Genetic Algorithms Applications"

Second edition, Chapman & Hall/CRC, 2001

[25] Charles L. Karr, L. Michael Freeman

"Industrial Applications of Genetic Algorithms"

CRC Press, 1999

[26] J.H. Holland

"Adaptation in Natural and Artificial Systems"

Ann Arbor, The University of Michigan Press, 1975

[27] Randy L. Haupt, Sue Ellen Haupt

"Practical Genetic Algorithms"

John Wiley & Sons, Inc, 1998

[28] Thomas Bäck

"Evolutionary Algorithms in Theory and Practice"

Oxford University Press, 1996

[29] Zbigniew Michalewicz

"Genetic Algorithms + Data Structures= Evolution Programs"

Third Edition, Springer, 1992

[30] R. D. Findlay

"Analysis of Two Layer Aluminum Conductor Steel Reinforced"

IEEE PES Winter Meeting, New York, January-February 1973

[31] R. D. Findlay, D. Brocilo, V. T. Morgan

"Sensitivity Analysis of Aluminum Conductor Steel Reinforced (ACSR) Using Historical Permeability Data From a Single Wire Versus Stranded Steel Core Permeability Data"

Canadian Conference on Electrical and Computer Engineering, Waterloo, Canada, 24-28 May 1998

[32] Lawrence Davis

"Handbook of Genetic Algorithms"

Van Nostrand Reinhold, New York, 1991

[33] Randy L. Haupt

"An Introduction to Genetic Algorithms for Electromagnetics"

IEEE Antennas and Propagation Magazine, Vol. 37, No. 2, April 1995